Investigating the role of MALAT1, a long non-coding RNA, in glioblastoma tumorigenesis

Inaugural dissertation

for the attainment of the title of doctor
in the Faculty of Mathematics and Natural Sciences
at the Heinrich Heine University Düsseldorf

presented by

Maike Langini
from Trier

Düsseldorf, September 2022

from the Molecular Proteomics Laboratory
of the institute for molecular medicine I
at the Heinrich Heine University Düsseldorf

Published by permission of the
Faculty of Mathematics and Natural Sciences at
Heinrich Heine University Düsseldorf

Supervisor: Prof Dr Kai Stühler
Co-supervisor: Prof Dr Lutz Schmitt

Date of the oral examination: 2nd November 2022

“Don’t be afraid of hard work. Nothing worthwhile comes easily. Don’t let others discourage you or tell you that you can’t do it. In my day I was told women didn’t go into chemistry. I saw no reason we couldn’t.” – Gertrude B. Elion

Abbreviations

Akt	protein kinase B
ANOVA	analysis of variance
ATRX	alpha-thalassemia/mental retardation, X-linked
CDK4	cyclin dependent kinase 4
CDK6	cyclin dependent kinase 6
cDNA	complementary deoxyribonucleic acid
CHART	capture hybridisation analysis of RNA targets
ChIRP	chromatin isolation by RNA purification
CLIP	cross-linking and immunoprecipitation
CNS	central nervous system
CRISPRi	clustered regularly interspaced short palindromic repeats interference
Crtl	control
CT	threshold cycle
DMEM	Dulbecco's Modified Eagle Medium
DMSO	dimethyl sulfoxide
EDTA	ethylenediaminetetraacetic acid
EFEMP1	EGF-containing fibulin-like extracellular matrix protein 1
EGF	epidermal growth factor
EGFR	epidermal growth factor receptor
EMT	epithelial-to-mesenchymal transition
ESI	electrospray ionisation
FBS	foetal bovine serum
FC	fold change
FDR	false discovery rate
GAPDH	glyceraldehyde-3-phosphate dehydrogenase
GBM	glioblastoma
gRNA	guide RNA
H3F3A	histone H3.3
HHIP-AS1	hedgehog interacting protein- antisense 1
HOTAIRM1	HOX antisense intergenic RNA myeloid 1
HRP	horse radish peroxidase
HT	high throughput
HuR	human antigen 1
IC50	half-maximal inhibitory concentration
IDH	isocitrate dehydrogenase
KD	knockdown
LC	liquid chromatography
lncRNA	long non-coding RNA
MALTA1	metastasis associated lung adenocarcinoma transcript 1
MAPK	mitogen-activated protein kinase
MB	medulloblastoma
miRNA	microRNA
MS	mass spectrometry
MS/MS	tandem mass spectrometry
NEAT1	nuclear paraspeckle assembly transcript 1
NF1	neurofibromin 1
PAIR	PNA assisted identification of RBPs
PBS	phosphate buffered saline
PCNA	proliferating cell nuclear antigen

PGK1	phosphoglycerate kinase 1
PI	propidium iodide
PI3K	phosphoinositol 3-kinases
PNA	peptide nucleic acid
PSM	peptide-spectrum match
PTEN	phosphatase and tensin homolog deleted on chromosome 10
PTM	post translational modification
PVDF	polyvinylidene difluoride
qPCR	quantitative polymerase chain reaction
R^2	coefficient of determination
RAP	RNA affinity purification
RB	retinoblastoma
RB1	retinoblastoma protein
RBP	RNA binding protein
RIP	RNA immunoprecipitation
RNA	ribonucleic acid
RRM	RNA recognition motif
RT	reverse transcriptase
SDS-PAGE	sodium dodecyl sulphate polyacrylamide **gel** electrophoresis
SETD2	SET domain containing 2, histone lysine methyltransferase
SHH	sonic hedgehog
siRNA	small interfering RNA
Sp1	Sp1 transcription factor
SRSF	serin/arginine-rich splicing factor
SSC	saline sodium citrate
TERT	telomerase reverse transcriptase
TFA	trifluoro acetic acid
TMZ	temozolomide
TP53	tumour protein p53
TRIM28	tripartite motif containing 28
WHO	World Health Organisation
Wnt	wingless-type
WT	wild type
ZNF10	zinc finger protein 10

List of Figures

List of Tables

Summary

This study aimed to increase the understanding of *MALAT1s*' influence on protein signatures in GBM a highly malignant brain tumour with 5-year survival rates of approx. 5 % as well as a 90 % recurrence rate through a combination of interactomics, phenotype, proteomics and drug screening analyses.

LncRNAs such as *MALAT1* previously thought to have no function could be employed as druggable targets as well as biomarkers. Therefore, investigation of their influence on protein signatures are necessary to increase the understanding of affected biological pathways and signalling cascades.

- Through RNA-centric affinity enrichment, previously unknown putative *MALAT1* interacting proteins were identified in established MB and GBM cell lines. In a GBM specific sample set involvement of *MALAT1* in EGFR/PI3K signalling and cell cycle progression from G1- to S-phase was observed.
- The phenotype study performed under application of the isogenic cell line pairs generated highlights the influence of *MALAT1* in migration and proliferation events in a cell line-specific manner based on varying underlying biology.
- Protein expression level analysis via nanoLC-MS approach shows that *MALAT1* levels can indirectly affect protein expression levels. The link to EGFR/PI3K signalling observed in the interactome study is corroborated in this analysis and a cell line specific influence of *MALAT1* based on the mutational background of the parental cell line was indicated.
- The high-throughput drug screen employing one of the generated isogenic cell line pairs resulted in the identification of ZSTK474 as a drug candidate affecting *MALAT1* linked signalling pathways in respective GBM cases. Orthogonal validation methods employed exhibited a treatment effect for ZSTK474 a pan PI3K inhibitor based on the *MALAT1* expression level in the isogenic cell lines generated.
- Through the combined data collected in this study several proteins, biological pathways, and phenotypical markers were shown to be affected by *MALAT1* expression changes. The proteins H3F3A, TRIM28, PCNA, EFEMP1, and ZNF10 were linked to *MALAT1* resulting in a potential linkage of this lncRNA to cell cycle progression, EGFR/PI3K, and DNA repair signalling pathways.

This study shows that *MALAT1* as a lncRNA can affect protein signatures in the investigated cell lines and that decreased *MALAT1* expression levels can lead to phenotypic changes as well as perturbations in protein signalling cascades. While *MALAT1* has already been shown to affect EGFR/PI3K signalling in tumours, the proposed modus operandi via transcriptional regulation of EFEMP1 and competitive binding to PCNA has not been described before in GBM. On basis of the data collected during this study, the observed effect of *MALAT1* on cell cycle progression is proposed to be linked to competitive binding of PCNA and TRIM28 in GBM. SETD2 is a well-known *MALAT1* interacting protein, however so far, no study has proposed the linkage between *MALAT1*, PCNA, H3F3A, and SETD2 to affect DNA repair signalling pathways via competitive binding events in GBM.

Putative *MALAT1* interactors identified in this study could be corroborated via reverse pulldowns with an RT-qPCR readout.

The data obtained increased the knowledge of *MALAT1s*' influence in GBM biology and revealed potential linkages to signalling pathways implicated in GBM tumorigenesis.

1 Introduction

1.1 Tumours of the central nervous system

A cluster of abnormal cells growing in the brain or spinal cord are classified as central nervous system, CNS, tumours. The tumours are divided into two groups benign and malignant. Benign or non-cancerous tumours rarely spread, while malignant or cancerous tumours spread into other brain tissue. Both benign and malignant CNS tumours are symptomatic. Their occurrence is not age restricted. In addition, a distinction is made between primary, originating in the brain, and metastatic, originating outside the brain, tumours.

To organise the plethora of different CNS tumours, the different tumours are grouped based on the cell type they originated from. For example, CNS tumours originating from astrocytes are called astrocytic tumours, oligodendroglioma originate from oligodendrocytes and medulloblastoma, MB, originate from neuronal progenitor cells (Figure 1). In addition, the World Health Organisation, WHO, defined a tumour grading system based on the rate of abnormality of the tumour cell as well as the growth rate and potential to spread. There are four different grades with grade I, low-grade tumours with a lower severity, and grade IV, high-grade tumours with a high severity. For example, pilocytic, diffuse, and anaplastic astrocytoma as well as glioblastoma, GBM, are all astrocytic tumours but their severity increases from grade I to grade IV in the listed order. [1, 2]

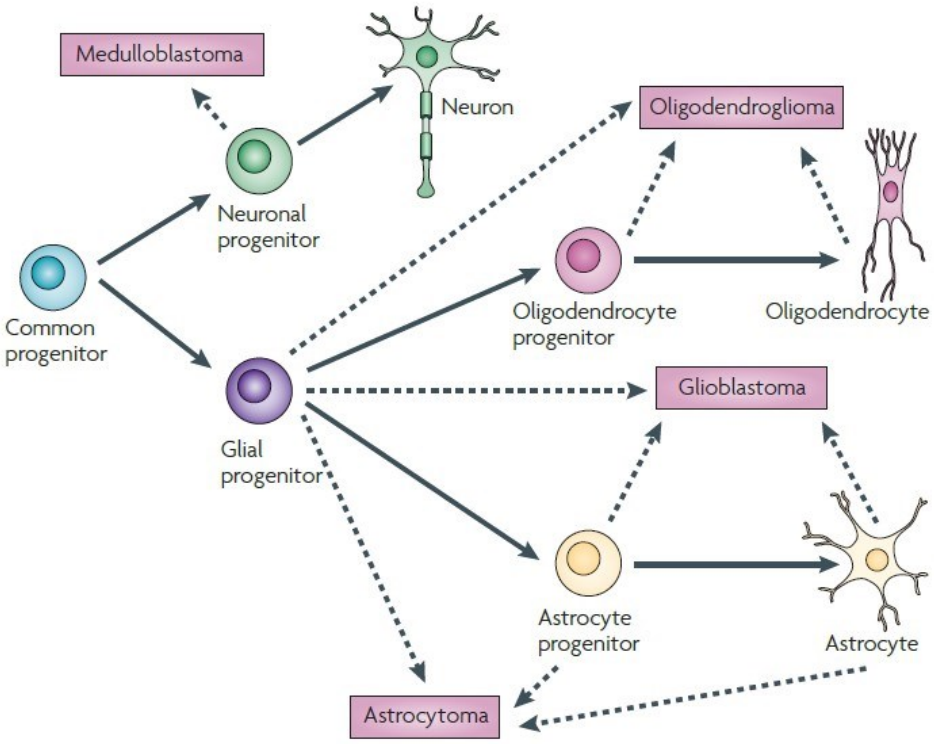

Figure 1 CNS tumours paired with their respective cells of origin. [3]

Symptoms of CNS tumours depend on the specific location of the tumour growth and range from nausea and headaches to seizures, changes in personality and difficulties with walking. Diagnosis can be achieved through a combination of biomarker panels, DNA analysis, imaging techniques, and biopsies. Treatment strategies most often include surgery, radiation therapy, chemotherapy, and targeted therapy. Even with these aggressive treatment options, survival rates are low for malignant

CNS tumours. Additionally, they have a high propensity for recurrence reducing overall survival rates even more and can become resistant to employed standard of care drugs like for example the observed temozolomide, TMZ, resistance in GBM. Novel treatment strategies such as immunotherapy, gene therapy, novel drug-delivery technologies, and targeted therapy are under development to reduce the necessity of highly invasive procedures and to increase overall survival rates. [1, 4-6]

An increased understanding of the underlying biological disturbances in the two most common malignant CNS tumour entities, GBM in adult and MB in paediatric patients, respectively, will aid in progressing the development of novel treatment options.

1.1.1 Glioblastoma

GBM is a highly malignant, heterogenous brain tumour. It is the most common primary brain tumour and can develop without age restriction [5, 7].

In 2016, WHO revised their classification of this tumour type adding molecular parameters to reflect recent findings. With this revision, GBM are classified based on the mutational state of isocitrate dehydrogenase, *IDH*. The two groups, *IDH*-wildtype, WT, and *IDH*-mutant GBM, closely resemble the previously employed classifications of primary and secondary GBM, respectively. 90 % of all GBM are *IDH*-wildtype GBM occurring de novo while 10 % are *IDH*-mutant GBM developing from diffuse or anaplastic astrocytoma. Both subtypes are classed as WHO grade IV tumours. Median age at diagnosis of the predominant *IDH*-wildtype GBM is 62 years and 44 years for *IDH*-mutant GBM [8].

Reported 5-year survival rate for GBM is 5.4 % [9]. Standard treatment consisting of surgical resection, radiation, and chemotherapy results in a median overall survival of 15 month [8]. This poor prognosis is based on the heterogeneous nature of the tumour, treatment resistances, the observed diffuse as well as rapid growth pattern, as well as a recurrence rate of 90 % [10-12].

Most common aberrations in *IDH*-wildtype GBM are telomerase reverse transcriptase, *TERT*, promoter, tumour protein p53, *TP53*, alpha thalassemia/mental retardation syndrome X-linked, *ATRX*,, and phosphatase and tensin homolog, *PTEN*, mutations as well as epidermal growth factor receptor, EGFR, amplification [8]. Potential genomic alteration in *IDH*-wildtype GBM include copy number alterations, gene mutations, gene overexpression, and promoter methylation but also altered noncoding ribonucleic acids, RNA, have been implicated in GBM tumour biology (Figure 2) [13].

EGFR amplification is present in approx. 36 to 60 % of all *IDH*-wildtype GBM [13]. However, this amplification is very rare in paediatric GBM as well as patients under the age of 35. There are different types of EGFR amplification such as a general gene overexpression of the WT molecule as well as genetic mutations leading to *EGFR* variants. The most frequent of these variants is *EGFR vIII*. This variant results in a constitutive activation of the respective signalling pathway. Both the variant and WT amplification result in increased signalling activity on mitogen-activated protein kinase, MAPK, and phosphoinositide 3-kinase, PI3K, signalling pathways. [13-15]

PTEN mutations are observed in approx. 15 to 40 % of all GBM. This mutation is highly uncommon in *IDH*-mutant GBM and leads to a loss of function of this tumour-suppressor gene. In non-cancerous cells PTEN negatively regulates the PI3K signalling pathway and can induce G1 cell cycle arrest. [13, 14]

Neurofibromin-1, *NF1*, loss of function mutations are present in approx. 20 % of all GBMs. Mutations in NF1 can cause a hereditary cancer predisposition called Neurofibromatosis type 1. The protein encoded by *NF1* is a negative regulator of Ras activity linking it to both the MAPK and PI3K pathways. [3, 13, 16]

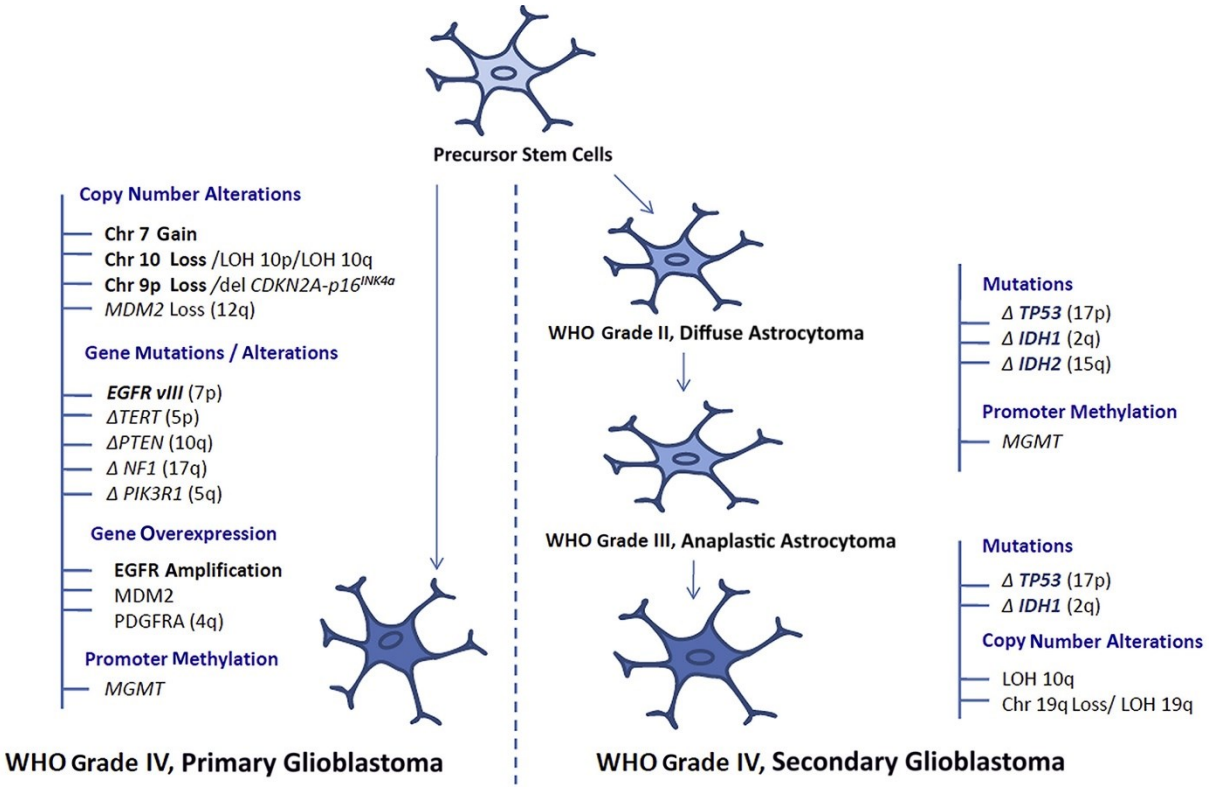

Figure 2 Chromosomal and genetic aberrations involved in the genesis of glioblastoma. [13]

These genetic aberrations lead to changes in protein signalling pathways such as the PI3K/protein kinase B, Akt, signalling pathway resulting in drug resistances, increased migration rates, and inhibition of apoptosis (Figure 3). [12, 17, 18]

Two highly important signalling pathways for GBM development are the MAPK and PI3K pathways. These pathways are linked to cell proliferation, cell cycle progression, and survival as well as migration. Through the described genomic aberrations, the activity of both pathways is increased. Amplification of EGFR protein activity is directly linked to the increased activity of the MAPK and PI3K pathway as they are directly activated through the receptor. In case of the PTEN and NF1 proteins which have a reduced expression due to the loss of function mutation, this activation is indirect as both proteins act as suppressors in a healthy cell. NF1 inhibits Ras and reduces the activation of downstream signalling. PTEN inactivates PI3K leading to a reduction in the activity of the downstream signalling events. [3, 13, 14, 19]

Another important signalling pathway for GBM development is the retinoblastoma, RB, tumour suppressor pathway. It is linked to the PI3K signalling axis via Akt. The pathways themself regulate cell cycle progression through the G_1/S checkpoint. The tumour suppressive effect of the RB pathway is due to the retinoblastoma protein, RB1, which negatively regulates the cell cycle. Increased phosphorylation of this protein via cyclin-dependent kinase 4, CDK4, and cyclin-dependent kinase 6, CDK6, initiates G_1 to S phase transition. Although mutations in the *RB1* gene are only found in approx.

11 % of GBMs, the activity of the pathway itself is deregulated in 78 % of GBMs. For example, this pathway can be deregulated through p21 based inactivation of CDK4 and CDK6 or proliferating cell nuclear antigen, PCNA, based activation of CDK4 and CDK6 resulting in G_1 to S cell cycle progression or arrest, respectively. [13, 20-22]

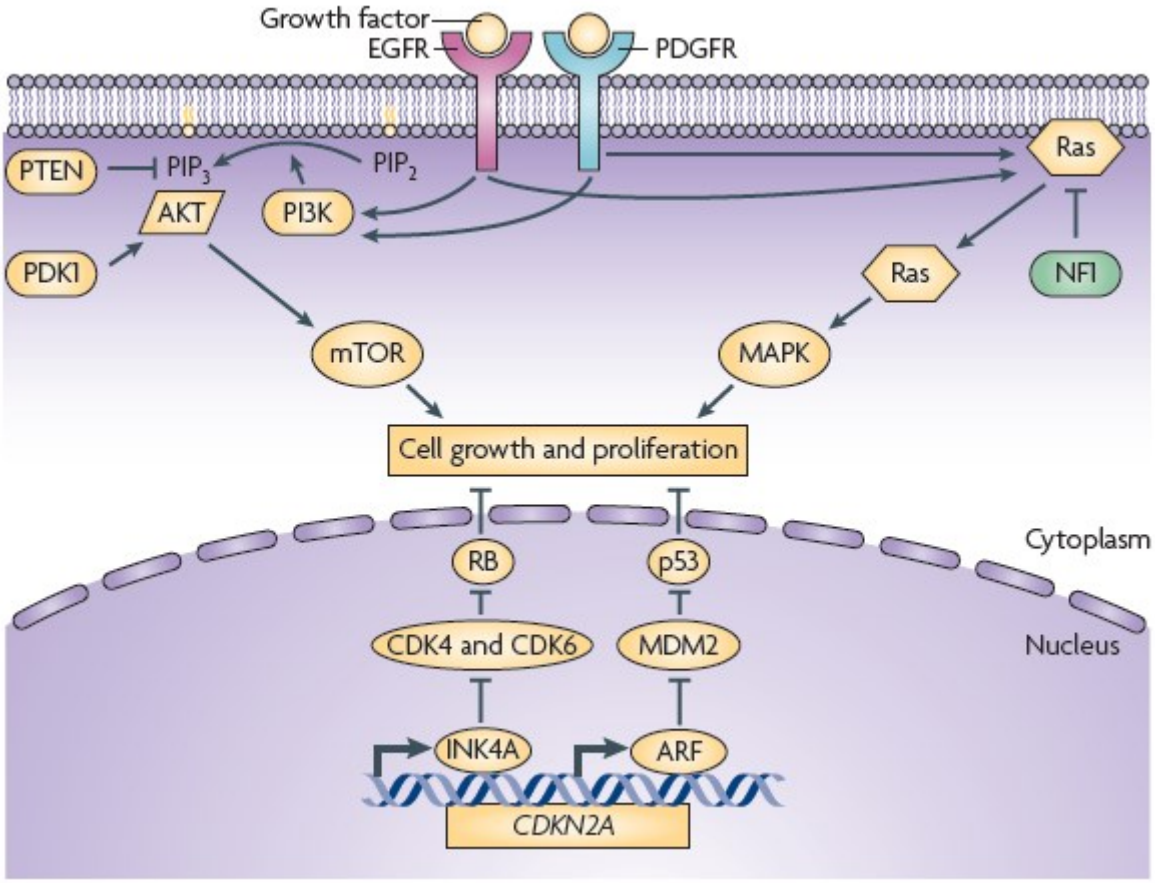

Figure 3 Protein signalling pathways involved in GBM pathogenesis. [3]

Although underlying disturbances in GBM tumour biology have already been described, the low overall survival rate necessitates further studies to increase the knowledge of GBM tumorigenesis.

1.1.2 Medulloblastoma

MB are considered the most frequent malignant tumour in children dependent on the WHO tumour grading. They are classified as grade IV tumours [23, 24]. Although MB are the most frequent brain tumours in children affecting one in five children diagnosed [25], in adults this tumour group accounts for less than 1 % of all brain tumours reported [26]. MB in adults exhibit higher number of recurrent mutations and mutations per tumour compared to numbers observed in paediatric MB [25].

Whilst the 5-year survival rate is at approx. 70%, one-third of patients diagnosed remain incurable. Current treatment strategies employ a synergy of surgical resection, radiotherapy and chemotherapy [27]. In long-term survivors, significant damage related to treatment regiments applied is observed influencing their quality of life. The most prominent treatment related sequelae observed result in an inability to finish school or obtain required work qualifications. [28-31]

Four distinct molecular subgroups were identified. Those four subgroups, wingless-type, Wnt, sonic hedgehog, SHH, Group 3, and Group 4, differ in abundance, age group affected, gender distribution, related histological subgroups, metastatic propensity as well as prognosis [25]. Classification of MB diagnosed results in the subsequent frequency distribution of 10 % cases in WNT-, 30 % cases in SHH subgroup, 25 % cases in Group 3 and 35 % cases in Group 4. In adults however, the subgroup distribution differs from the one observed in paediatric cases. No Group 3 MB are reported in adult cases presenting a tumour distribution by molecular subgroup with 72 % SHH-, 21 % Group 4- and 7 % WNT MB. Prognosis of adults with WNT MB is poorer compared to paediatric cases. Metastatic propensity is highest in group 3 MB and lowest in SHH and Wnt group MB. [32, 33]

Mutations in the *CTNNB1* gene characterise the Wnt subgroup. This subgroup has the most favourable outcome for patients out of the four groups. These activating mutations of *CTNNB1* result in increased Wnt signalling via stabilisation and nuclear translocation of ß-catenin. The SHH subgroup carries inactivating mutations of *PTCH1* and *SUFU* as well as activating mutations of *SMO*. In addition, somatic copy number aberrations of *MYCN* are observed as well. All these result in increased activity of the SHH signalling pathway. Mutations in the PTCH1 gene can cause Gorlin's syndrome or naevoid basal cell carcinoma syndrome which is linked to an increased incidence of SHH MB. Mutations in the regulatory genes for TGF-ß and NF-κB signalling pathways are observed in a subgroup specific manner in Group 3 and Group 4 MB, respectively [34]. Another difference between these two groups are the c-myc gene amplification observed in group 3 MB and the amplification of the MYCN and CDK6 genes observed in group4 MB. [3, 35]

MB development is driven through SHH and Wnt signalling routes (Figure 4). Other pathways involved in a subgroup specific manner are the TGF-ß and NF-κB signalling pathways. Additionally, MAPK and PI3K signalling have been linked to metastatic MB. In contrast to GBM tumour biology the MAPK and PI3K signalling axis do not appear to be the main driver pathways in this brain tumour type. [3, 35, 36]

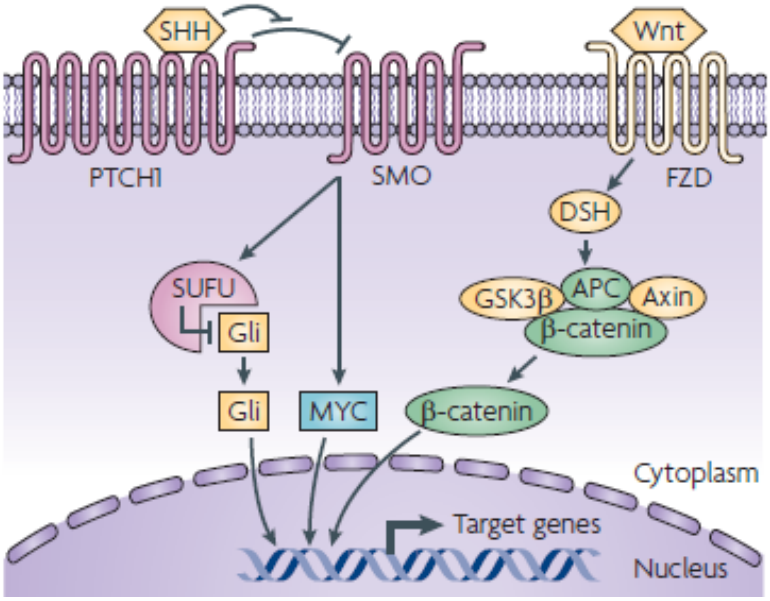

Figure 4 Protein signalling pathways involved in MB pathogenesis. [3]

To decrease treatment related long-term sequelae, subgroup specific targeted treatment strategies are being developed. Intrasubgroup heterogeneity observed via genomic analyses and the paucity of

recurrent oncogenic drivers responsible in two of the subgroups hinder significant advances in the development of targeted therapeutic interventions. This suggests further experimental efforts on a broader molecular scale are necessary to drive the development of accurate targeted therapy strategies in medulloblastoma. [33, 37]

1.2 Long non-coding RNA

Characterisation of tumours as well as disease states in general has mainly focused on genomics, transcriptomics (mostly messenger RNA), and increasingly proteomics up till now. In recent years, the interest in other RNA species such as microRNAs, miRNAs, and non-coding RNAs as well as their interaction partners as potential molecules of interest in tumour biology has increased.

Only a small portion of the human genome is actually transcribed into protein-coding RNA while a far bigger portion is being transcribed into non-coding RNA (Figure 5). Long non-coding RNA, lncRNA, are a subtype of RNAs. Their classification is based on the length of their nucleotide sequence with a minimum cut-off number of 200 nucleotides. Non-coding RNAs shorter than 200 nucleotides are classified as short non-coding RNAs. Two examples of these short non-coding RNAs are miRNAs, and small interfering RNAs, siRNAs. Whereas their function and mechanisms of action are in some cases well understood, the same can't be said about lncRNAs. Necsulea *et al*. showed that lncRNA numbers have grown alongside the evolutionary process reflecting on organisms complexity [38]. So far it is understood that lncRNAs form complex secondary and tertiary structures, can undergo post transcriptional modification, and are found in the cell nucleus as well as the cytoplasm. [39]

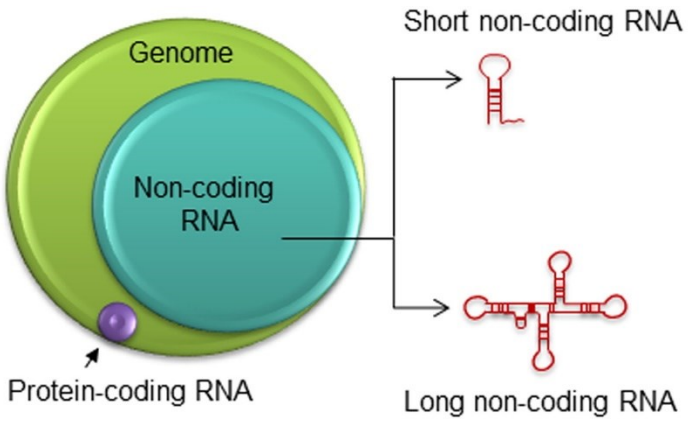

Figure 5 Depiction of protein-coding and non-coding RNA portions in reference to the human genome. [39]

LncRNAs have been shown to alter basic cellular biological processes and contribute to tumorigenesis through interaction with deoxyribonucleic acid, DNA, other RNA, and proteins (Figure 6 A, B, and C, respectively). These interactions result in the regulation of gene expression in most cases. The complex structure of lncRNAs enables various interactions with all those different molecules. For example, lncRNAs can act as miRNA sponges in the cytosol and thereby influence the respective target genes expression or they can interact with chromatin-modifying complexes guiding them to specific target DNA loci affecting their epigenetic modulation. [39-42]

The point of interest for this study is that lncRNAs can interact with proteins and thereby alter their localisation, modulate their activity, as well as act as scaffold or decoy binding partner. The knowledge about these interactions as well as their overall effects on cell biology and thereby their role in

tumorigenesis is still minor and highlights the necessity of further studies. However, some studies highlighting the different interaction effects are already available. [39-42]

The lncRNA HOX antisense intergenic RNA myeloid 1, *HOTAIRM1*, has been reported to interact with the proteins PRC2 and LSD1 to induce gene silencing via histone methylation and to compete with BRCA1 for binding to EZH2 resulting in modulation of the respective protein activity in breast cancer. The binding between *HOTAIRM1* and EZH2 is dependent on the phosphorylation state of the EZH2 protein. [43]

LncRNAs are able to relocate proteins through interacting with them as has been shown for nuclear paraspeckle assembly transcript 1, *NEAT1,* which binds directly to a heterodimer of SFPQ and NONO proteins. This interaction then results in a relocation of said dimer from the promoter region to paraspeckles mediating IL8 expression. [44]

The 1.2 kb yeast telomerase RNA *TLC1* acts as a flexible scaffold for proteins highlighting the potential of lncRNAs to act in a structural and organisational role through its interaction with proteins. [45]

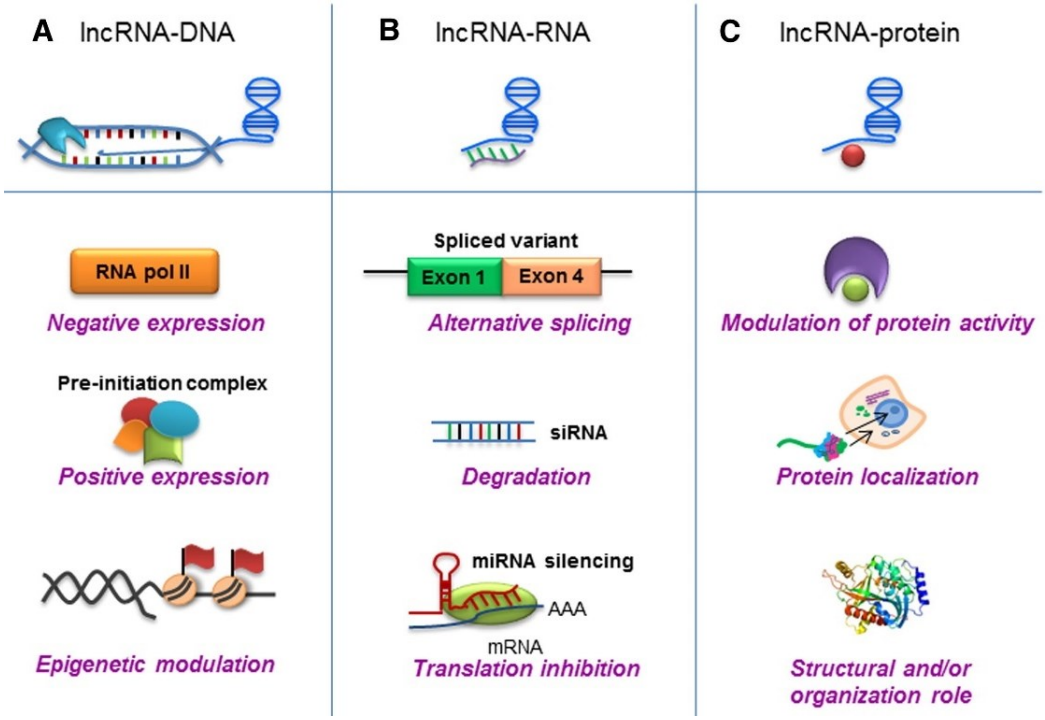

Figure 6 LncRNA interactions with DNA (A), RNA (B), and protein (C) and their respective effects on cell biology. [39]

In recent years, lncRNAs have emerged as potential biomarkers and therapeutic targets based on their tissue-specific expression levels as well as their ability to interfere with key signalling pathways in various diseases such as neuronal disorders, diabetes, cancer, and cardiovascular disease. It has been shown that lncRNAs can act as tumour suppressors as well as oncogenic drivers in brain tumours. [3, 46-48]

For example, they have been reported to contribute to disease progression via activating immune responses in cancer cells [49]. An example for a protective effect of lncRNAs has been reported by Flynn *et al.*. In their paper they described the interaction between the lncRNA *TERRA*, and the two proteins hnRNPA1 and POT1 promoting telomere capping to preserve genomic integrity [50].

Understanding of disease specific biology in brain tumours such as glioblastoma and medulloblastoma could be increased through investigations into lncRNA molecular interactions and their disease specific function.

1.2.1 Metastasis associated lung adenocarcinoma transcript 1

Metastasis associated lung adenocarcinoma transcript 1, *MALAT1*, is a well characterised, 8.5 kb lncRNA implicated in various diseases [51, 52]. Although *MALAT1* itself, has no protein coding potential, it can influence protein expression levels via DNA, RNA, and protein interaction. *MALAT1* is a highly conserved and highly expressed lncRNA linked to increased tumorigenesis in various tumour types such as non-small cell lung cancer, breast cancer and osteosarcoma [53-55]. In Glioblastoma, previous study results range from *MALAT1* as a marker for poor prognosis [56] and oncogene [57, 58] to *MALAT1* acting as a tumour suppressor [59].

MALAT1 has been shown to interact with several proteins such as serine/arginine-rich splicing factors, SRSF, 1, 3, and 6 as well as SET domain containing 2, SETD2, and human antigen R, HuR, in Hela and HEK293 cells [60, 61].

Reportedly this lncRNA is involved in a plethora of different signalling pathways (Figure 7) like for example MAPK [62], PI3K [63], Wnt [64], and NF-κB [65]. All these pathways are implicated in either GBM or MB. MALAT1 interference in signalling pathways in cancer modifies proliferation, migration, invasion, cell cycle progression, cell death, angiogenesis, and tumorigenicity. [66]

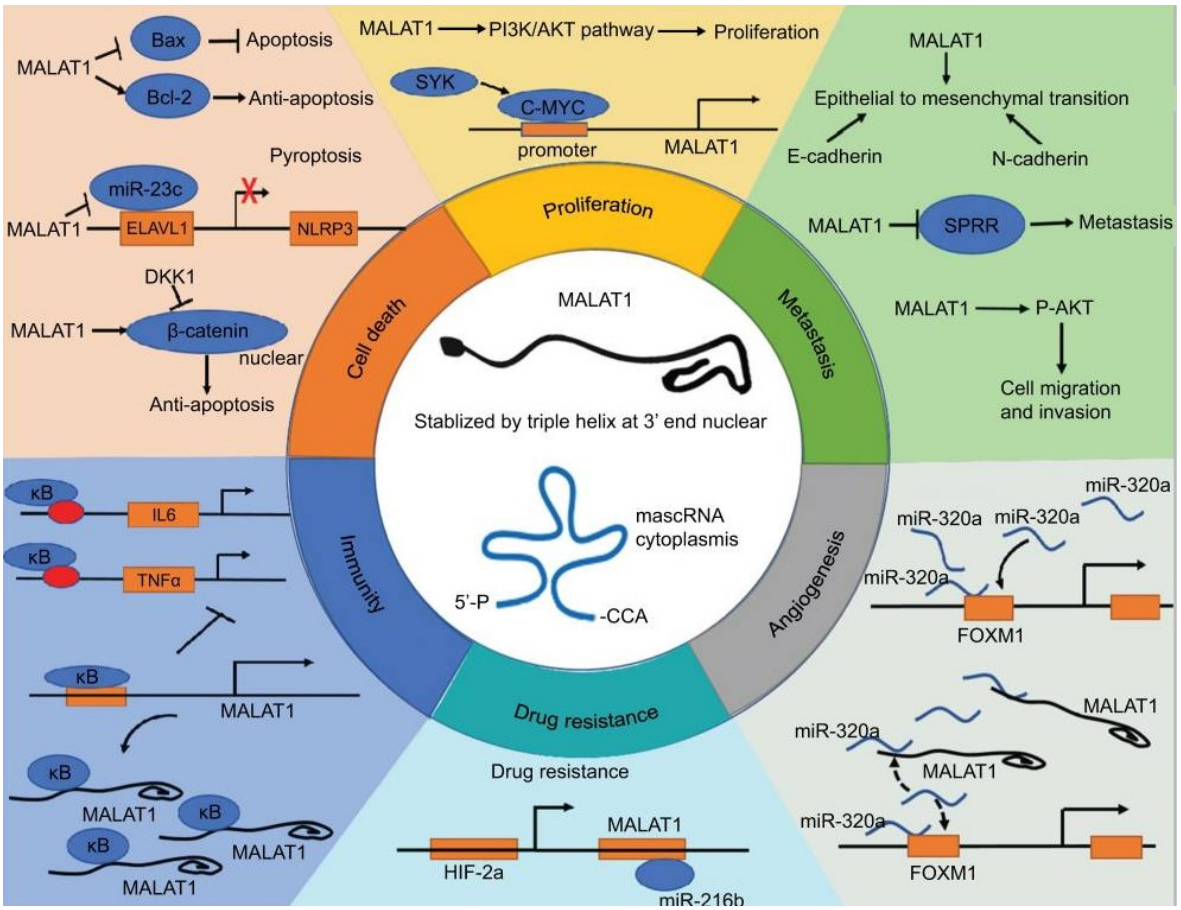

Figure 7 Cancer related signalling pathways affected by *MALAT1*. [66]

The spread of tumour cells to different parts of the body called metastasis reduces overall survival chances and hinders effective treatment. The process is primarily dependent on epithelial-to-mesenchymal transition, EMT, of cancer cells. *MALAT1* has been shown to be a driver of EMT in ovarian cancer via PI3K/Akt signalling [67]. Tumour growth is driven by cell proliferation which can be affected by several different pathway. *MALAT1* has been reported to drive cell proliferation as well as metastasis in osteosarcoma through increased activation of PI3K/Akt signalling [63].In a neuroblastoma-derived cell line, *MALAT1* has been shown to activate MAPK signalling resulting in neurite outgrowth [62]. A potential way for *MALAT1* to reduce MAPK signalling indirectly is through inhibiting miRNA-124 as has been shown in retinoblastoma by Liu *et al.* [68]. Another hindrance in the treatment of various cancers is drug resistance. A well-documented case of drug resistance in brain tumours is the resistance of GBM to TMZ. This resistance has been reversed through *MALAT1* knockdown, KD, in a GBM-derived cell line with the KD leading to an increase in miRNA-101 [69]. Regulation of alternative splicing in epithelial cell lines (HeLa, U2OS, and EpH4) through interaction with several SRSF proteins is another well-described function of MALAT1 [53]. [66]

1.3 Proteomics

Although the genomic information highlights signalling pathways of interest in GBM development additional information on the protein level is necessary to further the understanding of this highly malignant and heterogeneous brain tumour. This missing knowledge is still a big hurdle on the way to better treatment strategies and classification for GBM patients. Mass spectrometry based proteomic studies offer a strategy to directly analyse protein expression levels and could therefore increase the understanding of GBM biology. [12]

The proteome of a given species is dynamically changing dependent of a multitude of factors like pH value, temperature or life cycle phase. Therefore, performed proteomic analyses yield the actual protein composition at a given time under given conditions. Those results are subject to sample preparation steps performed, as the momentary protein composition is influenced by experimental conditions applied. Not once in the life cycle of a cell is its complete proteome, consisting of all proteins the cell is able to generate, present. In addition, transcriptomic predictions of protein expression patterns based on the genomic and transcriptomic information are unable to yield reliable results as post-translational modifications like phosphorylation, glycosylation or sulphation, as well as post-translational degradation processes are not inscribed. In summary, this highlights the necessity of a higher number of analytical experiments to obtain complete proteomic information on a species to further complete the genomic information. [70]

Historically two-dimensional gel electrophoresis has been employed to analyse protein expression levels in complex mixtures. Robustness of this approach was increased through 2D difference gel electrophoresis, DIGE, enabling direct comparison of two samples relative to a standard on one gel [71]. However, to identify individual proteins, spots had to be excised, digested, and analysed with for example mass spectrometers. Mass spectrometry, MS, is an analytical method applied to determine the exact mass of ions from an analyte compound. High-resolution instruments are able to perform measurements with high mass resolution as well as high mass accuracy enabling qualitative analysis via databases. The coupling of high-performance liquid chromatography, LC, with mass spectrometry results in a third analysis dimension, allowing for analysis of highly complex samples such as protein digests of whole cell lysates. [72-74]

Proteomic analysis via MS can be achieved through various strategies dependent on the research question. Currently, there are three main analysis strategies defined by the size of protein fragments to be analysed, bottom-up, middle-down, and top-down proteomics (Figure 8). Bottom-up proteomics focusses on small peptides of approx. 8 to 30 amino acids obtained by proteolysis. Respective peptide mixtures are separated via LC and identified via database searches of MS/MS fragments. Middle-down proteomics employs the same principle as bottom-up proteomics but focusses on peptide bigger than 30 amino acids. This strategy is often applied to analyse histone post translational modification, PTM, to retain information about co-existing PTMs on the same protein [75]. Top-down proteomics is the analysis of intact proteins to discern different proteoforms via MS after separation though for example LC [76]. The complexity of data analysis for the three approaches increases from bottom-up to top-down proteomics. [77]

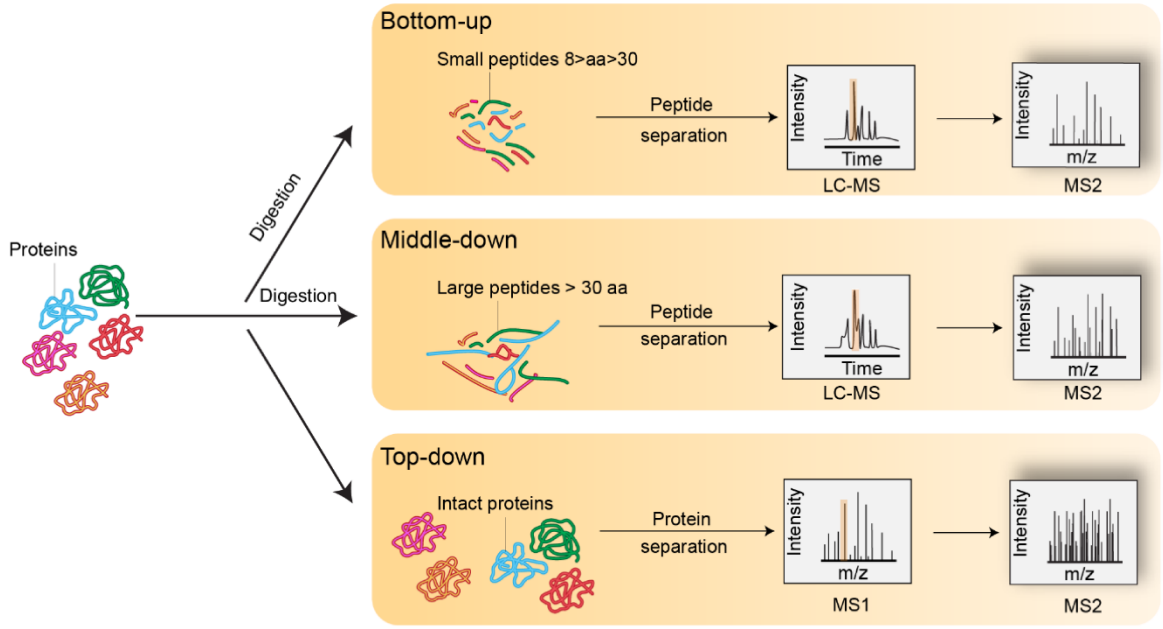

Figure 8 Common MS based analysis strategies in proteomics. [77]

Quantitative MS yields relative quantification results. Quantification via mass spectrometry requires high reproducibility in sample work-up and subsequent measurement. Through addition of internal standards absolute quantification can be performed whereas relative quantification is achievable for identical proteins in similar samples on basis of their respective peptides. [70]

Label-free and stable isotope labelling are two different main techniques applied in quantitative mass spectrometry. Stable isotope labelling can be achieved through metabolic approaches or chemical derivatisation and are therefore not applicable for all samples. Label-free approaches are more versatile but require higher measurement numbers as well as a higher dependence on work-up reproducibility. [73, 78-80]

To increase the accuracy of MS based proteomics approaches isotopic labelling can be employed during sample preparation (Figure 9). This strategy however is not applicable to all samples such as human derived sample tissues. Those samples can be chemically labelled at the protein or peptide label to increase measurement accuracy. Labelling at protein level is more accurate than labelling at peptide level. Another possibility is to spike a subset of labelled peptides for specific protein

quantification into a digested mixture. Alternatively, a whole labelled cell lysate can be spike into samples unlabelled samples to increase the overall measurement accuracy [81]. Although these approaches increase quantification accuracies, the linear dynamic range as well as the quantitative proteome coverage are reduced. In addition, labelling can only be applied to a set number of samples or sample states whereas label-free proteomics does have no restrictions in that regard. [82]

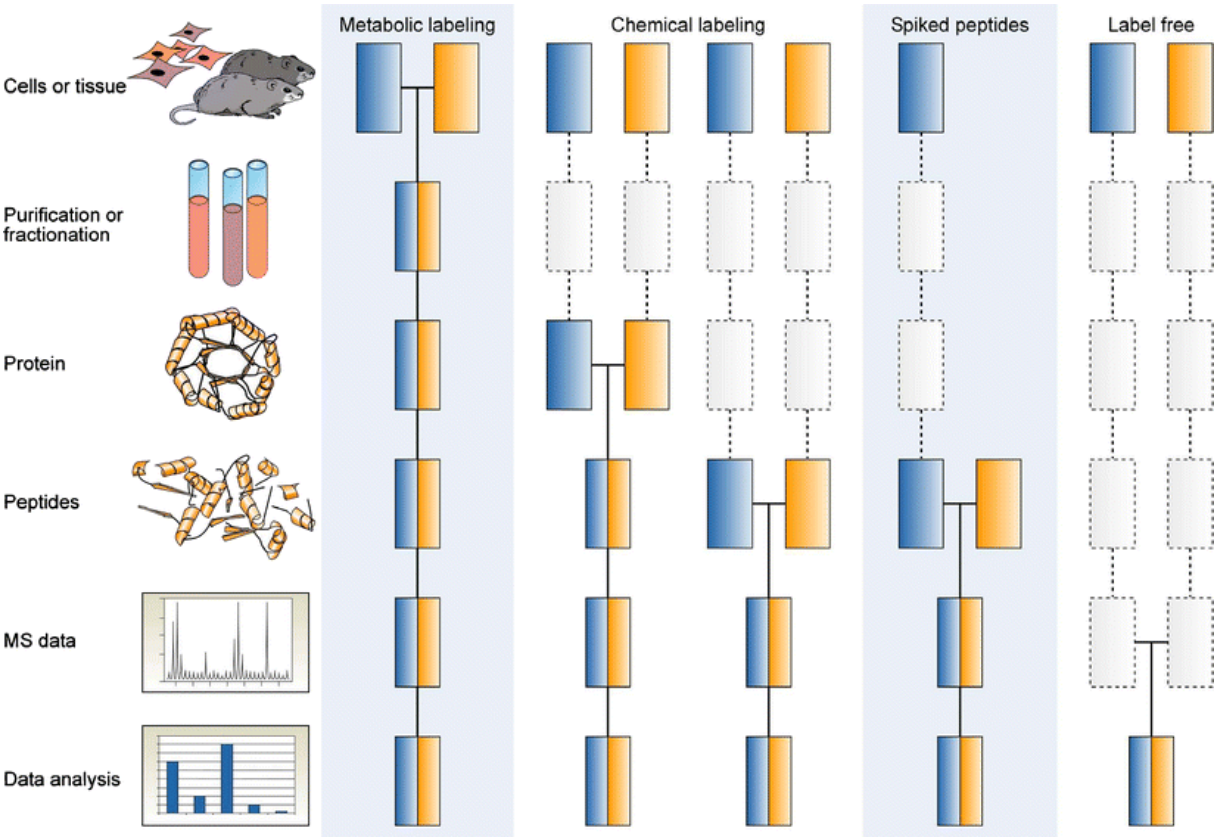

Figure 9 Common MS based quantitation strategies in proteomics. [82]

To this day, analysing the whole proteome of a sample in one biological state via proteomics remains challenging. In part this is due to the sheer number of different proteoforms as well as the high range of different protein expression levels. In addition, the number of quantifiable proteins per sample set is always lower compared to the number of identifiable proteins in the same sample set. Throughout the last years the percentage of identifiable and quantifiable proteins per sample set has been increasing due to several facture such as better MS instrumentation, automation of sample preparation, as well as progress in available data analysis strategies.

A label-free bottom-up approach as depicted in Figure 10 was chosen for this study. Samples for proteome analysis were obtained either directly through cell lysis of isogenic cell lines or through pre-treated cell lysates enriched for RNA-binding proteins. These complex protein mixtures were desalted via sodium dodecylsulphate polyacrylamide gel electrophoresis, SDS-PAGE, previous to reduction, alkylation and trypsin digestion in gel. Peptides thus obtained were eluted from the gel with sonication in a mixture of acetonitrile and water while trypsin is retained in the gel. These peptide mixtures were analysed on a nano LC-nano electrospray, ESI, MS system. The data obtained was analysed under application of Mascot and MSAmanda search algorithms embedded in a Proteome Discoverer

workflow for peptide and subsequent protein identification while quantification was achieved through relative intensity comparison in Progenesis QI for proteomics.

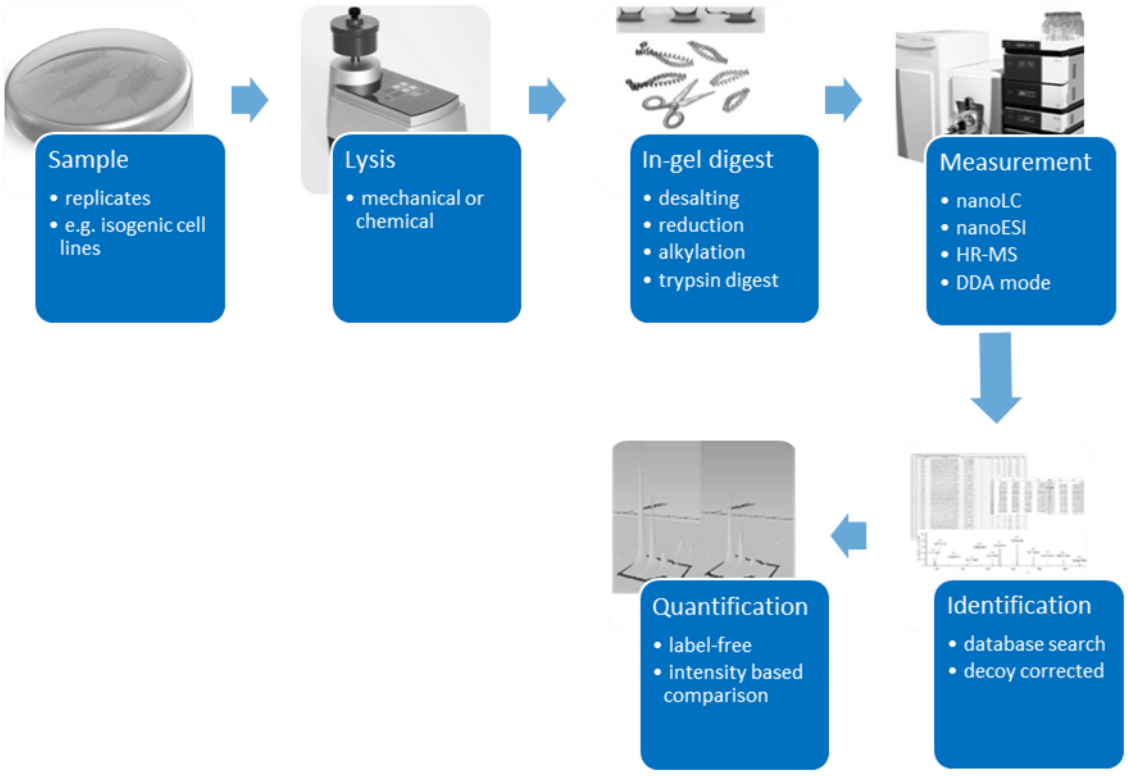

Figure 10: Schematic label-free bottom-up proteomics workflow.

In recent years, proteomics and phoshoproteomics studies are successfully employed to increase the knowledge of cancer biology. For example, Mertins *et al.* analysed 105 breast cancer samples with previous genomics data through quantitative protein and phosphoprotein characterisation via MS and were thereby able to connect observed somatic mutations to signalling events in breast cancer [83]. And Forget *et al.* added protein and phosphoprotein data to a set of MB samples with prior genomics data to further delineate group 3 and group 4 MB and highlight hallmark signalling pathways [84].

An example for a study focussing on the direct effect of a single molecule on proteomic signations in a given disease is the study from Ahmadov *et al.* where proteomics is employed to increase the understanding of *HOTAIRM1* a lncRNA in GBM tumour aggressiveness and radiotherapy resistance. A label-free bottom-up approach is employed to analyse *HOTAIRM1* KD as well as control cells identifying a link between *HOTAIRM1* and the protein transglutamise 2 expression levels in a GBM model cell line. [85]

These studies highlight the applicability of MS based proteomics approaches to increase the understanding of cell biology.

1.3.1 Interactomics

Molecular functions can be altered based on protein interaction partners resulting in an increase of functional diversity (Figure 11). This diversity offers the opportunity to investigate interactions between different molecules leading to the discovery of their functional relationship. The overall term employed to describe these studies is interactomics.

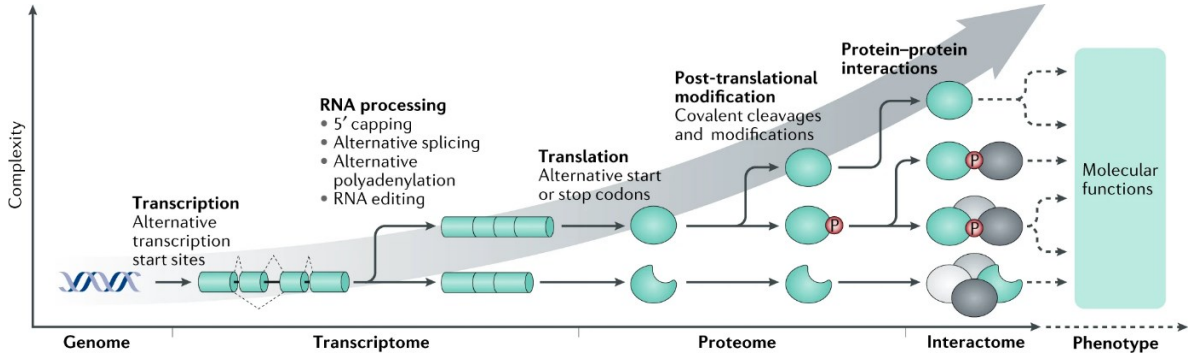

Figure 11 Functional diversity at various molecular instances. [86]

Interactomes can be analysed applying various strategies with several different readout setups such as fluorescence energy transfer [87], MS, or yeast phenotype analysis [88]. Most studies rely upon a standard bottom-up approach for the MS based measurements while the sample preparation beforehand is dependent on the type of interaction to be investigated (Figure 12). Affinity purification and co-fractionation methods can be employed for investigation of stable interactions while proximity labelling methods are employed in the study of transient interactions. As an approach to study short-term interactions, cross-linking methods can be applied. [86]

	Affinity purification coupled to mass spectrometry	Proximity labelling (BioID, APEX)	Cross-linking coupled to mass spectrometry	Co-fractionation coupled to mass spectrometry
Screening approach				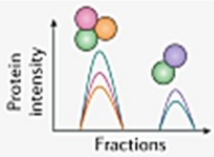
Measurement	MS/MS	MS/MS	MS/MS	MS/MS
Requirements	Genetic tagging or available antibody	Genetic tagging with enzyme	None	None
Type of interactions	Binary PPIs and complexes (only via reciprocal pull-downs)	Proximal proteins	Binary PPIs, complexes and structural information	Binary PPIs and complexes
	Very stable interactions	Transient interactions (down to ~1 min labelling speed)	Short-term interactions (~1 h cross-linking time)	Very stable interactions
Information from single experiment				
Proteome coverage	Proteome coverage depends on selected bait proteins	Proteome coverage depends on selected bait proteins	Good proteome coverage in a single assay	Good proteome coverage in a single assay

Figure 12 Overview of proteome-wide interactome investigation strategies. modified from [86]

Affinity purification strategies can be employed to investigate lncRNA-protein interactions. Different approaches can be split into two groups either protein- or RNA-centric based on the molecule of interest (Figure 13). Protein-centric approaches focus on the different RNAs able to interact with a specific protein while RNA-centric approaches focus on the different proteins able to interact with a specific RNA. Potential candidates emerging through application of the protein-centric approach can be validated with the RNA-centric approach and vice versa. Cross-linking can be employed to freeze weak and transient interactions and enable harsher treatment options in the sample workup. RNA immunoprecipitation, RIP, as well as cross-linking and immunoprecipitation, CLIP, are two different protein-centric strategies with a quantitative polymerase chain reaction, qPCR, or an RNA-sequencing based readout. Both employ antibodies to enrich the respective protein of interest as well as the interacting RNAs from complex mixtures. Capture hybridisation analysis of RNA targets, CHART, chromatin isolation by RNA purification, ChIRP, RNA affinity purification, RAP, and peptide nucleic acid, PNA, assisted identification of RNA binding proteins, RBP, PAIR, are RNA-centric pulldown approaches employing oligonucleotide probes to analyse interacting proteins. The PAIR approach utilises PNA analogue oligonucleotides as well as respective antisense PNA oligo pairs to enrich for RBPs and can be employed *in-vivo* while the others utilise biotinylated oligonucleotide probes to pulldown the respective RNA *in-vitro*. CHART, ChIRP, and RAP approaches differ in the length and number of employed probes as well as the employed cross-linking strategies. The MS2-TAG strategy adds an MS2 stem-loop cluster to the RNA of interest which is recognised by a bacteriophage protein initiating an in-vivo biotinylation of the RNA. Reliant on the biotin tag the RNA can be enriched via streptavidin beads from a cell lysate to study the protein interactors. Once the respective interacting proteins have been enriched, they can be analysed employing a bottom-up proteomics approach with MS readout. All of these approaches are applicable to investigate lncRNA-protein interactions. [89]

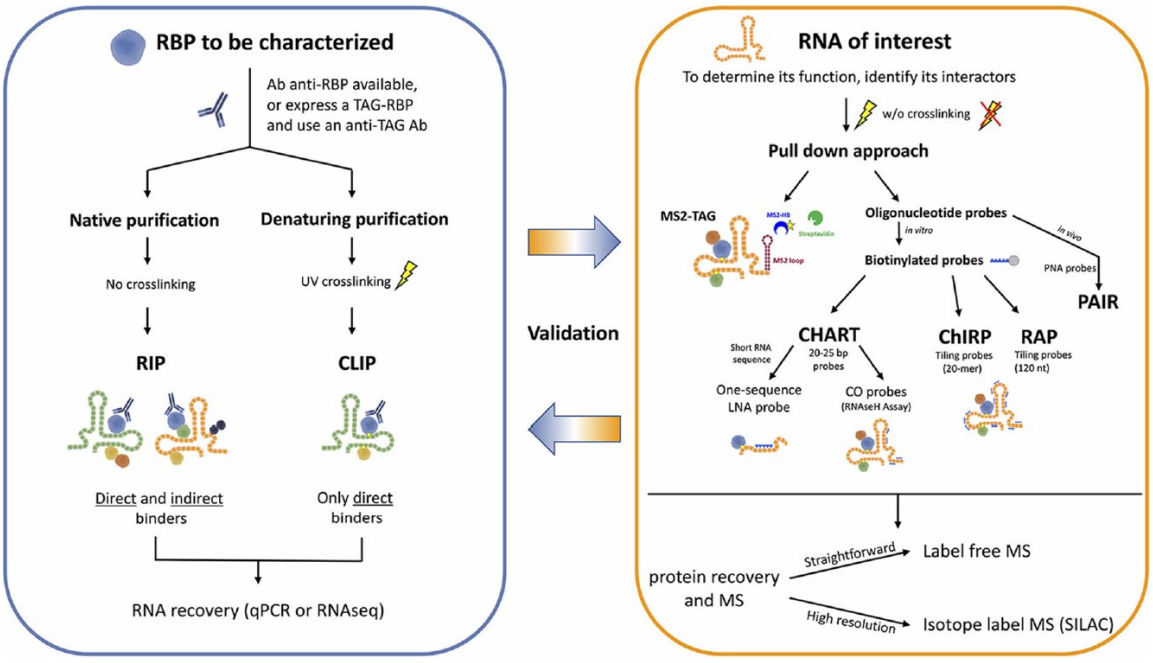

Figure 13 Overview of different strategies to investigate lncRNA-protein interactions. In the blue box protein-centric approaches are depicted while RNA-centric approaches are depicted in the orange box. **[89]**

While the knowledge of lncRNA-protein interactions is still limited the number of available tools being developed highlight the importance of these interactions in biological processes. In recent years, more

studies are focussing on these interactions to understand biological pathways in disease as well as in general.

For example, Smola *et al.* employed RNA-centric interactomics to study the function of *Xist*, a lncRNA essential for X-chromosome inactivation during female development to increase the knowledge of the underlying biological processes. [90]

In another study, Bartl et al. analyse protein interactors of the lncRNA *hedgehog interacting protein-antisense 1, HHIP-AS1*, in SHH MB. They show that HHIP-AS1 interacts with the protein dynein complex 1 and promotes tumorgenicity. [91]

These studies show that interactions between lncRNAs and proteins can affect biological pathways as well as the necessity to increase our knowledge about these interactions to better understand aberrant processes in disease.

2 Objectives

Even with advances in cancer research, therapeutic improvements, and personalised treatment strategies, GBM 5-year survival rates remain at approx. 5 % with a 90% recurrence rate. This poor prognosis highlights the need for a better understanding of the underlying biology.

Novel approaches and perspectives are necessary to advance the current disease knowledge. This in term will allow the development of novel treatment strategies or repurposing of drugs employed in other cancers and illnesses.

More and more evidence suggests, lncRNAs previously thought to have no function can be potential druggable targets as well as biomarkers. Investigation of their influence on protein signatures will increase the understanding of known biological pathways.

This thesis aims to investigate the influence of a specific lncRNA, namely *MALAT1*, on proteomic signatures in GBM cell lines to further the knowledge of this highly aggressive and common brain tumour species. The work will largely focus on potential proteinaceous *MALAT1* binding partners as well as protein expression level changes in relation to *MALAT1* expression levels.

- *MALAT1*-centric affinity enrichment will be performed to investigate proteinaceous interactors in established MB and GBM cell lines.
- Isogenic *MALAT1* KD as well as respective control cell lines will be generated to study phenotype changes based on the expression level of *MALAT1*.
- The influence of *MALAT1* on protein expression levels in the isogenic cell line pairs will be analysed via a bottom-up proteomics approach with a MS readout.
- A high-throughput drug screen in the isogenic cell lines generated will be performed to identify potential drug candidates affecting signalling pathways linked to *MALAT1*. Orthogonal validation methods will be employed to corroborate the results from the high-throughput drug screen.
- The combined data collected in this study will be applied to identify proteins, biological pathways, and phenotypical behaviour linked to *MALAT1* expression changes.

This study aims to increase the knowledge of *MALAT1*s' influence in GBM biology and reveal potential linkages to signalling pathways implicated in GBM tumorigenesis. Mass spectrometry based proteomics will be employed to gain a deeper understanding of MALATs' effect on protein signatures in GBM cell lines.

3 Materials and Methods

3.1 Materials

3.1.1 Instruments

All instruments applied in the methods detailed in section 3.2 are listed in Table 1.

Table 1 Specifications of utilised instruments.

Instrument type	Name	Firmware version	Supplier
Cell counter	Vi-CELL XR 2.03	-	Beckman Coulter
Centrifuge 1	Mikro 220R	-	Hettich
Centrifuge 2	5430 R	-	Eppendorf
Centrifuge 3	Rotina 46 R	-	Hettich
Electrophoresis chamber TGX	Mini-PROTEAN Tetra	-	Bio-Rad
Electrophoresis power supply	PowerPac™ Basic	-	Bio-Rad
Flow cytometer	CytoFlex	-	Beckman Coulter
Heated shaker	MKR 13	-	Heidolph
Horizontal shaker	Unimax 1010	-	Heidolph
imager	ChemiDoc MP	2.3.0.07	Bio-Rad
incubator	Heracell 240i	-	Thermo Fischer Scientific
Live cell imager	IncuCyte	2018B	Essen BioScience Inc.
Mass spectrometer	QExactive plus	-	Thermo Fischer Scientific
MaxWell	MaxWell RSC system	v4.17	Promega
Nano spectrometer	NanoDROP 2000	-	Thermo Fischer Scientific
nanoLC	RSLCnano U3000	-	Thermo Fischer Scientific
Precision scale	PCB	-	Kern
RT qPCR system	CFX384 Touch™	-	Bio-Rad
Scale	Entris	-	Sartorius
Semi-dry blotter	Trans-Blot Turbo	-	Bio-Rad
Spectrometer	DTX 880	-	Beckman Coulter
Sterile hood	Safe 2020	-	Thermo Fischer Scientific
Tissue lyser	TissueLyser LT	-	Qiagen
ultrasonicator	M220	-	Covaris
Vacuum concentrator	5301	-	Eppendorf
Xcelligence	Xcelligence 3x16	2.0.0.1301	ACEA Biosciences Inc.

3.1.2 Chemicals, Buffers and Solutions

All chemicals applied in the preparation of solutions, standards and buffers in Table 2 as well as in the methods in section 3.2, including buffer, solution and standard recipes, are listed in Table 2.

Table 2 Specifications of utilised commercial chemicals, buffers and solutions.

Name	Supplier	Catalogue number
20x Saline-sodium citrate ,SSC, buffer	Thermo Fischer Scientific	15557044
4 -12 % Bis-Tris polyacrylamide gel	Thermo Fischer Scientific	NP0321
4–15% Mini-PROTEAN® TGX™ Precast Protein Gels	Bio-Rad	4561084
acetonitrile	Fluka	14261
Aminocaproic acid	Sigma-Aldrich	A2504
ammonium bicarbonate	Sigma-Aldrich	S8875
Ammonium chloride	Merck	213330
Bovine serum albumin	Sigma-Aldrich	A2153
Bromophenol blue	Carl Roth	A512.1
CellTiter-Glo®	Promega	G7572
CHAPS	Sigma-Aldrich	C5070
Clarity Max Western ECL Substrate	Bio-Rad	1705062
dithiothreitol	Serva	20711.03
dNTP Mix	Promega	U1511
Dulbecco´s Modified Eagle´s Medium, DMEM	Thermo Fischer Scientific	31966021
Dulbecco´s Phosphate Buffered Saline, PBS	Thermo Fischer Scientific	14190250
Dynabeads™ MyOne™ Streptavidin T1	Thermo Fischer Scientific	65601
ECL Prime blocking reagent	cytiva	RPN418
Ethylene dinitrolo tetra acetic acid, EDTA	Merck	1.08421
Fetal bovine serum, FBS	Sigma-Aldrich	F9665
Formaldehyde	Sigma-Aldrich	F8775
formamide	Thermo Fischer Scientific	AM9342
Formic acid	Thermo Fischer Scientific	10596814
glycerin	Sigma-Aldrich	G7126
glycine	Sigma-Aldrich	G7126
Immobilon®-FL	Merck	ISEQ00010
iodoacetamide	Sigma-Aldrich	I6125
MALAT1-specific raPool	siTOOLs Biotech	-
Maxwell® RSC simplyRNA Tissue Kit	Promega	AS1340
M-MLV RT 5x buffer	Promega	M3681

Continuation of **Table 2 Specifications of utilised commercial chemicals, buffers and solutions.**

Name	Supplier	Catalogue number
M-MLV RT, Rnase (H-)	Promega	M368C
MOPS	Sigma-Aldrich	M1254
NE-PER™ Nuclear and Cytoplasmic Extraction Reagents	Thermo Fischer Scientific	78833
Nonident P-40 substitute	Sigma-Aldrich	74385
non-RNA binding raPool	siTOOLs Biotech	-
oligodT primer mix	Promega	C110A
Page ruler	Thermo Fischer Scientific	26616
Pierce 660nm	Thermo Fischer Scientific	22660
polybrene	Merck	TR-1003-G
Polyethylenimine	Merck	408727
potassium ferrocyanide	Merck	104973
Precision Blue Real-Time PCR dye	Bio-Rad	1725555
protease inhibitor	Roche	5892791001
Proteinase K	Promega	V3021
puromycin	InvivoGen	ant-pr-5
qPCR GoTaq 2x MasterMix	Promega	A6110
Random primer	Promega	C118A
ReliaPrep™ RNA Miniprep System	Promega	Z6012
Rnasin Plus Ribonuclease inhibitor	Promega	N2615
Sodium chloride	Sigma-Aldrich	S3014
sodium deoxycholate	Sigma-Aldrich	30970
Sodium dodecyl sulfate (SDS)	Sigma-Aldrich	L4509
sodium thiosulfate	Fluka	72051
Thiourea	Sigma-Aldrich	T7875
tricine	Sigma-Aldrich	T0377
trifluoroacetic acid	Fluka	40967
Tris	Sigma-Aldrich	T1503
Trypan Blue solution	Thermo Fischer Scientific	15250061
trypsin	Serva	37284.01
Tween 20	Sigma-Aldrich	P5927
Urea	Bio-Rad	161-0730

All non-commercial solutions, standards and buffers applied in the methods under 3.2. are listed with their respective preparation in Table 3.

Table 3 Listing of non-commercial solutions, standards and buffers applied with their respective preparation.

Name	Preparation
10x SDS buffer	250 mM Tris 1.92 M Glycine 35 mM SDS
10x TBS buffer	100 mM Tris 1.5 M NaCl pH 8.0
1x SDS sample buffer	7.5 % Glycerin (v/v) 4 % SDS (w/v) 37.5 mM Tris-Cl pH 7.0 bromophenol blue
20x MOPS buffer	1 M MOPS 1 M Tris Base 30 % SDS 20 mM EDTA pH 7.7 not adjusted
4x loading buffer	600 mM DTT 30 % Glycerin 12 % SDS 150 mM Tris pH 7.0. bromophenol blue
5x Hybridisation buffer	3.75 M NaCl 0.25 M Tris-Cl 10 mM EDTA pH 7.0
Anode blotting buffer	300 mM Tris 100 mM Tricine pH 8.7-8.8 not adjusted
Cathode blotting buffer	300 mM aminocaproic acid 30 mM Tris pH 8.6-8.7 not adjusted
Lysis buffer 1	50 mM NH4Cl 80 mM Tris protease inhibitor (add fresh before use) pH 8.0

Continuation of **Table 3 Listing of non-commercial solutions, standards and buffers applied with their respective preparation.**

Name	Preparation
Lysis buffer 2	20 mM NaCl 1 % sodium deoxycholate (w/v) 1 % NP-40 (v/v) 20 mM Tris pH 8.0
Pulldown wash buffer	2x SSC buffer 0.5 % SDS (w/v)
Proteinase K buffer	10 % SDS (w/v) 50 mM EDTA 10 mM Tris-Cl pH 7.4
Solvent A	0.1% (v/v) formic acid in water
Solvent B	0.1% (v/v) formic acid, 84% (v/v) acetonitrile in water
TBST buffer	1x TBS buffer 0.1 % Tween 20
TE buffer	10 mM Tris-Cl 1 mM EDTA pH ~ 7.5 not adjusted
Urea buffer	30 mM Tris Base 7 M Urea 2 M Thiourea 4 % CHAPS (w/v) adjust to pH 8.0 with HCl

3.1.3 Software

Every software applied in the detailed methods in section 3.2 is listed in Table 4.

Table 4 Specifications of utilised software.

Name	Version	Supplier
CFX manager 3.1	3.1.1517.0823	Bio-Rad
CytExpert 2.2	2.2.0.97	Beckman Coulter, Inc.
Image Lab	6.0.0 build 25	Bio-Rad
IncuCyte	2018B	Essen BioScience Inc.
Maxwell® RSC Application Software	v3.0.3	Promega
Progenesis QIP	2	Nonlinear Dynamics
Proteome Discoverer 2.3	2.3.0.523	Thermo Fischer Scientific
RTCA	1.0.0.1304	ACEA Biosciences Inc.
SoftMax Pro	06.05.2001	Molecular Devices
Xcalibur 2.2	SP1.48	Thermo Fischer Scientific

3.1.4 Antibodies

All antibodies applied in the methods in section 3.2 are listed in Table 5.

Table 5 Specifications of utilised antibodies.

Target protein	Specificity	Host	Molecular weight	Dilution	Supplier	Catalogue number
Anti-mouse IgG HRP	M	horse	-	1:5000	Cell Signalling	7076
Anti-rabbit IgG HRP	R	goat	-	1:5000	Cell Signalling	7074
AKT	H, M, R, Mk	rabbit	60 kDa	1:1000	Cell Signalling	4691P
EFEMP1	H	rabbit	56 kDa	1:50	Cell Signalling	HPA070841
Erk1/2	H, M, R, Mk	mouse	44, 42 kDa	1:2000	Cell Signalling	4696S
MEK1/2	H, M, R, Mk	rabbit	45 kDa	1:1000	Cell Signalling	8727T
pAKT S473	H, M, R, Mk	rabbit	60 kDa	1:2000	Cell Signalling	4060P
pAKT T308	H, M, R, Mk	rabbit	60 kDa	1:1000	Cell Signalling	2965P
pErk1/2	H, M, R, Mk	rabbit	44, 42 kDa	1:2000	Cell Signalling	4370S
pMEK1/2	H, M, R, Mk	rabbit	45 kDa	1:1000	Cell Signalling	9154T
Profilin-1	H, M, R, B	rabbit	15 kDa	1:500	Cell Signalling	3237
SRSF1	H, M, R, Mk	rabbit	33 kDa	1:500	Cell Signalling	14908
ß-Actin	H, M, R, Rb	mouse	42 kDa	1:2000	abcam	ab8226
TRIM28	H	mouse	100 kDa	1:1000	R&D biotech	MAB7785
ZNF10	H	rabbit	66 kDa	1:1000	novus bio	NBP2-59679

3.1.5 Vectors and guide RNA

All vectors, plasmids, and gRNAs applied in the methods in section 3.2 are listed in Table 6 and Table 7, respectively. All vectors were bought from Addgene, Massachusettes United States of America.

Table 6 Specifications of utilised vectors and plasmids.

Name	Category	Catalogue number	Reference
pMD2.G	envelope plasmid	12259	-
pMDL/pRRE	packaging plasmid	12251	[92]
pRSV-Rev	packaging plasmid	12253	[92]
pLV hU6-sgRNA-KRAB	sgRNA and dCas9 expression plasmid	71236	[93]

All gRNA sequences were bought from Integrated DNA Technologies, Iowa United States of America.

Table 7 Specifications of utilised gRNAs.

Name	Sequence	Direction
MALAT1.1	caccgAAAATGGCGCTGCGCTTAAG	forward
	aaacCTTAAGCGCAGCGCCATTTTc	reverse
MALAT1.2	caccGACAAAGCCATTCGCTTAGT	forward
	aaacACTAAGCGAATGGCTTTGTC	reverse
MALAT1.3	caccgAAAATTTCCGTGCGGGCCGT	forward
	aaacACGGCCCGCACGGAAATTTTc	reverse
Control	caccGTTCCGCGTTACATAACTTA	forward
	aaacTAAGTTATGTAACGCGGAAC	reverse

3.1.6 Primer

All primer sequences applied in the methods in section 3.2 are listed in Table 8. All primer sequences were bought from Integrated DNA Technologies, Iowa United States of America.

Table 8 Specifications of utilised primers.

Target DNA	Sequence	Direction
MALAT1	CCCAGGTGCTACACAGAAGT	forward
	ACTGGCTCCTGGACTCTTTT	reverse
PGK1	GACAGCAGCCTTAATCCTCTG	forward
	CTAACAAGCTGACGCTGGA	reverse
GAPDH	GTCAGCCGCATCTTCTTTTG	forward
	GCGCCCAATACGACCAAATC	reverse

3.2 Methods

3.2.1 Cell culture

The cell lines LN18, LN229, LN308, T98G, and U251 were a gift from Professor Guido Reifenberger, university Hospital Düsseldorf. The cell line HEK293T was a gift from Doctor Ute Fischer, university Hospital Düsseldorf. The cell lines D283, Med8A, ONS76, and UW-228-3 were a gift from Doctor Pablo Landgraf, university Hospital Düsseldorf. The cell line CHLA-259 was a gift from the Childhood Cancer Repository, Texas Tech University Health Sciences Center (http://www.ttuhsc.edu).

Cell line identity has been confirmed through STR profiling and cells were regularly tested for mycoplasma contamination. All steps requiring sterile working conditions were performed under a sterile hood.

Suspension cell lines, as well as adherent cell lines and their derivatives, were kept in culture intermittently for experiments performed during this work. Medulloblastoma, MB, associated cell lines CHLA-259, D283, Med8A, ONS76, and UW-228-3, as well as HEK 293T cells, were cultivated by Nan Qin and a subpopulation was supplied for the performed experiments. GBM associated cell lines LN18, LN229, LN308, T98G, and U251 were cultured in DMEM supplemented with 10 % (v/v) heat-inactivated FBS at 37°C in 5 % CO_2 in a humidified incubator.

Cell concentration was determined before experiments with an automated cell counter under application of Trypan blue staining to determine cell viability.

3.2.2 Cell harvest

Cells were grown on sterile cell culture dishes.

Adherent cells were washed two times with 5 mL ice-cold PBS after removal of culture medium. The cells were collected through scraping and stored in 1 mL ice-cold PBS in a tared 2.0 mL tube.

Suspension cells were transferred to a 15 mL tube and centrifuged at 1000 xg at 4°C for 5 min. The supernatant was discarded, and the pellet was washed two times in 5 mL ice-cold PBS through centrifugation. The pellet was resuspended in 1 mL ice-cold PBS and transferred to a tared 2.0 mL tube.

Afterwards, the cell suspensions were centrifuged at 1000 xg for 5 min at 4°C and the supernatant was discarded. The weight of the thus obtained pellets was determined and the pellet was frozen at -80°C.

3.2.3 RNA Isolation

RNA was extracted from harvested cell pellets in an automated process while in the case of RNA-centric pulldown samples the RNA was extracted by a manual column-based approach. The different extraction procedure for RNA-centric pulldown samples was chosen due to the low sample amount.

3.2.3.1 Automated RNA extraction

RNA was isolated from harvested cell pellets under application of the Maxwell® RSC simplyRNA Tissue Kit on the MaxWell system following the protocol provided by the supplier. Isolated RNA was quantified through spectrometric absorbance measurement at 260 nm.

3.2.3.2 Column based RNA extraction

RNA was isolated from RNA-centric pulldown samples under application of the ReliaPrep™ RNA Miniprep System following the protocol provided by the supplier.

3.2.4 Quantitative reverse transcription, RT, -qPCR

Complementary deoxyribonucleic acid, cDNA, was generated through reverse transcription of isolated RNA with M-MLV reverse transcriptase, RT. 1 mg RNA was mixed with 0.5 µL RT primer mix (1 pM oligodT primer mix and 50 µg/mL random primer in water), adjusted to 16.75 µL with water, and incubated at 70°C for 5 min. The mixture was placed on ice for 2 min. To each reaction, 5 µL M-MLV RT 5x buffer, 1.25 µL dNTP mix, 1 µL M-MLV RT, as well as 1 µL RNase inhibitor were added. The thus obtained mixture was incubated at 37°C for 60 min. Obtained cDNA was stored at -20°C.

Resulting cDNA was amplified under the application of specific primer sequences for *MALAT1, phosphoglycerate kinase 1, PGK1*, or *glyceraldehyde-3-phosphate dehydrogenase, GAPDH*, respectively (Table 8). Amplified cDNA levels were quantified through a fluorescent readout based on the DNA double-strand intercalating dye SYBR Green. All measurements were performed in triplicate. 1 µL cDNA was mixed with 2.63 µL water, 0.05 µL Precision Blue Real-time dye, 0.32 µL primer, and 4 µL qPCR GoTaq 2x MasterMix. The RT-qPCR was performed in triplicate on a CFX384 Touch Real-Time PCR system, and the data was analysed with the CFX manager software.

3.2.5 Pulldown

For the *MALAT1*-centric protein pulldown, RNA-protein complexes were crosslinked with formaldehyde in individual cell line samples before cell harvest and subsequent cell lysis. RNA and DNA contained in the samples was sheared before hybridisation with *MALAT1* specific or non-RNA binding biotinylated DNA probes. Under the application of the biotin tag, samples were purified based on streptavidin affinity retardation on magnetic beads. A small part of the sample was subjected to RNA isolation for analysis of *MALAT1* enrichment efficiency while the main sample part was subjected to protein elution, crosslink reversal, and bottom-up MS analysis.

Adherent cells were cultured on sterile cell culture dishes. The medium was removed, and the cells were washed three times with PBS. Following this, 8 mL 4 % formaldehyde (v/v) in PBS were added per culture dish before incubation at 37°C for 10 min. 500 mM glycine was added to each dish before incubation at 37°C for 5 min to stop the crosslinking. The solution was removed, and the cells were washed three times with ice-cold PBS previous to collection in 1.5 mL tubes through scraping. The cell pellet was obtained by centrifugation at 1000 xg for 5 min and the supernatant was discarded.

Suspension cells were transferred into 50 mL tubes and washed three times with PBS via centrifugation at 200 x g for 5 min. 10 mL preheated 4 % formaldehyde (v/v) in PBS was added and the suspension was incubated for 10 min at 37°C. A 500 mM glycine solution was added to each tube and the suspension was incubated for 5 min at 37°C. The cells were collected and washed twice with ice-cold PBS through centrifugation at 1000 x g for 5 min. The cell pellet was transferred into 1.5 mL tube in 1 mL ice-cold PBS and centrifuged at 1000 x g for 5 min. The supernatant was discarded.

The pellet amount per tube was determined and an equal amount of lysis buffer 1 and lysis buffer 2 was added. The suspension was incubated on ice and homogenised with a douncer 20 times. Lysates were adjusted to 800 µL with a 1:1 mix of lysis buffer 1 and lysis buffer 2. Per sample, 10 µL

Ribonuclease inhibitor was added. Contained RNA and DNA was sheared in an ultrasonicator at 3.3 intensity equal to 50-55 W, 7°C, 20 % duty cycle, 200 cycles per burst for 400 s in power tracking mode. The samples were centrifuged at 14,000 x g and 4°C for 10 min and the supernatant was collected.

160 µL 5x Hybridisation buffer, 80 µL 10x SDS and 150 µL formamide were added to each sample. The samples were divided to one half 4 µL *MALAT1*-specific raPool (25 pmol/µL) was added while 4 µL non-RNA binding raPool (25 pmol/µL) was added to the other half. The samples were incubated at 37°C and 500 rpm for 4 h.

100 µL Streptavidin beads per sample were washed thrice with a 1:1 mix of lysis buffer 1 and lysis buffer 2 and resuspended in the original volume of a 1:1 mix of lysis buffer 1 and lysis buffer 2.

The respective amount of washed beads was added to each raPool containing sample and incubated at 37°C and 450 rpm for 30 min. The beads were washed five times with 1 mL preheated pulldown wash buffer at 37°C and resuspended in 1 mL pulldown wash buffer.

50 µL of bead suspension was collected for column-based RNA extraction. The pulldown wash buffer was exchanged against 90 µL proteinase K buffer and 10 µL proteinase K at 20 mg/mL. The mixture was incubated at 55°C and 350 rpm for 50 min previous to RNA extraction.

The wash buffer was removed from the leftover bead containing sample and 30 µL 1x SDS sample buffer were added. The suspension was incubated at 95°C for 5 min and the supernatant was collected. 1.08 µL 1.4 M DTT was added to each protein sample before incubation at 95°C for 30 min.

The generated samples were prepared for MS analysis.

3.2.6 Sample workup for MS analysis

Samples were desalted through electrophoretic migration at 50 V for 10 min on a 4 -12 % Bis-Tris polyacrylamide gel. Protein bands were cut out after silver staining. Bands were destained with a 1:1 mixture of 30 mM sodium thiosulfate and 100 mM potassium ferrocyanide before being washed three times alternately with 10 mM ammonium bicarbonate and 10 mM ammonium bicarbonate in 50 % acetonitrile. Washed protein bands were reduced with 10 µM DTT in 50 mM ammonium bicarbonate for 45 min at 56°C and alkylated with 55 mM iodoacetamide in 50 mM ammonium bicarbonate for 30 min at room temperature. After alkylation protein bands were washed two times alternately with 10 mM ammonium bicarbonate and 10 mM ammonium bicarbonate in 50 % acetonitrile. Proteins were digested in-gel overnight at 37°C with trypsin at a 1:50 ratio. Generated peptides were extracted from the gel matrix via sonication on ice for 15 min in a 1:1 mixture of 0.1 % trifluoroacetic acid, TFA, and acetonitrile.

3.2.7 LC-MS/MS

For mass spectrometric analysis, 15 µL peptide solution per sample were analysed on a nano-high-performance liquid chromatography-electrospray ionisation mass spectrometer. The analytical system was composed of an RSLCnano U3000 HPLC coupled to a QExactive plus mass spectrometer via a nano-electrospray ion source. Injected peptides were concentrated and desalted at a flow rate of 6 µL/min on a trapping column (Acclaim PepMap C18, 2 cm x 100 µm x 3 µm particle size, 100 Å pore size) with 0.1 % TFA for 10 min. Subsequently, peptides were separated at a constant flow rate of 300 nL/min over a 120 min gradient on an analytical column (Acclaim PepMap RSLC C18, 25 cm x 75 µm x 2 µm

particle size, 100 Å pore size) at 60°C. The separation was achieved through a gradient from 4 to 40 % solvent B in solvent A. Afterwards, peptides were ionised via a nano-electrospray interface at a voltage of 1,400 V and transferred into the mass spectrometer operated in positive mode. MS scans were recorded in profile mode in a range from 350-2000 m/z at a resolution of 70,000 while tandem mass spectra were recorded at a resolution of 17,500. Tandem mass spectra were recorded with a data dependent Top10 method and 30% normalised collision energy. Dynamic exclusion was activated with a repeat count of 1 for 100 ms.

3.2.8 MS data analysis

Proteome Discoverer was applied for peptide/protein identification with Mascot and MS Amanda as search engines employing the UniProt database (human; including isoforms; date 2019-05-29). A false discovery rate of 1 % ($p \leq 0.01$) on peptide level was set as identification threshold. Proteins were quantified with Progenesis QIP.

3.2.9 Transfection

All plasmids were prepared by Frauke Meyer in *Escherichia coli* cells and supplied as frozen down stocks for the experiments in this thesis. All steps requiring sterile working conditions were performed under a sterile hood.

HEK293T cells were cultured in DMEM supplemented with 10 % (v/v) heat-inactivated FBS at 37°C in 5 % CO_2 in a humidified incubator on 15-cm tissue culture dishes with a seeding density of $2.5x10^6$ cells per plate three days before the start of virus production. Two hours before the addition of the viral production mix, the old medium was exchanged for fresh medium. Viral production mix was prepared by mixing the plasmids pMDL/pRRE 1.75 µL/mL, pRSV-Rev 1.375 µg/mL, pMD2.G 0.75 µg/mL, and the transfer vector 1.75 µg/mL with polyethene imine at 0.25 µL/mL in 4 mL DMEM. The mix was incubated at room temperature for 10 min before addition of 7 mL DMEM supplemented with 15 % (v/v) heat-inactivated FBS. This suspension was exchanged for the medium on one 15-cm tissue culture dish and the cells were incubated at 37°C in 5 % CO_2 in a humidified incubator overnight. After incubation, the medium was exchanged for 14 mL fresh DMEM supplemented with 10 % (v/v) heat-inactivated FBS and the cells were incubated for 24 h at 37°C in 5 % CO_2 in a humidified incubator. The medium was collected in a 50 mL tube and stored at 4°C and 10 mL DMEM supplemented with 10 % (v/v) heat-inactivated FBS was added to each plate. The cells were incubated for 24 h at 37°C in 5 % CO_2 in a humidified incubator before the medium was collected and added to the previous 50 mL tube. The collected virus suspension was centrifuged for 5 min at 500 xg and the pooled supernatant was filtered through a 0.45 µm filter unit.

GBM associated cells lines were grown on a 6-well plate with a seeding density of 300,000 cells per well. After 24 h 2 mL of the generated virus suspension supplemented with 4 µg/mL polybrene were added per well and the cells were incubated for 48 h at 37°C in 5 % CO_2 in a humidified incubator. Following the incubation period, the medium was discarded, and the cells were washed with PBS previous to trypsin mediated transfer to T75 flasks in DMEM supplemented with 10 % (v/v) heat-inactivated FBS. After 24 h the medium was discarded, and the antibiotic selection was initiated through addition of DMEM supplemented with 10 % (v/v) heat-inactivated FBS and 2.5 µg/mL puromycin. After 48 h the medium was exchanged for DMEM supplemented with 10 % (v/v) heat-inactivated FBS and 0.5 µg/mL puromycin. Antibiotic selection was performed for five days.

3.2.10 Phenotype assays

Proliferation or migration rate assays were employed to determine if *MALAT1* influences the phenotypical behaviour of the different cell lines. Results from phenotype assays were employed to further the understanding of *MALAT1* related cell biology.

All steps requiring sterile working conditions were performed under a sterile hood.

3.2.10.1 Proliferation

Cell proliferation assays were employed to determine the growth rate of isogenic GBM cell lines.

3.2.10.1.1.1 IncuCyte live cell proliferation analysis

Live cell proliferation analysis was performed through confluency measurement via IncuCyte® live cell analysis imaging system over a period of 120 h. Equal and defined cell numbers per cell line were seeded onto a culture plate and incubated under standard culture conditions in a live cell imager. For a period of 120 hours, two phase pictures per well were taken at 10x magnification every hour in an adjoining layout in the middle of the well. Cell lines were cultured in three separate wells each to obtain triplicate measurements. Data analysis was performed with the IncuCyte software and a two-sided Student's T-test was employed to calculate statistical significance.

3.2.10.1.1.2 XCelligence real-time proliferation analysis

Real-time proliferation rate was analysed through a one chamber XCelligence setup. Cells were suspended in either dimethyl sulfoxide, DMSO, - or inhibitor-containing medium and given into a well chamber. The well chamber contained gold impedance microelectrodes on the bottom. Cells adhering to the microelectrodes were resulting in a stable and continuous change in the impedance signal monitored over a defined time range. The impedance signal is directly correlated to the cell monolayer area. The measurement was performed in triplicates over 70 hours and a two-sided Student's T-test was employed to calculate statistical significance. Chamber wells containing cell-free media suspensions with either DMSO or inhibitor were employed as baseline measurement. Data analysis was performed with the RTCA software.

3.2.10.1.1.3 Doubling Time measurement

Equal numbered cell populations were seeded on six culture dishes per cell line. This cell population number was noted for time point 0 h. Seeded cell dishes were incubated under standard conditions for 24 h and 48 h. At each individual time point, three culture dishes per cell line were employed for determination of their respective cell number via automated cell counting with Trypan blue staining. Through application of the staining, the cell counter discriminates between viable and dead cells.

3.2.10.2 Cell migration assay via XCelligence

Cell migration assays were employed to determine the migration rate of isogenic GBM cell lines.

Real-time migration rate was analysed through a two-chamber XCelligence setup. Cells were suspended in serum-free medium and given into the upper chamber. Standard medium containing serum was added to the lower chamber, the serum was employed as a chemoattractant. The two chambers were separated by a microporous, cell-permeable membrane with gold impedance microelectrodes on the underside. The cells passed through the membrane and adhered to the microelectrodes resulting in a stable and continuous change in the impedance signal monitored over a defined time range.

Real-time cell migration analysis was performed in triplicates for a period of 30 hours of continuous measurements. Respective isogenic cell pairs consisting of control and KD cells were compared on basis of the curves' slope rates and tested for significance under application of a two-sided Student's t-test. The data was baseline corrected against chambers with cell-free media.

3.2.11 Protein extraction from cell pellets

Proteins were extracted from collected cell pellets by homogenisation in urea buffer in a tissue lyser and subsequent sonication on ice. After a 15 min centrifugation at 16,000 xg and 4°C, the supernatant containing the extracted proteins was collected. The resulting pellet was resuspended in urea buffer and homogenised in a tissue lyser. The suspension was sonicated on ice and centrifuged at 16,000 xg and 4°C for 15 min to collect the supernatant. Both supernatants were combined.

The protein concentration was determined against an albumin standard curve under application of the Pierce 660 nm Protein Assay on a spectrometer through absorbance measurements at 660 nm. Data was analysed with SoftMax Pro.

3.2.12 HT-drug screen

Isogenic LN18 *MALAT1* KD and respective control cells were seeded onto 384-well plates. The plates contained 641 inhibitors each in nine different concentrations (0.005 µM - 25 µM, logarithmic distribution) in addition to DMSO control wells. The inhibitors were dispensed in a randomised manner and DMSO concentration was normalised to 0.25% in each well. Cells were incubated for 72 h with the inhibitors. After incubation, the cell viability was measured through ATP quantification with luminescence-based readout under application of CellTiter-Glo® reagent. Half-maximal inhibitory concentration , IC_{50}, curves were generated through an in-house software script.

3.2.13 Cell cycle analysis via flow cytometry

For the analysis of cell-cycle stages, a flow cytometry assay based on propidium iodide, PI, is performed.

Cells were seeded onto 6-well plates in an inhibitor-containing medium at a density of 300,000 cells/well. After 48 h incubation, the cells were harvested and fixed in 70 % ethanol for 2 h at -20°C. Fixed cells were incubated for 30 min with 50 µL RNase (100 µg/mL) at 37°C under gentle mixing. Subsequently, cells were resuspended in 100 – 200 µL PI (50 µg/mL) and transferred onto a V-well 96-well plate. After overnight incubation at 4°C, the samples were measured on the flow cytometer. The data was analysed with the CytExpert software. All measurements were performed in triplicates. Significance was tested under application of Student's t-test.

3.2.14 Western blotting and immunolabelling

Extracted proteins were separated based on their molecular weight through SDS-PAGE at 50 V for 10 min and subsequently, 200V for 50 min on a 4 -12 % Bis-Tris polyacrylamide or on a 4–15% Mini-PROTEAN® TGX™ gel. 4 -12 % Bis-Tris polyacrylamide gels were combined with 1x MOPS running buffer while 4–15% Mini-PROTEAN® TGX™ were processed in 1x SDS running buffer. Separated proteins were transferred to a polyvinylidene difluoride, PVDF, membrane via semi-dry electroblotting. Membranes were blocked with ECL Prime blocking reagent in TBST buffer (1 g/50 mL) at room temperature for 30 min. For detection, protein-specific primary antibodies were employed which were detected through secondary antibodies conjugated to horse radish peroxidase, HRP. Primary antibody incubation was

performed at 4°C overnight in blocking solution. Secondary antibody incubation was performed at room temperature for 90 min in blocking solution. Blots were washed thrice for 5 min at room temperature in TBST buffer prior to incubation with secondary antibody as well as previous to incubation with ECL substrate. The readout was performed via accumulated detection of the chemiluminescence intensity of an enzymatic substrate conversion via HRP. Image analysis was performed with Image Lab software.

3.2.15 Nuclear and cytoplasmic protein fractionation

Nuclear and cytosolic protein fractionation was performed under application of the NE-PER™ Nuclear and Cytoplasmic Extraction Reagents kit following the protocol provided by the supplier with some exceptions as described hereafter.

Cells were grown on two 15-cm dishes to 90 % confluency under respective culturing conditions. Cells were washed twice with PBS before being harvested through scraping and centrifuged at 500 xg for 5 min to remove excess PBS. The cell pellet weight was determined, and Cer I reagents was added at five times the volume of the pellets' weight (mg to µL). The cell mixture was vigorously vortexed and incubated on ice for 10 min. After the incubation period, 0.275 times the volume of the pellets' weight of Cer II reagent was added to the mixture. After a 5-sec vortexing step, the mixture was incubated on ice for 1 min. The suspension was centrifuged at 16,000 xg and 4°C for 5 min and the supernatant was collected as cytoplasmic fraction. The pellet was resuspended in Cer I, vortexed for 15 sec, centrifuged at 16,000 xg and 4°C for 5 min, and the supernatant was added to the cytoplasmic fraction. The thus obtained pellet was resuspended in 2.5 times the volume of the original pellets' weight of NER reagent. The cell suspension was vortexed for 15 sec followed by a homogenisation step in a douncer with ten strokes and sonicated on ice four times for 10 sec. This step was repeated four times at 10 min intervals. The douncer was cleaned with water, ethanol, and water between samples. Overall, the cell suspension was incubated on ice for a total of 40 min. The suspension was centrifuged at 16,000 xg and 4°C for 10 min and the supernatant was collected as nuclear fraction.

4 Results

MALAT1 is a highly conserved and highly expressed lncRNA linked to increased tumorigenesis in various tumour types [53-55]. To deepen the understanding of *MALAT1s*' role in GBM tumorigenesis and to reveal the underlying mechanisms, this thesis aims to investigate the proteomic signatures influenced by *MALAT1* in GBM cell lines. Findings will be considered on a global basis supported by extensive previously published data.

4.1 Investigation of *MALAT1* interactome

To deepen the understanding of *MALAT1s*' role in GBM tumorigenesis, identification of proteinaceous interaction partners was performed. In this study, *MALAT1s*' protein interactors were analysed through an RNA-centric protein pulldown in GBM and MB cell lines through MS analysis. Analysis of MB cell lines and comparison of the results with those obtained through analysis of GBM cell lines was employed to gain insight into possible GBM specific *MALAT1* interaction partners.

4.1.1 RNA-based protein pulldown

First *MALAT1* expression levels were investigated in ten different GBM and MB cell lines to establish an expression level baseline as well as confirm *MALAT1* levels are in a high to medium expression range to enable RNA-centric pulldown experiments. Second *MALAT1* interactors are enriched through RNA-centric pulldown experiments and analysed via RT-qPCR and MS to ensure enrichment of *MALAT1* in the individual samples and to identify obtained interactors, respectively.

4.1.1.1 RNA analysis before pulldown

MALAT1 levels were analysed via RT-qPCR in a relative manner in five GBM (LN18, LN229, LN308, T98G, and U251) and five MB (CHLA-259, D283, Med8A, ONS76, and UW-228-3) cell lines. Measured levels for *MALAT1, GAPDH* and *PGK1* were normalised to a non-template control sample. *GAPDH* and *PGK1* measurements were employed as housekeeper RNA measurements for relative quantification. All measurements were performed in triplicates. Significance was tested under application of Student's t-test.

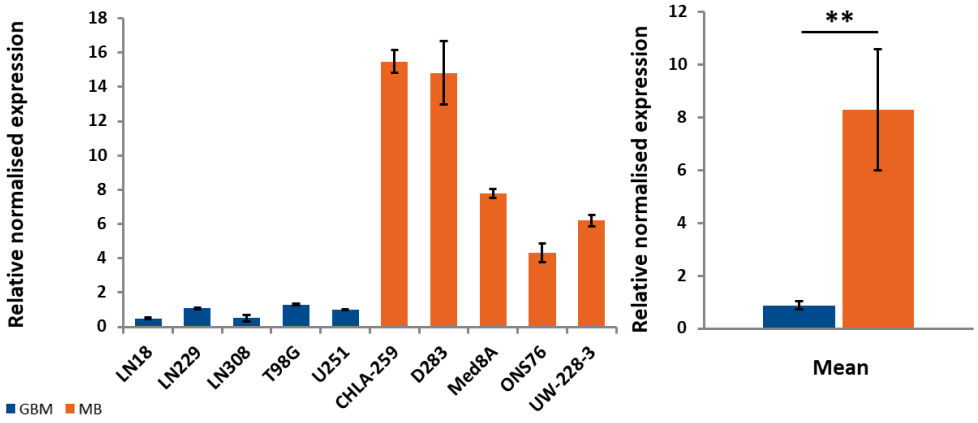

Figure 14 *MALAT1* expression levels in GBM and MB cell lines relative to *PGK1* and *GAPDH* housekeeper RNA levels determined by RT-qPCR (n=3). All measurements were performed in triplicate. Measured levels for *MALAT1* were normalised to a non-template control sample and are depicted relative to measured *GAPDH* and *PGK1* signals in the bar graph on the left side while mean relative, normalised *MALAT1* levels are depicted in the bar graph on the right side. GBM associated cell lines are depicted in blue while MB associated cell lines are depicted in orange. Mean values were calculated based on the associated tumour type to enable a group-based comparison. Measurement variance is indicated through error bars. Significance levels are indicated through ** for p-values < 0.01.

PGK1 was detected with a median threshold cycle, CT, value of 16.90 (± 1.86) and *GAPDH* with a median CT value of 13.55 (± 1.48) over all analysed cell lines. *MALAT1* was detected with a median CT value of 13.85 (± 1.09) over all analysed cell lines. For the system and primers employed in this analysis, analysis results with CT values under 35 are considered as reliable and quantitative.

All five MB cell lines exhibited higher *MALAT1* expression levels than GBM cell lines analysed (Figure 14). In GBM cell lines measured, *MALAT1* expression levels were comparable to housekeeper RNA levels (LN18: 0.49 ± 0.045; LN229: 1.08 ± 0.035; LN308: 0.52 ± 0.185; T98G: 1.29 ± 0.049; U251: 1.00 ± 0.033). In MB cell lines analysed, *MALAT1* expression levels were at least four times higher than housekeeper RNA levels measured (CHLA-259: 15.47 ± 0.664; D283: 14.82 ± 1.832; Med8A: 7.78 ± 0.253; ONS76: 4.31 ± 0.562; UW-228-3: 6.20 ± 0.342). Amongst these ten cell lines analysed, *MALAT1* expression levels were significantly (p-value = 4.8E-03) higher in MB cell lines compared to GBM cell lines with mean expression levels of 8.28 ± 2.293 and 0.88 ± 0.158, respectively.

MALAT1 CT values were well below the detection limit based cut-off value of 35 and individual expression levels were in the high range as they were comparable to those of highly expressed, standard housekeeper RNAs. Consequently, *MALAT1* expression levels were sufficient for *MALAT1*-centric protein pulldown in all ten cell lines analysed.

4.1.1.2 RNA analysis after pulldown

To confirm enrichment of *MALAT1*, its levels were analysed after total protein and DNA digestion via RT-qPCR in a defined part of each cell line sample pair. Each sample pair consisted of one RNA-based pulldown sample generated with a pool of biotinylated *MALAT1* specific DNA probes and one RNA-based pulldown sample generated with a pool of biotinylated non-RNA binding DNA probes. Pulldowns with non-RNA binding DNA probes were employed as negative controls in this analysis. Measured levels for *MALAT1, GAPDH* and *PGK1* were normalised to a non-template control sample. *GAPDH* and *PGK1* measurements were employed as housekeeper RNA measurements for relative quantification. All measurements were performed in triplicates and significance was tested under application of Student's t-test.

PGK1 was detected with a median CT value of 35.92 (± 0.82) and *GAPDH* with a median CT value of 33.51 (± 0.82) over all analysed cell lines. These mean CT values depict a distinct (p-value: *PGK1* 1.78E-25, *GAPDH* 1.33E-22) decrease of the housekeeper RNA levels compared to previously obtained values of 16.90 (± 1.86) and 13.55 (± 1.48) for *PGK1* (p-value = 1.78E-25) and *GAPDH* (p-value = 1.33E-22), respectively, in non-pulldown samples.

MALAT1 was detected in *MALAT1* specific samples as well as non-RNA binding samples over all analysed cell lines with median CT values of 20.33 (± 1.52) and 30.99 (± 1.61), respectively. This confirms a significant depletion of MALAT1 in non-RNA binding samples with a p-value of 2.43E-11.

The highest relative *MALAT1* levels were measured in *MALAT1* specific LN229 and UW-228-3 samples with 6.11 ± 1.7 and 5.26 ± 0.34, respectively. In LN308 and D283 non-RNA binding samples, the lowest relative *MALAT1* levels were measured with 0.0015 ± 0.0003 and 0.0019 ± 0.0009, respectively.

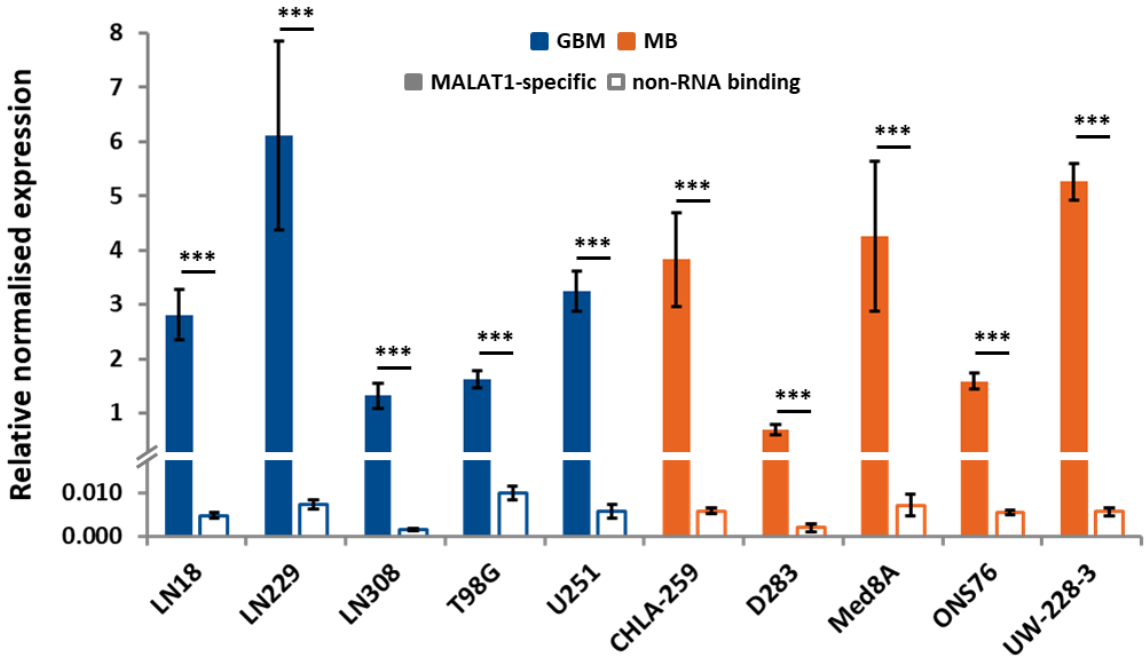

Figure 15 *MALAT1* expression levels in RNA-centric pulldown eluates relative to *PGK1* and *GAPDH* housekeeper RNA levels determined by RT-qPCR (n=3). All measurements were performed in triplicate. Measured levels for *MALAT1* were normalised to a non-template control sample and are depicted relative to measured *GAPDH* and *PGK1* signals in the bar graph. Significance was tested under application of Student's t-test. GBM associated cell lines are depicted in blue while MB associated cell lines are depicted in orange. Measurement variance is indicated through error bars. Significance levels are indicated through *** for p-values < 0.001. Samples generated with *MALAT1*-specific DNA probes are depicted as filled bars while samples generated with non-RNA binding DNA probes are depicted as unfilled bars. Refer to **Table 17** in Appendix B for individual values.

Throughout all samples, *MALAT1* levels in samples generated with *MALAT1*-specific DNA probes were significantly higher compared to respective levels in samples generated with non-RNA binding DNA probes (Figure 15 and Table 17). This additional checkpoint analysis confirmed the suspected increase in *MALAT1* levels in all *MALAT1*-specific pulldown samples in combination with decreased housekeeper RNA levels compared to previously measured baseline levels in the respective cell lines. In samples generated with non-RNA binding probes both *MALAT1* and housekeeper RNA levels were decreased compared to previously measured baseline levels in the respective cell lines.

MALAT1 CT values as well as relative expression levels confirmed distinct depletion of *MALAT1* in non-RNA binding samples was achieved. These checkpoint results increased the validity of identifying putative *MALAT1* interacting proteins through the chosen sample work-up. Based on these results the samples were employed to analyse *MALAT1s*' interactome.

4.1.1.3 *MALAT1* Interactome characterisation via shotgun proteomics

After RNA-centric affinity enrichment, the crosslinks were removed and the proteins eluted, desalted, and digested previous to separation via nano-HPLC. Peptides were analysed with a high-resolution mass spectrometer. Peptide identification was achieved through database searches of MS2 spectra recorded while quantification was achieved through MS1 intensity comparison. Interactome analysis was performed in five individual GBM cell line and five individual MB cell line sample pairs consisting of one *MALAT1*-specific and one non-RNA binding sample per cell line. Relative quantification of protein amounts per sample was achieved based on all non-conflicting peptide signals.

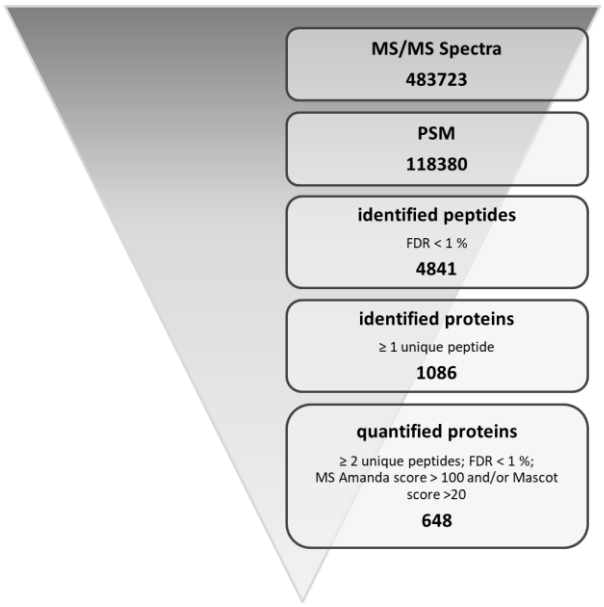

Figure 16 Summary of MS-based proteome data obtained for GBM and MB samples processed with *MALAT1* specific and non-RNA binding DNA probes as well as respective cut-off values implemented. The chart shows the hierarchical structure and defined cut-off values for each step in the analysis of recorded MS/MS spectra.

483,723 MS2 spectra were recorded over all 20 samples, 118,380 (24.5 %) of which were matched to database spectra under application of MS Amanda and Mascot search algorithms. These peptide-spectrum match, PSMs, lead to the identification of 4,841 peptides implementing a 1 % false discovery rate, FDR, cut-off at peptide level (Figure 16). In total 1,086 proteins were identified and 648 were quantified. For identification, at least one unique peptide per protein was necessary while for quantification two unique peptides per protein were required. Peptides were considered for protein quantification if their identification score from MS Amanda or Mascot was at least 100 or 20, respectively. Furthermore, only proteins with a FDR of at most 1 % were quantified.

This data fit the expectations for proteome analyses results of an affinity enrichment study with a nuclear lncRNA in the centre based on researched literature.

4.1.1.4 Determination of *MALAT1* interactome

Identification of putative *MALAT1* interacting proteins was performed through fold change comparison and one-way analysis of variance, ANOVA, significance testing. Individual samples generated with either *MALAT1*-specific or non-RNA binding DNA probes were directly compared in relation to their tumour association. This results in two separate datasets depicting the *MALAT1* interactome in analysed GBM and MB cell lines. Throughout all analysis steps, samples generated with non-RNA binding DNA probes were considered as negative control. In the volcano plots (Figure 17), negative, decimal logarithmic p-values were plotted against respective binary logarithmic fold changes for each quantified protein.

In this study, a p-value of at most 0.01 ($-\log(0.01) = 2$) and a fold change of at least 2 ($\log_2(2) = 1$) were chosen as significance and fold change cut-offs, respectively. Proteins were considered as putative *MALAT1* interactors if their amount in samples generated with *MALAT1*-specific DNA probes was higher compared to samples generated with non-RNA binding DNA probes. The five individual cell lines analysed per tumour type were considered as biological replicates for the overall comparison of *MALAT1* interactomes in GBM and MB.

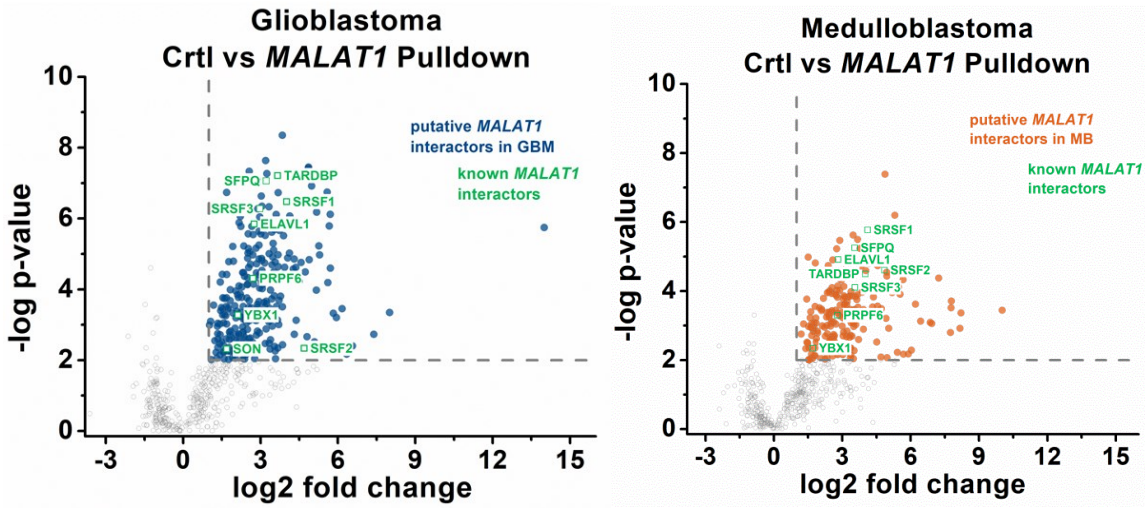

Figure 17 Differential analysis of proteins in GBM and MB associated cell line samples after RNA-centric pulldown. Volcano plots show negative, decimal logarithmic p-values against respective binary logarithmic fold changes for each quantified protein. Dashed lines indicate the significance cut-off values chosen in this study, namely a p-value of at most 0.01 (-log(0.01) = 2) and a fold change of at least 2 ($log_2(2) = 1$). One-way ANOVA significance testing was employed to the fold change, FC, comparison. Positive FC values are employed to indicate putative *MALAT1* interactors. Significant proteins are highlighted in blue for GBM associated samples (right plot), orange for MB associated samples (left plot) and known *MALAT1* interactors are marked in green.

In each tumour type analysed putative *MALAT1* interacting proteins were identified with the above mentioned cut off values (Figure 17). The GBM associated sample set yielded 264 putative *MALAT1* interacting proteins while the MB associated sample set yielded 213 putative *MALAT1* interacting proteins. In both sample sets, previously well-known *MALAT1* interactors were among the list of putative interactors [61]. These known *MALAT1* interactors are Serine/arginine-rich splicing factor 1 (Q07955; SRSF1), Serine/arginine-rich splicing factor 2 (Q01130; SRSF2), Serine/arginine-rich splicing factor 3 (P84103; SRSF3), Y-box-binding protein 1 (P67809; YBX1), Splicing factor, proline- and glutamine-rich (P23246; SFPQ), ELAV-like protein 1 (Q15717; ELAV1), TAR DNA-binding protein 43 (Q13148; TARDBP), Pre-mRNA-processing factor 6 (O94906; PRP6), and Protein SON (P18583; SON).

Table 9 Summary of enrichment analysis results for identified proteins in RNA-centric pulldown eluates. Enrichment was performed against the human proteome as background. Significance was tested under application of the hypergeometric Benjamini-Hochberg test. Enriched GO terms are listed with the percentage of identified proteins and the negative, decimal logarithmic p-value sorted by their GO category.

GO category	GO term	Identified proteins in %	p-value
Cellular component	Nucleus	87	1.5E-89
Molecular function	RNA binding	31.6	5.4E-86
Biological pathway	Gene Expression	28.1	6.0E-70
	mRNA splicing	24.6	4.3E-93
	Transcription	12.6	1.5E-30
Protein domain	RNA recognition motif	28.4	4.0E-93
	Histone 3 domain	3.9	7.2E-15
Expression site	Brain	74.7	4.3E-37

A full list of putative MALAT1 interacting proteins was included in Appendix A

Table 14 for GBM associated samples and Table 15 for MB associated samples. In addition, graphs depicting the dynamic range obtained for each respective sample group was included in Appendix A Figure 57.

Putative *MALAT1* interacting proteins identified in this affinity enrichment study were employed in an enrichment analysis with the human proteome as background (Table 9) to enable a descriptive analysis and to assess the validity of the generated affinity enrichment dataset. Significance was tested under application of the hypergeometric Benjamini-Hochberg test.

Enriched GO terms were in line with *MALAT1* literature as well as the location of GBM and MB tumours.

Nuclear proteins were enriched with a p-value of 1.5E-89 covering 87 % of putative *MALAT1* interacting proteins identified. The molecular function RNA binding was enriched with a p-value of 5.4E-86 covering 31.6 % of the putative interactors. Gene expression, mRNA splicing, and transcription were biological pathways enriched with p-values of 6.0E-70, 4.3E-93, and 1.5E-30 while covering 28.1 %, 24.6 %, and 12.6 % of the putative interactors identified, respectively. The RNA recognition motif, RRM, and the H3 domain were two enriched protein domains with respective p-values of 4.0E-93, and 7.2E-15 while covering 28.4 %, and 3.9 % of the putative interactors. In addition, enrichment of proteins expressed in the brain with a p-value of 4.3E-37 and protein coverage of 74.7 % was depicted in this dataset.

Observed enrichment of nuclear proteins, as well as RNA binding proteins, are in line with expectations based on *MALAT1s*' localisation in the nucleus and it being a lncRNA. Enrichments of proteins involved in gene expression, mRNA splicing, and transcription reflect current knowledge of *MALAT1s*' involvement in these biological pathways [61, 94]. Enrichment of proteins expressed in the brain is plausible since both analysed tumour types are located in the brain. While the enrichment of proteins containing an RNA recognition motif reflects the enrichment of RNA binding proteins and was therefore suspected. The enrichment of proteins containing a histone 3 domain is thought to be based on their role in transcription.

Enrichment analyses results showed appropriate results in regard to possible functions and location of the nuclear lncRNA MALAT1.

Respective lists of putative *MALAT1* interactors were overlaid with a list of previously proposed *MALAT1* interacting proteins combined from Spiniello *et al.* [95], Chen *et al.* [96] and the review article Gutschner *et al.* [61]. The overlap is depicted in a Venn diagram (Figure 18). Previous interactomics studies were performed in various cell lines namely Hep2G [96], a hepatocellular carcinoma cell line, PC-3 [95], a prostate adenocarcinoma cell line, Hela [53, 97-100], a cervical cancer cell line, HEK 293 [97, 101, 102], a human embryonic kidney cell line, SH-SY5Y [103], a neuroblastoma cell line, H9 [103], a human embryonic stem cell line, EpH4 [53, 99], a mouse breast epithelial cell line, YUSAC [104], a melanoma cell line, NIH/3T3 [104], a mouse embryonic fibroblast cell line, U2OS [53], an osteosarcoma cell line, and IMR-90 [97], a human normal lung fibroblast cell line.

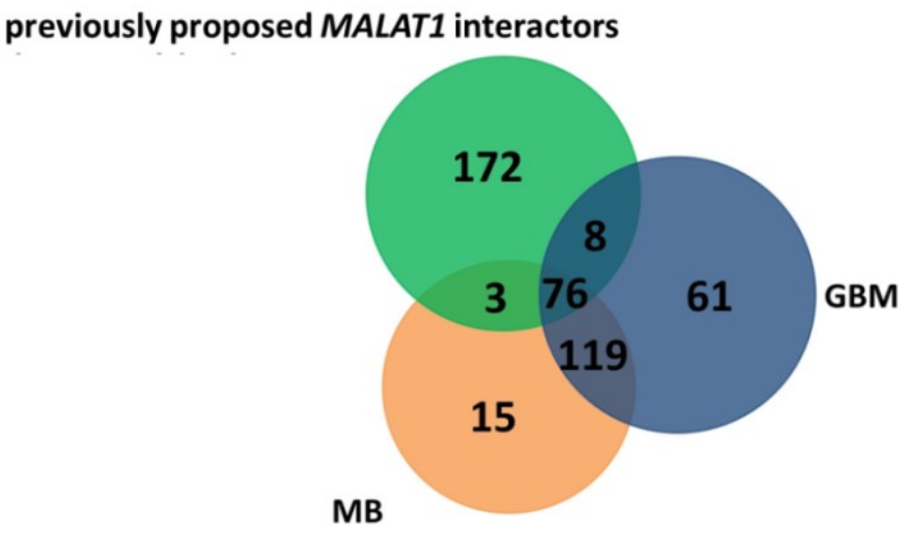

Figure 18 Depiction of overlap between putative MALAT1 interactors from this study with literature. VENN-diagram comparing putative MALAT1 interactors identified in this study with previously proposed MALAT1 interactors from literature. GBM associated samples are depicted in blue, MB associated samples are depicted in orange and previously proposed *MALAT1* interactors are depicted in green. In GBM associated samples, 264 putative MALAT1 interacting proteins were identified. In MB associated samples, 213 putative MALAT1 interacting proteins were identified. 259 proteins have been proposed as MALAT1 interactors in literature. Amongst GBM and MB associated sample sets, 195 putative *MALAT1* interactors were identical while 61 and 15 were only identified in the respective sample sets. 89 out of the 282 identified putative *MALAT1* interactors have been described as potential *MALAT1* interactors in at least one of the mentioned publications. Out of these 76 proteins were identified in both GBM and MB associated datasets.

In total, 282 putative *MALAT1* interacting proteins have been identified in the overall sample set. Amongst GBM and MB associated sample sets, 195 putative *MALAT1* interactors were identical while 61 and 15 were only identified in the respective sample sets. 87 out of the 282 identified putative *MALAT1* interactors have been described as potential *MALAT1* interactors in at least one of the mentioned publications. Out of these, 76 proteins were identified in both GBM and MB associated datasets. Previously proposed interactors were identified in various cell lines from different cancer types, disease states, the tissue of origin, and different organisms. For this study, the biological pathways represented by the 61 putative interactors that appear to be GBM exclusive were of predominant interest.

Putative *MALAT1* interacting proteins exclusively identified in one of the tumour associated datasets from this affinity enrichment study, as well as previously proposed MALAT1 interactors, were employed in an enrichment analysis with the human proteome as background (Figure 19) to enable a descriptive analysis of processes influenced by *MALAT1* in a sample group-specific analysis. Significance was tested under application of the hypergeometric Benjamini-Hochberg test. This analysis was employed to identify GBM exclusive pathways influenced by *MALAT1* able to drive tumour aggressiveness.

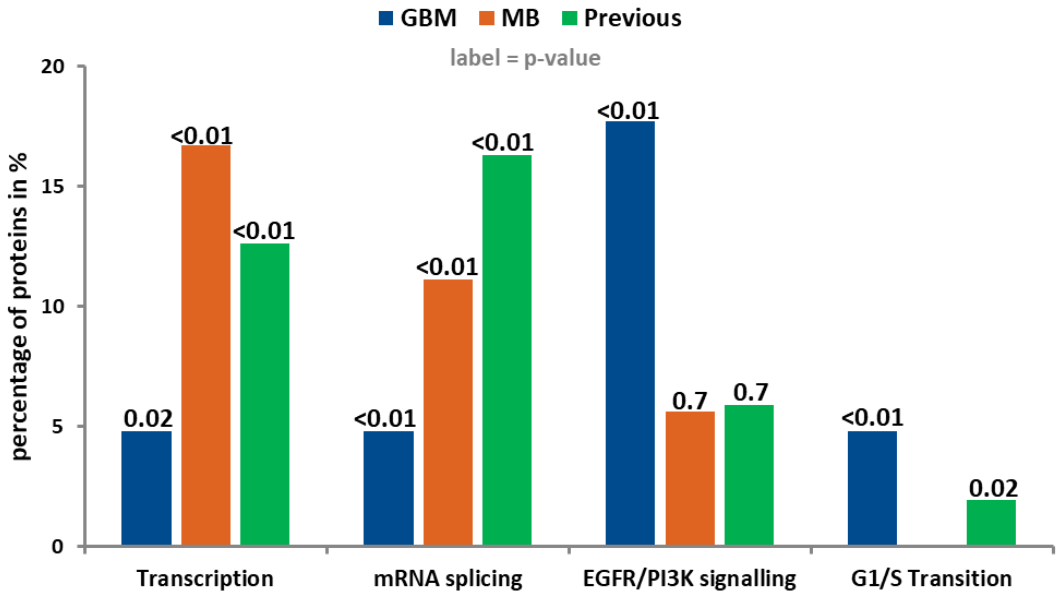

Figure 19 Summary of enrichment analysis results for putative *MALAT1* interacting proteins exclusively identified in one sample group. Enrichment was performed against the human proteome as background. Significance was tested under application of the hypergeometric Benjamini-Hochberg test. Enriched GO terms are depicted by the percentage of identified proteins for each individual sample group and their p-value listed on top of each bar. GBM associated samples are depicted in blue, MB associated samples are depicted in orange and previously proposed *MALAT1* interactors are depicted in green.

Covering 4.8 % of putative GBM specific *MALAT1* interactors each, proteins associated with transcription (p-value = 2.0E-02) and mRNA splicing (p-value = 5.0E-03) appeared underrepresented compared to 16.7 % (p-value = 5.8E-04) and 11.1 % (p-value = 4.5E-03) of putative MB specific *MALAT1* interactors as well as 12.6 % (p-value = 8.1E-29) and 16.3 % (p-value = 8.9E-54) of previously proposed *MALAT1* interactors, respectively. Proteins associated with EGFR/PI3K signalling events appeared overrepresented in putative GBM specific *MALAT1* interactors with 17.7 % (p-value = 2.5E-03) of putative interactors compared to putative MB specific *MALAT1* interactors with 5.6 % (p-value = 7.1E-01) of putative interactors and previously proposed interactors with 5.9 % (p-value = 7.2E-01). Proteins associated with G1/S transition in the cell cycle covering 4.8 % (p-value = 6.5E-03) of putative GBM specific *MALAT1* interactors, were overrepresented compared to previously proposed interactors covering 1.9 % (p-value = 2.5E-02). In the list of putative MB specific *MALAT1* interactors, no proteins associated to G1/S transition in the cell cycle were present.

Regulation of transcription and mRNA splicing are two well-described modes of action for *MALAT1* in human cancers [51]. On the other hand, proteins involved in EGFR/PI3K signalling and G1/S transition appear to be more prevalent in the list of putative GBM specific interactors compared to the MB specific and previously proposed interactors. Proliferating cell nuclear antigen (P12004; PCNA) is associated with both biological pathways, EGFR/PI3K signalling [105, 106] as well as G1/S transition [107], and has been identified as a putative GBM specific *MALAT1* interacting protein in this study.

Putative GBM specific *MALAT1* interacting proteins were less involved in transcription and mRNA splicing processes compared to putative MB specific and previously proposed *MALAT1* interactors. Higher involvement of putative GBM specific *MALAT1* interacting proteins was observed in EGFR/PI3K signalling and G1/S transition compared to putative MB specific and previously proposed *MALAT1* interactors.

4.2 Investigation of MALAT1s' influence on the phenotype in GBM cell lines

To further investigate the influence of *MALAT1* in GBM tumour biology, stable *MALAT1* KD as well as respective control cell lines generated through a clustered regularly interspaced short palindromic repeats interference, CRISPRi, strategy were employed in phenotype analysis assays.

4.2.1 *MALAT1* expression in GBM cell lines

To identify suitable cell lines for investigation of proteomic signatures influenced by the lncRNA *MALAT1*, its expression in seven established glioblastoma cell lines was analysed via RT-qPCR. A suitable cell line should express a high level of *MALAT1*, be easy to culture as well as transfect, be well established in literature, and represent the broader GBM tumour biology. MALAT1 levels were considered as high if they were in the same range as the employed housekeeper RNA levels.

Measured levels for *MALAT1, GAPDH* and *PGK1* were normalised to a non-template control sample. *GAPDH* and *PGK1* measurements were employed as housekeeper RNA measurements for relative quantification. All measurements were performed in triplicates. Significance was tested under application of Student's t-test. Analysed cell lines LN18, LN229, LN308, T98G, TP365, U251 and U87 represent the diverse mutational landscape and patient backgrounds of glioblastoma [108-113].

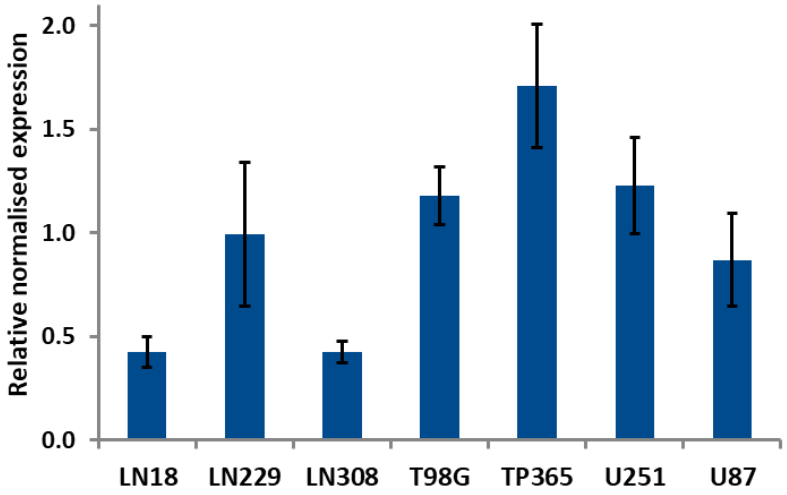

Figure 20 *MALAT1* expression levels in glioblastoma cell lines relative to *PGK1* and *GAPDH* housekeeper RNA levels determined by RT-qPCR (n=3). Measured levels for *MALAT1* were normalised to a non-template control sample. Mean *MALAT1* levels for individual GBM cell lines are depicted relative to measured *GAPDH* and *PGK1* signals in the bar graph. Measurement variance is indicated through error bars. Refer to Table 18 in Appendix B for individual values.

PGK1 was detected with a median CT value of 16.84 (± 0.81) and *GAPDH* with a median CT value of 13.77 (± 0.58) over all analysed cell lines. *MALAT1* was detected with a median CT value of 15.45 (± 0.98) over all analysed cell lines. For the system and primers employed in this analysis, results with CT values under 35 were considered as reliable and quantitative.

MALAT1 expression levels measured were comparable to the levels of analysed housekeeper RNAs, *PGK1* and *GAPDH* (Figure 20 and Table 18). Relative expression values normalised to housekeeper RNA levels measured ranged from 0.42 (± 0.075) for LN18 to 1.71 (± 0.30) for TP365 with respective CT values between 16.64 (± 0.17) and 14.12 (± 0.20).

All analysed GBM cell lines express high levels of MALAT1 and would therefore be suitable for the generation of MALAT1 KD cell lines.

On basis of these results as well as previous knowledge about transfection efficiency, necessary culture conditions, STR profiling (Table 16), and panel sequencing results (Table 20), cell lines LN18, LN229, LN308 and U251 were chosen for further experiments. All four chosen cell lines were grown under the same culture conditions as well as in identical growth medium and culture flasks for adherent cells. They were split under application of the same parameters and detachment agent. The chosen cell lines were comparable in their size and grow as monolayers to high confluency rates. In addition, these four cell lines are according to literature search *IDH*-WT cell lines [114-116] and therefore belong to the same GBM subclass according to the WHO classification [8].

4.2.2 Establishment of *MALAT1* KD cell lines

Stable *MALAT1* KD and respective control cell lines were generated with CRISPRi technology. For the generation of isogenic control cell lines, a population of each respective cell line was transfected with a vector missing a specific guide RNA, gRNA. Three different gRNAs (Table 7) were tested in all four cell lines to identify the gRNA resulting in the strongest *MALAT1* KD (results not shown). One gRNA, gRNA01, consistently yielded the highest *MALAT1* KD efficiency in all four cell lines.

To determine final *MALAT1* KD efficiency in the stable isogenic cell lines generated, RT-qPCR measurements for *MALAT1*, *GAPDH* and *PGK1* were performed in triplicates. *MALAT1* expression levels were normalised to *GAPDH* and *PGK1* acting as housekeeper RNAs. KD efficiency was deduced by *MALAT1* expression level comparison amongst the respective control and KD cell lines in a relative manner (Figure 21).

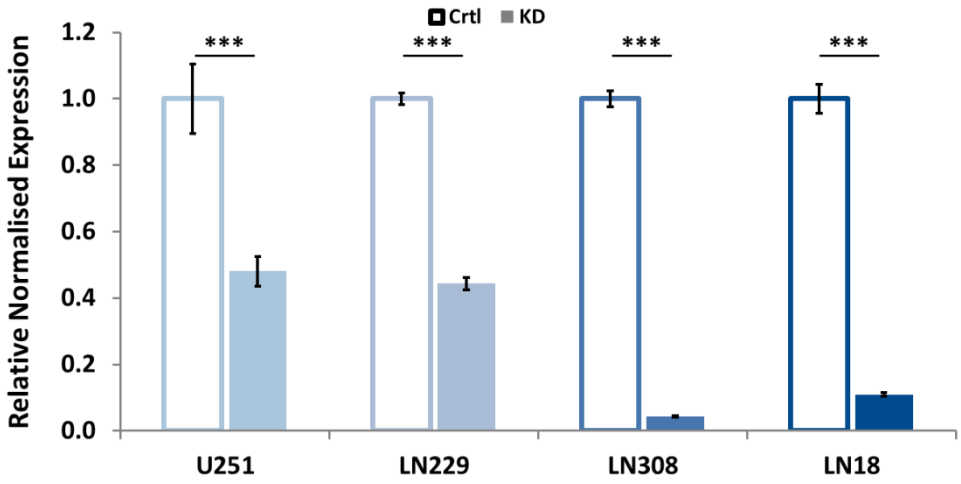

Figure 21 *MALAT1* KD efficiency determined by RT-qPCR of control and respective KD cell lines generated (n=3) normalised to *GAPDH* and *PGK1* levels. All measurements were performed in triplicate. Measured levels for *MALAT1* were normalised to measured *GAPDH* and *PGK1* signals and compared to measured *MALAT1* levels in respective isogenic control cell lines in a relative manner. Two-sided Student's t-test was employed for significance calculation. The bar graph shows individual *MALAT1* levels in isogenic *MALAT1* KD cell lines relative to respective *MALAT1* levels in isogenic control cell lines. Measurement variance is indicated through error bars. Significance levels are indicated through *** for p-values < 0.001. Refer to Table 19 in Appendix B for individual values.

Achieved *MALAT1* KD efficiencies were 52 % in U251, 56 % in LN229, 95 % in LN308 and 89 % in LN18. Reduction in *MALAT1* levels was significant in all four cell line pairs. Significance was tested under application of the two-sided Student's t-test.

Regarding the achieved *MALAT1* KD efficiency, the isogenic cell line pairs based on LN18 and LN308 were chosen for further analysis steps in this thesis.

4.2.3 Phenotypical characterisation of *MALAT1* KD cell lines generated

In previous studies, *MALAT1* has mostly been associated with a migration phenotype [55, 57]. A cancer cell's ability to migrate is directly linked to tumour metastasis, the leading reason for mortality in cancer [117-120]. Abnormal or increased proliferation is an influential aspect of tumour growth and onset of primary tumours [121]. Therefore, *MALAT1*'s influence on cell migration and proliferation was analysed in this study through well-established phenotype assays.

4.2.3.1 Real-time migration analysis of isogenic cell pairs

Real-time migration rate was analysed through a two-chamber XCelligence setup. Cell migration analysis was performed in triplicates for a period of 30 hours of continuous measurements. Respective isogenic cell pairs consisting of control and KD cells were compared on basis of the curves' slope rate and tested for significance under application of a two-sided Student's t-test. The data was baseline corrected against chambers with cell-free media. The two-chamber system chosen for this measurement determines the ability of a cell to migrate towards a chemoattractant, in this case, FBS. The system is set up to mimic tumour cell migration on basis of chemoattractant stimuli in the external matrix [122, 123].

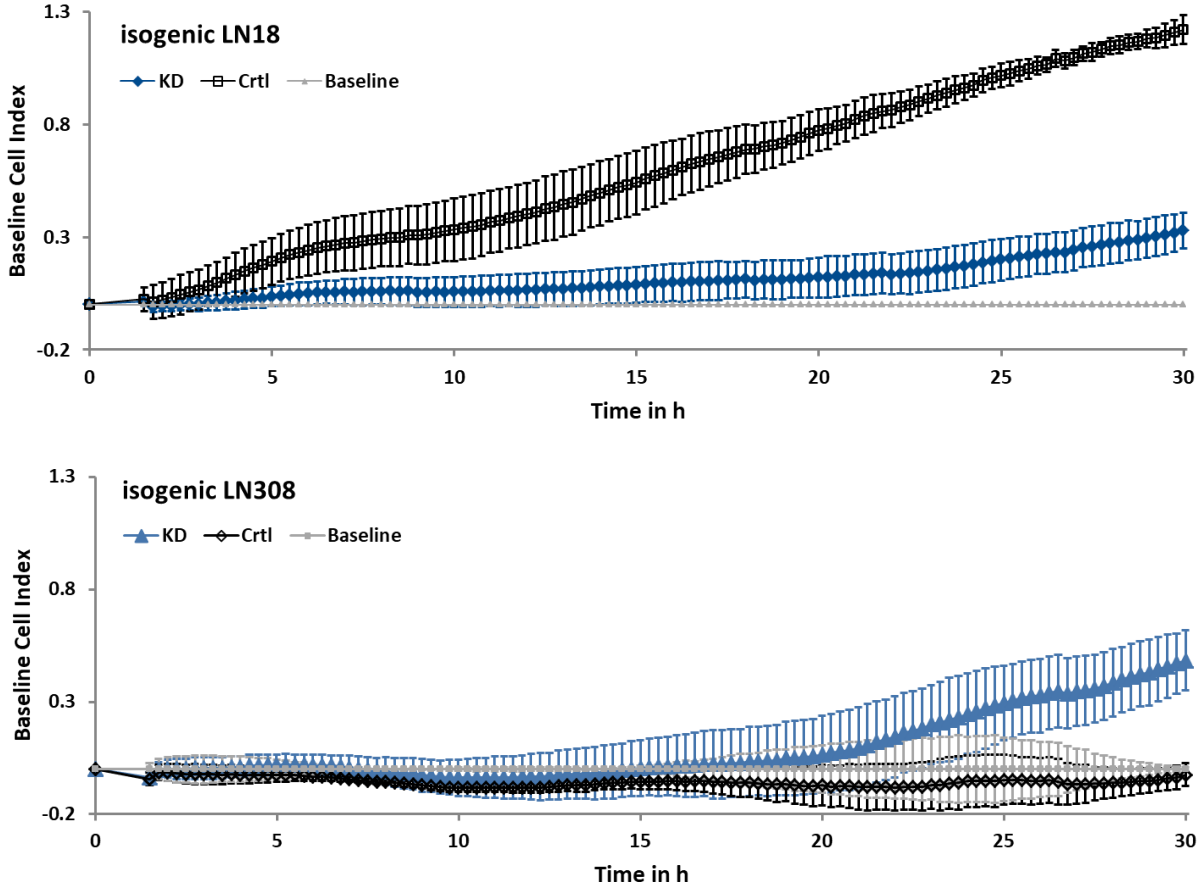

Figure 22 Real-time cell migration analysis of isogenic LN18 and LN308 cell models generated. The scatter plots show the baseline-corrected mean migration rate for the individual cell lines dependant on time. Measurement variance is indicated through error bars. Measurements for isogenic LN18 cell lines are depicted in the top graph with control cells in black and *MALAT1* KD cells in blue. In the bottom plot measurements for isogenic LN308 cell lines are depicted with control cells in black and *MALAT1* KD cells in blue. The baseline is indicated in light grey in both graphs.

Amongst LN18 control and KD cell populations, a distinct migration rate reduction was observed (Figure 22). Median migration rates for LN18 control and *MALAT1* KD cells were measured with 0.038 1/h (± 1.89E-03) and 0.005 1/h (± 1.92E-03), respectively. LN18 *MALAT1* KD cells showed a highly significant (p-value = 6.67E-05) reduction in their measured migration rate. For LN308 control and *MALAT1* KD cells, respective median migration rates of -0.001 1/h (± 1.80E-03) and 0.0148 1/h (± 4.73E-03) were measured. A median migration rate of -0.001 1/h indicates that no cells migrated from the upper to the lower chamber during the monitored timeframe. Comparison of these results indicated a significant (p-value = 0.012) increase in migration rates upon *MALAT1* KD (Figure 22).

In LN18 control, the cells started migrating from the upper to the lower chamber at the beginning of the 30 h incubation time. Respective *MALAT1* KD cells exhibited a delayed migration start at approx. 15 h incubation point. In LN308 *MALAT1* KD the cells did not start to migrate to the lower chamber until approx. 20 hours of the incubation period passed and LN308 control did not show any migrating cells over the whole 30 h time course.

4.2.3.2 Live cell proliferation analysis of isogenic cell pairs

Live cell proliferation analysis was performed through confluency measurement via IncuCyte® live cell analysis imaging system for 120 h. Cell lines were cultured in three separate wells each to obtain triplicate measurements.

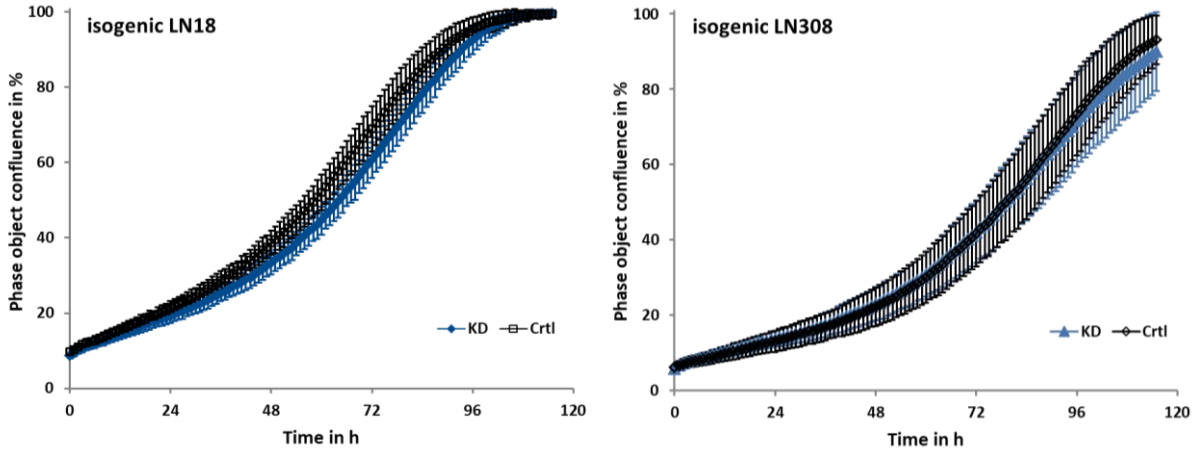

Figure 23 Live-cell proliferation analysis of isogenic LN18 and LN308 control and KD cells. The scatter plots show the mean confluence in percent for the individual cell lines dependant on time. Measurement variance is indicated through error bars. Measurements for isogenic LN18 cell lines are depicted in the left graph with control cells in black and *MALAT1* KD cells in blue. In the right plot measurements for isogenic LN308 cell lines are depicted with control cells in black and *MALAT1* KD cells in blue.

Phase object confluence was measured progressively for 120 h. Comparison of the respective control and *MALAT1* KD cell line pairs was achieved through a curve comparison. Phase object confluence measured was plotted as a percentage against the respective measurement time. Due to triplicate measurements, a standard deviation was calculated and added to each data point obtained.

The resulting curves overlapped in case of both isogenic cell line pairs, showing no significant difference in cellular proliferation rate amongst respective control and *MALAT1* KD cell lines (Figure 23).

4.2.3.3 Doubling time analysis of isogenic cell pairs

Through determination of cell numbers at subsequent time points after seeding, a doubling time was calculated for a given cell line. For the doubling time analysis, only viable cells were considered. The analysis was performed in triplicates.

Respective isogenic cell pairs consisting of control and KD cells were compared on basis of their calculated doubling time and tested for significance under application of a two-sided Student's t-test. LN18 control and *MALAT1* KD cells displayed no significant difference (p-value = 0.734) in their doubling time of 24.41 h (± 2.8) and 23.47 h (± 2.4), respectively. Isogenic *MALAT1* KD cells exhibited a significant (p-value = 5.79E-03) increase in doubling time compared to their control cell line from 25.88 h (± 0.92) for the control cell line to 30.74 h (± 0.89) for the *MALAT1* KD cell line (Figure 24).

With p-values of 0.51 and 0.25 neither the LN18 control cell line nor the LN18 *MALAT1* KD cell line exhibited significantly distinct doubling times compared to LN308 control. In comparison to LN18 control and *MALAT1* KD cell lines doubling time of LN308 *MALAT1* KD was significantly increased with p-values of 0.037 and 0.015, respectively.

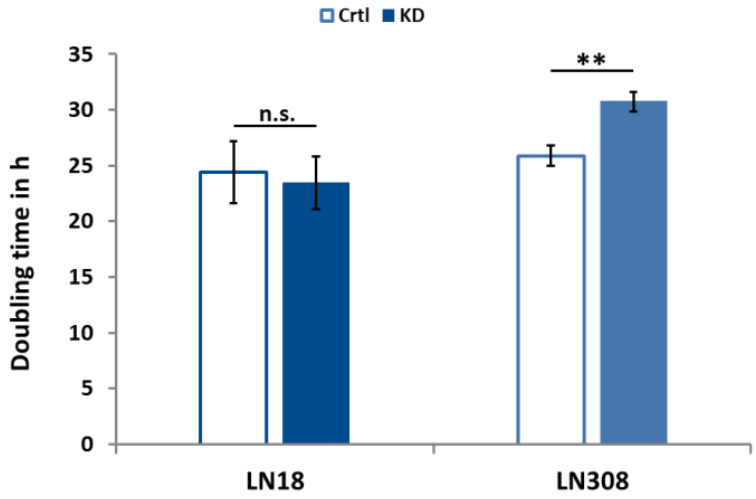

Figure 24 Doubling time analysis of isogenic LN18 and LN308 cell models generated (n=3). The bar graph depicts the calculated doubling time values for the respective isogenic cell lines. For the doubling time analysis, only viable cells were considered in the doubling time calculation performed. Significance was tested under application of a two-sided Student's t-test. Measurement variance is indicated through error bars. Significance levels are indicated through ** for p-values < 0.01 and *** for p-values < 0.001.

Differential migration rates observed in isogenic LN308 cell lines did not relate to a migratory phenotype. Based on the late onset of migration in combination with the doubling time variation observed in isogenic LN308 cell lines, any cell migration measured was due to space restrictions and overpopulating of the upper chamber. However, in isogenic LN18 cell lines, differential migration rates were observed starting at approx. five hours after seeding while no difference in either proliferation rate or doubling time was observed.

4.3 Analysis of *MALAT1* based perturbations in the cellular proteome

Protein based dysregulations in cellular signalling pathways are a common occurrence in cancer cells leading to e.g., aberrant proliferation, increased migration rates or apoptosis resistance [124-127]. Migratory phenotype observed for isogenic LN18 cell lines could have been caused through protein expression changes dependent on *MALAT1* levels. *MALAT1* based perturbations in cellular proteomes were analysed to investigate if *MALAT1* levels influence cellular protein signalling pathways. In this study, cellular proteomes of all four cell lines were determined through a classic bottom-up mass spectrometric approach.

4.3.1 Proteome characterisation isogenic LN18 and LN308 cell lines

For proteome analysis, cell lysates were analysed following a classic bottom-up approach with high-resolution MS readout. Proteome analysis was performed in quintuplicates for LN18 and LN308 isogenic cell line pairs. Absolute quantification of protein amounts per sample was achieved through spike-in peptide mixture of known concentration.

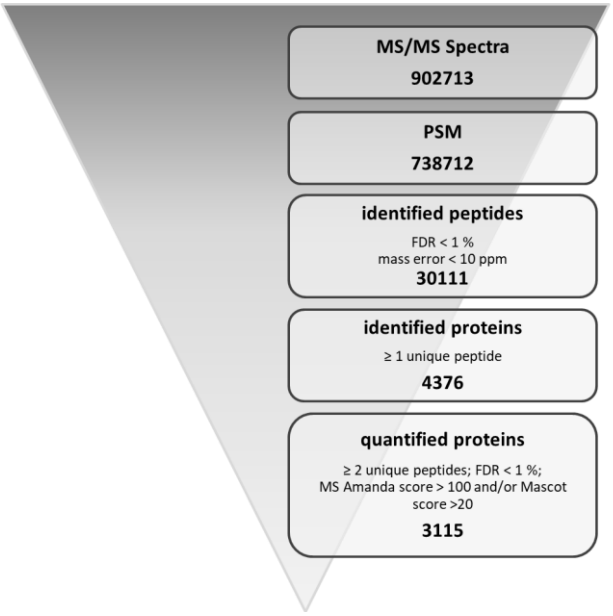

Figure 25 Summary of MS-based proteome data obtained for isogenic LN18 and LN308 cells and respective cut-off values implemented. The chart shows the hierarchical structure and defined cut-off values for each step in the analysis of recorded MS/MS spectra.

Over all 20 samples, 902,713 MS2 spectra were recorded, 738,712 (81.8 %) of which were matched to peptides under application of MS Amanda and Mascot search algorithms. These PSMs lead to the identification of 30,111 peptides implementing a 1 % FDR cut-off at peptide level as well as a mass error cut-off of at most 10 ppm (Figure 25). In total 4,376 proteins were identified and 3,115 were quantified. For identification, at least one unique peptide per protein was necessary while for quantification two unique peptides per protein were required. Peptides were considered for protein quantification if their identification score from MS Amanda or Mascot was at least 100 or 20, respectively. Furthermore, only proteins with a FDR of at most 1 % were quantified. Proteins were quantified in an absolute manner under application of a spike-in peptide mixture and Top5 method.

Overall, this data fit the expectations for standard cell culture-based proteome analysis data under application of the method employed in this work.

4.3.2 Enrichment analysis of proteomic results

Enrichment-interaction analyses of all significant proteins in the isogenic LN18 and LN308 datasets, respectively, were performed via FunRich [128, 129] against a human proteome background. Statistical analysis was performed under application of the hypergeometric Benjamini-Hochberg test.

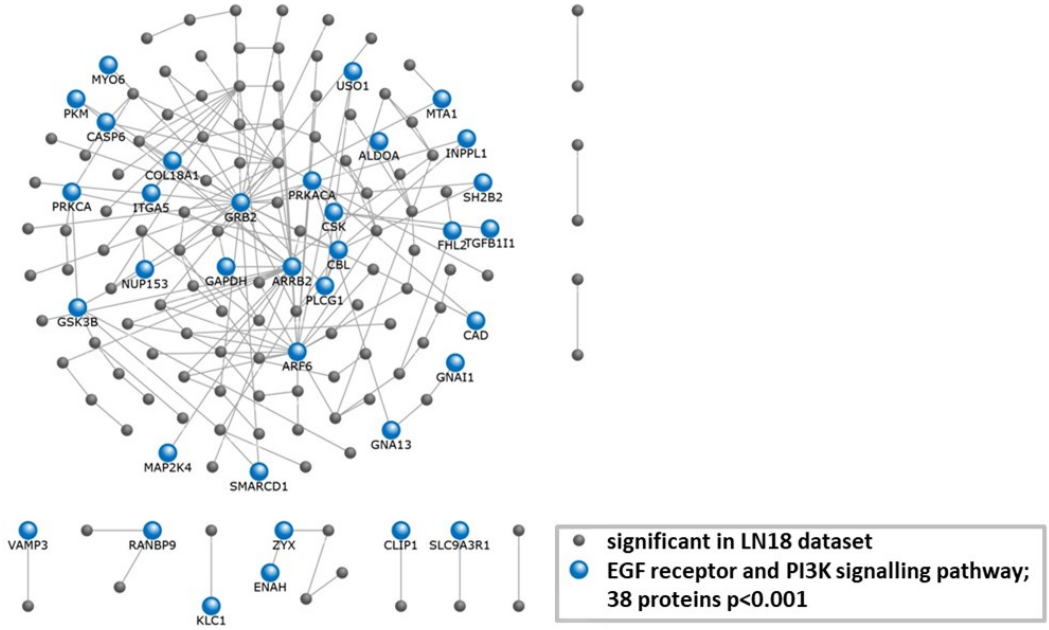

Figure 26 Enrichment Analysis of significant proteins in isogenic LN18 cell lines. Enrichment-interaction analysis performed via FunRich against a human proteome background highlighted 38 proteins in the interaction network with involvement in EGF receptor and PI3K signalling pathways. Statistical analysis was performed under application of the hypergeometric Benjamini-Hochberg test.

Enrichment-interaction analysis in the isogenic LN18 dataset highlighted 38 proteins in the interaction network with involvement in epidermal growth factor, EGF, receptor and PI3K signalling pathways (Figure 26). With these proteins, EGFR and PI3K signalling proteins exhibited significant enrichment with a p-value < 0.001. Deregulation of these pathways is a common occurrence in GBM leading to increased migration, drug resistance e.g. TMZ, and faster proliferation [19, 130].

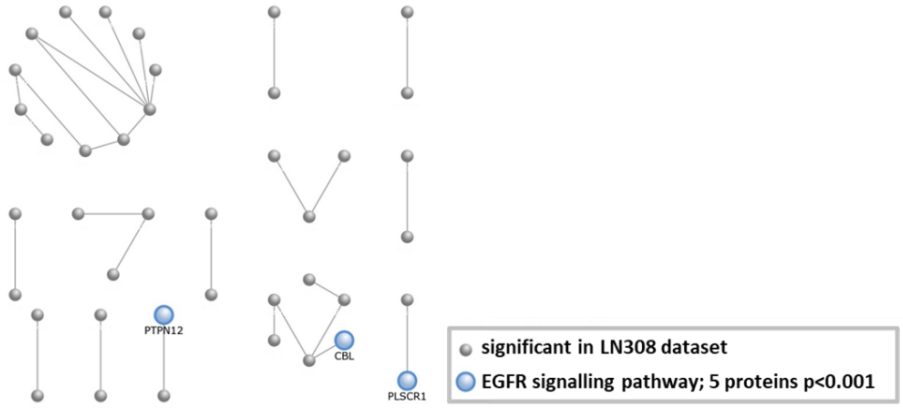

Figure 27 Enrichment Analysis of significant proteins in isogenic LN308 cell lines. Enrichment-interaction analysis performed via FunRich against a human proteome background highlighted 5 proteins in the interaction network with involvement in EGF receptor signalling pathway. Statistical analysis was performed under application of the hypergeometric Benjamini-Hochberg test.

Corresponding analysis in the isogenic LN308 dataset highlighted 5 proteins in the interaction network with involvement in the EGF receptor signalling pathway (Figure 27). With these proteins, EGFR signalling proteins exhibited significant enrichment with a p-value < 0.001.

Enrichment of proteins involved in EGF receptor and PI3K signalling pathways can be linked to the migratory phenotype observed.

4.3.3 Differential analysis LN18 and LN308

Identification of protein level perturbations in relation to *MALAT1* levels was performed through fold change comparison and one-way ANOVA significance testing. Individual isogenic cell line pairs were compared on basis of respective absolute protein amounts in fmol after normalisation. In the volcano plots (Figure 28), negative, decimal logarithmic p-values were plotted against respective binary logarithmic fold changes for each quantified protein. With *MALAT1* being a lncRNA, expected numbers of regulated proteins range from 20 up to 400 (data based on previous studies in-house; not shown here).

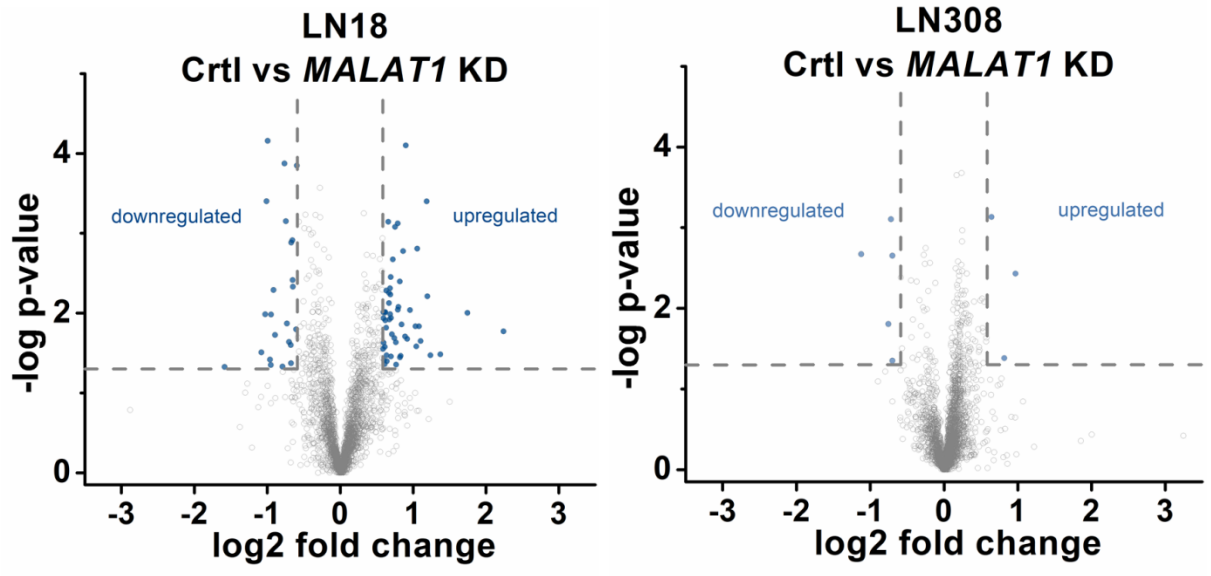

Figure 28 Differential analysis of proteins in isogenic LN18 LN308 cell line pairs. Volcano plots show negative, decimal logarithmic p-values against respective binary logarithmic fold changes for each quantified protein. Dashed lines indicate significance cut-off values chosen in this study, namely a p-value of at most 0.05 (-log(0.05) = 1.301) and a fold change of at least 1.5 (log_2(1.5) = 0.585). One-way ANOVA significance testing was employed to the FC comparison. Negative FC values are employed to indicate a downregulation upon MALAT1 KD while positive FC values are employed to indicate an upregulation upon MALAT1 KD. Significant proteins were highlighted in blue while all other quantified proteins are indicated in grey. The left volcano plot shows the results for isogenic LN18 cell lines while the right one shows results for isogenic LN308 cell lines.

In this study, a p-value of at most 0.05 (-log(0.05) = 1.301) and a fold change of at least 1.5 (log_2(1.5) = 0.585) were chosen as significance and fold change cut-offs, respectively. Proteins were considered as upregulated if their amount in *MALAT1* KD cells was higher compared to control cells and considered as downregulated if their amount in *MALAT1* KD cells was lower compared to control cells.

Both cell line pairs exhibited differentially regulated proteins upon *MALAT1* KD (Figure 28 and Figure 29). The number of differentially regulated proteins was higher in isogenic LN18 compared to isogenic LN308 cell line pairs. Whilst in isogenic LN18 112 proteins exhibited differential regulation, only eight proteins exhibited differential regulation in isogenic LN308.

In isogenic LN18 cell line samples, 83 proteins were significantly upregulated and 29 were significantly downregulated (p-value ≤ 0.05 and FC ≥ 1.5; Figure 29). The highest FC for a significantly upregulated protein was 4.81 for Transcription factor ETV6 (P41212; ETV6). Rho-related GTP-binding protein RhoE (P61587; RND3) exhibited with -2.43 the highest FC for downregulated proteins. A full list of differentially regulated proteins was included in Appendix C Table 21.

In isogenic LN308 cell line samples, three proteins were significantly upregulated and five were significantly downregulated (p-value ≤ 0.05 and FC ≥ 1.5; Figure 29). Amongst those upregulated proteins, the highest FC measured was 1.96 for Tether containing UBX domain for GLUT4 (Q9BZE9; ASPSCR1). In the list of downregulated proteins, Dynein light chain Tctex-type 3 (P51808; DYNLT3) exhibited with -2.18 the highest measured FC. A full list of differentially regulated proteins was included in Appendix C Table 22. In addition, graphs depicting the dynamic range obtained for each respective sample group were added in Figure 58 under Appendix C.

Enrichment analysis performed on basis of the lists of differentially regulated proteins per isogenic cell line pair depicted a distinct enrichment of proteins with an Sp1 transcription factor, Sp1, promoter site. In the isogenic LN18 cell line pair, 59.5 % of all regulated proteins had an Sp1 promoter site. This enrichment was statistically significant with a p-value of 1.41E-06. In the isogenic LN308 cell line pair, proteins with an Sp1 promoter region constituted 62.5 % of all differentially regulated proteins. Although the percentage was comparable to that of the isogenic LN18 cell line pair this enrichment was not statistically significant with a p-value of 0.132.

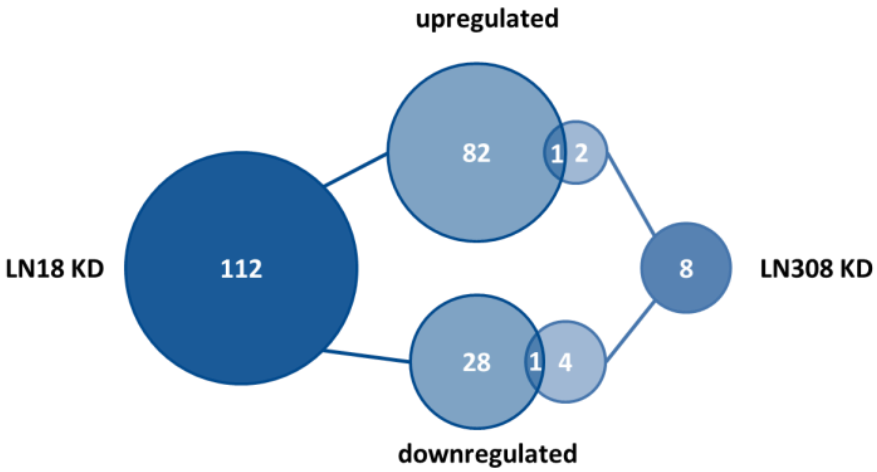

Figure 29 Depiction of overlap between differential proteins from isogenic LN18 and LN308 cell line pairs. VENN-diagram comparing differential proteins from isogenic LN18 and LN308 cell line pairs analysed. In isogenic LN18 cells, 112 proteins exhibited differential regulation upon *MALAT1* KD. In isogenic LN308 cells, eight proteins exhibited differential regulation upon *MALAT1* KD. The following cut-off values were applied p-value ≤ 0.05 and FC ≥ 1.5.

Amongst isogenic LN18 and LN308 cell line pairs only two of the differentially regulated proteins were found in both cell line pairs depicting equal regulation. These were EGF-containing fibulin-like extracellular matrix protein 1 (Q12805; EFEMP1), and Zinc finger protein 10 (P21506; ZNF10). EFEMP1 was downregulated upon *MALAT1* KD while ZNF10 was upregulated upon *MALAT1* KD.

Isogenic cell line pairs generated differed in the number of *MALAT1* expression-based perturbations in the proteome. The number of differentially regulated proteins amongst isogenic LN18 cell lines was 14-fold higher than amongst isogenic LN308 cell lines. While the chosen candidate proteins showed

comparable regulations upon *MALAT1* KD, they were the sum of the general overlap of differentially regulated proteins amongst both cell line pairs.

A literature search was performed for each protein differentially regulated in this proteome analysis. On basis of these search results, several proteins were chosen for further consideration as possible candidate proteins for further validation and consideration in subsequent analyses.

Table 10 Upregulated proteins in isogenic LN18 MALAT1 KD cells chosen for further consideration. Proteins are listed with their UniProt accession, gene name, p-value and FC measured as well as their function described in literature.

Function	Accession	Protein name	ANOVA p-value	FC	source
Transcriptional regulators	P41212	ETV6	4.69E-02	4.81	[131]
	Q9UQR1	ZNF148	1.07E-02	2.05	[132, 133]
	P21506	ZNF10	1.51E-04	1.78	[134, 135]
	Q9H4L7	SMARCAD1	4.89E-02	1.74	[136]
	Q15047	SETDB1	3.35E-02	1.65	[137, 138]
	Q9H9T3	ELP3	4.72E-03	1.62	[139]
	Q96GM5	SMARD1	5.10E-03	1.57	[140]
	Q9UPN9	TRIM33	1.24E-02	1.56	[141, 142]
	Q8NDX5	PHC3	2.44E-02	1.51	[143, 144]
	P56524	HDAC4	2.57E-02	1.51	[145]
Involved in cancer-related signalling cascades	Q9Y6D6	ARFGEF1	2.16E-02	2.06	[146, 147]
	Q9NWT1	PAK1IP1	1.06E-02	1.74	[148]
	O15357	INPPL1	2.25E-02	1.6	[149-151]
	O14492	SH2B2	5.35E-03	1.56	[152]
	O94887	FARP2	3.03E-02	1.56	[153]
	Q8IZ07	ANKRD13A	1.14E-02	1.52	[154]
	P08648	ITGA5	3.69E-02	1.52	[155]
Migratory processes	Q8IZ81	ELMOD2	2.36E-02	2.12	[156, 157]
	Q4L180	FILIP1L	3.42E-02	1.63	[158-160]
	Q9H9T3	ELP3	4.72E-03	1.62	[161]
	Q5VT25	CDC42BPA	6.82E-03	1.56	[162]
Tumour suppressor	Q86X76	NIT1	1.57E-04	1.98	[163, 164]
	Q13635	PTC1	4.21E-02	1.66	[165]
Involved in apoptosis; GBM therapy resistance	Q9BXK5	BCL2L13	2.82E-02	1.53	[166-168]

In Table 10, 23 of the 83 upregulated proteins in isogenic LN18 cell lines were listed with their UniProt accession, gene name, p-value and FC measured as well as their function described in literature. These 23 upregulated proteins were chosen for further validation and consideration based on the literature search performed. Out of those 23 proteins listed, ten proteins act as transcriptional regulators (ETV6, ZNF148, ZNF10, SMARCAD1, SETDB1, ELP3, SMARD1, TRIM33, PHC3, and HDAC4), seven are involved in cancer-related signalling cascades (ARFGEF1, PAK1IP1, INPPL1, SH2B2, FARP2, ANKRD13A, and ITGA5), four are involved in migratory processes (ELMOD2, FILIP1L, ELP3, and CDC42BPA), two are known tumour suppressors (NIT1, and PTC1), and BCL2L13 is involved in apoptosis as well as GBM therapy resistance processes.

Table 11 Downregulated proteins in isogenic LN18 MALAT1 KD cells chosen for further consideration. Proteins are listed with their UniProt accession, gene name, p-value and FC measured as well as their function described in literature.

Function	Accession	Protein Name	ANOVA p-value	FC	source
Migratory processes	P61587	RND3	3.38E-02	-2.43	[169]
	Q12805	EFEMP1	2.30E-05	-2	[170]
	P39060	COL18A1	8.34E-03	-1.86	[171]
	Q9UPQ0	LIMCH1	3.09E-02	-1.73	[172]
	O43294	TGFB1I1	1.60E-02	-1.68	[173]
	P08962	CD63	1.22E-03	-1.57	[174, 175]
	Q13501	SQSTM1	3.42E-02	-1.55	[96, 176]
Involved in cancer-related signalling cascades	Q9NQS7	INCENP	4.50E-02	-2.06	[177-179]
	Q12805	EFEMP1	2.30E-05	-2	[170]
	P39060	COL18A1	8.34E-03	-1.86	[171]
	O43294	TGFB1I1	1.60E-02	-1.68	[173]
	Q8N653	LZTR1	9.82E-03	-1.65	[180, 181]
	P08962	CD63	1.22E-03	-1.57	[174, 175]
previously described MALAT1 interactor	Q96QR8	PURB	7.83E-04	-1.64	[96]
	Q13501	SQSTM1	3.42E-02	-1.55	[96, 176]

In Table 11, nine of the 29 downregulated proteins in isogenic LN18 cell lines were listed with their UniProt accession, gene name, p-value and FC measured as well as their function described in literature. These nine downregulated proteins were chosen for further validation and consideration based on the literature search performed. From those nine proteins seven are involved in migratory processes (RND3, EFEMP1, COL18A1, LIMCH1, TGFB1I1, CD63, and SQSTM1), six are involved in cancer-related signalling pathways (INCENP, EFEMP1, COL18A1, TGFB1I1, LZTR1, and CD63), and two are previously described *MALAT1* interactors (PURB, and SQSTM1).

Table 12 Upregulated proteins in isogenic LN308 MALAT1 KD cells chosen for further consideration. Proteins are listed with their UniProt accession, gene name, p-value and FC measured as well as their function described in literature.

Function	Accession	Protein name	ANOVA p-value	FC	source
Transcriptional regulator	P21506	ZNF10	7.39E-04	1.56	[134, 135]
ASPSCR1–TFE3 fusion oncoprotein	Q9BZE9	ASPSCR1	3.71E-03	1.96	[182]
Involved in DNA repair	Q9NXR7	BABAM2	4.14E-02	1.76	[183]

In Table 12, all three upregulated proteins in isogenic LN308 cell lines were listed with their UniProt accession, gene name, p-value and FC measured as well as their function described in literature. P21506 is a transcriptional repressor, ASPSCR1 acts as oncoprotein if fused to TFE3, and BABAM2 is involved in DNA repair. Of these three, only ZNF10 was differentially regulated amongst isogenic LN18 cell line pairs.

Table 13 Downregulated proteins in isogenic LN308 MALAT1 KD cells chosen for further consideration. Proteins are listed with their UniProt accession, gene name, p-value and FC measured as well as their function described in literature.

Function	Accession	Protein name	ANOVA p-value	FC	source
Promote migration	P51808	DYNLT3	2.13E-03	-2.18	[184, 185]
	Q12805	EFEMP1	1.90E-03	-1.65	[170]
	Q9Y316	MEMO1	7.85E-04	-1.64	[186]
Involved in DNA damage control	Q9BY42	RTF2	1.57E-02	-1.69	[187]
Transcriptional regulator	Q9NZN8	CNOT2	4.47E-02	-1.62	[188]

In Table 13, all five downregulated proteins in isogenic LN308 cell lines were listed with their UniProt accession, gene name, p-value and FC measured as well as their function described in literature. MEMO1 acts as a migratory promoter, DYNLT3 is involved in migratory processes of ovarian cancer cells, EFEMP1 is an EGFR activator promoting migration in GBM, RTF2 is involved in DNA damage control, and CNOT2 acts as a transcriptional regulator. EFEMP1 was the only protein differentially upregulated amongst both isogenic cell line pairs.

All differentially regulated proteins amongst isogenic LN18 cell lines listed in Table 10 and Table 11 were considered as possible candidate proteins while proteins only differentially regulated amongst isogenic LN308 cell lines were not considered.

4.4 High-throughput drug screening

High-throughput drug screening was performed to further investigate *MALAT1s'* role in tumour biology and to determine if its oncogenic function can be influenced through pharmacological intervention. Cell cycle and proliferation analysis were performed to validate obtained results for the inhibitor candidate with the greatest difference in inhibition.

4.4.1 Characterisation of *MALAT1* based drug dependencies

An in-house library of inhibitors with clinical approval was employed in a high-throughput drug screening approach based on cell viability readout. The compounds in this library comprised clinically well-established inhibitors (Appendix D Table 23). The IC_{50} curves generated for isogenic LN18 *MALAT1* KD and their respective control cells were compared for each inhibitor.

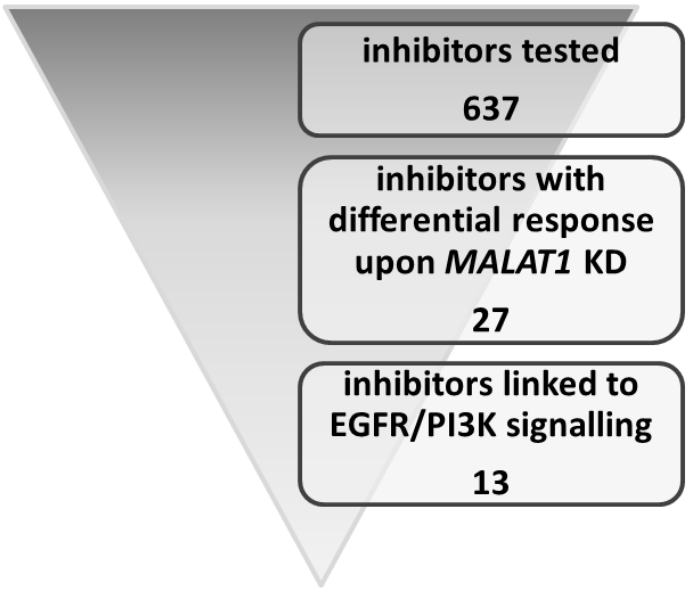

Figure 30 Summary of high-throughput drug screening results in isogenic LN18 cell lines. The chart shows the hierarchical structure and results of the performed screen.

Out of the tested 641 inhibitors, 27 inhibitors exhibited a differential dose-response amongst isogenic LN18 *MALAT1* KD and control cells (Figure 30). Inhibitors linked to EGFR/PI3K signalling pathway represent the majority with 13 different inhibitors [189-195]. Five inhibitors are implicated in tumour growth [195-198] and DNA replication/transcription processes [195], respectively. Three inhibitors are linked to protein degradation [195] and one is implicated in redox signalling pathways [199].

Amongst the 13 inhibitors linked to EGFR/PI3K signalling, ZSTK474 exhibited the strongest difference between isogenic LN18 *MALAT1* KD and respective control cells (Figure 31).

The chemotherapeutic agent TMZ standard of care in GBM was also tested in this HT screen. No difference in the inhibition of the tested isogenic LN18 cell lines was observed. According to literature LN18 cells are TMZ resistant while LN308 cells are TMZ sensitive [5, 200].

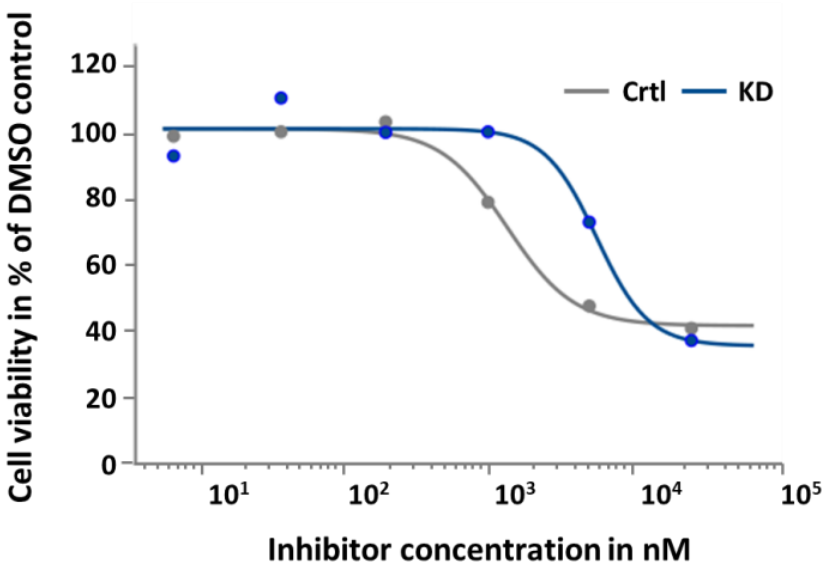

Figure 31 *MALAT1*-expression based differences in ZSTK474 efficacy in isogenic LN18 cell lines. The scatter plot depicts the cell viability normalised to the DMSO control measured as a percentage dependant of the inhibitor concentration in isogenic LN18 cell lines. Results for *MALAT1* KD cells are depicted in blue and results for control cells are depicted in grey. Respective curves were fitted under application of a sigmoidal fit.

Dose-response curves were fitted under application of a sigmoidal function for individual results of isogenic LN18 *MALAT1* KD and respective control cells. The coefficient of determination, R^2, indicated a high accuracy for the obtained curve fit for results obtained with the inhibitor ZSTK474 with values of 0.96 and 0.99 for isogenic LN18 *MALAT1* KD and control cells, respectively (Figure 31). With a value of 5106 nM, the calculated IC_{50} for ZSTK474 in LN18 *MALAT1* KD cells was considerably higher than the calculated IC_{50} for ZSTK474 in LN18 control cells with a value of 1144 nM.

ZSTK474, a PI3K inhibitor, appeared to be an interesting candidate inhibitor for further analysis. Due to the number of tested inhibitors this analysis was not performed in triplicates, therefore, no significance can be calculated. The results obtained have to be verified under application of orthogonal methods or repeat measurements.

4.4.2 Verification of *MALAT1* expression-based difference in response to ZSTK474 via cell cycle

Since treatment with ZSTK474 in various cancer-associated cell lines has been described to result in G0/G1 cell cycle arrest in previous studies [201, 202], cell cycle analysis was employed to verify results obtained for ZSTK474 by the high-throughput drug screening in this study.

Isogenic LN18 and LN308 *MALAT1* KD cells as well as their respective control cells were treated with 4 µM ZSTK474 and DMSO as control previous to cell cycle analysis based on flow cytometric measurements of propidium iodide staining. The analysis was performed in triplicate and significance was tested under application of Student's T-test and two-way ANOVA.

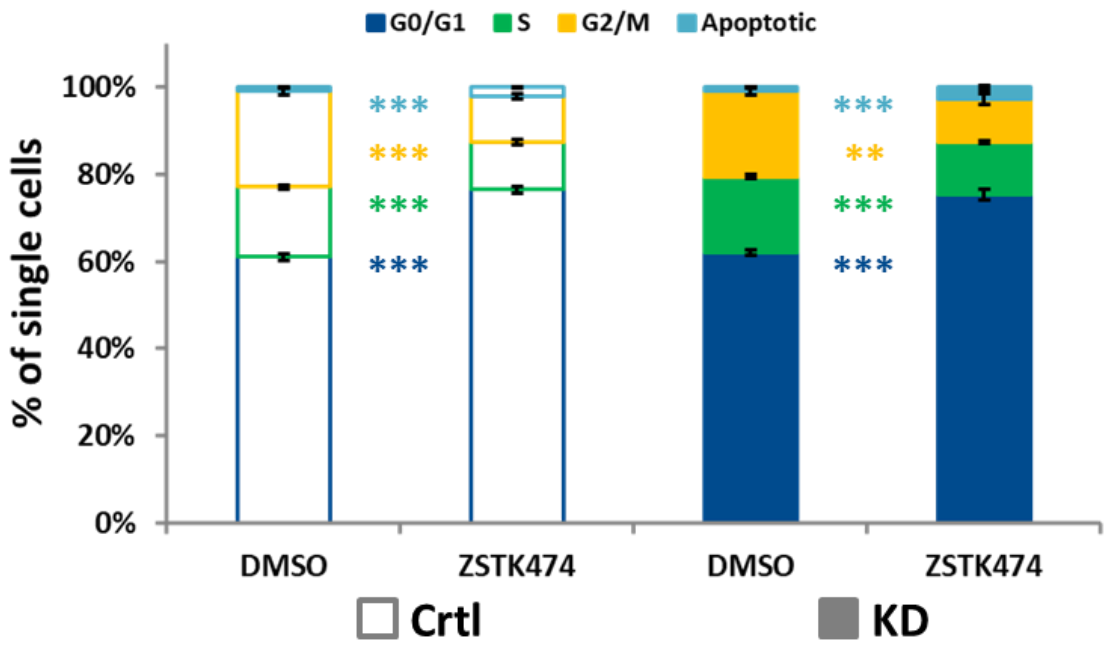

Figure 32 Cell cycle analysis of isogenic LN18 cell lines with and without ZSTK474 treatment (4 µM; n=3). The bar graphs depict the percentage of single cells respective of their cell cycle stage for each isogenic LN18 cell line treated with either DMSO or 4 µM ZSTK474. Control cells are depicted as unfilled bars and *MALAT1* KD cells as filled bars. Cell cycle phases are indicated through different colours with dark blue representing cells in G0/G1-phase, green representing cells in S-phase, yellow representing cells in G2/M-phase and light blue representing apoptotic cells. Measurement variance is indicated through error bars. Student's t-test significance levels are indicated through with ** for p-values < 0.01, and *** for p-values < 0.001.

Measured distribution values for G0/G1-phase in isogenic LN18 *MALAT1* KD, as well as control cells of 61.93 % (±0.84) and 75.30 % (±2.59) as well as 60.83 % (±0.81) and 76.34 % (±0.82), treated with DMSO and ZSTK474, respectively, exhibited a highly significant increase with respective p-values of 4.72E-04 and 4.53E-05. In isogenic LN18 control cells, the percentage of apoptotic cells significantly increased from 0.85 % (±0.01) to 2.10 % (±0.18) upon ZSTK treatment with a p-value of 5.88E-04 while in isogenic LN18 *MALAT1* KD cells the percentage of apoptotic cells significantly increased from 0.84 % (±0.07) to 2.59 % (±0.46) with a p-value of 6.12E-03. Distribution values measured for S-phase in isogenic LN18 MALAT1 KD, as well as control cells of 17.42 % (±0.53) and 12.03 % (±0.26) as well as 16.03 % (±0.43) and 10.96 % (±0.47), treated with DMSO and ZSTK474, respectively, exhibited highly significant deregulation with p-values of 2.08E-04 and 3.55E-04. In isogenic LN18 control cells, the percentage of cells in G2/M-phase significantly decreased from 21.97 % (±0.74) to 10.45 % (±0.50) upon ZSTK treatment with a p-value of 5.42E-05 while in isogenic LN18 *MALAT1* KD cells the percentage of cells in G2/M-phase significantly decreased from 19.59 % (±1.02) to 9.97 % (±1.30) with a p-value of 1.18E-03 (Figure 32).

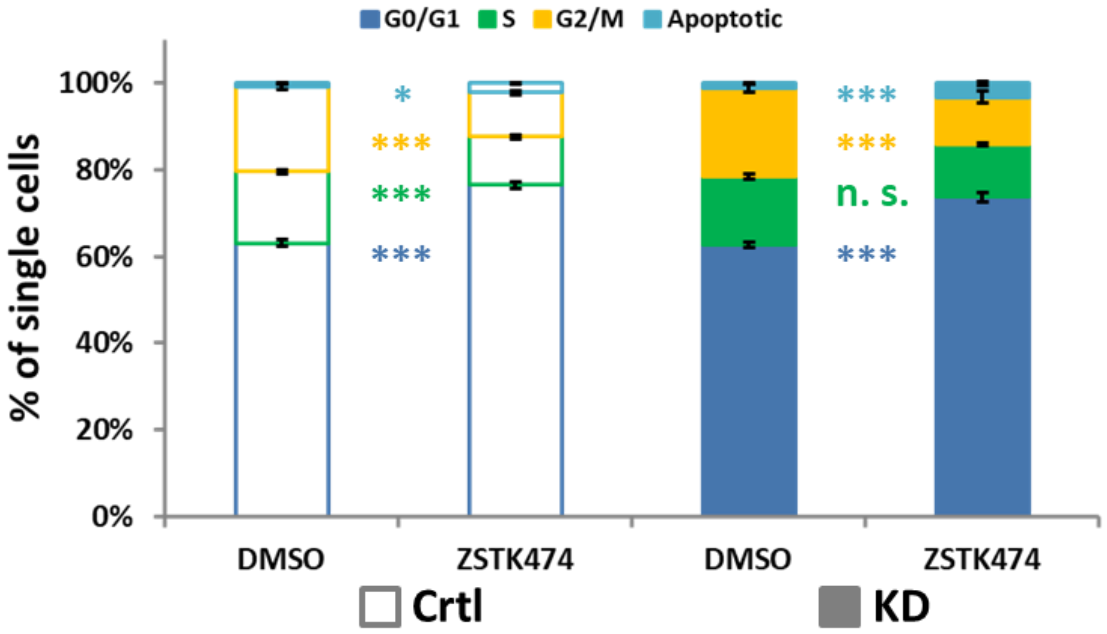

Figure 33 Cell cycle analysis of isogenic LN308 cell lines with and without ZSTK474 treatment (4 µM; n=3). The bar graphs depict the percentage of single cells respective of their cell cycle stage for each isogenic LN18 and LN308 cell line treated with either DMSO or 4 µM ZSTK474. Control cells are depicted as unfilled bars and *MALAT1* KD cells as filled bars. Cell cycle phases are indicated through different colours with blue representing cells in G0/G1-phase, green representing cells in S-phase, yellow representing cells in G2/M-phase and light blue representing apoptotic cells. Measurement variance is indicated through error bars. Student's t-test significance levels are indicated through with * for p-values < 0.05, and *** for p-values < 0.001.

Distribution values measured for G0/G1-phase in isogenic LN308 *MALAT1* KD as well as control cells of 62.38 % (±2.22) and 73.60 % (±1.12) as well as 62.93 % (±0.64) and 76.43 % (±1.55) either treated with DMSO and ZSTK474, respectively, resulted in p-values of 3.11E-03 and 3.38E-04 (Figure 33). The number of cells in G0/G1 phase exhibited highly significant increase upon ZSTK474 treatment. In isogenic LN308 control cells, the percentage of apoptotic cells significantly increased from 0.80 % (±0.04) to 2.16 % (±0.57) upon ZSTK treatment resulting in a p-value of 2.80E-02 while in isogenic LN308 *MALAT1* KD cells the percentage of apoptotic cells significantly increased from 1.08 % (±0.11) to 3.20 % (±0.37) resulting in a p-value of 1.44E-03. Measured distribution values for S-phase in isogenic LN308 *MALAT1* KD as well as control cells of 15.66 % (±2.20) and 12.21 % (±0.97) as well as 16.50 % (±0.30) and 11.17 % (±0.13) treated with DMSO and ZSTK474, respectively, resulted in p-values of 1.13E-01 and 2.08E-05. Cells measured in S-phase exhibited a significant downregulation in isogenic LN308 control cells only. In isogenic LN308 control cells, the percentage of cells in G2/M-phase decreased significantly from 19.59 % (±0.56) to 10.15 % (±0.93) upon ZSTK treatment resulting in a p-value of 2.49E-04 while in isogenic LN308 *MALAT1* KD cells the percentage of cells in G2/M-phase decreased significantly from 20.38 % (±0.26) to 10.86 % (±1.81) resulting in a p-value of 1.79E-03.

Treatment with ZSTK474 influenced the cell cycle in all four analysed cell lines (Figure 32 and Figure 33) corroborating the data obtained from the high-throughput drug screening.

Isogenic LN18 *MALAT1* KD, respective LN18 control and LN308 isogenic control cells exhibited a highly significant increase of cells in G0/G1-phase and apoptotic cells as well as a highly significant decrease of cells in S- and G2/M-phase upon ZSTK474 treatment. Isogenic LN308 *MALAT* KD cells also exhibited a highly significant increase of cells in G0/G1- phase and apoptotic cells as well as a highly significant

decrease of cells in G2/M- phase upon ZSTK474 treatment while the decrease of cells in S-phase was not significant.

Comparison of results obtained for control versus *MALAT1* KD cells exhibited equal distribution of cells throughout the cell cycle with three exceptions. A significant increase of cells in S-phase amongst isogenic LN18 control and *MALAT1* KD cells from 16.03 % (±0.43) to 17.42 % (±0.53) upon DMSO treatment resulted in a p-value of 4.43E-02 and from 10.96 % (±0.47) to 12.02 % (±0.26) upon ZSTK474 treatment resulted in a p-value of 4.83E-02. In addition, a significant increase of apoptotic cells from 0.80 % (±0.04) to 1.08 % (±0.11) upon DMSO treatment resulted in a p-value of 3.04E-02 in isogenic LN308 control versus *MALAT1* KD cells.

Under application of the two way ANOVA significance test, an interactive effect in the isogenic LN18 cell line pair for *MALAT1* KD and ZSTK474 treatment was observed with a p-value of 2.85E-02 for the observed increase of cells in G0/G1-phase. This highlighted a possible interplay between biological pathways influenced by *MALAT1* and biological pathways affected by ZSTK474 treatment in LN18 cells while in LN308 cells there appears to be no interplay between the two. Since ZSTK474 is a PI3K inhibitor and proteins involved in this pathway were enriched in the proteome analysis in isogenic LN18 but not in isogenic LN308, this data is in line with previous results obtained in this study.

The analysis of the four tested cell lines confirmed a treatment effect for ZSTK474 on the cell cycle leading to an arrest in G0/G1-phase. The treatment efficacy was significantly lower in isogenic LN18 MALAT1 KD cells compared to their respective control cells. Results obtained under application of the two-way ANOVA highlighted the involvement of *MALAT1* in PI3K linked signalling in a cell line dependent manner.

4.4.3 Validation of inhibitor of interest through proliferation analysis

As a second orthogonal verification strategy, real-time proliferation analysis was performed for isogenic LN18 and LN308 cell line pairs upon DMSO and ZSTK474 treatment.

Real-time proliferation rate was analysed through a one chamber XCelligence setup. The measurement was performed in triplicates over 70 hours and Student's T-test was employed to calculate statistical significance. Chamber wells containing cell-free media suspensions with either DMSO or inhibitor were employed as baseline measurement.

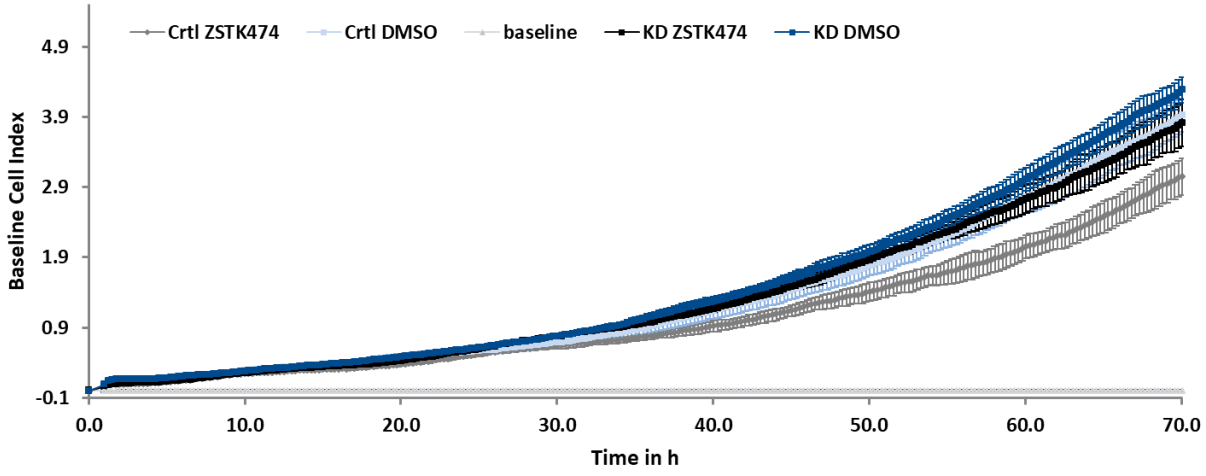

Figure 34 Real-time cell proliferation analysis of isogenic LN18 cell lines treated with ZSTK474 and DMSO. The scatter plot shows the baseline-corrected mean proliferation rate for the individual cell lines dependant on time. Measurement variance is indicated through error bars. Measurements for isogenic LN18 control cells treated with DMSO are depicted in light blue, measurements for isogenic LN18 control cells treated with ZSTK474 are depicted in dark grey, measurements for isogenic LN18 *MALAT1* KD cells treated with DMSO are depicted in dark blue, and measurements for isogenic LN18 *MALAT1* KD cells treated with ZSTK474 are depicted in black. The baseline is indicated in light grey.

In isogenic LN18 *MALAT1* KD and respective control cells treated with either DMSO as control or ZSTK474, real-time proliferation curves exhibited a high level of overlap except for LN18 control cells treated with ZSTK474 (Figure 34). Median proliferation rates for LN18 control cells upon DMSO and ZSTK474 treatment were measured with 0.050 1/h (± 3.04E-03) and 0.038 1/h (± 2.45E-03), respectively. Isogenic LN18 control cells showed a significant (p-value = 3.43E-02) reduction in their measured proliferation rate upon ZSTK474 treatment. Isogenic LN18 *MALAT1* KD cells exhibited no significant (p-value = 1.32E-01) difference in their proliferation rate upon ZSTK474 treatment with respective proliferation rate values of 0.056 1/h (±2.33E-03) and 0.051 1/h (±3.18E-03) for DMSO and ZSTK474 treated cells.

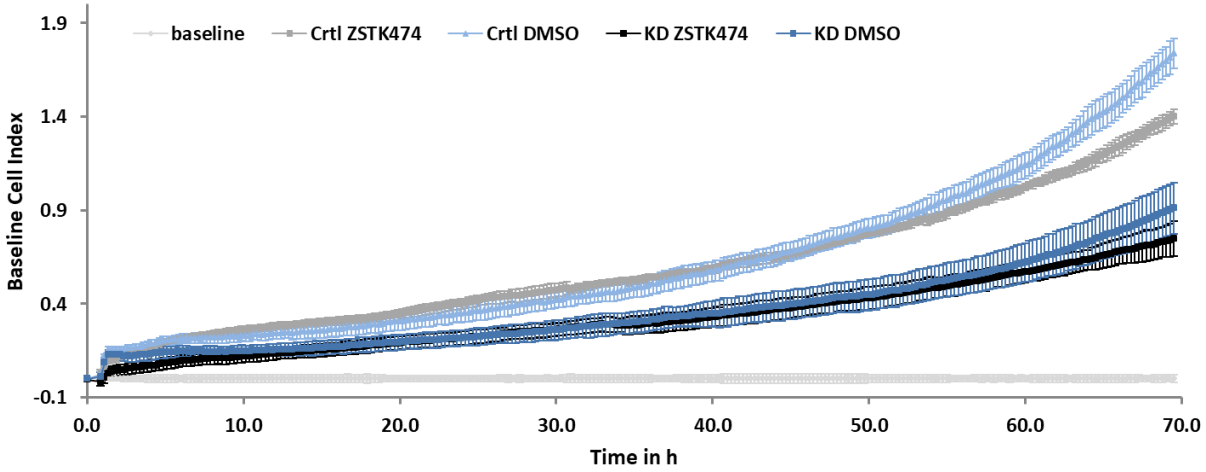

Figure 35 Real-time cell proliferation analysis of isogenic LN308 cell lines treated with ZSTK474 and DMSO. The scatter plot shows the baseline-corrected mean proliferation rate for the individual cell lines dependant on time. Measurement variance is indicated through error bars. Measurements for isogenic LN308 control cells treated with DMSO are depicted in light blue, measurements for isogenic LN308 control cells treated with ZSTK474 are depicted in dark grey, measurements for isogenic LN308 *MALAT1* KD cells treated with DMSO are depicted in dark blue, and measurements for isogenic LN18 *MALAT1* KD cells treated with ZSTK474 are depicted in black. The baseline is indicated in light grey.

For LN308 control cells upon DMSO and ZSTK474 treatment respective median migration rate values of 0.020 1/h (±7.87E-04) and 0.016 1/h (±5.10E-04) were measured (Figure 35). Comparison of these results indicated a significant (p-value = 7.62E-03) reduction in proliferation rates upon ZSTK474 treatment. Median proliferation rates for isogenic LN308 *MALAT1* KD cells exhibited no significant (p-value = 5.06E-01) difference upon treatment with respective proliferation rate values of 0.010 1/h (±1.28E-03) and 0.009 1/h (±6.13E-03) for DMSO and ZSTK474 treated cells.

The discrepancy with previous proliferation rate results in this study could be based on the different methods applied in the proliferation measurement. The previous analysis was performed based on phase confluency measurements while this analysis is based on impedance measurements. The confluency measurement is dependent on the contrast of the images obtained and the successful establishment of a confluency mask. In this study, one confluency mask was employed for all four cell lines which might have led to incorrect confluency measurements. In addition, the cell monolayer in

the images contained a high number of not clearly defined cell wall structures. In contrast, the impedance measurement performed in this analysis is not reliant on image contrast, it is not necessary to establish a mask and the values obtained were baseline corrected. Overall, the data from this proliferation analysis was considered as correct based on the measurement method and the corroboration of the doubling time results.

Obtained proliferation data corroborates the finding that treatment with the PI3K inhibitor, ZSTK474, appears to be more effective in cells with higher *MALAT1* levels.

4.5 Proteome and *MALAT1* interactome interplay

The datasets obtained in this study from the high-throughput drug screening, the differential proteome analysis amongst *MALAT1* KD and control cell lines, as well as from the *MALAT1* interactome study in GBM and MB associated cell lines were analysed to identify possible correlations. This analysis was substantiated through a literature search employed to further the understanding of *MALAT1*s' role in GBM.

All results obtained in this study so far highlight MALAT1 as an influencing factor in EGFR/PI3K signalling events. All further validation experiments focus on this hypothesis intending to unravel the biological events responsible for the observed migratory phenotype.

4.5.1 In-depth analysis of proteins for further validation

Protein candidate selection was performed under consideration of their function as it was described in the literature, observed phenotype in this study, and interaction data from the literature.

Under consideration of *MALAT1* centric pulldown data, the data obtained through the mass spectrometric proteome investigation of *MALAT1* KD cell lines and their respective controls, as well as the results from the phenotype investigation of the MALAT1 KD cell lines generated, the proteins Histone H3.3 (H3F3A; P84243), Transcription intermediary factor 1-beta (TRIM28; Q13263), Proliferating cell nuclear antigen (PCNA; P12004), EGF-containing fibulin-like extracellular matrix protein 1 (EFEMP1; Q12805), and Zinc finger protein 10 (ZNF10; P21506), were chosen as proteins of interest in this study (Figure 36, Figure 37, Figure 38, Figure 39, and Figure 41).

H3F3A (P84243) is a known transcriptional regulator [203, 204] and negative transcriptional regulation of tumour suppressor genes through interaction with *MALAT1* has been described by Stamato *et al.* [205].

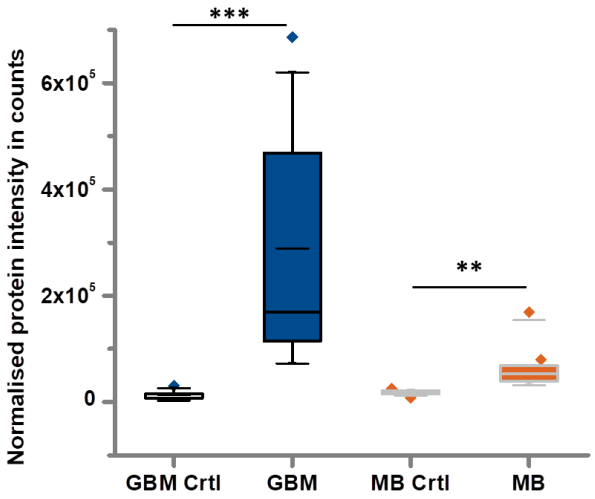

Figure 36 MS data recorded for H3F3A in consolidated RNA-centric pulldown non-RNA binding and *MALAT1*-specific samples. The boxplot depicts the normalised protein intensity in counts on the y-axis for each sample per sample group. Significance levels are indicated through ** for p-values < 0.01, and *** for p-values < 0.001.

In the GBM associated affinity enrichment sample set, H3F3A was significantly enriched with a FC of 20.85 and a p-value of 7.48E-04 (Figure 36). It was identified and quantified on basis of two unique peptides, respectively. Identification scores for H3F3A from Mascot and MSAmanda were with 783 and 15578, respectively, well above individually set thresholds of 20 and 100. In total, 199 PSMs were

obtained resulting in coverage of 49 % with the identified peptides spaced over the whole protein sequence.

The *MALAT1* protein interactome study depicted a significant binding of H3F3A to the *MALAT1*-specific DNA probes employed in both GBM and MB associated datasets. H3F3A has been linked to tumorigenesis through specific mutations as well as aberrant PTM states. Mutations in H3F3A were first identified and linked to tumorigenesis in paediatric tumours but recent studies show these mutations also occur in adult gliomas [206, 207]. These mutations lead to deregulation of chromatin which results in transcriptional changes. While further investigations are necessary to understand the full impact of these mutations, it has been shown that the known mutations K27M and K36M influence the methylation status of H3K36 resulting in transcriptional variations [206]. Even without a mutation in H3F3A in the chosen cell lines, aberrant methylation profiles are possible and would lead to the same perturbations in cell biological processes. West *et al.* have shown that *MALAT1* associates with active chromatin sites such as H3K36me3 [208] depicting a possible link between *MALAT1*-protein interactions and the proteins methylation status. In addition, H3F3A has been linked to DNA damage repair [209] as well as aberrations in this process leading to tumorigenesis. In this study, no mutation could be identified in the H3F3A protein but the identified peptides in the initial search were all located from the middle towards the C-terminal end of the amino acid chain while the mentioned mutation sides are located on the N-terminal side. Since none of the employed cell lines has been described as carrying a mutation in H3F3A no search directly allowing these was performed in this study. Even so, H3F3A was chosen as a protein of interest due to its distinct enrichment with *MALAT1*-specific DNA probes and its underlying biological relevance.

TRIM28 (Q13263) is a transcription factor known to interact with ZNF10, SETDB1 and H3F3A to suppress transcription [135, 137, 210-212] and has been shown to promote metastasis in breast cancer cells [213] as well as lung adenocarcinoma [214]. Next to TRIM28, ZNF10, and H3F3A which have been selected as proteins of further interest in this study, SETDB1 is also significantly upregulated in LN18 *MALAT1* KD cell samples compared to their respective control with a FC of 1.65 and an ANOVA p-value of 3.35E-02 (Table 10) underlining the selection of TRIM28.

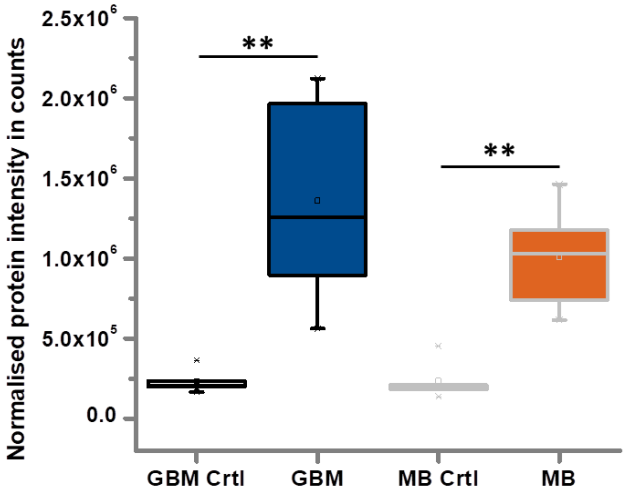

Figure 37 TRIM28 MS data recorded in consolidated RNA-centric pulldown non-RNA binding and *MALAT1*-specific samples. The boxplot depicts the normalised protein intensity in counts on the y-axis for each sample per sample group. Significance levels are indicated with ** for p-values < 0.01.

TRIM28 was significantly enriched with a FC of 5.83 and a p-value of 3.26E-04 in the GBM associated affinity enrichment sample set (Figure 37). It was identified and quantified on basis of twelve unique peptides. Identification scores for TRIM28 from Mascot and MSAmanda were with 1458 and 24985, respectively, well above individually set thresholds of 20 and 100. In total, 238 PSMs were obtained resulting in coverage of 22 % with the identified peptides spaced over the whole protein sequence.

This protein is involved in DNA damage-induced cell cycle checkpoints regulating progression from G1- to S-phase through interaction with p21 [215]. TRIM28 was identified as a potential *MALAT1* interacting protein in GBM and MB associated samples during this study and its interactors ZNF10 as well as SETDB1 (Q15047) were found to be upregulated upon *MALAT1* KD in the isogenic LN18 based sample set. In the isogenic LN308 based sample set only ZNF10 was found to be significantly upregulated while SETDB1 depicted no significant change in expression.

PCNA (P12004) is involved in both biological pathways exclusively depicting a significant enrichment in the GBM associated sample set, EGFR/PI3K signalling [105, 106] as well as G1/S transition [107].

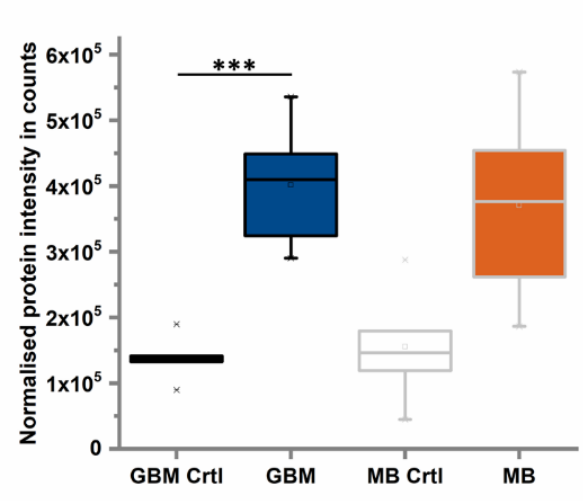

Figure 38 PCNA MS data recorded in consolidated RNA-centric pulldown non-RNA binding and *MALAT1*-specific samples. The boxplot depicts the normalised protein intensity in counts on the y-axis for each sample per sample group. Significance levels are indicated with *** for p-values < 0.001.

PCNA was identified as a putative *MALAT1* interacting protein in the GBM associated dataset of this study. In the MB associated dataset, this protein showed no enrichment with the *MALAT1* specific DNA probes. This discrepancy was regarded with great interest since it could be employed to identify tumour specific *MALAT1* interactions. As was seen in the enrichment study of *MALAT1* interacting proteins exclusively identified in one of the tumour-specific datasets from this study or the collective set of previously proposed interactors, *MALAT1* appeared to be involved in diverse biological pathways dependent on the tumour entity. In the GBM associated affinity enrichment sample set, PCNA was significantly enriched with a FC of 2.91 and a p-value of 1.74E-04 (Figure 38). It was identified and quantified on basis of two unique peptides, respectively. Identification scores for PCNA from Mascot and MSAmanda were with 256 and 8055, respectively, well above individually set thresholds of 20 and 100. In total, 86 PSMs were obtained resulting in coverage of 8 %. Identified peptides were located on the middle and c-terminal side of the protein sequence.

Release of PCNA from p21 by AKT results in cell cycle progression from G1- to S-phase [216] and according to Olaisen *et al.* PCNA is able to bind to NF1 and alter its activity in the EGFR/PI3K signalling cascade [105]. Both pathways have been linked to *MALAT1* in GBM during this study through the interactomics, proteomics and HT drug screening analyses. Furthermore, PCNA has been shown to bind to chromatin and is activated through phosphorylation by nuclear EGFR [107]. Silencing of PCNA in the lung cancer cell line A549 through miR-204 resulted in inhibition of cell proliferation and migration [217] and *MALAT1* has been previously described to act as a miRNA sponge in regards to miR-204 decreasing its functionality and promoting proliferation and migration [218-220]. These links to migrational behaviour fit with the decreased migration observed for isogenic LN18 *MALAT1* KD cells compared to their respective control. Under consideration of the combined data obtained in this study, PCNA appears to be a protein of interest for understanding *MALAT1* based perturbations in GBM biology.

EFEMP1 (Q12805) also known as fibulin-3 has been shown to compete with EGF for EGFR binding. This binding can activate autophosphorylation of EGFR initiating downstream signalling events on the AKT and MAPK axis leading to increased migration rates [15]. EFEMP1 is highly upregulated in malignant gliomas leading to increased cell motility and invasion [170]. Transcription of EFEMP1 is regulated through three Sp1 and one oestrogen response element-binding sites [221].

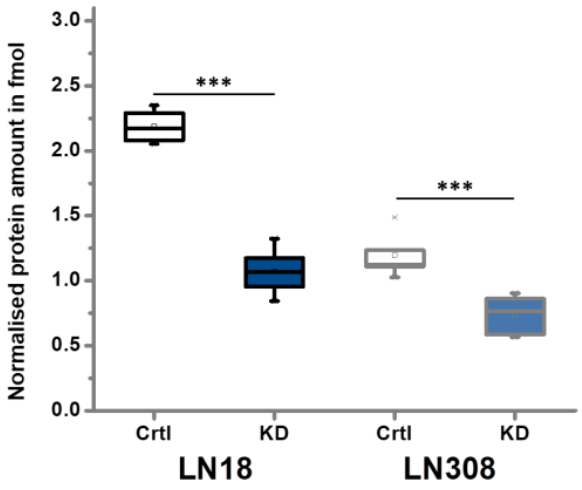

Figure 39 EFEMP1 MS data recorded in isogenic LN18 and LN308 cell line pairs. The boxplot depicts the normalised protein amount in fmol on the y-axis for each sample per sample group. Significance levels are indicated through *** for p-values < 0.001.

EFEMP1 was the most significant downregulated protein amongst isogenic LN18 cell lines with a p-value and FC of 2.3E-05 and -2.00, respectively (Figure 39). It was identified and quantified on basis of six and five unique peptides, respectively. Identification scores for EFEMP1 from Mascot and MSAmanda were with 1078 and 16137, respectively, well above individually set thresholds of 20 and 100. In total, 122 PSMs were obtained resulting in coverage of 18 % with the identified peptides spaced over the whole protein sequence.

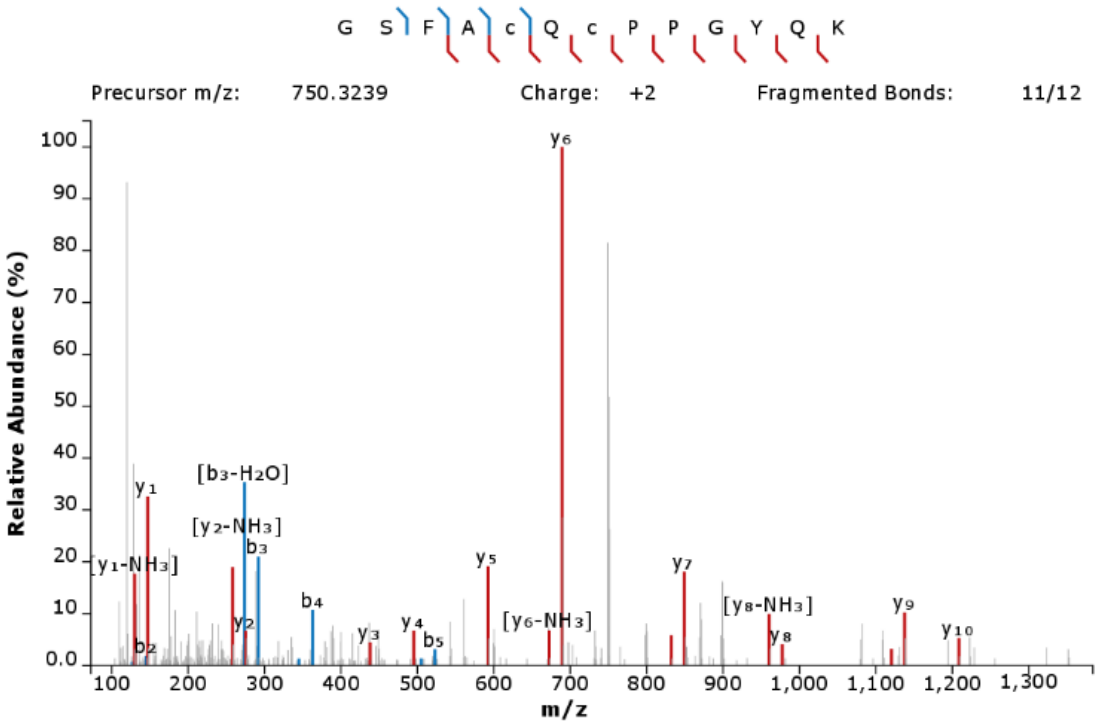

Figure 40 EFEMP1 peptide fragment match spectra. The mass spectrum on the right depicts the recorded mass spectrum matched to theoretical m/z values for the peptide GSFACQCPPGYQK employed in its identification. Recorded m/z values consistent with respective theoretical values for y-ions are highlighted in red while the ones for b-ions are highlighted in blue.

The peptide GSFACQCPPGYQK responsible for EGFR activation was identified with an Amanda Score of 264, a Mascot score of 28 and 10 PSM [15]. The fragment match spectra depicted a high coverage of respective fragment ions by a serious of y-, and b-ions (Figure 40). In addition, this specific peptide was quantified with a FC -1.69 and an ANOVA p-value 0.15 as well as with a FC -3.71 and an ANOVA p-value 0.03 in the isogenic LN18 and LN308 datasets, respectively.

EFEMP1 is able to activate autophosphorylation of EGFR initiating downstream signalling events on the AKT and MAPK axis leading to increased migration rates as has been shown by Camaj *et al.* in pancreatic carcinoma cells [15]. The peptide GSFACQCPPGYQK responsible for EGFR proliferation has been identified and quantified in all samples from the *MALAT1* KD proteomics study. While it was found to be downregulated in both isogenic LN18 and LN308 *MALAT1* KD cells compared to their respective control, the regulation was only significant in the LN308 based dataset. In isogenic LN18 samples, the quantification is impacted by an interfering signal which led to the exclusion of this peptide from the quantification of EFEMP1. A clear picture of the regulation of this peptide in isogenic LN18 *MALAT1* KD cells was not obtained in this study. Hu *et al.* described EFEMP1 as highly upregulated in malignant gliomas leading to increased cell motility and invasion [170]. EFEMP1 contains a signalling peptide enabling classical secretion of this protein to the extracellular matrix enabling EGFR activation as well as the promotion of invasion and migration processes [15, 170]. Transcription of EFEMP1 is regulated through three Sp1 and one oestrogen response element-binding sites [221]. In this study, EFEMP1 has been shown to be downregulated upon *MALAT1* KD in both isogenic LN18 and LN308 datasets. Findings from the performed literature search link EFEMP1 to the observed migration phenotype as well as the EGFR/PI3K signalling pathways highlighted in the interactomics, proteomics and HT drug screening datasets. This in addition to the linkage with malignant gliomas leads to the selection of EFEMP1 as a protein of interest in this study.

ZNF10 (P21506) also known as KOX1 is a zinc finger protein shown to act as a transcriptional repressor in cooperation with TRIM28 and H3F3A in the cell nucleus [134, 135]. Transcriptional repression has been previously shown to be initiated through binding of ZNF10 to Sp1 sites in the promoter region [222].

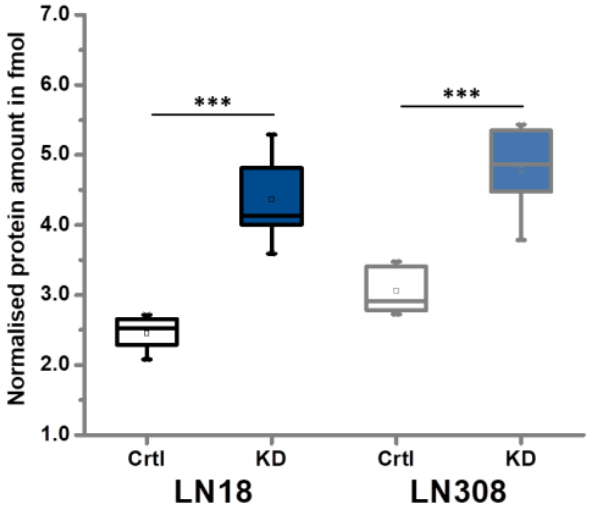

Figure 41 ZNF10 MS data recorded in isogenic LN18 and LN308 cell line pairs. The boxplot depicts the normalised protein amount in fmol on the y-axis for each sample per sample group. Significance levels are indicated through with *** for p-values < 0.001.

ZNF10 was the second most significant upregulated protein amongst isogenic LN18 cell lines with a p-value and FC of 1.51E-04 and 1.78, respectively (Figure 41). Five unique peptides were employed as basis for identification and quantification. With a Mascot score of 2082 and an MSAmanda score of 26488 as identification scores, both respective search-engine based thresholds were exceeded. 195 PSMs were obtained resulting in coverage of 9 %. All five unique peptides were located among the first 100 amino acid residues covering the KRAB domain spanning from amino acid 14 to 85 in the n-terminal protein region.

ZNF10 was found to be upregulated upon *MALAT1* KD in both isogenic sample sets during this study in the proteomics analysis. Since TRIM28 and H3F3A have already been declared as proteins of interest, ZNF10 was added to the list of interesting proteins. Furthermore, Nishitsuji *et al.* have shown that ZNF10 can repress transcription through binding to Sp1 sites in the promoter regions of protein-coding DNA [222]. This directly links ZNF10 as well as TRIM28 and H3F3A to the differential regulation observed for EFEMP1 based on *MALAT1* expression levels observed in this study since EFEMP1 is regulated through three Sp1 promoter regions [221]. Furthermore, this connection is of utmost interest as over half of all protein to be found differentially regulated during this study depict transcriptional regulation based on SP1 promoter regions.

The combinatorial analysis of the obtained data as well as literature resulted in the selection of TRIM28, H3F3A, PCNA, EFEMP1, and ZNF10 as key proteins to understand MALAT1s' influence on tumour biology in GBM. To strengthen the insights gained in this study, additional corroborating analyses of these proteins were planned.

4.5.2 Corroborating analyses of specific proteins of interest inferred from analysis results

Proteins of interest identified in this study, H3F3A, TRIM28, EFEMP1, and ZNF10, were analysed through a complementary method for validation and to gain a deeper insight into underlying biology. In addition, global as well as phospho-protein expression levels for checkpoint proteins from the PI3K and EGFR signalling pathways were examined. As a complementary method to substantiate results obtained via interactome and proteome MS data analysis and for analysis of specific phospho-proteins, immunolabelling was employed. Interactome based candidates, H3F3A and TRIM28, were further substantiated through second round search and ZNF10 localisation change analysis, respectively.

4.5.2.1 Expression changes observed via immunoblot

The abundance of the candidate proteins EFEMP1 and ZNF10 was validated by immunoblotting. These analyses were repeated three times. Measured intensities were normalised to the loading control signal obtained through actin measurements and compared to respective measurements from control cell lines. Student's t-test was employed for significance testing. Target antibodies employed in this analysis were raised against EFEMP1 and ZNF10 (Table 5).

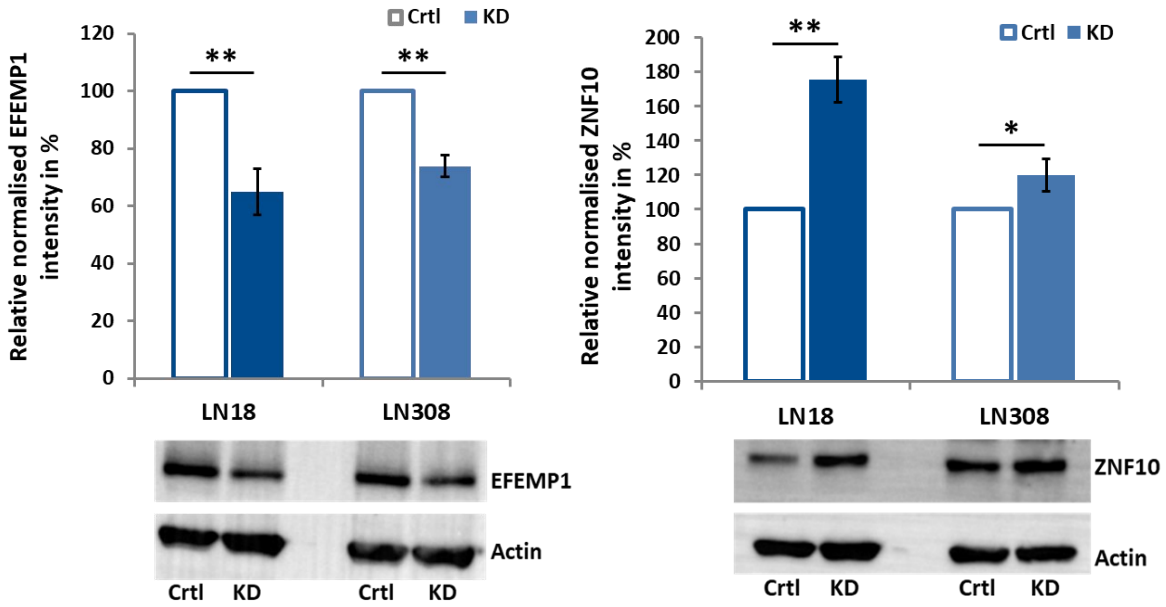

Figure 42 Protein expression analysis via immunolabelling of EFEMP1 (left) and ZNF10 (right) in isogenic LN18 and LN308 cell lines (n=3). Measured intensities were normalised to the loading control signal and compared to respective measurements from control cell lines. Student's t-test was employed for significance testing. Target antibodies employed in this analysis were raised against EFEMP1 and ZNF10 (Table 5). Bar graphs show the relative normalised protein intensity in percent for each isogenic cell line analysed with control cells as unfilled bars and *MALAT1* KD cells as blue filled bars. Immunolabelling pictures are depicted exemplarily underneath the respective bar graphs. Measurement variance is indicated through error bars. Significance levels are indicated through ** for p-values < 0.01 and * for p-values < 0.05.

Immunolabelling analyses substantiated obtained MS results. EFEMP1 signal intensities were significantly decreased to 65 % (± 8.11; p-value = 3.6E-03) and 74 % (± 3.87; p-value = 2.9E-03) in isogenic LN18 and LN308 *MALAT1* KD cells, respectively, compared to their individual control cells (Figure 42). ZNF10 signal intensities observed were significantly upregulated by 76 % (± 13.28; p-value = 1.3E-03) and 20 % (± 9.47; p-value = 4.9E-02) in isogenic LN18 and LN308 *MALAT1* KD cells, respectively, compared to their individual control cells (Figure 42).

To corroborate the downregulation of EFEMP1 as well as the upregulation of ZNF10 upon *MALAT1* KD, immunoblotting was performed as an orthogonal validation method. The immunoblots obtained depict the downregulation of EFEMP1 as well as the upregulation upon *MALAT1* KD in both isogenic cell line pairs. This additional result further strengthens the findings obtained in the proteomics study.

Candidate proteins H3F3A and TRIM28 derived from the interactome dataset were analysed via immunoblot together with the well-known *MALAT1*-interactor SRSF1. Because levels obtained in the RNA-centric pulldown experiment were insufficient in most samples for this kind of analysis, immunoblotting was only performed for one representative sample per tumour type, the GBM associated cell line T98G and the MB associated cell line CHLA-259. Target antibodies employed in this analysis were raised against TRIM28 and H3F3A (Table 5).

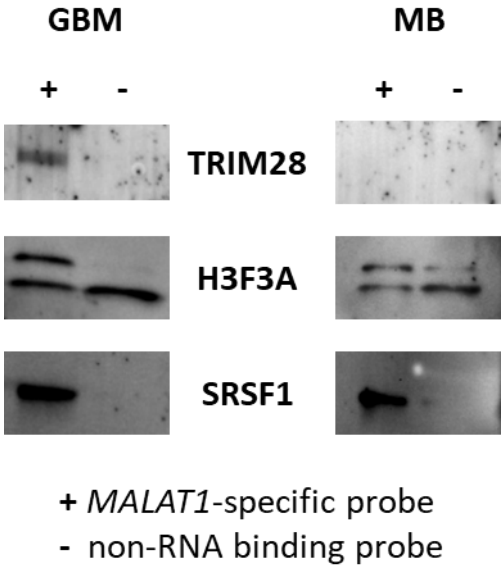

Figure 43 Protein expression analysis via immunolabelling of TRIM28, H3F3A, and SRSF1 in RNA-centric pulldown samples from GBM associated T98G and MB associated CHLA-259 cells (n=1). Target antibodies employed in this analysis were raised against TRIM28, H3F3A, and SRSF1 (Table 5). + indicates that a *MALAT1*-specific pulldown probe was employed in sample generation while – indicates that a non-RNA binding probe was employed.

The protein SRSF1 is a well-known and well-documented *MALAT1*-interacting protein [61] and was employed as a marker to confirm a successful pulldown experiment. Both samples obtained with the *MALAT1*-specific probe showed a distinct signal for SRSF1 while in the samples generated with non-RNA binding probes no signal was detected with the SRSF1 antibody (Figure 43).

In contrast to that, the putative *MALAT1*-interactor H3F3A yielded a signal in every one of the four samples but the obtained signal pattern was distinctly varied between the samples. All the samples resulted in a signal for H3F3A at approx. 15 kDa while a second signal at approx. 17 kDa was observed in all samples except for the GBM associated sample generated with the non-RNA binding probe. The signal at approx. 17 kDa for H3F3A in the MB associated samples was stronger in the sample generated with the *MALAT1*-specific probe compared to the non-RNA binding probe. As H3F3A is a DNA binding protein, a signal band with the non-RNA binding probe was not unexpected. This finding was reflective of the proteomics dataset. A shift in signal height could result from a differential PTM status of the detected protein. The apparent lack of a double band in the GBM associated sample generated with the non-RNA binding probe was unexpected. The observed double band could be due to differential

PTM statuses of H3F3A leading to increased interaction between H3F3A and *MALAT1* corroborating previous findings documented in literature stating that *MALAT1* binds H3K36me3 [208].

Furthermore, the immunoblot analysis yielded a distinct signal band for TRIM28 in the GBM associated sample generated through the application of the *MALAT1*-specific probes. Both samples generated with the non-RNA binding probes depicted no signal for TRIM28. Surprisingly, no signal for TRIM28 was detected in the MB associated sample generated with *MALAT1*-specific probes. The absent signal in the MB associated sample was thought to be based on the protein amount in the sample in addition to the sensitivity of the immunolabelling method as well as the applied antibody. In the MS-based analysis, the signal intensities obtained in MB associated samples were also lower compared to the signal intensities in GBM associated samples. These findings resulted in the choice of TRIM28 as another protein of interest in this study.

The putative interaction between *MALAT1* and H3F3A was corroborated through immunoblot analysis in a representative sample for each tumour type, GBM and MB. To ensure that the enrichment worked, the well documented *MALAT1* interacting protein SRSF1 was analysed in addition [61]. A putative interaction between MALAT1 and TRIM28 was only corroborated in the representative GBM sample through this immunoblot analysis.

4.5.2.2 Analysis of key proteins in the EGFR/PI3K signalling pathway

Immunoblot analysis was performed to investigate the abundance of key proteins in the EGFR/PI3K signalling pathway. The analysis was performed for the proteins AKT, ERK and MEK as well as their respective, activating phosphorylation sites pAKT S473, pAKT T308, pERK and pMEK S217/221 (target antibody information Table 5). Profilin-1 measurements were employed as loading control. Global protein intensities were normalised to respective loading control intensities while phospho-protein intensities were normalised to global protein intensities.

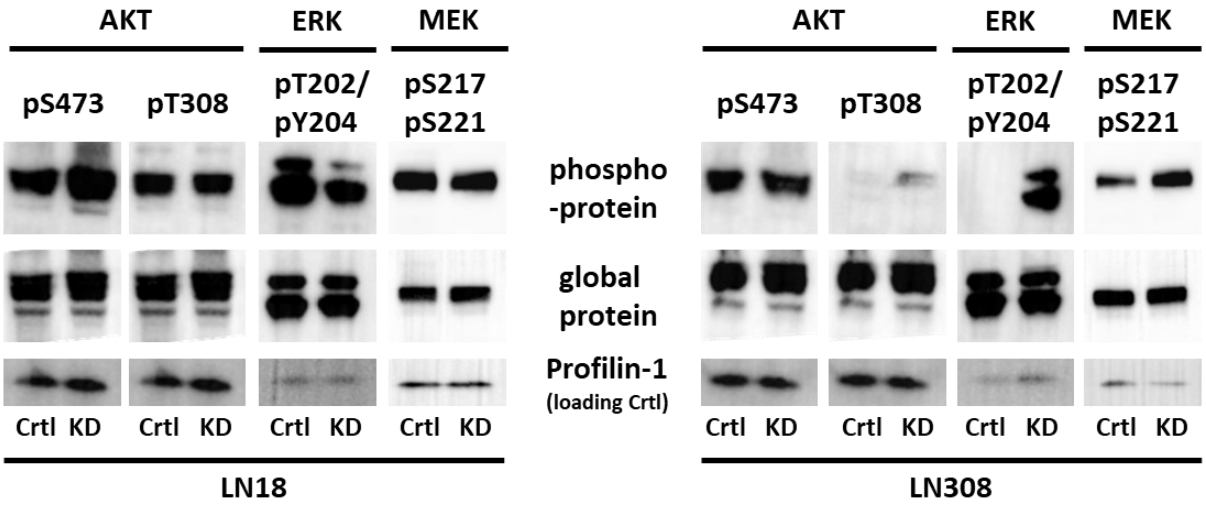

Figure 44 Protein expression analysis via immunolabelling of key proteins in the EGFR/PI3K pathway in isogenic LN18 cell lines (left) and isogenic LN308 cell lines (right) (n=1). Profilin-1 measurements were employed as loading control. Target antibodies employed in this analysis were raised against AKT, ERK and MEK as well as their respective, activating phosphorylation sites pAKT S473, pAKT T308, pERK and pMEK S217/221 (Table 5). Immunoblot pictures show the protein intensity for each isogenic cell line analysed. Measurements for isogenic LN18 cell lines are depicted on the left and measurements for isogenic LN308 cell lines are depicted on the right.

AKT, ERK and MEK are downstream targets in PI3K and EGFR signalling cascades. Their activation is achieved through phosphorylation. The abundance of AKT, ERK, nor MEK was changed upon *MALAT1* KD in either isogenic cell line pair. In isogenic LN18 *MALAT1* KD cells compared to their control cells signal intensities for phosphorylation at AKT S473 were increased while signal intensities for phosphorylation at AKT T308, ERK T202/Y204, and MEK S217/221 were decreased. In isogenic LN308 *MALAT1* KD cells compared to their respective control cells signal intensities for phosphorylation at AKT S473 were unchanged while signal intensities for phosphorylation at AKT T308, and MEK S217/221 were increased. Phosphorylation of ERK at T202/Y204 was not detectable in isogenic LN308 control cell lines whereas the respective MALAT1 KD cell line exhibited high levels of this phosphorylation (Figure 44).

EGFR/PI3K signalling was highlighted in the interactomics, proteomics, and HT drug screening analyses. In addition, EFEMP1 has been linked to this signalling cascade[15]. On basis of this, immunoblot analysis was performed for key proteins from the EGFR/PI3K signalling pathway on a global level as well as for the phosphorylated proteins in the isogenic cell lines generated. This analysis depicts that the protein expression is not influenced by the *MALAT1* level in GBM associated cell lines analysed. However, the analysis of the respective phosphorylated proteins indicated distinct differences based on the *MALAT1* expression level in the isogenic cell lines. Since the global protein levels were equal amongst isogenic *MALAT1* KD and their respective control cell lines, the observed changes on the phosphorylation level were assumed to be due to differential activation of this signalling cascade. In isogenic LN18 *MALAT1* KD cells, an increase in pAKT S473 and a decrease in pAKT T308, pERK, as well as pMEK was observed. In isogenic LN308 *MALAT1* KD cells, the opposite effect on protein phosphorylation was observed. These results indicate vice versa signalling events in isogenic LN18 and LN308 cell lines generated. Both effects are described in the literature in various cell lines hinting at a differential response to EFEMP1 based on the mutational background in the analysed cell lines [15, 223, 224]. These differential phosphorylation levels reflect the differential behaviour of the isogenic *MALAT1* KD cells in the phenotype analyses performed. Although, these immunoblots were performed once so the results lack statistical relevance.

All employed antibodies yielded distinct and specific signals at target protein-specific migration heights compared to a molecular size marker. Results for isogenic LN18 *MALAT1* KD cells show decreased phosphorylation levels for ERK, MEK, and AKT T308 as well as increased phosphorylation levels for AKT S473. The results are vice versa in isogenic LN308 *MALAT1* KD cells.

4.5.2.3 Localisation analysis of ZNF10

ZNF10 was selected for further analysis based on the differential proteome study in isogenic LN18 control and *MALAT1* KD cells. The protein itself was significantly upregulated in *MALAT1* KD cells and acts as a transcription repressor in nuclei [134, 135]. The putative *MALAT1* interactor TRIM28 is known to relocate ZNF10 from the cytosol into the nucleus initiating transcriptional repression[210]. To investigate the effect of *MALAT1* KD on the localisation of ZNF10, immunoblotting of ZNF10 in cytosolic and nuclear cell fractions in LN18 *MALAT1* KD and respective control cells was performed. According to literature EFEMP1, the other protein selected for further analysis, does not change its subcellular localisation due to interaction with either H3F3A or TRIM28.

Proteins were extracted in cytosol and nuclear specific fractions. Profilin-1 and SRSF1 measurements were employed as cytosolic and nuclear control, respectively. Measured intensities were normalised

to the control signal and the obtained signal in the cytosolic fraction of LN18 isogenic control cells was employed as reference. Student's t-test was employed for significance testing. Cytosolic and nuclear markers, Profilin-1 and SRSF1, depicted equal distribution patterns amongst the fractions in both analysed isogenic cell lines.

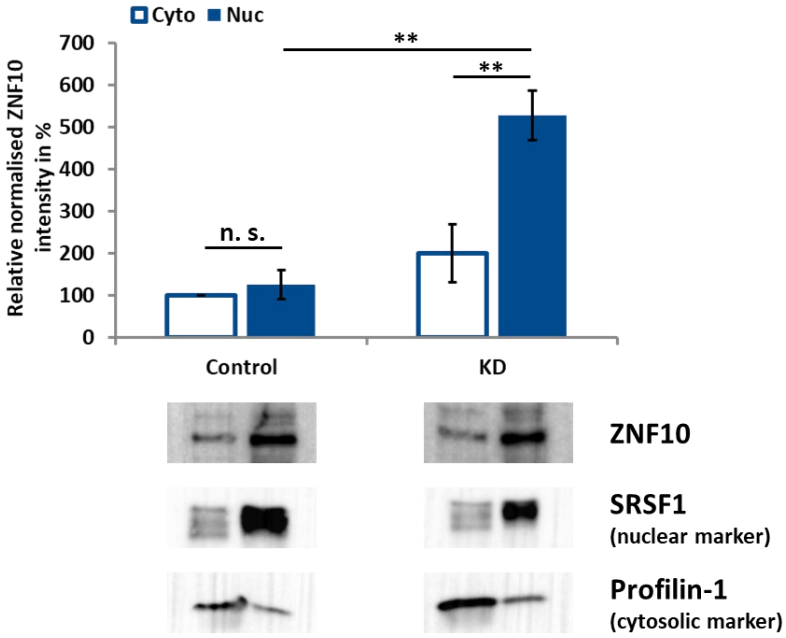

Figure 45 Protein expression analysis via immunolabelling of ZNF10 in cytosolic and nuclear fractions of isogenic LN18 (n=3). Measured intensities were normalised to the loading control signal and compared to the respective measurement in the cytosolic control cell line fraction. Student's t-test was employed for significance testing. SRSF1 measurements were employed as nuclear control and Profilin-1 as cytosolic control. Target antibodies employed in this analysis were raised against ZNF10 (Table 5). The bar graph shows the relative normalised protein intensity in percent for each isogenic LN18 cell line analysed with cytosolic fractions as unfilled bars and nuclear fractions as blue filled bars. Immunoblot pictures are depicted exemplarily underneath the respective bar graphs. Measurement variance is indicated through error bars. Significance levels are indicated through ** for p-values < 0.01.

Normalised ZNF10 levels were not significantly different between the cytosolic and nuclear fraction of isogenic LN18 control cells with a p-value of 0.349 and respective relative, normalised intensities of 100 % (±0.00) to 125 % (±34.5). In isogenic LN18 *MALAT1* KD cells, relative, normalised ZNF10 levels were significantly higher in the nuclear fraction compared to the cytosolic fraction with a p-value of 0.007 and relative, normalised intensities of 528 % (±59.8) and 201 % (±69.1). Amongst the cytosolic fractions from isogenic LN18 control and *MALAT1* KD cells, ZNF10 levels were not significantly different with a p-value of 0.109. However, a comparison of the nuclear fractions from isogenic LN18 control and *MALAT1* KD cells showed with a p-value of 0.001 a significant increase in ZNF10 in the isogenic *MALAT1* KD cells (Figure 45).

ZNF10 is located in the cytosol as well as the nucleus. TRIM28 relocates cytosolic ZNF10 into the nucleus where transcriptional repression complexes can be formed [210]. To analyse if there is an increased level of ZNF10 in the nuclei in *MALAT1* KD cells, cytosolic and nuclear protein fractions were analysed via immunoblot in the isogenic LN18 cell line pair. This analysis indicates a significant increase in nuclear ZNF10 upon *MALAT1* KD in LN18. These results could hint towards a potential blocking of the respective ZNF10 binding site on TRIM28 through *MALAT1* leading to a decrease in nuclear ZNF10.

In addition, the immunoblot clearly shows the increase in ZNF10 levels upon *MALAT1* KD observed in previous immunoblots as well as in the proteomics dataset.

4.5.2.4 Investigation of Histone PTM status

H3F3A function is regulated through PTMs like mono-, di-, and trimethylation. *MALAT1* has been associated with H3F3A trimethylation at K27 [51] and K36 [208]. To investigate the effect of *MALAT1* KD on H3F3A PTMs as well as the effect of H3F3A PTMs on its binding to *MALAT1* the generated proteome and interactome datasets were analysed through a second-round search.

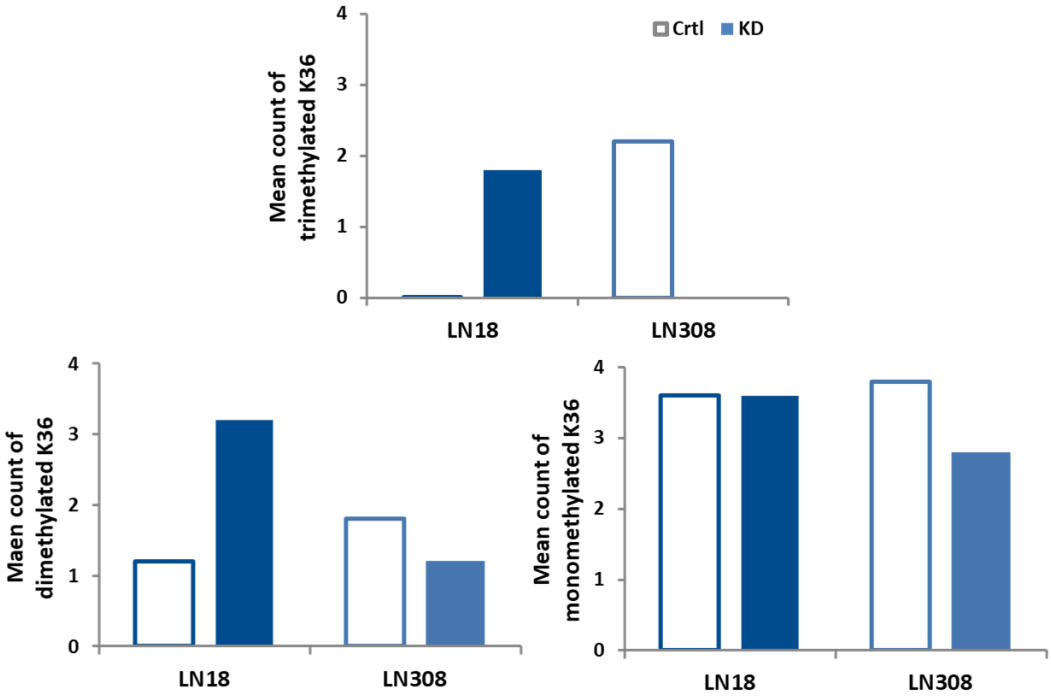

Figure 46 PTMs of H3F3A in isogenic LN18 and LN308 cell lines analysed by second-round search (n=5). The bar graphs depict the mean PSM count of mono-, di-, and trimethylated Lysine[36] in H3F3A per analysed cell line, respectively. Control cells are depicted as unfilled bars and *MALAT1* KD cells are depicted as blue filled bars.

Peptides from proteins identified in the previous datasets were employed as a starting point for the analyses of their PTM status. While in the first search queried PTMs were restricted and the complete human peptide space was considered, this second round search was an unrestricted PTM query with a restricted peptide list. This search strategy allowed for independent identification of PTMs. To be considered in this analysis the PTM had to be listed for the peptide on UniProt as well as PhosphositePlus. In addition, the PTM had to be identified in three samples per group.

The trimethylation of lysine[36] (K36) was the only identified PTM fulfilling all set criteria in the isogenic LN18 and LN308 *MALAT1* KD cell samples as well as in their respective control cell samples. With an average number of 1.8 PSMs in isogenic LN18 *MALAT1* KD cell samples and zero in their respective control cell samples, isogenic LN18 cell lines exhibited a vice versa K36 trimethylation status compared to isogenic LN308 cell lines with zero PSMs in *MALAT1* KD cell samples and an average number of 2.2 PSMs in respective control cell samples. The trimethylation at K36 (K36me3) was identified in three out of five isogenic LN18 *MALAT1* KD samples and four out of five isogenic LN308 control cell samples. Average PSM numbers for dimethylation at K36 (K36me2) depict a similar, albeit less obvious trend compared to K36me3 in both isogenic cell line pairs. Monomethylation at K36 (K36me) appeared to

be equal between isogenic LN18 control and MALAT1 KD cells while it was slightly reduced in isogenic LN308 MALAT1 KD cells compared to the respective control cell line (Figure 46).

Subsequent to the performed second round search, a peptide search was performed allowing for oxidation of methionine, carbamidomethylation of cysteine, and methylation of lysine as potential PTMs considering the complete human peptide space. The search was performed under application of the Mascot and MSAmanda search algorithms on a combined spectrum dataset generated from the whole isogenic *MALAT1* KD dataset. Therefore, no sample-specific information was gained through this analysis. This search was employed to corroborate the findings from the second-round search.

The H3F3A peptide SAPSTGGVKKPHR was identified in the database with a dimethyl as well as a trimethyl group at K36. The dimethylated peptide was identified with a Mascot score of 11, an MSAmanda score of 258.96, and 12 PSMs while the trimethylated peptide was identified with a Mascot score of 9, an MSAmanda score of 139.18, and 13 PSMs. In addition, the H3F3A peptide KSAPSTGGVKKPHR was identified carrying two dimethyl groups with a Mascot score of 34, an MSAmanda score of 388.45, and 2 PSMs. These peptides represent the H3F3A amino acid sequence from position 28 to 40 and 27 to 40, respectively, if the starting methionine is neglected as was done in the counting for the second-round search. In the initial search, these peptides were not identified which was potentially based on their PTM status as this was restricted to oxidation of methionine and carbamidomethylation of cysteine during that search. The peptides were identified allowing missed cleavage sites as the methylation of lysine blocks trypsin activity at these sites [225, 226].

In LN18 cells, this result could be due to a reduced binding between *MALAT1* and SETD2, upon *MALAT1* KD while the methylation status of H3F3A is not affected in isogenic LN308 control cells due to the existence of functional SETD5 in addition to SETD2. The reduction in H3F3A K36me3 upon *MALAT1* KD in isogenic LN308 cells was unexpected and does not fit with this theory. This points to a further influencing factor that is as of yet unidentified. A subsequent peptide search allowing for methylation as a potential PTM, resulted in the identification of the di- and trimethylated K36 H3F3A peptide increasing the credibility of the findings from the second-round search. This peptide has not been observed in the initial search and therefore increase the sequence coverage of the protein. In addition, the peptide covering the potential mutation site K27 was identified in this subsequent search as well. This finding is in line with mutational data of the employed cell lines [227].

The missing coverage of H3F3As' N-terminal amino acid chain was shown to be based on the PTM restrictions in the initial search. The performed investigation of H3F3As' PTM status via second-round search indicates a putative involvement of *MALAT1* in H3F3A methylation in glioblastoma associated cell lines. TRIM28, EFEMP1, and ZNF10 did not show any changes in their PTMs in the second-round search data. Di- and trimethylation of H3F3A K36 was corroborated by subsequent PTM restricted peptide identification.

Data obtained during this study lead to the selection of H3F3A, TRIM28, PCNA, EFEMP1, as well as ZNF10 as proteins of interest to understand the influence of *MALAT1* expression levels in tumour biology. Orthogonal and corroborating analyses performed emphasize this choice and strengthen the belief that *MALAT1s*' influence on tumour biology is highly dependent on the mutational status of the cell.

5 Discussion

At this time, lncRNA based effects on cellular mechanisms are still poorly understood. While several studies have shown that lncRNAs like *MALAT1* are able to interact with DNA, RNA, and proteins, general knowledge regarding the implications of those interactions as well as their breadth are still lacking [39, 41, 42, 53, 61, 228]. The objective of this study was to investigate whether the lncRNA *MALAT1* effects protein signatures in GBM and thereby tumorigenicity. Furthermore, this study aimed to identify key proteins as well as biological pathways affected by *MALAT1* to gain a deeper understanding of *MALAT1* dysregulation effects in GBM.

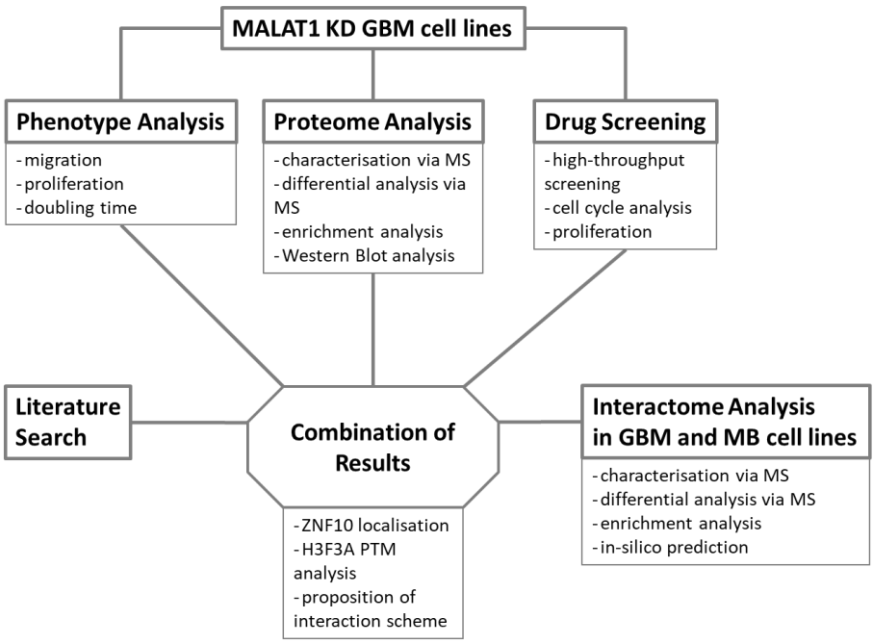

Figure 47 Schematic of different analysis steps.

To date, *MALAT1* is one of the best-studied lncRNAs and has been linked to tumourigenesis in several cancer types [53-55]. Several studies focused on *MALAT1s*' role in GBM resulting in the proposal of different functions from oncogene [57, 58] to tumour suppressor [59]. Through a combination of interactomics, phenotype, proteomics and drug screening analyses, this study aims to increase the understanding of *MALAT1s*' influence on protein signatures in GBM (Figure 47).

5.1 *MALAT1* interactome is tumour specific

Elucidation of proteinaceous interaction partners gives access to underlying functional processes. In this study, *MALAT1s*' proteinaceous interaction partners were revealed through an RNA-centric protein pulldown. Results from MB cell lines were employed as an in-house reference dataset in addition to previously published datasets [61, 95, 96] to identify potential GBM-specific interacting proteins. Several aspects were employed as checkpoints to ensure the validity of this affinity enrichment study.

In the overall dataset, 264 and 213 proteins were identified as potential *MALAT1* interacting proteins in GBM and MB associated cell lines, respectively. Nine out of 17 well-known *MALAT1* interactors were among the list of putative interactors in both sample sets [61]. The review paper from Gutschner *et al.* [61] lists eight additional *MALAT1* interacting proteins which were not identified as potential

interactors during this study. This might be due to the overall size of above 200 kDa for two of these proteins (Q03164 (KMT2A), and Q9BYW2 (SETD2)) and the low expression levels in brain cells of five other proteins (Q8IYX4 (DND1), Q9UKV8 (AGO2), Q8WYQ5 (DGRCR8), Q9BYW2 (SETD2), and Q13563 (PKD2)) from that list. In addition, this list was combined from a number of studies in various cell lines from different tumour types and it is possible that those proteins interact with *MALAT1* in a tissue-specific background.

Putative *MALAT1* interacting proteins identified in this affinity enrichment study were employed in GO term enrichment analyses to obtain insight into *MALAT1*s' role in these tumours. Results obtained matched results from previous studies focussed on *MALAT1* pathway involvement as well as general knowledge about *MALAT1* such as its nuclear localisation and it being a lncRNA [61, 94]. Eleven out of 282 putative *MALAT1* interacting proteins possess a histone 3 domain. In previous studies, *MALAT1* has been associated with active chromatin sites by West et al. [208] specifically H3K36me3 sites. This previous finding corroborates the enrichment of proteinaceous *MALAT1* interaction partners possessing a histone 3 domain and links *MALAT1* to histone 3 based transcriptional processes.

The data was analysed to identify proteins that specifically interact with *MALAT1* in GBM. In this study, 282 putative *MALAT1* interacting proteins were identified. Out of these, 87 proteins have been identified in previous studies and 195 were newly identified as putative *MALAT1* interactors in this study. None of the previous studies were performed in GBM associated cell lines. The majority of putative *MALAT1* interactors with 195 proteins were identical between both MB and GBM associated sample sets. While 61 and 15 proteins, respectively, were identified as putative *MALAT1* interactors in a GBM- and MB-specific background. While both the MB associated dataset and the list of previously proposed *MALAT1* interactors contain a high number of proteins associated with transcription and mRNA splicing, these proteins seem to be underrepresented in the GBM specific interactor list in comparison. This result indicates that MALAT1s' involvement in these biological pathways is lower in GBM associated cell lines. Enrichment of proteins linked to EGFR/PI3K signalling and cell cycle progression from G1- to S-phase specifically in GBM associated cell lines depicts a further difference between *MALAT1s*' involvement in biological pathways in a tumour specific manner. This data highlights a differential influence of *MALAT1* in GBM associated cell lines compared to the other cell lines employed in *MALAT1* interactomics studies so far. Furthermore, this indicates a deviation from the well described influence of *MALAT1* on cell biology in GBM associated cell lines.

Direct and indirect interaction of *MALAT1* with proteins involved in cell cycle regulation has been reported previously in various tumour backgrounds [228-231]. However, while *MALAT1* has been linked to activation of the PI3K/AKT signalling resulting in increased proliferation, migration and invasion in previous studies of various cancer types no direct interaction with associated proteins has been reported so far [230, 232-235].

Through RNA-centric affinity enrichment, 195 previously unknown putative *MALAT1* interacting proteins were identified. Furthermore, 61 proteins were identified to show specific interaction with *MALAT1* in GBM associated cell lines. These proteins lead to the discovery of possible involvement of *MALAT1* in EGFR/PI3K signalling and cell cycle progression from G1- to S-phase in GBM associated cell lines.

5.2 *MALAT1* influences migration and proliferation in a cell line specific manner in GBM

Stable *MALAT1* KD as well as respective control cell lines generated through a CRISPRi strategy were employed in phenotype analysis assays to increase the understanding of *MALAT1s*' influence on tumour biology in GBM.

Achieved KD efficiencies ranged from 52 to 95 % and resulted in the selection of the LN18 and LN308 based cell line pairs for all further analysis. KD efficiencies of 89 and 95 % as achieved in LN18 and LN308 cells were in the range of previously reported KD efficiencies of 90 % in A549 a lung adenocarcinoma cell line as well as K526 a chronic myelogenous leukaemia cell line without clonal selection [236]. KD efficiency rates can be affected by the size and nuclear localisation of the target lncRNA as well as the high baseline expression level [236]. Out of the four transfected cell lines, the two cell lines, LN229 and U251, with lower KD efficiency of 52 and 56 %, respectively, depicted higher baseline *MALAT1* expression levels compared to LN18 and LN308. The transfection outcomes obtained reflect current theories on lncRNA KD efficiencies and hindrances.

A distinct reduction in the migration rate of LN18 cells upon *MALAT1* KD was measured concurring with previous studies linking *MALAT1* to a migrational phenotype [55, 57]. However, in LN308 *MALAT1* KD cells this reduction has not been observed. While in LN18 control cells first migration events were observed after a culture period of 5 h in the other three tested cell lines no migration events are observed before the 20 h mark. The late onset of migration events might reflect spacial restrictions instead of migrational behaviour. Obtained results are still accepted as based on *MALAT1* levels as the cell pairs are treated equally in the experiment and thus all result variations must be due to the variable factor, in this case, the *MALAT1* level.

The employed migration assay can be affected through variations in cell proliferation rates [122, 123]. Therefore, cell proliferation in both isogenic cell line pairs has been analysed via confluency measurement as well as doubling time analysis. No discernible difference in proliferation rates was measured in the confluency-based analysis for either of the two isogenic cell line pairs. The measured doubling time of the isogenic LN18 cell line pair depicted no discernible differences, leading to the assumption that the difference in migration rates observed amongst isogenic LN18 control and *MALAT1* KD cells was solely based on the difference in *MALAT1* level. However, in isogenic LN308 *MALAT1* KD cells the doubling time appears to be increased compared to the respective control cell line. This observed increase in doubling time for LN308 *MALAT1* KD cells does not directly reflect the proposed increase in migration rate due to overpopulation of the chamber. The observed increase in doubling time for isogenic LN308 *MALAT1* KD cells indicates a reduction in proliferation rate for this cell line compared to the respective control. The discrepancy to the confluency-based measurement might be due to measuring inaccuracy of the employed confluency measurement. On basis of the measured doubling times for the isogenic LN308 cell line pair, the migration rate would be expected to depict an earlier onset in LN308 control cells with a later onset in LN308 *MALAT1* KD cells. This finding is vice versa compared to the results obtained through the migration analysis in the isogenic LN308 cell line pair.

This phenotype study highlights the influence of *MALAT1* in migration and proliferation events in a cell line-specific manner based on varying underlying biology.

5.3 Proteins linked to EGFR/PI3K signalling depict *MALAT1* based perturbations in the cellular proteome

MALAT1 based perturbations in cellular proteome expression levels of generated isogenic cell lines were analysed to increase the understanding of *MALAT1* based effects on cellular protein signalling pathways.

Analysis of the data was performed in a base cell line dependent manner since the phenotype study hinted at base cell line-specific biological events. Enrichment analysis in the LN18 associated sample set depicted a significant enrichment of proteins linked to EGFR/PI3K signalling. In GBM, deregulation of these pathways leads to increased migration, drug resistance, and faster proliferation [19, 130]. Proteins linked to EGFR/PI3K signalling have already been identified as important in the *MALAT1*-centric interaction study. In LN308 associated isogenic cell lines, proteins involved in EGFR signalling were found to be significantly enriched while no enrichment of proteins linked to PI3K signalling was observed. These results indicate as did the results in the phenotype analysis that *MALAT1* influences protein signatures differently in the tested GBM associated cell lines. The recurrence of the EGFR enrichment, as well as the observed migratory phenotype in LN18 based isogenic cell lines, give credence to a possible *MALAT1* expression level-based effect on this pathway.

Differential proteome analyses further highlight a possible base cell line-specific behaviour of *MALAT1* amongst the analysed cell lines. While in LN18 a decrease in *MALAT1* expression levels resulted in a differential expression of 112 proteins, in LN308 only eight proteins depicted a perturbed expression level. Interestingly, comparing the two lists of differentially expressed proteins two proteins were found to be regulated in the same manner in both isogenic cell line pairs. Both depicted a significant downregulation of EFEMP1 and a significant upregulation of ZNF10. In isogenic LN18 *MALAT1* KD cells, several proteins involved in transcriptional regulation [121, 124, 127, 134, 141-144], cancer-related signalling, and migratory processes were found to be differentially regulated. In addition, two previously described *MALAT1* interactors not identified in the *MALAT1* interactomics study performed were found to be downregulated in this dataset (Q96QR8 (PURB) and Q13501 (SQSTM1)). Proteins differentially regulated in isogenic LN308 *MALAT1* KD cells are involved in migratory processes, DNA damage control, as well as transcriptional regulation. Although there were distinct differences between isogenic LN18 and LN308 based cell lines, *MALAT1* appears to affect the same pathways in both albeit with various intensity and on different adjusting screws. This observed difference could be based to some part on the mutational status of the base cell lines.

The performed enrichment analysis on basis of proteins found to be regulated upon *MALAT1* KD in the isogenic cell line pairs distinctly highlighted the importance of the Sp1 promoter region in this dataset. Although the enrichment of proteins transcriptionally regulated through this Sp1 promoter site was not statistically significant in both isogenic cell line pairs, this is thought to be based on the low number of differentially regulated proteins detected in the isogenic LN308 dataset.

The protein analysis clearly shows that *MALAT1* levels can indirectly affect protein expression levels potentially on basis of the Sp1 promoter region although *MALAT1* has no coding potential. Furthermore, this data corroborates the link to EGFR/PI3K signalling observed in the interactome study as well as a base cell line specific influence of *MALAT1*. This could be due to a difference in mutational background of these cell lines.

5.4 *MALAT1* affects drug efficacies of EGFR/PI3K inhibitors

To determine if *MALAT1s*' oncogenic function can be influenced through pharmacological intervention, high-throughput drug screening was performed under application of an in-house clinical inhibitor library.

The performed high-throughput screen depicted *MALAT1* based drug dependencies in isogenic LN18 cell lines in approx. 4 % of the tested inhibitors. Out of the list of inhibitors depicting possible *MALAT1* based dependencies, 48 % were linked to EGFR/PI3K signalling [189-195]. Other inhibitors were involved in general tumour growth [195-198], transcriptional processes [195], protein degradation [195], and redox signalling pathways [199]. ZSTK474, a PI3K inhibitor, depicted the highest level of difference in its dose-response curve out of all tested inhibitors.

The pan PI3K inhibitor ZSTK474 has previously been described to reduce pAKT levels and induce G0/G1 cell cycle arrest in GBM as well as breast, prostate, lung, and colorectal cancer-associated cell lines and xenografts [201, 202, 237]. Treatment with ZSTK474 led to an increase in cells in G0/G1-phase as well as apoptotic cells and a decrease in cells in S-phase and G2/M-phase with the exception of isogenic LN308 *MALAT1* KD which did not depict a significant reduction in S-phase cells. These results corroborate results for ZSTK474 treatment from previous studies mentioned and show that the tested cell lines undergo G0/G1 cell cycle arrest through the inhibitor treatment. Furthermore, in isogenic LN18 *MALAT1* KD cells the percentage of cells in S-phase was consistently higher compared to the respective control cell in both populations treated with DMSO and ZSTK474. This reflects the reduced effectiveness of ZSTK474 observed in isogenic LN18 *MALAT1* KD cells in the initial drug screen and indicates an effect of *MALAT1* on the cell cycle of LN18 cells in general. While the drug appeared to have a differential effect on the cell cycle based on *MALAT1* expression levels in isogenic LN18 cell lines, this cell cycle-based difference was not present in isogenic LN308 cell lines. Further analysis of the cell cycle data identified a synergistic effect between *MALAT1* expression levels and ZSTK474 treatment in isogenic LN18 cell lines. This finding suggests that *MALAT1* could affect the same signalling pathways in LN18 but not LN308 cells as does ZSTK474. This finding reflects the results obtained through the enrichment analyses performed on the proteomics datasets obtained for both isogenic cell line pairs.

In addition to cell cycle analysis, proliferation rates were measured after treatment with DMSO and ZSTK474, respectively, in all four isogenic cell lines. In isogenic LN18 *MALAT1* cells the proliferation appears to be unaffected by ZSTK474 treatment while it is distinctly decreased in respective control cells upon treatment with ZSTK474. These findings reflect previous results from the high-throughput drug screening as well as from the phenotype analysis. Although in isogenic LN308 cells ZSTK474 only appears to affect the proliferation in isogenic control cells comparable to the results from the isogenic LN18 cell lines, the overall proliferation rate in isogenic *MALAT1* KD cells appeared to be decreased compared to the control cells. This change in proliferation rate upon *MALAT1* KD could reflect the prolonged doubling time previously observed for LN308 *MALAT1* KD cells compared to their respective control.

The high-throughput drug screen as well as the orthogonal validation methods exhibited a treatment effect for ZSTK474. The treatment efficacy on the proliferation was reduced in both isogenic *MALAT1* KD cells compared to their respective control cells. Results obtained highlighted the involvement of *MALAT1* in PI3K linked signalling affecting the cell cycle in a cell line dependent manner.

5.5 *MALAT1* perturbs several signalling pathways in a cell line specific manner

The combined data collected in this study highlighted several proteins, biological pathways, and phenotypical markers affected by *MALAT1* expression changes. The proteins H3F3A, TRIM28, PCNA, EFEMP1, and ZNF10 were investigated in the literature to supplement the findings from this study and to gain a deeper knowledge of cellular processes influenced by *MALAT1* expression levels. Cell cycle progression, EGFR/PI3K signalling, and DNA repair came up numerous times. On basis of these findings, various signalling diagrams are suggested to explain the differential protein regulation, the observed phenotype changes, the influence of *MALAT1* on tumorigenesis, as well as the effects observed after treatment with the pan PI3K inhibitor ZSTK474. These proposed schemata do not represent the full signalling landscape but rather an abbreviated snapshot and only depict a potential explanation on basis of the data obtained in this study.

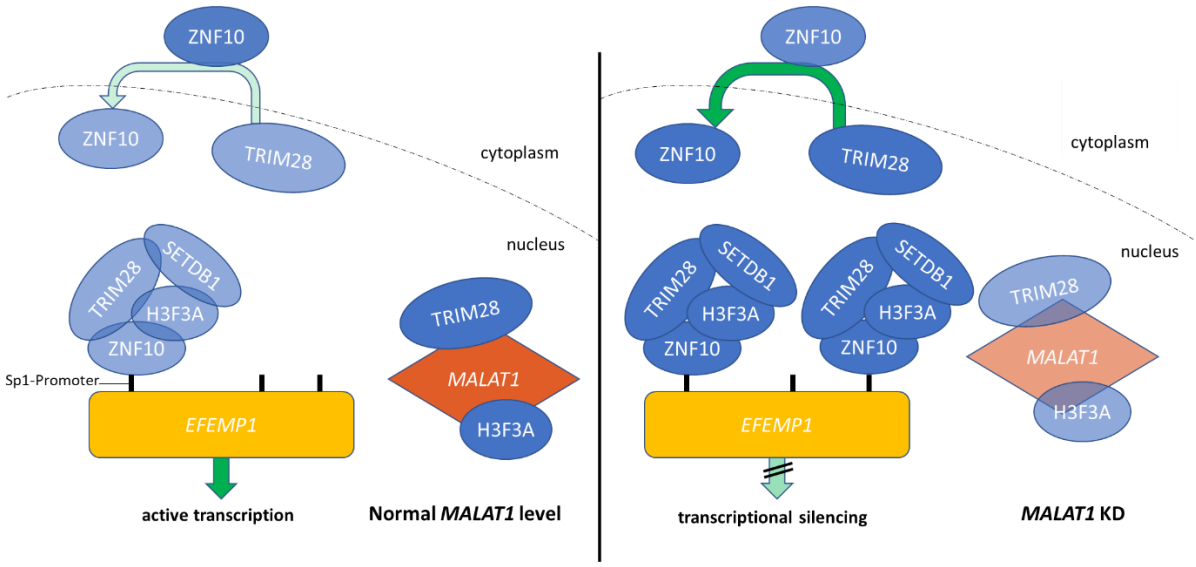

Figure 48 Proposed pathway for regulation of EFEMP1 dependent on *MALAT1* level in isogenic LN18 and LN308 control (left) and *MALAT1* KD (right) cells. Yellow rectangles represent DNA, red diamonds represent lncRNA, blue ovals represent proteins and green arrows indicate a process. The colour saturation of the proteins and lncRNA indicates the level present at the depicted site, the higher the saturation the higher the level at the depicted site. While the colour saturation of the process arrows indicates the activity level of this process, the higher the saturation the higher the activity of the process.

Expression changes observed for EFEMP1 upon *MALAT1* KD in both isogenic cell line pairs could be due to the proposed interaction between *MALAT1* and TRIM28 as well as H3F3A combined with the increased ZNF10 and SETDB1 levels in addition to the increase of ZNF10 in the nuclei upon *MALAT1* KD (Figure 48). In the control cells, *MALAT1* levels are high enough to have sufficient binding of TRIM28 and H3F3A and thus block the relocalisation of ZNF10 from the cytosol to the nucleus. The resulting lower levels of free TRIM28, H3F3A, and ZNF10 in the nuclei decrease the formation of the transcriptional silencing complex as well as its binding to the Sp1 promoter sites of *EFEMP1*. Also, the levels of ZNF10 and SETDB1 are overall lower in these cells hindering the formation of the complex further. Thus EFEMP1 is actively transcribed. In contrast in the *MALAT1* KD cells, the expression level of *MALAT1* is reduced leading to lower amounts of bound TRIM28 and H3F3A. Therefore, TRIM28 is able to relocate more ZNF10 to the nucleus and the formation of the transcriptional silencing complex is increased. This results in a higher occupancy of the Sp1 promoter sites on *EFEMP1* and therefore transcriptional silencing. In addition, these cells have a higher base level of ZNF10 and SETDB1 allowing

for a higher number of complexes to be formed. These interactions result in lower EFEMP1 levels in isogenic *MALAT1* KD cells compared to their respective control cells.

This highly simplified diagram recapitulates the observations from the differential proteome analysis upon *MALAT1* KD, the MS-based investigation of proteinaceous *MALAT1* interactors, as well as the immunolabelling analysis of ZNF10s' localisation in the cell. In isogenic LN308 *MALAT1* KD cells, no differential regulation of SETDB1 was observed and the localisation of ZNF10 has not been analysed in this cell line pair. Nevertheless, it appears as if the proposed diagram holds for the isogenic LN308 cell line pair as well since the reduction in EFEMP1 levels was observed in both isogenic cell line pairs upon *MALAT1* KD. Potential binding between *MALAT1* and H3F3A, as well as TRIM28, has been observed in both parental cell lines and the increase of ZNF10 was observed in both cell line pairs upon *MALAT1* KD. Although the diagram depicts the regulation of EFEMP1 on basis of the MALAT1 expression level, the depicted interaction and signalling pathways are based on the existence of Sp1 promoter sites in the respective protein-coding DNA regions. Meaning that the diagram could depict a general pathway for *MALAT1* based protein regulation. Upon *MALAT1* KD in both isogenic cell line pairs investigated proteins were found to be downregulated as well as upregulated suggesting further regulatory checkpoints. For example, the transcription of the protein integrin α-5 (ITGA5) upregulated upon *MALAT1* KD in isogenic LN18 cells is regulated through Sp1 promoter sites [238]. This highlights that there are as of yet unknown factors influencing the postulated regulatory event.

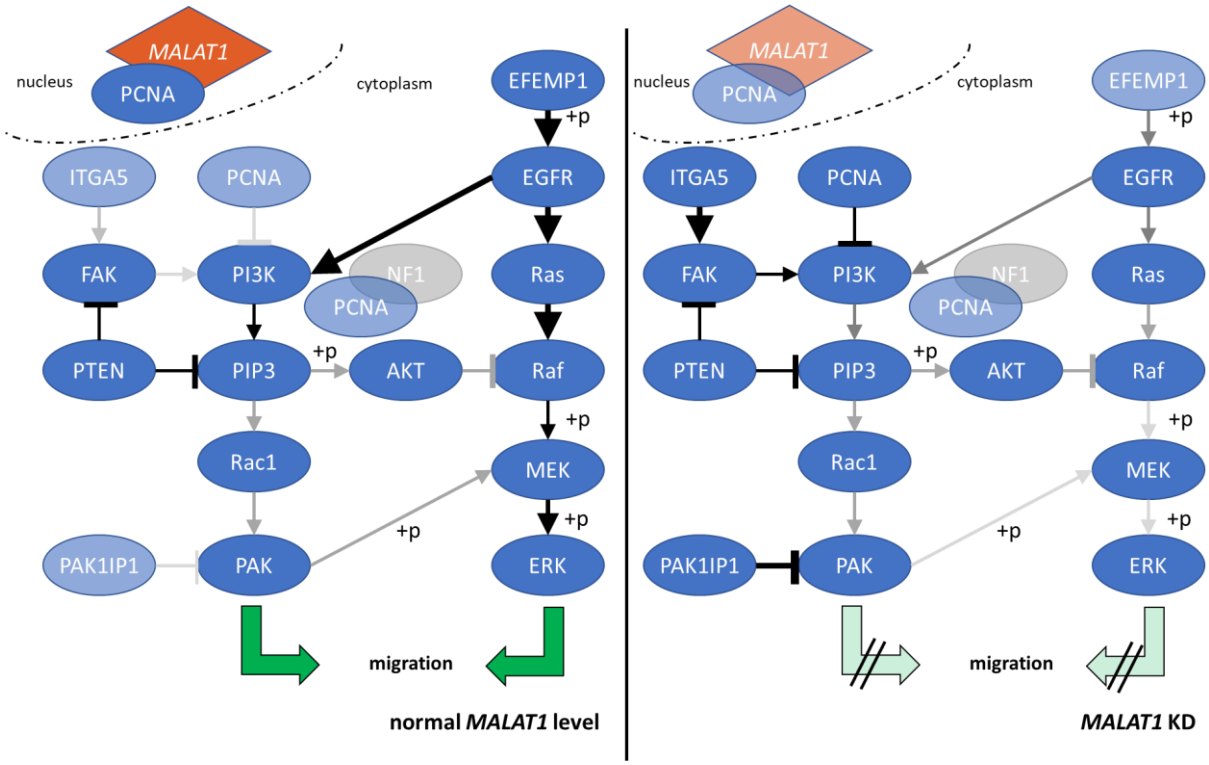

Figure 49 Proposed pathway for migration effect observed in isogenic LN18 control (left) and *MALAT1* KD (right) cells. Blue ovals represent proteins, red diamonds represent lncRNA, grey ovals represent proteins affected by silencing mutations, grey, as well as black arrows, indicate signalling events, and green block arrows indicate a process. The colour saturation of the proteins and lncRNA indicate the level present at the depicted site, the higher the saturation the higher the level at the depicted site. While the colour saturation of the process arrows indicates the activity level of this process, the higher the saturation the higher the activity of the process. The colour and thickness of the signalling event arrows indicate the activity level for this event, the darker and bolder the arrow the higher the activity level of the signalling event. The +p indicates where the activation is achieved through phosphorylation of the respective protein.

The reduction in migration rate upon *MALAT1* KD observed in the isogenic LN18 cell line pair could be based on the reduced binding of PCNA to *MALAT1*, on the increase in ITGA5 as well as PAK1IP1 levels, on the reduction of EFEMP1 levels, and the thus reduced activity of the EGFR/PI3K signalling axis (Figure 49). In the control cells, PCNA is mostly bound to *MALAT1* reducing its ability to block PI3K signalling [239]. The EGFR/PI3K signalling cascade is activated through EFEMP1 and to a lower extent through integrin ITGA5 resulting in cell migration [15, 19, 155, 240-244]. Both FAK and PI3K are blocked though PTEN reducing the activity of PIP3 and therefore the level of pAKT as well as activated Rac1 and PAK. PAK1IP1 further reduces the level of active PAK and thus in turn the level of phosphorylated MEK and ERK. Decreased pAKT levels result in reduced inhibition of Raf and a higher level of phosphorylated MEK and ERK. Both activated PAK and phosphorylated ERK instigate cell migration through further downstream signalling. In comparison, isogenic LN18 *MALAT1* KD cells possess a higher level of unbound PCNA as well as higher levels of ITGA5 and PAK1IP1 in addition to reduced levels of EFEMP1. These changes lead to reduced activation of the EGFR/PI3K signalling cascade resulting in lower levels of phosphorylated MEK and ERK, lower levels of activated PAK and thus a decrease in migration rate.

This diagram reflects the observed protein expression level changes upon *MALAT1* KD of EFEMP1, ITGA5, and PAK1IP1 in the isogenic LN18 cell line pair, the potential interaction between MALAT1 and PCNA, as well as the decrease in AKT T308, MEK, and ERK phosphorylation levels. The observed increase in AKT phosphorylation at S473 is not reflected in this diagram. Phosphorylation of AKT at S473 has been linked to the mTOR signalling pathway which is not represented in the diagram [245]. Additional activation of the mTOR signalling cascade could result in the observed increase in pAKT S473 but has not been investigated during this study.

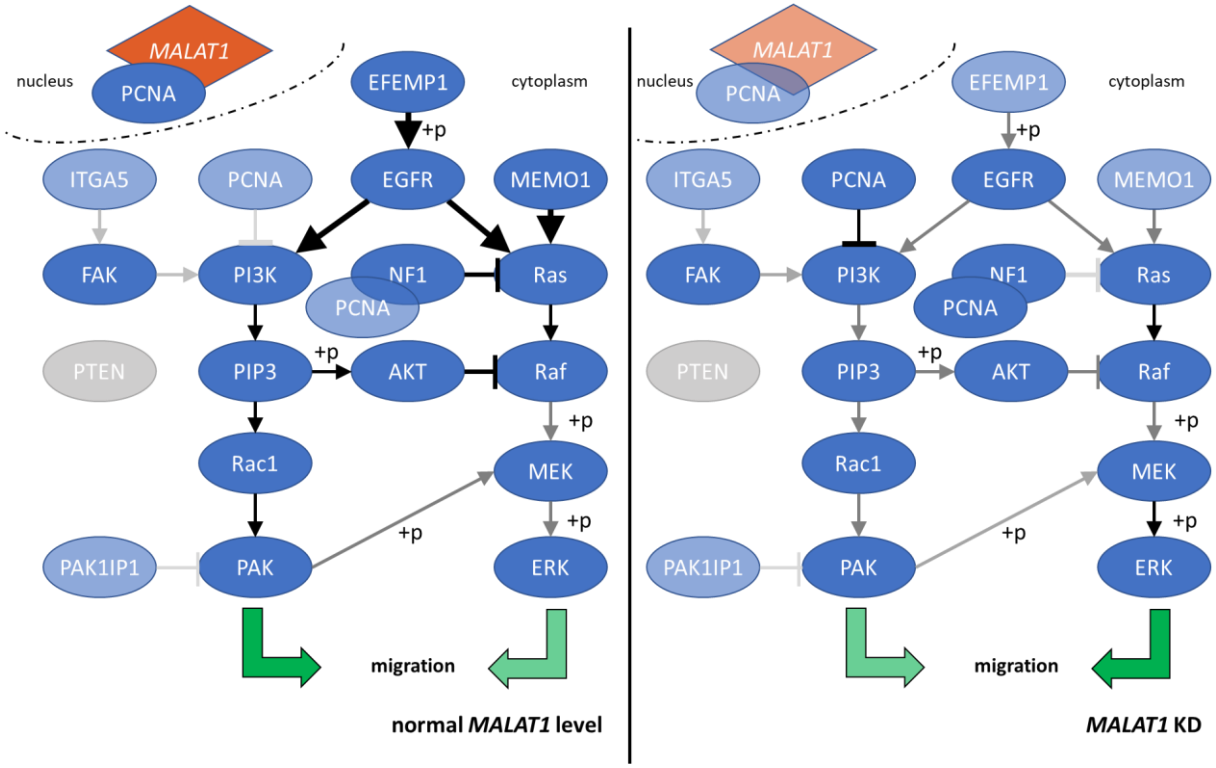

Figure 50 Proposed pathway for migration effect observed in isogenic LN308 control (left) and *MALAT1* KD (right) cells. Blue ovals represent proteins, red diamonds represent lncRNA, grey ovals represent proteins affected by silencing mutations, grey, as well as black arrows, indicate signalling events, and green block arrows indicate a process. The colour saturation of

the proteins and lncRNA indicate the level present at the depicted site, the higher the saturation the higher the level at the depicted site. While the colour saturation of the process arrows indicates the activity level of this process, the higher the saturation the higher the activity of the process. The colour and thickness of the signalling event arrows indicate the activity level for this event, the darker and bolder the arrow the higher the activity level of the signalling event. The +p indicates where the activation is achieved through phosphorylation of the respective protein.

The steady migration rate in isogenic LN308 *MALAT1* KD and respective control cells observed could be based on the reduced binding of PCNA to *MALAT1*, on the reduction of EFEMP1, as well as MEMO1, levels, and the thus reduced activity of the EGFR/PI3K signalling axis (Figure 50). Contrary to LN18 cells, LN308 cells carry a mutation leading to *PTEN* silencing while NF1 is normally expressed and functioning. Therefore, FAK and PIP3 activity levels are not reduced through PTEN in this cell line leading to increased phosphorylation of AKT and activation of Rac1. Due to the resulting higher level of pAKT, EGFR signalling activity is reduced at Raf. However, increased activity of Rac1 leads to increased activity of PAK resulting in activation of downstream signalling events. Since PCNA is mostly bound to *MALAT1* in the isogenic control cells, NF1 is able to reduce the EFEMP1 activated EGFR signalling through inhibition of Ras. Meanwhile, Ras activity levels in these cells are increased by MEMO1 negating the influence of NF1 based inhibition. Overall, the activity of the PK axis in the isogenic LN308 control cells might by higher through the PI3K based axis compared to the Ras-MEK-ERK axis. In isogenic *MALAT1* KD cells, PCNA inhibits PI3K and NF1 activity. The inhibition of NF1 together with the lower activation of EGFR through EFEMP1, in addition to the reduced activation of Ras by MEMO1, due to reduced expression levels cancel each other out resulting in an overall unchanged activity level for this pathway. The reduction in PI3K signalling results in a reduction of pAKT which results in a decreased inhibition of Raf as well as a reduced activity of Rac1 resulting in lower activity levels of PAK and higher activity levels of Raf. Overall, these perturbations result in an increased activation through the Ras-MEK-ERK axis and a decreased activity through the PI3K axis.

The diagram reflects results obtained from the MS-based proteomics study, the affinity enrichment based *MALAT1* interactomics analysis, and the immunoblot results obtained. The observed decrease upon *MALAT1* KD increase of pAKT T308 could be based on the measurement inaccuracy of the method especially since this immunoblot was only performed one time. However, the observed increase in MEK and ERK phosphorylation upon *MALAT1* KD is distinct enough to be unaffected by this inaccuracy. This observed increase in phosphorylation level could be based on the additional downregulation of MEMO1 in isogenic LN308 *MALAT1* KD cells. This protein activates Ras and might be the reason for the observed increase in phosphorylation of MEK and ERK [186]. This downregulation is not observed in isogenic LN18 *MALAT1* KD cells. The increased activation of MEK and ERK upon *MALAT1* KD in isogenic LN308 cells observed via immunoblot does not correlate with the unperturbed migration rate compared to the respective isogenic control cells. As suggested in the diagram, it is possible that the activity shifts between the two depicted signalling axes and therefore balancing the activation of respective downstream targets resulting in an unperturbed migration rate upon *MALAT1* KD. The seemingly higher activation of the Ras-MEK-ERK axis in combination with an unperturbed migration rate, in this case, could also be explained through the analysis of further downstream signalling targets as the EGFR signalling axis activates a broad range of downstream targets affecting various cellular responses such as proliferation, differentiation and development [246]. No further analysis of any downstream targets has been performed during this thesis since the data obtained during this study is not highlighting any particular area of interest for this cell line.

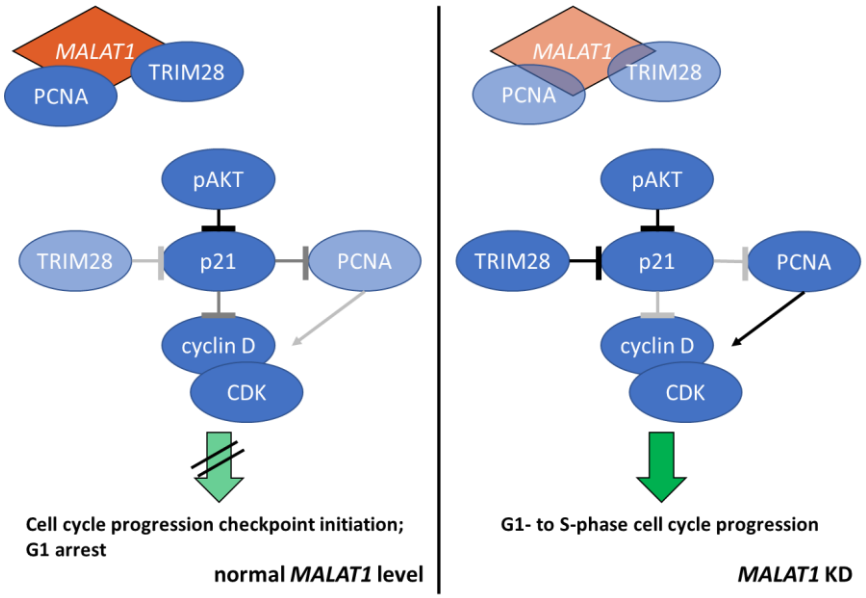

Figure 51 Proposed pathway for cell cycle effect observed in isogenic LN18 control (left) and *MALAT1* KD (right) cells. Blue ovals represent proteins, red diamonds represent lncRNA, grey, as well as black arrows, indicate signalling events, and green block arrows indicate a process. The colour saturation of the proteins and lncRNA indicate the level present at the depicted site, the higher the saturation the higher the level at the depicted site. While the colour saturation of the process arrows indicates the activity level of this process, the higher the saturation the higher the activity of the process. The colour and thickness of the signalling event arrows indicate the activity level for this event, the darker and bolder the arrow the higher the activity level of the signalling event. The +p indicates where the activation is achieved through phosphorylation of the respective protein.

In isogenic LN18 *MALAT1* KD cells compared to their respective control cells, cell cycle analysis depicted a significantly higher percentage of cells in S-phase. Combining findings from the investigation of proteinaceous *MALAT1* interactors, performed cell cycle analysis, as well as the proposed pathway diagram reflecting the effects of EFEMP1 dysregulation (Figure 49) discovered in the proteomics analysis, a pathway for cell cycle regulation in isogenic LN18 control and *MALAT1* KD cells was proposed (Figure 51) [20, 215, 216, 247, 248]. In isogenic control cells, TRIM28 and PCNA are thought to be mostly bound to *MALAT1* resulting in reduced inhibition of p21 through TRIM28 as well as reduced activation of the cyclin D/CDK complex through PCNA. This reduction in inhibition results in checkpoint activation and G1 arrest through inhibition of the cyclin D/CDK protein complex and PCNA via p21. Contrarily in isogenic LN18 *MALAT1* KD cells, the p21 based inhibition of G1- to S-phase is reduced since unbound TRIM28 inhibits the p21 protein activity. The reduction in p21 protein activity also results in reduced inhibition of unbound PCNA. Levels of pAKT in isogenic LN18 *MALAT1* KD cells are either equal to those of the respective control cells or higher. In case of higher pAKT levels, the inhibition of p21 would be further increased upon *MALAT1* KD in LN18 derived isogenic cells.

The proposed diagram reflects the observed increase in S-phase cells upon *MALAT1* KD in isogenic LN18 cells, the proposed interaction between *MALAT1* and TRIM28/PCNA as well as the potential increase in pAKT levels upon *MALAT1* KD observed through immunolabelling analysis. While an increase in the percentage of cells in S-phase could indicate a higher rate of cell cycle progression upon *MALAT1* KD in isogenic LN18 cells no change in their proliferation rate has been observed during this study. On the other hand, an increase in cells in S-phase could also reflect a blockage of the progression of cells into G2/M-phase. S-phase is an important part of the cell cycle as this phase not only includes DNA replication but also DNA repair [249, 250]. During S-phase cells have to pass several checkpoints

to ensure genome stability to progress into G2/M-phase. The proposed *MALAT1* interacting protein PCNA has been described to be essential for G1 and G2 cell cycle progression in a p21 dependent manner in p53 deficient cells by Cayrol *et al.*, this proposed interaction highlights a fine-tuned regulation of p21 activity influenced by *MALAT1* through interaction with PCNA and TRIM28 [20]. Both parent cell lines, LN18 and LN308, are p53 deficient (Appendix B Table 20) fitting with the proposed regulation pathway. The observed increase in cells during S-phase upon *MALAT1* KD in isogenic LN18 cells could be due to a decrease in G1 arrest as well as an increase in S-phase arrest at this point both scenarios are equally possible.

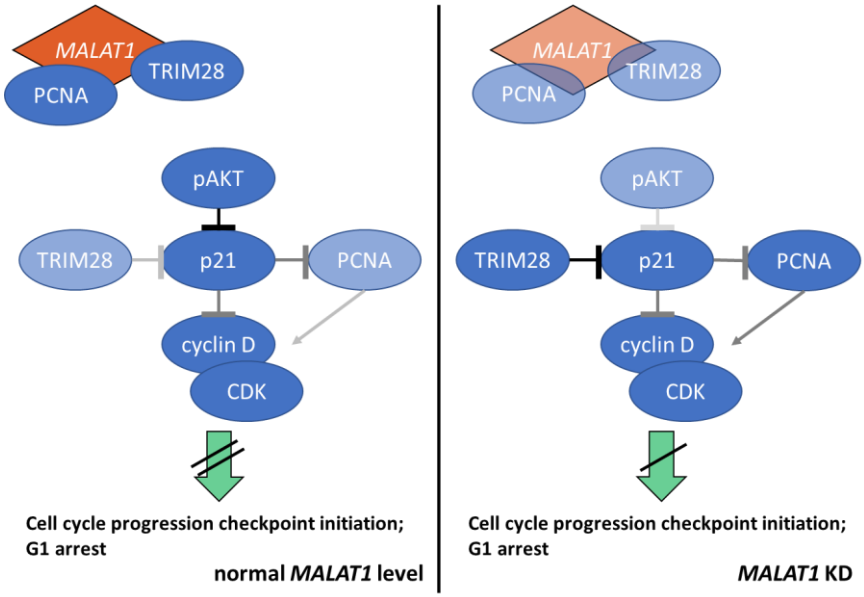

Figure 52 Proposed pathway for cell cycle effect observed in isogenic LN308 control (left) and *MALAT1* KD (right) cells. Blue ovals represent proteins, red diamonds represent lncRNA, grey, as well as black arrows, indicate signalling events, and green block arrows indicate a process. The colour saturation of the proteins and lncRNA indicate the level present at the depicted site, the higher the saturation the higher the level at the depicted site. While the colour saturation of the process arrows indicates the activity level of this process, the higher the saturation the higher the activity of the process. The colour and thickness of the signalling event arrows indicate the activity level for this event, the darker and bolder the arrow the higher the activity level of the signalling event. The +p indicates where the activation is achieved through phosphorylation of the respective protein.

No statistically relevant differences were observed in the cell cycle of isogenic LN308 *MALAT1* KD cells in comparison to their respective control cells. Combining findings from the investigation of proteinaceous *MALAT1* interactors, performed cell cycle analysis, as well as the proposed pathway diagram reflecting the effects of EFEMP1 and MEMO1 dysregulation (Figure 50) discovered in the proteomics analysis, a pathway for cell cycle regulation in isogenic LN308 control and *MALAT1* KD cells was proposed (Figure 52) [20, 215, 216, 247, 248]. In comparison to the proposed pathway in isogenic LN18 *MALAT1* KD cells (Figure 51), pAKT levels were found to be reduced in isogenic LN308 *MALAT1* KD cells. This reduction is thought to level out the increased inhibition of p21 via TRIM28 described previously. While the increase in unbound PCNA increases the overall activation of the cyclin D/CDK complex slightly.

The proposed diagram reflects the results from the cell cycle analysis in the isogenic LN308 cell line pair depicting equal cell distributions over the analysed cell cycle phases. The increased doubling time observed for isogenic LN308 *MALAT1* KD cells could be due to a decrease in pPCNA levels resulting from the decreased pEGFR levels proposed for isogenic LN308 *MALAT1* KD cells (Figure 50) [251].

Activated EGFR has been shown to directly phosphorylate PCNA leading to increased cell growth in cancer cells [251, 252]. This regulatory action is independent of the proposed pathway for the cell-cycle results based on p21 activity and therefore not reflected in the diagram. The only statistically relevant difference observed in the cell cycle analysis between isogenic LN308 *MALAT1* KD and their respective control cells was an increase in the population of apoptotic cells upon *MALAT1* KD. This finding has not been depicted in this diagram since the increase is minimal, from 0.80 % (±0.04) to 1.08 % (±0.11), especially considering the measurement variance reported.

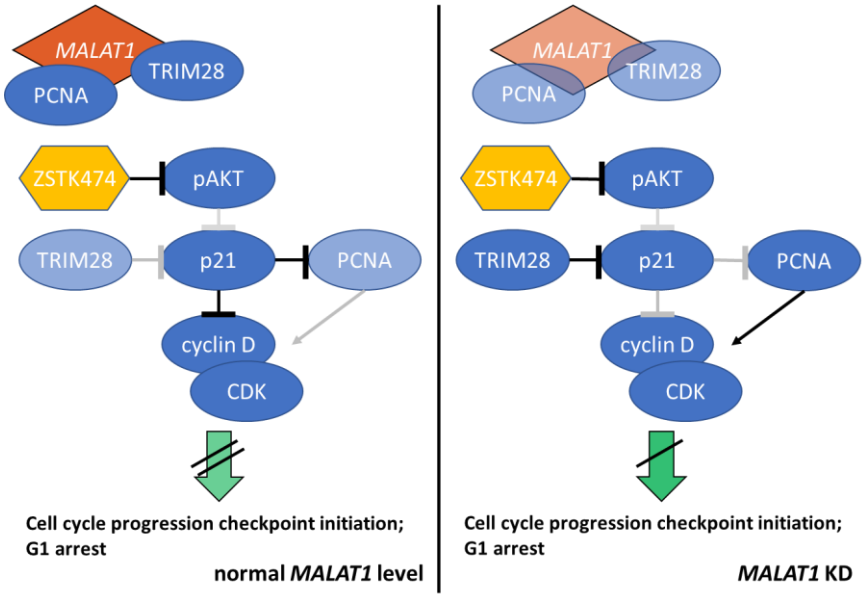

Figure 53 Proposed pathway for cell cycle effect observed in isogenic LN18 control (left) and *MALAT1* KD (right) cells treated with ZSTK474. Blue ovals represent proteins, yellow hexagons represent inhibitor molecules, red diamonds represent lncRNA, grey, as well as black arrows, indicate signalling events, and green block arrows indicate a process. The colour saturation of the proteins and lncRNA indicate the level present at the depicted site, the higher the saturation the higher the level at the depicted site. While the colour saturation of the process arrows indicates the activity level of this process, the higher the saturation the higher the activity of the process. The colour and thickness of the signalling event arrows indicate the activity level for this event, the darker and bolder the arrow the higher the activity level of the signalling event. The +p indicates where the activation is achieved through phosphorylation of the respective protein.

Treatment with the PI3K inhibitor ZSTK474 affected the cell cycle in all four isogenic cell lines analysed identically but to different degrees. Observed changes were an increase in the percentage of cells in G1-phase as well as apoptotic cells, and the subsequent decrease of cells in S- as well as G2/M-phase. The percentage of cells in S-phase after treatment with ZSTK474 was significantly higher in isogenic LN18 *MALAT1* KD cells compared to their respective control cells. In addition, the proliferation rate of the isogenic control cell lines was reduced upon treatment with ZSTK474 compared to respective cell populations treated with DMSO. This treatment effect was not observed in isogenic *MALAT1* KD cells. Combining findings from the investigation of proteinaceous *MALAT1* interactors, performed cell cycle analysis, as well as the proposed pathway diagram reflecting the effects of EFEMP1 dysregulation (Figure 49) discovered in the proteomics analysis, a pathway for cell cycle regulation in isogenic LN18 control and *MALAT1* KD cells upon treatment with ZSTK474 was proposed (Figure 53) on basis of the proposed cell cycle pathway (Figure 51) [20, 215, 216, 247, 248]. The diagram depicts the additional inhibition of pAKT via ZSTK474 resulting in a decreased inhibition of p21 in both isogenic LN18 cell line models [201, 202, 253]. This decreased inhibition leads to higher inhibition of the cyclin D/CDK complex resulting in increased G1 arrest. Due to the differential levels of unbound TRIM28 and PCNA, this effect

was significantly different amongst the isogenic LN18 cell line pair. Thus, a higher cell cycle inhibition in the G1-phase was observed for isogenic LN18 control cells.

The proposed diagram reflects analysis results obtained in this study for isogenic LN18 cell lines as well as previous literature. The higher percentage of cells in S-phase after treatment with ZSTK474 upon *MALAT1* KD in isogenic LN18 cells, align with the findings from the HT drug screen depicting a lower treatment efficacy of ZST474 in *MALAT1* KD cells. Statistical analysis revealed an interactive effect between *MALAT1* expression levels and ZSTK474 treatment. This observed interaction highlights a linkage between the cell signalling pathways affected through *MALAT1* and the ones affected through ZSTK474 treatment. This statistically significant interaction is reflected in the proposed pathway diagram.

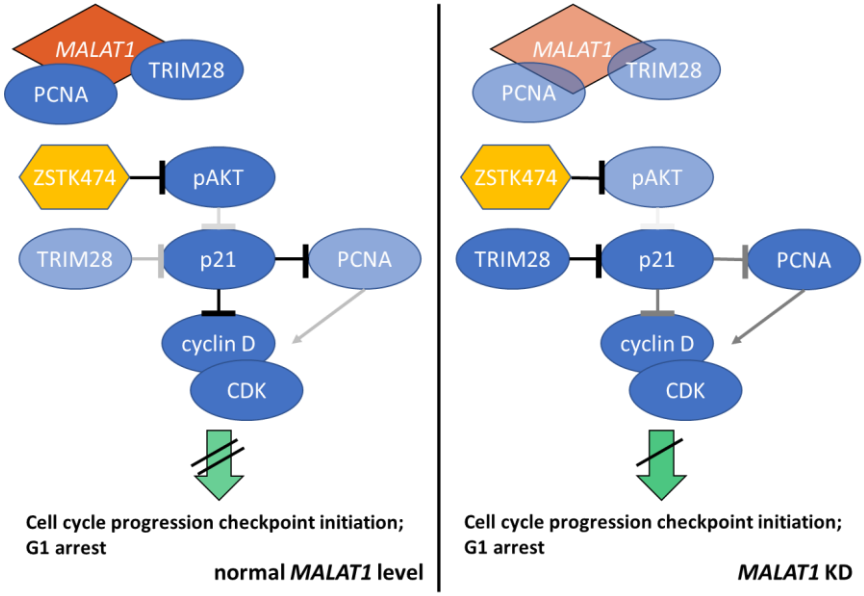

Figure 54 Proposed pathway for cell cycle effect observed in isogenic LN308 control (left) and *MALAT1* KD (right) cells treated with ZSTK474. Blue ovals represent proteins, yellow hexagons represent inhibitor molecules, red diamonds represents lncRNA, grey, as well as black arrows, indicate signalling events, and green block arrows indicate a process. The colour saturation of the proteins and lncRNA indicate the level present at the depicted site; the higher the saturation the higher the level at the depicted site. While the colour saturation of the process arrows indicates the activity level of this process; the higher the saturation the higher the activity of the process. The colour and thickness of the signalling event arrows indicate the activity level for this event, the darker and bolder the arrow the higher the activity level of the signalling event. The +p indicates where the activation is achieved through phosphorylation of the respective protein.

In isogenic LN308 cell lines, ZSTK474 treatment leads to the increase of cells in G1-phase, and a decrease of cells in G2/M-phase. A significant decrease of cells in S-phase was only observed in isogenic LN308 control cells upon ZSTK474 treatment. Combining findings from the investigation of proteinaceous *MALAT1* interactors, performed cell cycle analysis, as well as the proposed pathway diagram reflecting the effects of EFEMP1 and MEMO1 dysregulation (Figure 50) discovered in the proteomics analysis, a pathway for cell cycle regulation in isogenic LN308 control and *MALAT1* KD cells upon treatment with ZSTK474 was proposed (Figure 54) on basis of the proposed cell cycle pathway (Figure 52) [20, 215, 216, 247, 248]. As proposed for isogenic LN18 cell lines ZSTK474 inhibits pAKT and thereby reduces inhibition of p21 [201, 202, 253]. This reduced inhibition of p21 leads to increased inhibition of the cyclin D/CDK complex resulting in a stronger G1 arrest in both isogenic cell lines. In comparison to the isogenic LN18 cell line pair, the pAKT level was proposed to be reduced upon *MALAT1* KD in isogenic LN308 cells resulting in reduced efficacy of ZSTK474 treatment in these cells.

While measurements in the isogenic LN308 cell line pair depicted an overall identical response to ZSTK474 treatment on the cell cycle and proliferation, no significant interaction amongst *MALAT1* expression levels and ZSTK474 treatment was observed. Also, the percentage of cells in S-phase was not found to be increased upon *MALAT1* KD in isogenic LN308 cells compared to their respective control cells after treatment with ZSTK474, aligning with the observations from the cell cycle comparison of DMSO treated cells dependent on the *MALAT1* expression level. The percentage of cells in S-phase upon treatment with ZSTK474 while reduced was not found to be significantly reduced in isogenic LN308 *MALAT1* KD cells compared to the DMSO treated cells. This could be due to the high measurement variance observed or the change could have been to minor for the applied detection method. The obtained proliferation and cell cycle data suggest a reduced efficacy for treatment with the PI3K inhibitor ZSTK474 upon *MALAT1* KD in isogenic LN308 as has been observed for the isogenic LN18 cells but without any additional data on the dose-response in the two isogenic LN308 cell lines, no definitive statement can be made on a potentially differential efficacy of ZSTK474 treatment.

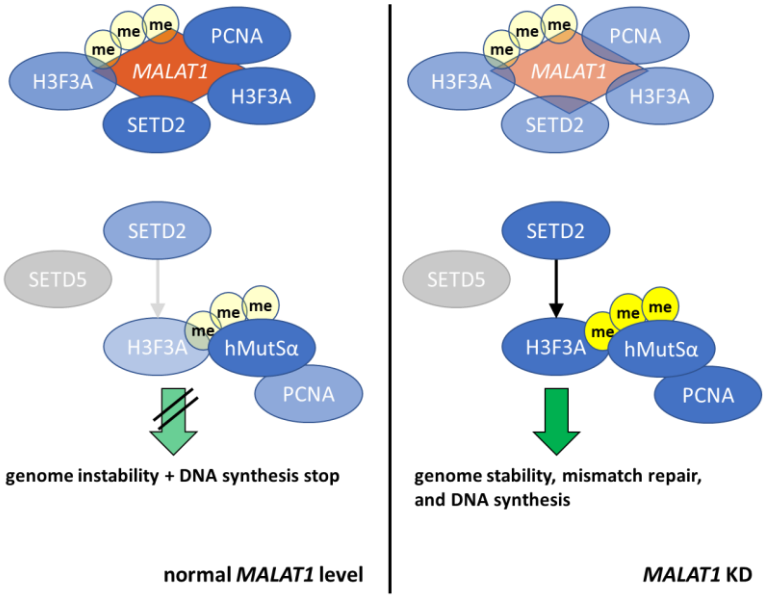

Figure 55 Proposed pathway for H3F3A PTM deregulation in isogenic LN18 control (left) and *MALAT1* KD (right) cells. Blue ovals represent proteins, yellow circles represent a methyl group, red diamonds represent lncRNA, grey, as well as black arrows, indicate signalling events, and green block arrows indicate a process. The colour saturation of the proteins and lncRNA indicate the level present at the depicted site, the higher the saturation the higher the level at the depicted site. While the colour saturation of the process arrows indicates the activity level of this process, the higher the saturation the higher the activity of the process. The colour and thickness of the signalling event arrows indicate the activity level for this event, the darker and bolder the arrow the higher the activity level of the signalling event. The +p indicates where the activation is achieved through phosphorylation of the respective protein.

H3F3A K36me3 levels appeared to be deregulated on basis of *MALAT1* expression levels according to the performed second round search. In isogenic LN18 *MALAT1* KD cells the level of H3F3A K36me3 appeared to be higher compared to its respective control cell line. Since the LN18 cell line carries a silencing mutation of SETD5 (according to the depmap portal accessed on 17/08/2020), trimethylation of H3F3A K36 is dependent on the known *MALAT1* interactor SETD2 [61, 227]. The methylation status at K36 affects genome stability through DNA synthesis as well as DNA repair pathways via interaction with hMutSα and PCNA [106, 254]. The diagram depicts a proposed pathway for the effects of H3F3A PTM deregulation based on *MALAT1* levels in isogenic LN18 cell lines (Figure 55). In the isogenic LN18 control cells, H3F3A, H3F3A K36me3, PCNA, and SETD2 are mostly bound to *MALAT1*. This binding is

thought to result in reduced levels of H3F3A K36me3, reducing the formation of the H3F3A K36me3/hMutSα/PCNA complex and therefore reducing DNA synthesis and mismatch repair. The isogenic LN18 *MALAT1* KD cells, in contrast, have higher levels of unbound H3F3A and SETD2 leading to higher levels of H3F3A K36me3. Since less H3F3A K36me3 and PCNA is bound to *MALAT1*, the H3F3A K36me3/hMutSα/PCNA complex is able to form and initiate DNA synthesis and mismatch repair.

A reduction in DNA mismatch repair leads to increased genome instability and thus increased tumorigenesis [209, 255, 256]. While DNA synthesis is necessary for cell cycle progression. The putative *MALAT1* interacting protein PCNA identified in this study has been linked to both processes in a regulatory function [248]. The diagram depicts a potential explanation for the increase in H3F3A K36me3 upon *MALAT1* KD in isogenic LN18 cells and proposes a potential impact on DNA damage repair and cell cycle pathways through interaction with PCNA. Accumulation of the H3F3A K36me3/hMutSα/PCNA complex at damaged DNA sites could result in S-phase arrest, explaining the differences observed in the isogenic LN18 *MALAT* KD cells compared to their respective control cells in the cell cycle analysis without any change in doubling time or proliferation rate.[248]

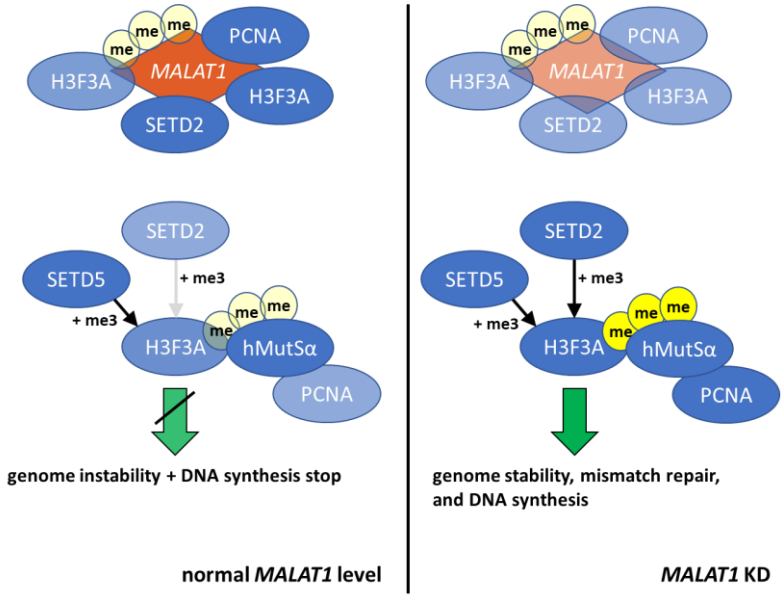

Figure 56 Proposed pathway for H3F3A PTM deregulation in isogenic LN308 control (left) and *MALAT1* KD (right) cells. Blue ovals represent proteins, yellow circles represent a methyl group, red diamonds represent lncRNA, grey, as well as black arrows, indicate signalling events, and green block arrows indicate a process. The colour saturation of the proteins and lncRNA indicate the level present at the depicted site, the higher the saturation the higher the level at the depicted site. While the colour saturation of the process arrows indicates the activity level of this process, the higher the saturation the higher the activity of the process. The colour and thickness of the signalling event arrows indicate the activity level for this event, the darker and bolder the arrow the higher the activity level of the signalling event. The +p indicates where the activation is achieved through phosphorylation of the respective protein.

Based on the data collected in this study, a pathway for the dysregulation of H3F3A K36 methylation status and its effects in isogenic LN308 cells cannot be proposed under consideration of all observations. Overall, the pathway proposed for isogenic LN18 cells should be identical to the one for isogenic LN308 cells with the addition of functional SETD5 (Figure 56). This proposed pathway would result in the same albeit slightly less extreme deregulation of H3F3A K36me3 upon *MALAT1* KD in isogenic LN308 cells as described for isogenic LN18 cells. However, the second-round search data suggests a vice versa regulation amongst the isogenic cell line pairs.

No clear pathway for the observed reduction of H3F3A K36me3 upon MALAT1 KD in isogenic LN308 cells can be proposed based on the data obtained in this study. The proposed increase in the H3F3A K36me3/hMutSα/PCNA complex upon *MALAT1* KD could result in the induction of a subsequent G1 arrest based on DNA-damage identified during S-phase [257]. This, in turn, could explain the lower doubling time observed for isogenic LN308 *MALAT1* KD cells as well as the equal distribution of cells in the different cell cycle stages amongst isogenic LN308 cells. The cells could be stalled in the S-phase due to DNA damage repair and therefore increase the cells doubling time. And the accumulation of the H3F3A K36me3/hMutSα/PCNA complex at DNA damage sites could lead to a subsequent G1 arrest counterbalancing the reduction of G1 arrest previously described in the proposed cell cycle pathway dependent on p21 upon *MALAT1* KD in isogenic LN308 cells.

Combination of all the data obtained during this study as well as an extensive literature search resulted in the proposal of several signalling pathways affected by *MALAT1* expression levels in both isogenic cell line pairs. These proposed pathways are employed to gain a better understanding of *MALAT1s*' influence on tumour biology and their protein interaction networks. In addition, they can be employed to set up further studies and experiments to unravel the influence *MALAT1* has on protein signatures in GBM.

6 Outlook

Although this study increased the knowledge about *MALAT1*s' influence in GBM biology, the data obtained gives rise to new questions and points out new putative focus areas.

As the analysed isogenic cell lines yielded distinctively different results potentially related to their mutational status, it would be beneficial to generate additional isogenic *MALAT1* KD cell lines with a matching mutational status, repeat the analyses, and compare results. In addition, the phosphorylation analysis of key proteins in the EGFR/PI3K signalling cascade should be repeated and broadened to include mTOR related AKT regulators. It might be beneficial to switch to an MS-based readout instead of the employed immunoblotting to increase sensitivity such as a parallel reaction monitoring method. Another worthwhile experiment would be to analyse secretomes from the isogenic cell lines since EFEMP1 is a classically secreted protein and investigate if culturing isogenic LN18 *MALAT1* KD cells with EFEMP1 containing media affects the migration rate. Culturing the isogenic *MALAT1* KD cells in conditioned medium from respective isogenic control cells might be the easiest way to perform this kind of experiment since synthesised proteins might differ in their folding or PTM status and therefore affect the treated cells differently. To corroborate the putative *MALAT1* interactors identified in this study, reverse pulldowns with an RT-qPCR readout should be performed to investigate if *MALAT1* RNA is binding to the respective protein. In case the binding is confirmed this setup could be employed to determine the specific region in the *MALAT1* sequence responsible for interacting with the respective protein employed in the reverse pulldown experiment.

7 Conclusion

In this study aimed at analysing *MALAT1* based protein signatures, several signalling pathways of known importance in GBM biology were linked to *MALAT1* biology.

Although the lncRNA *MALAT1* is highly expressed in a number of different tumours, its protein interactome has been shown to be specific between MB and GBM tumour cell lines.

The isogenic *MALAT1* cell lines generated depicted cell line specific differences in the employed phenotype characterisation assays. These highlighted phenotypic differences could be based on the distinct mutational background of the chosen parental cell lines. The change in migratory phenotype of isogenic LN18 cell lines fits well with the data obtained in the cellular proteome perturbation analysis. Although the downregulation of EFEMP1 via the described TRIM28/ZNF10 axis upon *MALAT1* KD depicts a global effect on both isogenic KD cells, the effects observed differ between the cell lines. This difference in effect is not unexpected in a highly heterogeneous tumour species such as GBM.

The PI3K/EGFR signalling cascade directly activated by EFEMP1 appears to be linked to *MALAT1* biology through the data obtained in this study. In addition, *MALAT1* appears to perturb signalling pathways for cell cycle regulation and DNA repair.

This study clearly shows that *MALAT1* as a lncRNA can affect protein signatures in the investigated cell lines and that decreased *MALAT1* expression levels can lead to phenotypic changes as well as perturbations in protein signalling cascades.

8 Bibliography

1. PDQ_Adult_Treatment_Editorial_Board. *PDQ Adult Central Nervous System Tumors Treatment*. 2022 [cited 2022 23/08/2022]; Available from: https://www.cancer.gov/types/brain/patient/adult-brain-treatment-pdq.
2. Compton, P.D., N.L. Kelleher, and J. Gunawardena, *Estimating the Distribution of Protein Post-Translational Modification States by Mass Spectrometry.* J Proteome Res, 2018. **17**(8): p. 2727-2734.
3. Huse, J.T. and E.C. Holland, *Targeting brain cancer: advances in the molecular pathology of malignant glioma and medulloblastoma.* Nature Reviews Cancer, 2010. **10**(5): p. 319-331.
4. Ostrom, Q.T., S.S. Francis, and J.S. Barnholtz-Sloan, *Epidemiology of Brain and Other CNS Tumors.* Current Neurology and Neuroscience Reports, 2021. **21**(12): p. 68.
5. Singh, N., et al., *Mechanisms of temozolomide resistance in glioblastoma - a comprehensive review.* Cancer drug resistance (Alhambra, Calif.), 2021. **4**(1): p. 17-43.
6. Lapointe, S., A. Perry, and N.A. Butowski, *Primary brain tumours in adults.* The Lancet, 2018. **392**(10145): p. 432-446.
7. Weller, M., et al., *Glioma.* Nature Reviews Disease Primers, 2015. **1**(1): p. 15017.
8. Louis, D.N., et al., *The 2016 World Health Organization Classification of Tumors of the Central Nervous System: a summary.* Acta Neuropathologica, 2016. **131**(6): p. 803-820.
9. Ostrom, Q.T., et al., *Adult Glioma Incidence and Survival by Race or Ethnicity in the United States From 2000 to 2014.* JAMA oncology, 2018. **4**(9): p. 1254-1262.
10. Delgado-López, P.D. and E.M. Corrales-García, *Survival in glioblastoma: a review on the impact of treatment modalities.* Clinical and Translational Oncology, 2016. **18**(11): p. 1062-1071.
11. Weller, M., et al., *Standards of care for treatment of recurrent glioblastoma—are we there yet?* Neuro-Oncology, 2012. **15**(1): p. 4-27.
12. Pirlog, R., et al., *Proteomic Advances in Glial Tumors through Mass Spectrometry Approaches.* Medicina, 2019. **55**(8): p. 412.
13. Crespo, I., et al., *Molecular and Genomic Alterations in Glioblastoma Multiforme.* The American Journal of Pathology, 2015. **185**(7): p. 1820-1833.
14. Ohgaki, H. and P. Kleihues, *Genetic pathways to primary and secondary glioblastoma.* Am J Pathol, 2007. **170**(5): p. 1445-53.
15. Camaj, P., et al., *EFEMP1 binds the EGF receptor and activates MAPK and Akt pathways in pancreatic carcinoma cells.* Biol Chem, 2009. **390**(12): p. 1293-302.
16. Lobbous, M., et al., *An Update on Neurofibromatosis Type 1-Associated Gliomas.* Cancers (Basel), 2020. **12**(1).
17. Markwell, S.M., et al., *Necrotic reshaping of the glioma microenvironment drives disease progression.* Acta Neuropathologica, 2022. **143**(3): p. 291-310.
18. Ross, J.L., et al., *5-Aminolevulinic Acid Guided Sampling of Glioblastoma Microenvironments Identifies Pro-Survival Signaling at Infiltrative Margins.* Sci Rep, 2017. **7**(1): p. 15593.
19. Li, X., et al., *PI3K/Akt/mTOR signaling pathway and targeted therapy for glioblastoma.* Oncotarget, 2016. **7**(22): p. 33440-33450.
20. Cayrol, C., M. Knibiehler, and B. Ducommun, *p21 binding to PCNA causes G1 and G2 cell cycle arrest in p53-deficient cells.* Oncogene, 1998. **16**(3): p. 311-320.
21. Biasoli, D., et al., *Retinoblastoma protein regulates the crosstalk between autophagy and apoptosis, and favors glioblastoma resistance to etoposide.* Cell Death & Disease, 2013. **4**(8): p. e767-e767.
22. Pearson, J.R. and T. Regad, *Targeting cellular pathways in glioblastoma multiforme.* Signal transduction and targeted therapy, 2017. **2**(1): p. 1-11.

23. Ostrom, Q.T., et al., *Alex's Lemonade Stand Foundation Infant and Childhood Primary Brain and Central Nervous System Tumors Diagnosed in the United States in 2007–2011.* Neuro-Oncology, 2015. **16**(suppl 10): p. x1-x36.
24. Louis, D.N., et al., *The 2007 WHO Classification of Tumours of the Central Nervous System.* Acta Neuropathologica, 2007. **114**(2): p. 97-109.
25. Gottardo, N.G., et al., *Medulloblastoma Down Under 2013: a report from the third annual meeting of the International Medulloblastoma Working Group.* Acta Neuropathologica, 2014. **127**(2): p. 189-201.
26. Kim, W., et al., *The tumor biology and molecular characteristics of medulloblastoma identifying prognostic factors associated with survival outcomes and prognosis.* Journal of Clinical Neuroscience, 2011. **18**(7): p. 886-890.
27. Bartlett, F., R. Kortmann, and F. Saran, *Medulloblastoma.* Clinical Oncology, 2013. **25**(1): p. 36-45.
28. Gilbertson, R.J. and D.W. Ellison, *The Origins of Medulloblastoma Subtypes.* Annual Review of Pathology: Mechanisms of Disease, 2008. **3**(1): p. 341-365.
29. Mabbott, D.J., et al., *Serial Evaluation of Academic and Behavioral Outcome After Treatment With Cranial Radiation in Childhood.* Journal of Clinical Oncology, 2005. **23**(10): p. 2256-2263.
30. Mulhern, R.K., et al., *Neurocognitive Consequences of Risk-Adapted Therapy for Childhood Medulloblastoma.* Journal of Clinical Oncology, 2005. **23**(24): p. 5511-5519.
31. Thomas, A. and G. Noël, *Medulloblastoma: optimizing care with a multidisciplinary approach.* Journal of multidisciplinary healthcare, 2019. **12**: p. 335.
32. Remke, M., et al., *Adult Medulloblastoma Comprises Three Major Molecular Variants.* Journal of Clinical Oncology, 2011. **29**(19): p. 2717-2723.
33. Remke, M., V. Ramaswamy, and M.D. Taylor, *Medulloblastoma molecular dissection: the way toward targeted therapy.* Current Opinion in Oncology, 2013. **25**(6): p. 674-681.
34. Northcott, P.A., et al., *Subgroup-specific structural variation across 1,000 medulloblastoma genomes.* Nature, 2012. **488**(7409): p. 49-56.
35. Dimitrova, V. and A. Arcaro, *Targeting the PI3K/AKT/mTOR signaling pathway in medulloblastoma.* Curr Mol Med, 2015. **15**(1): p. 82-93.
36. MacDonald, T.J., et al., *Expression profiling of medulloblastoma: PDGFRA and the RAS/MAPK pathway as therapeutic targets for metastatic disease.* Nature Genetics, 2001. **29**(2): p. 143-152.
37. Hatten, M.E. and M.F. Roussel, *Development and cancer of the cerebellum.* Trends in Neurosciences, 2011. **34**(3): p. 134-142.
38. Necsulea, A., et al., *The evolution of lncRNA repertoires and expression patterns in tetrapods.* Nature, 2014. **505**(7485): p. 635-640.
39. Parasramka, M.A., et al., *Long non-coding RNAs as novel targets for therapy in hepatocellular carcinoma.* Pharmacology & Therapeutics, 2016. **161**: p. 67-78.
40. Statello, L., et al., *Gene regulation by long non-coding RNAs and its biological functions.* Nature Reviews Molecular Cell Biology, 2021. **22**(2): p. 96-118.
41. Cech, Thomas R. and Joan A. Steitz, *The Noncoding RNA Revolution—Trashing Old Rules to Forge New Ones.* Cell, 2014. **157**(1): p. 77-94.
42. Fatica, A. and I. Bozzoni, *Long non-coding RNAs: new players in cell differentiation and development.* Nature Reviews Genetics, 2014. **15**(1): p. 7-21.
43. Bhan, A. and S.S. Mandal, *LncRNA HOTAIR: A master regulator of chromatin dynamics and cancer.* Biochimica et Biophysica Acta (BBA) - Reviews on Cancer, 2015. **1856**(1): p. 151-164.
44. Imamura, K., et al., *Long Noncoding RNA NEAT1-Dependent SFPQ Relocation from Promoter Region to Paraspeckle Mediates IL8 Expression upon Immune Stimuli.* Molecular Cell, 2014. **53**(3): p. 393-406.
45. Zappulla, D.C. and T.R. Cech, *Yeast telomerase RNA: a flexible scaffold for protein subunits.* Proc Natl Acad Sci U S A, 2004. **101**(27): p. 10024-9.

46. DiStefano, J.K., *The Emerging Role of Long Noncoding RNAs in Human Disease.* Methods Mol Biol, 2018. **1706**: p. 91-110.
47. Zhang, Y., W. Du, and B. Yang, *Long non-coding RNAs as new regulators of cardiac electrophysiology and arrhythmias: Molecular mechanisms, therapeutic implications and challenges.* Pharmacology & Therapeutics, 2019. **203**: p. 107389.
48. Katsushima, K., et al., *Long non-coding RNAs in brain tumors.* NAR Cancer, 2021. **3**(1).
49. Tanne, A., et al., *Distinguishing the immunostimulatory properties of noncoding RNAs expressed in cancer cells.* Proceedings of the National Academy of Sciences, 2015. **112**(49): p. 15154-15159.
50. Flynn, R.L., et al., *TERRA and hnRNPA1 orchestrate an RPA-to-POT1 switch on telomeric single-stranded DNA.* Nature, 2011. **471**(7339): p. 532-536.
51. Amodio, N., et al., *MALAT1: a druggable long non-coding RNA for targeted anti-cancer approaches.* Journal of Hematology & Oncology, 2018. **11**(1): p. 63.
52. Hutchinson, J.N., et al., *A screen for nuclear transcripts identifies two linked noncoding RNAs associated with SC35 splicing domains.* BMC Genomics, 2007. **8**(1): p. 39.
53. Tripathi, V., et al., *The nuclear-retained noncoding RNA MALAT1 regulates alternative splicing by modulating SR splicing factor phosphorylation.* Molecular cell, 2010. **39**(6): p. 925-938.
54. Lin, R., et al., *A large noncoding RNA is a marker for murine hepatocellular carcinomas and a spectrum of human carcinomas.* Oncogene, 2006. **26**: p. 851.
55. Ji, P., et al., *MALAT-1, a novel noncoding RNA, and thymosin β4 predict metastasis and survival in early-stage non-small cell lung cancer.* Oncogene, 2003. **22**(39): p. 8031-8041.
56. Ma, K.-x., et al., *Long noncoding RNA MALAT1 associates with the malignant status and poor prognosis in glioma.* Tumor Biology, 2015. **36**(5): p. 3355-3359.
57. Vassallo, I., et al., *WIF1 re-expression in glioblastoma inhibits migration through attenuation of non-canonical WNT signaling by downregulating the lncRNA MALAT1.* Oncogene, 2015. **35**: p. 12.
58. Chen, W., et al., *MALAT1 is a prognostic factor in glioblastoma multiforme and induces chemoresistance to temozolomide through suppressing miR-203 and promoting thymidylate synthase expression.* Oncotarget, 2017. **8**(14): p. 22783-22799.
59. Cao, S., et al., *Tumor-suppressive function of long noncoding RNA MALAT1 in glioma cells by suppressing miR-155 expression and activating FBXW7 function.* American journal of cancer research, 2016. **6**(11): p. 2561-2574.
60. Scherer, M., et al., *Quantitative Proteomics to Identify Nuclear RNA-Binding Proteins of Malat1.* International Journal of Molecular Sciences, 2020. **21**(3): p. 1166.
61. Gutschner, T., M. Hammerle, and S. Diederichs, *MALAT1 -- a paradigm for long noncoding RNA function in cancer.* J Mol Med (Berl), 2013. **91**(7): p. 791-801.
62. Chen, L., et al., *Long non-coding RNA Malat1 promotes neurite outgrowth through activation of ERK/MAPK signalling pathway in N2a cells.* J Cell Mol Med, 2016. **20**(11): p. 2102-2110.
63. Dong, Y., et al., *MALAT1 promotes the proliferation and metastasis of osteosarcoma cells by activating the PI3K/Akt pathway.* Tumour Biol, 2015. **36**(3): p. 1477-86.
64. Liang, J., et al., *MALAT1 induces tongue cancer cells' EMT and inhibits apoptosis through Wnt/β-catenin signaling pathway.* J Oral Pathol Med, 2017. **46**(2): p. 98-105.
65. Zhao, G., et al., *The long noncoding RNA MALAT1 regulates the lipopolysaccharide-induced inflammatory response through its interaction with NF-κB.* FEBS Lett, 2016. **590**(17): p. 2884-95.
66. Li, Z.X., et al., *MALAT1: a potential biomarker in cancer.* Cancer Manag Res, 2018. **10**: p. 6757-6768.
67. Jin, Y., et al., *LncRNA MALAT1 promotes proliferation and metastasis in epithelial ovarian cancer via the PI3K-AKT pathway.* Eur Rev Med Pharmacol Sci, 2017. **21**(14): p. 3176-3184.
68. Liu, S., et al., *Knockdown of Long Noncoding RNA (lncRNA) Metastasis-Associated Lung Adenocarcinoma Transcript 1 (MALAT1) Inhibits Proliferation, Migration, and Invasion and*

Promotes Apoptosis by Targeting miR-124 in Retinoblastoma. Oncol Res, 2018. **26**(4): p. 581-591.
69. Cai, T., Y. Liu, and J. Xiao, *Long noncoding RNA MALAT1 knockdown reverses chemoresistance to temozolomide via promoting microRNA-101 in glioblastoma.* Cancer Med, 2018. **7**(4): p. 1404-1415.
70. Lottspeich, F. and J. Engels, *Bioanalytik*. third ed. 2012, Heidelberg: Springer Spektrum.
71. Minden, J.S., et al., *Difference gel electrophoresis.* ELECTROPHORESIS, 2009. **30**(S1): p. S156-S161.
72. Gross, J.H., *Mass Spectrometry - A Textbook*. 2nd ed. 2011, Heidelberg: Springer Verlag.
73. Unwin, R.D., C.A. Evans, and A.D. Whetton, *Relative quantification in proteomics: new approaches for biochemistry.* Trends in Biochemical Sciences, 2006. **31**(8): p. 473-484.
74. Zhang, Y., et al., *Protein analysis by shotgun/bottom-up proteomics.* Chemical reviews, 2013. **113**(4): p. 2343-2394.
75. Sidoli, S. and B.A. Garcia, *Middle-down proteomics: a still unexploited resource for chromatin biology.* Expert Rev Proteomics, 2017. **14**(7): p. 617-626.
76. Toby, T.K., L. Fornelli, and N.L. Kelleher, *Progress in Top-Down Proteomics and the Analysis of Proteoforms.* Annu Rev Anal Chem (Palo Alto Calif), 2016. **9**(1): p. 499-519.
77. El Kennani, S., et al., *Proteomic Analysis of Histone Variants and Their PTMs: Strategies and Pitfalls.* Proteomes, 2018. **6**(3): p. 29.
78. Neilson, K.A., et al., *Less label, more free: Approaches in label-free quantitative mass spectrometry.* PROTEOMICS, 2011. **11**(4): p. 535-553.
79. Nahnsen, S., et al., *Tools for label-free peptide quantification.* Mol Cell Proteomics, 2013. **12**(3): p. 549-56.
80. Rauniyar, N. and J.R. Yates, 3rd, *Isobaric labeling-based relative quantification in shotgun proteomics.* J Proteome Res, 2014. **13**(12): p. 5293-309.
81. Geiger, T., et al., *Super-SILAC mix for quantitative proteomics of human tumor tissue.* Nature methods, 2010. **7**(5): p. 383-385.
82. Bantscheff, M., et al., *Quantitative mass spectrometry in proteomics: a critical review.* Analytical and Bioanalytical Chemistry, 2007. **389**(4): p. 1017-1031.
83. Mertins, P., et al., *Proteogenomics connects somatic mutations to signalling in breast cancer.* Nature, 2016. **534**(7605): p. 55-62.
84. Forget, A., et al., *Aberrant ERBB4-SRC Signaling as a Hallmark of Group 4 Medulloblastoma Revealed by Integrative Phosphoproteomic Profiling.* Cancer Cell, 2018. **34**(3): p. 379-395.e7.
85. Ahmadov, U., et al., *The long non-coding RNA HOTAIRM1 promotes tumor aggressiveness and radiotherapy resistance in glioblastoma.* Cell Death Dis, 2021. **12**(10): p. 885.
86. Bludau, I. and R. Aebersold, *Proteomic and interactomic insights into the molecular basis of cell functional diversity.* Nature Reviews Molecular Cell Biology, 2020. **21**(6): p. 327-340.
87. Bunt, G. and F.S. Wouters, *FRET from single to multiplexed signaling events.* Biophys Rev, 2017. **9**(2): p. 119-129.
88. Fields, S. and O.-k. Song, *A novel genetic system to detect protein–protein interactions.* Nature, 1989. **340**(6230): p. 245-246.
89. Barra, J. and E. Leucci, *Probing Long Non-coding RNA-Protein Interactions.* Frontiers in Molecular Biosciences, 2017. **4**.
90. Smola, M.J., et al., *SHAPE reveals transcript-wide interactions, complex structural domains, and protein interactions across the Xist lncRNA in living cells.* Proceedings of the National Academy of Sciences, 2016. **113**(37): p. 10322-10327.
91. Bartl, J., et al., *The HHIP-AS1 lncRNA promotes tumorigenicity through stabilization of dynein complex 1 in human SHH-driven tumors.* Nature Communications, 2022. **13**(1): p. 4061.
92. Dull, T., et al., *A third-generation lentivirus vector with a conditional packaging system.* Journal of virology, 1998. **72**(11): p. 8463-8471.

93. Thakore, P.I., et al., *Highly specific epigenome editing by CRISPR-Cas9 repressors for silencing of distal regulatory elements.* Nature methods, 2015. **12**(12): p. 1143-1149.
94. Arun, G., D. Aggarwal, and D.L. Spector, *MALAT1 Long Non-Coding RNA: Functional Implications.* Non-coding RNA, 2020. **6**(2): p. 22.
95. Spiniello, M., et al., *HyPR-MS for Multiplexed Discovery of MALAT1, NEAT1, and NORAD lncRNA Protein Interactomes.* J Proteome Res, 2018. **17**(9): p. 3022-3038.
96. Chen, R., et al., *Quantitative proteomics reveals that long non-coding RNA MALAT1 interacts with DBC1 to regulate p53 acetylation.* Nucleic Acids Research, 2017. **45**(17): p. 9947-9959.
97. Yang, L., et al., *ncRNA- and Pc2 methylation-dependent gene relocation between nuclear structures mediates gene activation programs.* Cell, 2011. **147**(4): p. 773-788.
98. Lebedeva, S., et al., *Transcriptome-wide Analysis of Regulatory Interactions of the RNA-Binding Protein HuR.* Molecular Cell, 2011. **43**(3): p. 340-352.
99. Wilusz, J.E., S.M. Freier, and D.L. Spector, *3' end processing of a long nuclear-retained noncoding RNA yields a tRNA-like cytoplasmic RNA.* Cell, 2008. **135**(5): p. 919-932.
100. Miyagawa, R., et al., *Identification of cis- and trans-acting factors involved in the localization of MALAT-1 noncoding RNA to nuclear speckles.* RNA (New York, N.Y.), 2012. **18**(4): p. 738-751.
101. Weinmann, L., et al., *Importin 8 Is a Gene Silencing Factor that Targets Argonaute Proteins to Distinct mRNAs.* Cell, 2009. **136**(3): p. 496-507.
102. Macias, S., et al., *DGCR8 HITS-CLIP reveals novel functions for the Microprocessor.* Nature structural & molecular biology, 2012. **19**(8): p. 760-766.
103. Tollervey, J.R., et al., *Characterizing the RNA targets and position-dependent splicing regulation by TDP-43.* Nature neuroscience, 2011. **14**(4): p. 452-458.
104. Li, L., et al., *Role of human noncoding RNAs in the control of tumorigenesis.* Proceedings of the National Academy of Sciences of the United States of America, 2009. **106**(31): p. 12956-12961.
105. Olaisen, C., et al., *PCNA-interacting peptides reduce Akt phosphorylation and TLR-mediated cytokine secretion suggesting a role of PCNA in cellular signaling.* Cellular Signalling, 2015. **27**(7): p. 1478-1487.
106. Ortega, J., et al., *Phosphorylation of PCNA by EGFR inhibits mismatch repair and promotes misincorporation during DNA synthesis.* Proceedings of the National Academy of Sciences, 2015. **112**(18): p. 5667-5672.
107. Wang, S.-C., et al., *Tyrosine phosphorylation controls PCNA function through protein stability.* Nature Cell Biology, 2006. **8**(12): p. 1359-1368.
108. Diserens, A.C., et al., *Characterization of an established human malignant glioma cell line: LN-18.* Acta Neuropathologica, 1981. **53**(1): p. 21-28.
109. Studer, A., et al., *Characterization of four human malignant glioma cell lines.* Acta Neuropathologica, 1985. **66**(3): p. 208-217.
110. Stein, G.H., *T98G: An anchorage-independent human tumor cell line that exhibits stationary phase G1 arrest in vitro.* Journal of Cellular Physiology, 1979. **99**(1): p. 43-54.
111. Bady, P., et al., *DNA fingerprinting of glioma cell lines and considerations on similarity measurements.* Neuro-oncology, 2012. **14**(6): p. 701-711.
112. Ishii, N., et al., *Frequent Co-Alterations of TP53, p16/CDKN2A, p14ARF, PTEN Tumor Suppressor Genes in Human Glioma Cell Lines.* Brain Pathology, 1999. **9**(3): p. 469-479.
113. Allen, M., et al., *Origin of the U87MG glioma cell line: Good news and bad news.* Science Translational Medicine, 2016. **8**(354): p. 354re3-354re3.
114. Lita, A., et al., *IDH1 mutations induce organelle defects via dysregulated phospholipids.* Nature Communications, 2021. **12**(1): p. 614.
115. Heinzen, D., et al., *Second Generation mTOR Inhibitors as a Double-Edged Sword in Malignant Glioma Treatment.* International Journal of Molecular Sciences, 2019. **20**(18): p. 4474.

116. Hollinshead, K.E.R., et al., *Oncogenic IDH1 Mutations Promote Enhanced Proline Synthesis through PYCR1 to Support the Maintenance of Mitochondrial Redox Homeostasis.* Cell Reports, 2018. **22**(12): p. 3107-3114.
117. Welch, D.R. and D.R. Hurst, *Defining the Hallmarks of Metastasis.* Cancer research, 2019. **79**(12): p. 3011-3027.
118. Yamaguchi, H., J. Wyckoff, and J. Condeelis, *Cell migration in tumors.* Current Opinion in Cell Biology, 2005. **17**(5): p. 559-564.
119. Kramer, N., et al., *In vitro cell migration and invasion assays.* Mutation Research/Reviews in Mutation Research, 2013. **752**(1): p. 10-24.
120. Wirtz, D., K. Konstantopoulos, and P.C. Searson, *The physics of cancer: the role of physical interactions and mechanical forces in metastasis.* Nature reviews. Cancer, 2011. **11**(7): p. 512-522.
121. Feitelson, M.A., et al., *Sustained proliferation in cancer: Mechanisms and novel therapeutic targets.* Seminars in cancer biology, 2015. **35 Suppl**(Suppl): p. S25-S54.
122. Justus, C.R., et al., *In vitro cell migration and invasion assays.* Journal of visualized experiments : JoVE, 2014(88): p. 51046.
123. Green, C.E., et al., *Chemoattractant Signaling between Tumor Cells and Macrophages Regulates Cancer Cell Migration, Metastasis and Neovascularization.* PLOS ONE, 2009. **4**(8): p. e6713.
124. Sever, R. and J.S. Brugge, *Signal transduction in cancer.* Cold Spring Harbor perspectives in medicine, 2015. **5**(4): p. a006098.
125. Sanchez-Vega, F., et al., *Oncogenic Signaling Pathways in The Cancer Genome Atlas.* Cell, 2018. **173**(2): p. 321-337.e10.
126. Shaw, R.J. and L.C. Cantley, *Ras, PI (3) K and mTOR signalling controls tumour cell growth.* Nature, 2006. **441**(7092): p. 424.
127. Karin, M., *Nuclear factor-κB in cancer development and progression.* Nature, 2006. **441**(7092): p. 431.
128. Pathan, M., et al., *FunRich: An open access standalone functional enrichment and interaction network analysis tool.* PROTEOMICS, 2015. **15**(15): p. 2597-2601.
129. Pathan, M., et al., *A novel community driven software for functional enrichment analysis of extracellular vesicles data.* Journal of extracellular vesicles, 2017. **6**(1): p. 1321455-1321455.
130. Zhao, H.-F., et al., *Recent advances in the use of PI3K inhibitors for glioblastoma multiforme: current preclinical and clinical development.* Molecular cancer, 2017. **16**(1): p. 100-100.
131. Zhang, M.Y., et al., *Germline ETV6 mutations in familial thrombocytopenia and hematologic malignancy.* Nature genetics, 2015. **47**(2): p. 180-185.
132. De Bustos, C., et al., *A PDGFRA promoter polymorphism, which disrupts the binding of ZNF148, is associated with primitive neuroectodermal tumours and ependymomas.* Journal of medical genetics, 2005. **42**(1): p. 31-37.
133. Fang, J., et al., *Functional characterization of a multi-cancer risk locus on chr5p15.33 reveals regulation of TERT by ZNF148.* Nature Communications, 2017. **8**: p. 15034.
134. Lorenz, P., D. Koczan, and H.-J. Thiesen, *Transcriptional repression mediated by the KRAB domain of the human C2H2 zinc finger protein Kox1/ZNF10 does not require histone deacetylation.* Biological chemistry, 2001. **382**(4): p. 637-644.
135. Moosmann, P., et al., *Transcriptional repression by RING finger protein TIF1 beta that interacts with the KRAB repressor domain of KOX1.* Nucleic acids research, 1996. **24**(24): p. 4859-4867.
136. Rowbotham, S.P., et al., *Maintenance of silent chromatin through replication requires SWI/SNF-like chromatin remodeler SMARCAD1.* Mol Cell, 2011. **42**(3): p. 285-96.
137. Schultz, D.C., et al., *SETDB1: a novel KAP-1-associated histone H3, lysine 9-specific methyltransferase that contributes to HP1-mediated silencing of euchromatic genes by KRAB zinc-finger proteins.* Genes & development, 2002. **16**(8): p. 919-932.

138. Valle-García, D., et al., *ATRX binds to atypical chromatin domains at the 3' exons of zinc finger genes to preserve H3K9me3 enrichment.* Epigenetics, 2016. **11**(6): p. 398-414.
139. Li, F., et al., *The Elp3 subunit of human Elongator complex is functionally similar to its counterpart in yeast.* Mol Genet Genomics, 2005. **273**(3): p. 264-72.
140. Wang, W., et al., *Diversity and specialization of mammalian SWI/SNF complexes.* Genes & Development, 1996. **10**(17): p. 2117-2130.
141. Venturini, L., et al., *TIF1γ, a novel member of the transcriptional intermediary factor 1 family.* Oncogene, 1999. **18**(5): p. 1209-1217.
142. He, W., et al., *Hematopoiesis Controlled by Distinct TIF1γ and Smad4 Branches of the TGFβ Pathway.* Cell, 2006. **125**(5): p. 929-941.
143. Levine, S.S., et al., *The core of the polycomb repressive complex is compositionally and functionally conserved in flies and humans.* Molecular and cellular biology, 2002. **22**(17): p. 6070-6078.
144. Deshpande, A.M., et al., *PHC3, a component of the hPRC-H complex, associates with E2F6 during G0 and is lost in osteosarcoma tumors.* Oncogene, 2007. **26**(12): p. 1714-1722.
145. Wang, A.H., et al., *HDAC4, a human histone deacetylase related to yeast HDA1, is a transcriptional corepressor.* Molecular and cellular biology, 1999. **19**(11): p. 7816-7827.
146. Schmidt, A. and A. Hall, *Guanine nucleotide exchange factors for Rho GTPases: turning on the switch.* Genes & Development, 2002. **16**(13): p. 1587-1609.
147. Saeki, N., H. Tokuo, and M. Ikebe, *BIG1 Is a Binding Partner of Myosin IXb and Regulates Its Rho-GTPase Activating Protein Activity.* Journal of Biological Chemistry, 2005. **280**(11): p. 10128-10134.
148. Xia, C., et al., *Regulation of the p21-activated kinase (PAK) by a human Gbeta -like WD-repeat protein, hPIP1.* Proceedings of the National Academy of Sciences of the United States of America, 2001. **98**(11): p. 6174-6179.
149. Pesesse, X., et al., *The Src Homology 2 Domain Containing Inositol 5-Phosphatase SHIP2 Is Recruited to the Epidermal Growth Factor (EGF) Receptor and Dephosphorylates Phosphatidylinositol 3,4,5-Trisphosphate in EGF-stimulated COS-7 Cells.* Journal of Biological Chemistry, 2001. **276**(30): p. 28348-28355.
150. Prasad, N.K. and S.J. Decker, *SH2-containing 5'-Inositol Phosphatase, SHIP2, Regulates Cytoskeleton Organization and Ligand-dependent Down-regulation of the Epidermal Growth Factor Receptor.* Journal of Biological Chemistry, 2005. **280**(13): p. 13129-13136.
151. Pengal, R.A., et al., *SHIP-2 Inositol Phosphatase Is Inducibly Expressed in Human Monocytes and Serves to Regulate Fcγ Receptor-mediated Signaling.* Journal of Biological Chemistry, 2003. **278**(25): p. 22657-22663.
152. Wakioka, T., et al., *APS, an adaptor protein containing Pleckstrin homology (PH) and Src homology-2 (SH2) domains inhibits the JAK-STAT pathway in collaboration with c-Cbl.* Leukemia, 1999. **13**(5): p. 760.
153. Kubo, T., et al., *A Novel FERM Domain Including Guanine Nucleotide Exchange Factor Is Involved in Rac Signaling and Regulates Neurite Remodeling.* The Journal of Neuroscience, 2002. **22**(19): p. 8504-8513.
154. Tanno, H., et al., *The Ankrd 13 family of UIM-bearing proteins regulates EGF receptor endocytosis from the plasma membrane.* Molecular biology of the cell, 2012. **23**(7): p. 1343-1353.
155. Murillo, C.A., P.G. Rychahou, and B.M. Evers, *Inhibition of alpha5 integrin decreases PI3K activation and cell adhesion of human colon cancers.* Surgery, 2004. **136**(2): p. 143-9.
156. Sabe, H., *Requirement for Arf6 in Cell Adhesion, Migration, and Cancer Cell Invasion.* The Journal of Biochemistry, 2003. **134**(4): p. 485-489.
157. Bowzard, J.B., et al., *ELMOD2 Is an Arl2 GTPase-activating Protein That Also Acts on Arfs.* Journal of Biological Chemistry, 2007. **282**(24): p. 17568-17580.

158. Kwon, M., et al., *Down-regulation of Filamin A interacting protein 1-like Is associated with promoter methylation and an invasive phenotype in breast, colon, lung and pancreatic cancers [corrected].* PloS one, 2013. **8**(12): p. e82620-e82620.
159. Kwon, M. and S.K. Libutti, *Filamin A interacting protein 1-like as a therapeutic target in cancer.* Expert Opinion on Therapeutic Targets, 2014. **18**(12): p. 1435-1447.
160. Kwon, M., et al., *Functional characterization of filamin a interacting protein 1-like, a novel candidate for antivascular cancer therapy.* Cancer research, 2008. **68**(18): p. 7332-7341.
161. Creppe, C., et al., *Elongator Controls the Migration and Differentiation of Cortical Neurons through Acetylation of α-Tubulin.* Cell, 2009. **136**(3): p. 551-564.
162. Tan, I., et al., *A Tripartite Complex Containing MRCK Modulates Lamellar Actomyosin Retrograde Flow.* Cell, 2008. **135**(1): p. 123-136.
163. Lin, C., et al., *NIT1 suppresses tumour proliferation by activating the TGFβ1-Smad2/3 signalling pathway in colorectal cancer.* Cell death & disease, 2018. **9**(3): p. 263-263.
164. Sun, J., et al., *Nit1 and Fhit tumor suppressor activities are additive.* Journal of cellular biochemistry, 2009. **107**(6): p. 1097-1106.
165. Ågren, M., et al., *Expression of the PTCH1 tumor suppressor gene is regulated by alternative promoters and a single functional Gli-binding site.* Gene, 2004. **330**: p. 101-114.
166. Fujiwara, M., et al., *The mitophagy receptor Bcl-2–like protein 13 stimulates adipogenesis by regulating mitochondrial oxidative phosphorylation and apoptosis in mice.* Journal of Biological Chemistry, 2019. **294**(34): p. 12683-12694.
167. Jensen, S.A., et al., *Bcl2L13 is a ceramide synthase inhibitor in glioblastoma.* Proceedings of the National Academy of Sciences of the United States of America, 2014. **111**(15): p. 5682-5687.
168. Murakawa, T., et al., *Bcl-2-like protein 13 is a mammalian Atg32 homologue that mediates mitophagy and mitochondrial fragmentation.* Nature communications, 2015. **6**: p. 7527-7527.
169. Clarke, K., et al., *Inference of Low and High-Grade Glioma Gene Regulatory Networks Delineates the Role of Rnd3 in Establishing Multiple Hallmarks of Cancer.* PLOS Genetics, 2015. **11**(7): p. e1005325.
170. Hu, B., et al., *Fibulin-3 is uniquely upregulated in malignant gliomas and promotes tumor cell motility and invasion.* Molecular cancer research : MCR, 2009. **7**(11): p. 1756-1770.
171. Kuo, C.J., et al., *Oligomerization-dependent regulation of motility and morphogenesis by the collagen XVIII NC1/endostatin domain.* The Journal of cell biology, 2001. **152**(6): p. 1233-1246.
172. Lin, Y.-H., et al., *LIMCH1 regulates nonmuscle myosin-II activity and suppresses cell migration.* Molecular Biology of the Cell, 2017. **28**(8): p. 1054-1065.
173. Sheta, R., et al., *Hic-5 regulates epithelial to mesenchymal transition in ovarian cancer cells in a TGFβ1-independent manner.* Oncotarget, 2017. **8**(47): p. 82506-82530.
174. Lee, Soo Y., et al., *TIMP-1 modulates chemotaxis of human neural stem cells through CD63 and integrin signalling.* Biochemical Journal, 2014. **459**(3): p. 565-576.
175. Jung, K.-K., et al., *Identification of CD63 as a tissue inhibitor of metalloproteinase-1 interacting cell surface protein.* The EMBO journal, 2006. **25**(17): p. 3934-3942.
176. Galavotti, S., et al., *The autophagy-associated factors DRAM1 and p62 regulate cell migration and invasion in glioblastoma stem cells.* Oncogene, 2012. **32**: p. 699.
177. Li, X., et al., *Direct Association with Inner Centromere Protein (INCENP) Activates the Novel Chromosomal Passenger Protein, Aurora-C.* Journal of Biological Chemistry, 2004. **279**(45): p. 47201-47211.
178. Honda, R., R. Körner, and E.A. Nigg, *Exploring the functional interactions between Aurora B, INCENP, and survivin in mitosis.* Molecular biology of the cell, 2003. **14**(8): p. 3325-3341.

179. Sasai, K., et al., *Aurora-C Interactions with Survivin and INCENP Reveal Shared and Distinct Features Compared with Aurora-B Chromosome Passenger Protein Complex.* PloS one, 2016. **11**(6): p. e0157305-e0157305.
180. Bigenzahn, J.W., et al., *LZTR1 is a regulator of RAS ubiquitination and signaling.* Science, 2018. **362**(6419): p. 1171-1177.
181. Steklov, M., et al., *Mutations in LZTR1 drive human disease by dysregulating RAS ubiquitination.* Science, 2018. **362**(6419): p. 1177-1182.
182. Kobos, R., et al., *Combining integrated genomics and functional genomics to dissect the biology of a cancer-associated, aberrant transcription factor, the ASPSCR1–TFE3 fusion oncoprotein.* The Journal of Pathology, 2013. **229**(5): p. 743-754.
183. Dong, Y., et al., *Regulation of BRCC, a Holoenzyme Complex Containing BRCA1 and BRCA2, by a Signalosome-like Subunit and Its Role in DNA Repair.* Molecular Cell, 2003. **12**(5): p. 1087-1099.
184. Lo, K.W.-H., J.M. Kogoy, and K.K. Pfister, *The DYNLT3 Light Chain Directly Links Cytoplasmic Dynein to a Spindle Checkpoint Protein, Bub3.* Journal of Biological Chemistry, 2007. **282**(15): p. 11205-11212.
185. Zhou, L., et al., *Effects of dynein light chain Tctex-type 3 on the biological behavior of ovarian cancer.* Cancer management and research, 2019. **11**: p. 5925-5938.
186. Marone, R., et al., *Memo mediates ErbB2-driven cell motility.* Nat Cell Biol, 2004. **6**(6): p. 515-22.
187. Kottemann, M.C., et al., *Removal of RTF2 from Stalled Replisomes Promotes Maintenance of Genome Integrity.* Mol Cell, 2018. **69**(1): p. 24-35 e5.
188. Zwartjes, C.G.M., et al., *Repression of Promoter Activity by CNOT2, a Subunit of the Transcription Regulatory Ccr4-Not Complex.* Journal of Biological Chemistry, 2004. **279**(12): p. 10848-10854.
189. Modi, P.K., et al., *Interplay between MEK-ERK signaling, cyclin D1, and cyclin-dependent kinase 5 regulates cell cycle reentry and apoptosis of neurons.* Molecular biology of the cell, 2012. **23**(18): p. 3722-3730.
190. Dhillon, A.S., et al., *MAP kinase signalling pathways in cancer.* Oncogene, 2007. **26**(22): p. 3279-3290.
191. McKay, M. and D. Morrison, *Integrating signals from RTKs to ERK/MAPK.* Oncogene, 2007. **26**(22): p. 3113-3121.
192. Karnoub, A.E. and R.A. Weinberg, *Ras oncogenes: split personalities.* Nature reviews. Molecular cell biology, 2008. **9**(7): p. 517-531.
193. Wang, B., et al., *Autophagy of macrophages is regulated by PI3k/Akt/mTOR signalling in the development of diabetic encephalopathy.* Aging, 2018. **10**(10): p. 2772-2782.
194. Iershov, A., et al., *The class 3 PI3K coordinates autophagy and mitochondrial lipid catabolism by controlling nuclear receptor PPARα.* Nature Communications, 2019. **10**(1): p. 1566.
195. Wishart, D.S., et al., *DrugBank 5.0: a major update to the DrugBank database for 2018.* Nucleic acids research, 2018. **46**(D1): p. D1074-D1082.
196. Gil-Ad, I., et al., *Evaluation of the potential anti-cancer activity of the antidepressant sertraline in human colon cancer cell lines and in colorectal cancer-xenografted mice.* International journal of oncology, 2008. **33**(2): p. 277-286.
197. Thebault, S., et al., *Novel role of cold/menthol-sensitive transient receptor potential melastatine family member 8 (TRPM8) in the activation of store-operated channels in LNCaP human prostate cancer epithelial cells.* Journal of Biological Chemistry, 2005. **280**(47): p. 39423-39435.
198. Perez, E.A., *Microtubule inhibitors: Differentiating tubulin-inhibiting agents based on mechanisms of action, clinical activity, and resistance.* Molecular Cancer Therapeutics, 2009. **8**(8): p. 2086-2095.

199. Saccoccia, F., et al., *Thioredoxin reductase and its inhibitors.* Current protein & peptide science, 2014. **15**(6): p. 621-646.
200. Lee, S.Y., *Temozolomide resistance in glioblastoma multiforme.* Genes & diseases, 2016. **3**(3): p. 198-210.
201. Dan, S., et al., *Inhibition of PI3K by ZSTK474 suppressed tumor growth not via apoptosis but G0/G1 arrest.* Biochemical and Biophysical Research Communications, 2009. **379**(1): p. 104-109.
202. Wang, Y., et al., *ZSTK474, a specific class I phosphatidylinositol 3-kinase inhibitor, induces G1 arrest and autophagy in human breast cancer MCF-7 cells.* Oncotarget, 2016. **7**(15): p. 19897-19909.
203. Chow, C.-M., et al., *Variant histone H3.3 marks promoters of transcriptionally active genes during mammalian cell division.* EMBO reports, 2005. **6**(4): p. 354-360.
204. Daury, L., et al., *Histone H3.3 deposition at E2F-regulated genes is linked to transcription.* EMBO reports, 2006. **7**(1): p. 66-71.
205. Stamato, M.A., et al., *Inhibition of EZH2 triggers the tumor suppressive miR-29b network in multiple myeloma.* Oncotarget, 2017. **8**(63): p. 106527-106537.
206. Lowe, B.R., et al., *Histone H3 Mutations: An Updated View of Their Role in Chromatin Deregulation and Cancer.* Cancers, 2019. **11**(5): p. 660.
207. Meyronet, D., et al., *Characteristics of H3 K27M-mutant gliomas in adults.* Neuro-Oncology, 2017. **19**(8): p. 1127-1134.
208. West, J.A., et al., *The long noncoding RNAs NEAT1 and MALAT1 bind active chromatin sites.* Mol Cell, 2014. **55**(5): p. 791-802.
209. Sun, Z., et al., *H3K36me3, message from chromatin to DNA damage repair.* Cell & Bioscience, 2020. **10**(1): p. 9.
210. Wang, W., et al., *Novel activity of KRAB domain that functions to reinforce nuclear localization of KRAB-containing zinc finger proteins by interacting with KAP1.* Cellular and Molecular Life Sciences, 2013. **70**(20): p. 3947-3958.
211. O'Geen, H., et al., *Genome-Wide Analysis of KAP1 Binding Suggests Autoregulation of KRAB-ZNFs.* PLOS Genetics, 2007. **3**(6): p. e89.
212. Friedman, J.R., et al., *KAP-1, a novel corepressor for the highly conserved KRAB repression domain.* Genes & Development, 1996. **10**(16): p. 2067-2078.
213. Addison, J.B., et al., *KAP1 Promotes Proliferation and Metastatic Progression of Breast Cancer Cells.* Cancer Research, 2015. **75**(2): p. 344-355.
214. Chen, L., T. Muñoz-Antonia, and W.D. Cress, *Trim28 Contributes to EMT via Regulation of E-Cadherin and N-Cadherin in Lung Cancer Cell Lines.* PLOS ONE, 2014. **9**(7): p. e101040.
215. Donehower, L.A., *Phosphatases reverse p53-mediated cell cycle checkpoints.* Proc Natl Acad Sci U S A, 2014. **111**(20): p. 7172-3.
216. Chang, F., et al., *Involvement of PI3K/Akt pathway in cell cycle progression, apoptosis, and neoplastic transformation: a target for cancer chemotherapy.* Leukemia, 2003. **17**(3): p. 590-603.
217. Li, P., Q. Wang, and H. Wang, *MicroRNA-204 inhibits the proliferation, migration and invasion of human lung cancer cells by targeting PCNA-1 and inhibits tumor growth in vivo.* International journal of molecular medicine, 2019. **43**(3): p. 1149-1156.
218. Li, J., et al., *LncRNA MALAT1 exerts oncogenic functions in lung adenocarcinoma by targeting miR-204.* American journal of cancer research, 2016. **6**(5): p. 1099-1107.
219. Xiao, X., et al., *LncRNA MALAT1 sponges miR-204 to promote osteoblast differentiation of human aortic valve interstitial cells through up-regulating Smad4.* International Journal of Cardiology, 2017. **243**: p. 404-412.
220. Hou, Z., et al., *The long non-coding RNA MALAT1 promotes the migration and invasion of hepatocellular carcinoma by sponging miR-204 and releasing SIRT1.* Tumor Biology, 2017. **39**(7): p. 1010428317718135.

221. Blackburn, J., et al., *Transcriptional Regulation and Expression of the Dominant Drusen Gene FBLN3 (EFEMP1) in Mammalian Retina.* Investigative Ophthalmology & Visual Science, 2003. **44**(11): p. 4613-4621.
222. Nishitsuji, H., et al., *ZNF10 inhibits HIV-1 LTR activity through interaction with NF-κB and Sp1 binding motifs.* FEBS Letters, 2015. **589**(15): p. 2019-2025.
223. Yin, X., et al., *EFEMP1 promotes ovarian cancer cell growth, invasion and metastasis via activated the AKT pathway.* Oncotarget, 2016. **7**(30): p. 47938-47953.
224. Hu, Y., et al., *EFEMP1 suppresses malignant glioma growth and exerts its action within the tumor extracellular compartment.* Molecular Cancer, 2011. **10**(1): p. 123.
225. Huesgen, P.F., et al., *LysargiNase mirrors trypsin for protein C-terminal and methylation-site identification.* Nature Methods, 2015. **12**(1): p. 55-58.
226. Garcia, B.A., et al., *Chemical derivatization of histones for facilitated analysis by mass spectrometry.* Nature protocols, 2007. **2**(4): p. 933.
227. Ghandi, M., et al., *Next-generation characterization of the Cancer Cell Line Encyclopedia.* Nature, 2019. **569**(7757): p. 503-508.
228. Tripathi, V., et al., *Long noncoding RNA MALAT1 controls cell cycle progression by regulating the expression of oncogenic transcription factor B-MYB.* PLoS Genet, 2013. **9**(3): p. e1003368.
229. Yang, F., et al., *MALAT-1 interacts with hnRNP C in cell cycle regulation.* FEBS Letters, 2013. **587**(19): p. 3175-3181.
230. Dai, Q., T. Zhang, and C. Li, *LncRNA MALAT1 Regulates the Cell Proliferation and Cisplatin Resistance in Gastric Cancer via PI3K/AKT Pathway.* Cancer management and research, 2020. **12**: p. 1929-1939.
231. Dai, X., et al., *Silencing of lncRNA MALAT1 inhibits cell cycle progression via androgen receptor signaling in prostate cancer cells.* Pathology - Research and Practice, 2019. **215**(4): p. 712-721.
232. Zhu, K., Q. Ren, and Y. Zhao, *lncRNA MALAT1 overexpression promotes proliferation, migration and invasion of gastric cancer by activating the PI3K/AKT pathway.* Oncol Lett, 2019. **17**(6): p. 5335-5342.
233. Chen, Y., et al., *LncRNA MALAT1 Promotes Cancer Metastasis in Osteosarcoma via Activation of the PI3K-Akt Signaling Pathway.* Cell Physiol Biochem, 2018. **51**(3): p. 1313-1326.
234. Wang, C., et al., *Long non-coding RNA MALAT1 promotes cholangiocarcinoma cell proliferation and invasion by activating PI3K/Akt pathway.* Neoplasma, 2017. **64**(5): p. 725-731.
235. Li, H.B., et al., *Long Non-Coding RNA-MALAT1 Mediates Retinal Ganglion Cell Apoptosis Through the PI3K/Akt Signaling Pathway in Rats with Glaucoma.* Cellular Physiology and Biochemistry, 2017. **43**(5): p. 2117-2132.
236. Gutschner, T., M. Baas, and S. Diederichs, *Noncoding RNA gene silencing through genomic integration of RNA destabilizing elements using zinc finger nucleases.* Genome Res, 2011. **21**(11): p. 1944-54.
237. Lin, L., et al., *Dual targeting of glioblastoma multiforme with a proteasome inhibitor (Velcade) and a phosphatidylinositol 3-kinase inhibitor (ZSTK474).* International journal of oncology, 2014. **44**(2): p. 557-562.
238. Dufour, S., F. Broders-Bondon, and N. Bondurand, *Chapter 13 - β1-Integrin Function and Interplay during Enteric Nervous System Development*, in *Neural Surface Antigens*, J. Pruszak, Editor. 2015, Academic Press: Boston. p. 153-166.
239. Olaisen, C., et al., *PCNA-interacting peptides reduce Akt phosphorylation and TLR-mediated cytokine secretion suggesting a role of PCNA in cellular signaling.* Cell Signal, 2015. **27**(7): p. 1478-87.
240. Wang, H., et al., *Deep multiomics profiling of brain tumors identifies signaling networks downstream of cancer driver genes.* Nat Commun, 2019. **10**(1): p. 3718.

241. Tamura, M., et al., *PTEN interactions with focal adhesion kinase and suppression of the extracellular matrix-dependent phosphatidylinositol 3-kinase/Akt cell survival pathway.* Journal of Biological Chemistry, 1999. **274**(29): p. 20693-20703.
242. Mischel, P.S. and T.F. Cloughesy, *Targeted Molecular Therapy of GBM.* Brain Pathology, 2003. **13**(1): p. 52-61.
243. Crespo, S., M. Kind, and A. Arcaro, *The role of the PI3K/AKT/mTOR pathway in brain tumor metastasis.* Journal of Cancer Metastasis and Treatment, 2016. **2**(3): p. 80.
244. Mitra, S.K. and D.D. Schlaepfer, *Integrin-regulated FAK-Src signaling in normal and cancer cells.* Curr Opin Cell Biol, 2006. **18**(5): p. 516-23.
245. Engelman, J.A., *Targeting PI3K signalling in cancer: opportunities, challenges and limitations.* Nature Reviews Cancer, 2009. **9**(8): p. 550-562.
246. Zhang, W. and H.T. Liu, *MAPK signal pathways in the regulation of cell proliferation in mammalian cells.* Cell Research, 2002. **12**(1): p. 9-18.
247. Xu, N., et al., *Akt: a double-edged sword in cell proliferation and genome stability.* Journal of oncology, 2012. **2012**: p. 951724-951724.
248. Maga, G. and U. Hübscher, *Proliferating cell nuclear antigen (PCNA): a dancer with many partners.* Journal of Cell Science, 2003. **116**(15): p. 3051-3060.
249. Bartek, J., C. Lukas, and J. Lukas, *Checking on DNA damage in S phase.* Nature Reviews Molecular Cell Biology, 2004. **5**(10): p. 792-804.
250. Willis, N. and N. Rhind, *Regulation of DNA replication by the S-phase DNA damage checkpoint.* Cell division, 2009. **4**: p. 13-13.
251. Zhao, H., et al., *Targeting Tyrosine Phosphorylation of PCNA Inhibits Prostate Cancer Growth.* Molecular Cancer Therapeutics, 2011. **10**(1): p. 29-36.
252. Wang, S.-C., *PCNA: a silent housekeeper or a potential therapeutic target?* Trends in Pharmacological Sciences, 2014. **35**(4): p. 178-186.
253. Dan, S., et al., *ZSTK474, a specific phosphatidylinositol 3-kinase inhibitor, induces G1 arrest of the cell cycle in vivo.* European Journal of Cancer, 2012. **48**(6): p. 936-943.
254. Li, F., et al., *The histone mark H3K36me3 regulates human DNA mismatch repair through its interaction with MutSalpha.* Cell, 2013. **153**(3): p. 590-600.
255. Pai, C.-C., et al., *A histone H3K36 chromatin switch coordinates DNA double-strand break repair pathway choice.* Nature Communications, 2014. **5**(1): p. 4091.
256. Li, F., et al., *Regulation of mismatch repair by histone code and posttranslational modifications in eukaryotic cells.* DNA Repair, 2016. **38**: p. 68-74.
257. Barr, A.R., et al., *DNA damage during S-phase mediates the proliferation-quiescence decision in the subsequent G1 via p21 expression.* Nature Communications, 2017. **8**(1): p. 14728.

Appendix A

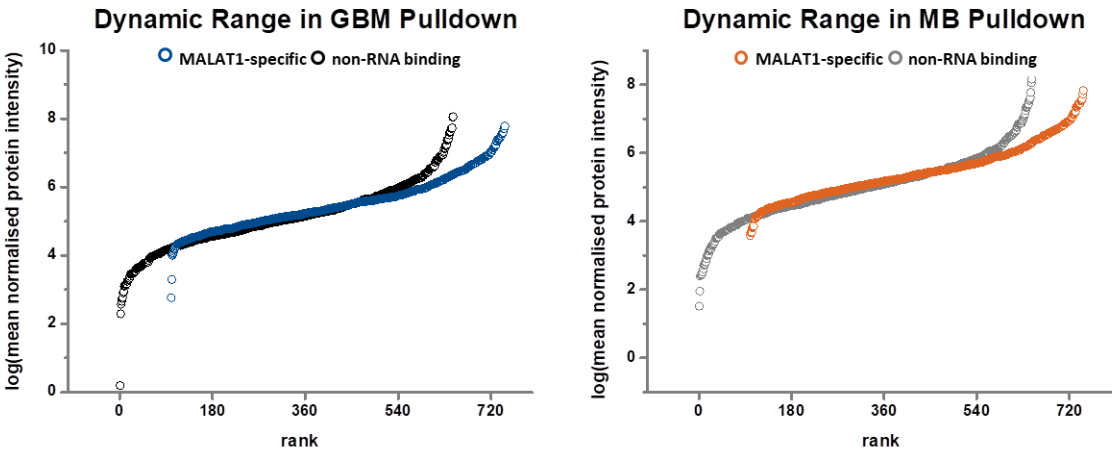

Figure 57 Distribution of dynamic range for all quantified proteins in GBM (left) and MB (right) associated samples generated with MALAT1 specific and non-RNA binding DNA probes. In these scatter plots logarithmic mean normalised protein intensities were plotted against their abundance ranked from lowest to highest. Abundance ranks for quantified proteins in samples enriched with *MALAT1* specific DNA probes start at 100 to increase visibility. Measurements for GBM associated samples are depicted in the left graph with non-RNA binding generated samples in black and *MALAT1*-specific generated samples in blue. In the right plot measurements for MB associated samples are depicted with non-RNA binding generated samples in black and *MALAT1*-specific generated samples in blue.

Table 14 List of putative *MALAT1* interacting proteins in GBM associated samples. Proteins are listed with their UniProt accession, associated gene name, peptide as well as unique peptide count in addition to p-value and FC measured.

Accession	Gene	Peptides	Unique peptides	p-value	FC
Q10570	*CPSF1*	2	2	2.42E-11	Infinity
Q9Y224	*C14orf166*	2	2	2.59E-10	Infinity
O75494-2	*SRSF10*	6	6	6.30E-09	14.52
P23246	*SFPQ*	21	13	8.46E-09	12.70
Q13247-3	*SRSF6*	16	15	1.54E-08	12.21
Q8IXT5	*RBM12B*	18	17	2.21E-08	11.55
Q9UHX1-4	*PUF60*	9	9	2.60E-08	8.99
Q05519-2	*SRSF11*	5	5	3.53E-08	29.07
Q00839	*HNRNPU*	32	31	4.93E-08	6.84
Q13148	*TARDBP*	8	8	6.13E-08	12.68
Q96AE4-2	*FUBP1*	20	4	7.91E-08	9.68
P62995	*TRA2B*	7	5	8.25E-08	23.73
Q14498-2	*RBM39*	11	11	1.10E-07	29.72
P26368-2	*U2AF2*	8	4	1.48E-07	4.22
P38159-2	*RBMX*	11	4	1.51E-07	9.41
Q15717-2	*ELAVL1*	8	4	1.52E-07	5.79
Q01844-6	*EWSR1*	5	5	1.83E-07	3.22
O43390	*HNRNPR*	16	4	1.93E-07	16.15
Q16629-4	*SRSF7*	6	4	3.33E-07	9.92
Q9BUJ2-2	*HNRNPUL1*	12	11	3.55E-07	8.79
P17844-2	*DDX5*	14	5	3.69E-07	7.79
Q13242	*SRSF9*	12	10	5.08E-07	10.78

P09651-2	*HNRNPA1*	57	40	6.58E-07	8.26
P62314	*SNRPD1*	5	5	7.69E-07	12.18
Q15427	*SF3B4*	3	3	8.47E-07	17.56
Q9BXP5-4	*SRRT*	8	3	1.13E-06	32.54
P62304	*SNRPE*	3	3	1.13E-06	9.29
Q07955	*SRSF1*	15	5	1.35E-06	4.02
O14979-3	*HNRNPDL*	8	2	1.48E-06	10.79
O43809	*NUDT21*	11	10	1.52E-06	8.89
P26599	*PTBP1*	16	15	1.54E-06	6.72
Q29RF7	*PDS5A*	2	2	1.79E-06	16383.71
P84103-2	*SRSF3*	7	2	1.86E-06	6.52
Q07955-2	*SRSF1*	15	7	2.24E-06	20.01
P62318-2	*SNRPD3*	4	4	2.43E-06	10.84
P17987	*TCP1*	3	3	2.56E-06	10.03
Q15233	*NONO*	16	14	2.75E-06	7.99
Q99729-3	*HNRNPAB*	12	10	2.80E-06	5.72
Q96T37	*RBM15*	3	3	2.93E-06	15.08
P31943	*HNRNPH1*	18	9	3.05E-06	6.45
Q96EP5-2	*DAZAP1*	4	4	3.06E-06	14.87
Q9Y2W1	*THRAP3*	6	6	3.16E-06	11.16
P61978-2	*HNRNPK*	31	2	3.23E-06	11.36
P07910-2	*HNRNPC*	22	22	3.60E-06	6.35
O43390-3	*HNRNPR*	14	2	3.65E-06	9.67
Q86W50	*METTL16*	3	3	3.71E-06	37.26
Q7Z7K6-3	*CENPV*	2	2	4.08E-06	26.40
O60264	*SMARCA5*	7	7	5.47E-06	11.47
Q8IYB3-2	*SRRM1*	3	3	5.94E-06	38.37
Q96MU7-2	*YTHDC1*	3	3	6.46E-06	8.05
P14866	*HNRNPL*	12	12	6.49E-06	4.58
P52597	*HNRNPF*	19	16	7.19E-06	5.55
P61978-3	*HNRNPK*	34	5	7.62E-06	5.75
Q14966	*ZNF638*	7	7	7.65E-06	10.35
P55795	*HNRNPH2*	12	6	7.67E-06	6.26
P82979	*SARNP*	5	5	8.91E-06	6.02
P22626	*HNRNPA2B1*	48	31	8.98E-06	6.93
O43684-2	*BUB3*	4	4	9.26E-06	11.33
Q9BUQ8	*DDX23*	5	5	9.88E-06	10.09
O43143	*DHX15*	17	17	1.01E-05	7.01
Q53GS9-3	*USP39*	4	4	1.07E-05	39.13
P52272-2	*HNRNPM*	25	23	1.16E-05	11.11
Q9H307-2	*PNN*	2	2	1.24E-05	13.15
Q15365	*PCBP1*	10	7	1.32E-05	5.66
P63241	*EIF5A*	4	4	1.32E-05	5.63
Q8IWX8	*CHERP*	4	4	1.40E-05	19.75
Q08211	*DHX9*	36	33	1.46E-05	7.68
P19338	*NCL*	15	15	1.47E-05	3.54
Q96PK6	*RBM14*	9	7	1.48E-05	8.67
P27694	*RPA1*	3	3	1.62E-05	17.65
Q13435	*SF3B2*	6	6	1.81E-05	42.44

Q14103-3	*HNRNPD*	17	14	1.82E-05	4.33
Q96DI7	*SNRNP40*	2	2	2.42E-05	13.26
Q2TAY7	*SMU1*	7	7	2.57E-05	14.11
Q9UQ35	*SRRM2*	4	4	2.81E-05	36.52
P51991	*HNRNPA3*	30	13	3.22E-05	2.50
O14979	*HNRNPDL*	8	3	3.56E-05	5.43
Q92879-5	*CELF1*	2	2	3.72E-05	12.76
Q9UMS4	*PRPF19*	7	6	3.73E-05	8.27
Q9UL40-3	*ZNF346*	2	2	3.80E-05	3.23
Q12905	*ILF2*	14	14	3.87E-05	5.17
Q92973-2	*TNPO1*	7	7	4.01E-05	13.63
P51991-2	*HNRNPA3*	18	4	4.02E-05	9.43
Q8WXF1-2	*PSPC1*	7	7	4.07E-05	14.29
Q96I24	*FUBP3*	5	3	4.14E-05	10.92
P62140	*PPP1CB*	5	2	4.29E-05	5.93
O75340-2	*PDCD6*	2	2	4.42E-05	4.95
P14678-2	*SNRPB*	7	7	4.50E-05	7.53
O94906-2	*PRPF6*	5	5	4.91E-05	6.52
P38919	*EIF4A3*	13	10	4.99E-05	7.03
Q9H0D6	*XRN2*	9	5	6.08E-05	10.41
Q12906	*ILF3*	14	8	6.80E-05	6.69
P0DN76	*U2AF1L5*	3	3	7.39E-05	5.61
Q9Y383	*LUC7L2*	5	5	7.55E-05	17.15
Q86XP3-2	*DDX42*	8	5	7.95E-05	6.41
P08621-2	*SNRNP70*	10	3	7.97E-05	1716.69
P31942-2	*HNRNPH3*	9	7	8.29E-05	4.25
P09874	*PARP1*	14	14	8.70E-05	4.82
Q13838	*DDX39B*	15	8	8.78E-05	6.54
P33240-2	*CSTF2*	3	3	9.21E-05	11.75
Q8N163-2	*CCAR2*	8	4	9.23E-05	7.28
P20073-2	*ANXA7*	5	5	1.01E-04	5.67
P43243	*MATR3*	15	14	1.19E-04	5.76
Q15459	*SF3A1*	14	14	1.20E-04	10.14
Q92841	*DDX17*	13	2	1.43E-04	687.85
O76003	*GLRX3*	3	3	1.43E-04	4.34
P33993	*MCM7*	11	10	1.47E-04	10.26
Q14151	*SAFB2*	16	5	1.50E-04	9.05
O60506	*SYNCRIP*	11	6	1.74E-04	5.50
P12004	*PCNA*	2	2	1.74E-04	2.91
P12956	*XRCC6*	12	9	1.75E-04	8.22
P33992	*MCM5*	5	5	1.76E-04	12.56
P13010	*XRCC5*	15	15	1.77E-04	5.70
P09012	*SNRPA*	3	2	1.77E-04	7.43
P08758	*ANXA5*	8	8	1.82E-04	3.06
P07737	*PFN1*	9	9	1.91E-04	2.78
O15042-2	*U2SURP*	3	3	1.93E-04	6.55
O43670-2	*ZNF207*	2	2	2.02E-04	13.15
P11388-4	*TOP2A*	6	6	2.07E-04	9.27
Q15393	*SF3B3*	27	26	2.20E-04	4.27

Q99873-3	*PRMT1*	12	7	2.33E-04	9.25
P17844	*DDX5*	20	10	2.35E-04	2.23
P35637-2	*FUS*	15	12	2.39E-04	3.40
Q09161	*NCBP1*	6	6	2.89E-04	10.51
O95232	*LUC7L3*	3	3	2.95E-04	16.08
Q15233-2	*NONO*	4	3	3.02E-04	5.80
P78347-2	*GTF2I*	4	4	3.05E-04	5.02
O75937	*DNAJC8*	2	2	3.12E-04	14.42
Q92841-1	*DDX17*	21	8	3.14E-04	7.09
P46063	*RECQL*	3	3	3.15E-04	9.39
P61289-2	*PSME3*	5	4	3.24E-04	3.19
Q13263	*TRIM28*	12	11	3.27E-04	5.79
Q9UKM9-2	*RALY*	11	11	3.49E-04	7.18
Q92804-2	*TAF15*	7	4	3.52E-04	71.61
Q12996	*CSTF3*	4	4	3.62E-04	36.94
O14776-2	*TCERG1*	7	7	3.91E-04	3.07
P98179	*RBM3*	3	3	4.05E-04	5.79
Q9P258	*RCC2*	5	5	4.06E-04	6.63
Q1KMD3	*HNRNPUL2*	14	14	4.34E-04	8.24
Q9Y5S9-2	*RBM8A*	2	2	4.64E-04	3.81
Q5BKZ1	*ZNF326*	4	4	4.75E-04	56.66
Q9Y265-2	*RUVBL1*	5	4	4.77E-04	6.59
Q9NQG5	*RPRD1B*	3	3	4.94E-04	245.75
Q8N1F7	*NUP93*	3	3	5.14E-04	10.78
P12956-2	*XRCC6*	11	9	5.17E-04	5.36
P67809	*YBX1*	2	2	5.31E-04	4.35
O43172-2	*PRPF4*	5	4	5.54E-04	3.14
Q99459	*CDC5L*	7	7	5.70E-04	4.21
Q9UKF6	*CPSF3*	5	5	5.86E-04	7.01
P31153	*MAT2A*	2	2	5.89E-04	4.66
Q9UQ88-4	*CDK11A*	2	2	5.90E-04	7.84
Q08945	*SSRP1*	5	5	6.18E-04	8.93
Q96T88-2	*UHRF1*	2	2	6.27E-04	61.59
Q92843-2	*BCL2L2*	3	3	6.42E-04	4.13
Q05048	*CSTF1*	3	3	6.48E-04	15.13
P68036-3	*UBE2L3*	3	3	6.91E-04	6.06
P84243	*H3F3A*	10	2	6.92E-04	21.34
P53999	*SUB1*	3	3	7.11E-04	3.30
P61081	*UBE2M*	2	2	7.16E-04	5.33
Q12874	*SF3A3*	5	5	7.33E-04	13.58
P39748-2	*FEN1*	4	2	7.43E-04	7.94
Q86VP6	*CAND1*	5	5	7.77E-04	4.06
P11142	*HSPA8*	32	24	7.84E-04	2.78
P62826	*RAN*	6	6	8.02E-04	2.78
Q96A72	*MAGOHB*	4	3	8.05E-04	7.79
O00422	*SAP18*	2	2	8.39E-04	7.90
P62829	*RPL23*	3	3	8.82E-04	5.33
P04083	*ANXA1*	12	12	9.07E-04	2.59
Q92499	*DDX1*	11	10	9.08E-04	6.09

P62888	*RPL30*	2	2	9.15E-04	2.53
P11940-2	*PABPC1*	12	6	1.02E-03	2.03
Q9Y3I0	*RTCB*	5	5	1.04E-03	8.67
P55060-3	*CSE1L*	15	12	1.05E-03	6.70
Q14566	*MCM6*	7	7	1.14E-03	6.20
Q04760-2	*GLO1*	2	2	1.21E-03	4.68
P18754-2	*RCC1*	6	4	1.22E-03	5.39
Q07666	*KHDRBS1*	6	4	1.24E-03	319.89
O14980	*XPO1*	5	5	1.25E-03	6.43
P78527-2	*PRKDC*	35	18	1.26E-03	8.36
P53396	*ACLY*	15	9	1.28E-03	4.03
P09382	*LGALS1*	2	2	1.35E-03	5.61
Q15637-5	*SF1*	8	8	1.44E-03	3.88
P20700	*LMNB1*	18	14	1.44E-03	4.41
P11387	*TOP1*	3	2	1.47E-03	5.89
P49915	*GMPS*	3	2	1.53E-03	11.89
P98175-4	*RBM10*	4	3	1.57E-03	145.77
Q13185	*CBX3*	6	6	1.58E-03	5.13
Q8N684-2	*CPSF7*	6	6	1.59E-03	5.05
P53621	*COPA*	4	4	1.63E-03	3.38
Q9Y230	*RUVBL2*	2	2	1.69E-03	2.84
Q96AE4	*FUBP1*	18	3	1.79E-03	3.37
P34932	*HSPA4*	3	2	1.82E-03	10.97
Q13123	*IK*	2	2	1.86E-03	167.83
P18583-2	*SON*	2	2	2.05E-03	5.43
Q13595	*TRA2A*	3	3	2.16E-03	2.86
Q71DI3	*HIST2H3A*	12	4	2.18E-03	27.89
Q9NTZ6	*RBM12*	3	3	2.23E-03	4.13
Q15181	*PPA1*	2	2	2.38E-03	6.07
P08621	*SNRNP70*	7	2	2.58E-03	9.01
O43447	*PPIH*	2	2	2.71E-03	2.30
P09661	*SNRPA1*	6	6	2.81E-03	2.35
P67775-2	*PPP2CA*	2	2	2.94E-03	4.48
P52701	*MSH6*	2	2	3.02E-03	10.67
O60828-2	*PQBP1*	2	2	3.05E-03	34.15
Q00610	*CLTC*	6	2	3.07E-03	3.58
P35579	*MYH9*	14	11	3.11E-03	2.71
Q15366-7	*PCBP2*	6	2	3.22E-03	7.06
P39748	*FEN1*	8	6	3.36E-03	5.59
P09429	*HMGB1*	7	6	3.37E-03	6.40
Q16666-3	*IFI16*	4	4	3.37E-03	9.10
P33991	*MCM4*	5	5	3.42E-03	17.13
O75533	*SF3B1*	11	11	3.47E-03	4.35
P49756	*RBM25*	5	5	3.51E-03	2.42
P30086	*PEBP1*	5	5	3.86E-03	4.45
Q96QD9-3	*FYTTD1*	2	2	3.97E-03	94.68
Q00610-2	*CLTC*	16	12	4.18E-03	2.74
P62979	*RPS27A*	10	9	4.36E-03	3.42
Q96QE3	*ATAD5*	2	2	4.46E-03	-2.57

P63241-2	*EIF5A*	3	3	4.53E-03	3.32
P49773	*HINT1*	3	3	4.55E-03	12.74
P37802	*TAGLN2*	5	2	4.58E-03	8.74
Q01130-2	*SRSF2*	2	2	4.62E-03	25.79
O75131	*CPNE3*	3	3	4.64E-03	9.59
P62701	*RPS4X*	2	2	4.74E-03	2.68
P78527	*PRKDC*	27	10	4.81E-03	6.39
O75475	*PSIP1*	4	4	5.07E-03	10.08
P62937	*PPIA*	11	11	5.16E-03	2.75
Q9P035	*HACD3*	2	2	5.43E-03	3.63
P23527	*HIST1H2BO*	25	4	5.48E-03	3.12
P50502	*ST13*	2	2	5.51E-03	3.31
Q5JTV8-3	*TOR1AIP1*	3	3	5.52E-03	11.88
P25205	*MCM3*	9	9	5.71E-03	3.57
Q13151	*HNRNPA0*	18	8	5.86E-03	3.00
Q13243	*SRSF5*	4	3	5.86E-03	2.41
Q8WXA9-2	*SREK1*	3	2	5.91E-03	6.05
P57053	*H2BFS*	24	3	6.26E-03	3.39
Q9BZZ5-2	*API5*	12	5	6.79E-03	5.28
O43148-2	*RNMT*	2	2	6.82E-03	5.45
Q7L014	*DDX46*	5	5	7.81E-03	2.77
O43290	*SART1*	2	2	8.69E-03	4.62
Q8IX12-2	*CCAR1*	2	2	8.78E-03	4.06
Q16658	*FSCN1*	7	7	8.91E-03	2.11
P62913	*RPL11*	2	2	8.91E-03	2.18
Q92688-2	*ANP32B*	3	3	8.96E-03	6.85
P37802-2	*TAGLN2*	6	3	9.39E-03	2.06
P22102	*GART*	2	2	9.58E-03	3.23
Q9NWH9	*SLTM*	3	3	9.63E-03	68.75
P51149	*RAB7A*	2	2	9.65E-03	2.13
P27708	*CAD*	2	2	9.71E-03	14.45

Table 15 List of putative *MALAT1* interacting proteins in MB associated samples. Proteins are listed with their UniProt accession, associated gene name, peptide as well as unique peptide count in addition to p-value and FC measured.

Accession	Gene	Peptides	Unique peptides	p-value	FC
Q9Y2W1	*THRAP3*	6	6	4.38E-06	12.08
O14979-3	*HNRNPDL*	8	2	1.54E-05	10.51
Q15717-2	*ELAVL1*	8	4	1.83E-05	5.90
Q8WXF1-2	*PSPC1*	7	7	2.24E-05	22.10
Q13242	*SRSF9*	12	10	2.86E-05	9.52
Q13148	*TARDBP*	8	8	3.21E-05	16.15
Q14966	*ZNF638*	7	7	3.44E-05	8.38
O43809	*NUDT21*	11	10	3.91E-05	8.52
Q9UMS4	*PRPF19*	7	6	4.66E-05	7.14
Q13435	*SF3B2*	6	6	4.89E-05	78.83
Q9BUJ2-2	*HNRNPUL1*	12	11	5.41E-05	7.58
P38159-2	*RBMX*	11	4	6.36E-05	11.56
O14979	*HNRNPDL*	8	3	9.66E-05	6.36

P31942-2	*HNRNPH3*	9	7	1.32E-04	4.07
Q9UHX1-4	*PUF60*	9	9	1.36E-04	9.84
P35637-2	*FUS*	15	12	1.39E-04	4.36
P22314	*UBA1*	10	9	3.06E-04	7.85
Q9H0D6	*XRN2*	9	5	3.34E-04	7.29
Q13185	*CBX3*	6	6	3.42E-04	8.09
Q13263	*TRIM28*	12	11	3.56E-04	4.18
P26368-2	*U2AF2*	8	4	3.61E-04	2.97
P08621-2	*SNRNP70*	10	3	3.78E-04	253.03
P14678-2	*SNRPB*	7	7	3.98E-04	8.69
Q13151	*HNRNPA0*	18	8	4.00E-04	3.07
Q2TAY7	*SMU1*	7	7	5.32E-04	11.51
O75533	*SF3B1*	11	11	5.34E-04	4.70
P33993	*MCM7*	11	10	6.42E-04	10.91
Q99459	*CDC5L*	7	7	6.77E-04	4.13
Q8N163-2	*CCAR2*	8	4	6.79E-04	5.37
P12956-2	*XRCC6*	11	9	7.36E-04	4.54
Q8N684-2	*CPSF7*	6	6	7.98E-04	6.17
Q86XP3-2	*DDX42*	8	5	8.48E-04	5.35
P09661	*SNRPA1*	6	6	1.11E-03	3.39
P55795	*HNRNPH2*	12	6	1.35E-03	5.14
Q96E39	*RBMXL1*	7	2	1.60E-03	215.05
Q9BZZ5-2	*API5*	12	5	1.92E-03	5.40
P00558	*PGK1*	12	6	2.01E-03	11.45
P42166	*TMPO*	11	5	2.03E-03	10.75
O00148	*DDX39A*	10	3	2.07E-03	10.72
O60264	*SMARCA5*	7	7	2.12E-03	9.37
P08621	*SNRNP70*	7	2	2.48E-03	4.70
Q15365	*PCBP1*	10	7	2.90E-03	6.30
Q99873-3	*PRMT1*	12	7	3.64E-03	6.52
P51659	*HSD17B4*	6	6	3.87E-03	6.61
P39748	*FEN1*	8	6	5.47E-03	5.19
Q92973-2	*TNPO1*	7	7	6.31E-03	6.93
P25205	*MCM3*	9	9	6.96E-03	3.49
P07737	*PFN1*	9	9	8.68E-03	3.31

Appendix B

Table 16 STR-profiling results of employed cell lines performed by DKFZ in Heidelberg on 27th November 2015 via multiplexion analyses.

Cell line	Identity in %	Result	Genotype code
LN18	98	confirmed, in database	TTTTTTAAAAATAAAATTATATTTTTAWA
			WAAAAATAWAATTTTAATT
LN229	98	confirmed, in database	AAATAAAATTAATTAAAAATATATTTAAT
			TAAATAWAWTTTTWTAAAT
LN308	100	confirmed, no database, alias LN-Z308	AWTTTTAAWTTTAAWTTTATAATTATW
			TATAATTATATAATTATTTTT
U251	98	confirmed, in database	AATTAAAAAAAAAAAATTATAATTTTAA
			AAAAAAATATAATTAATTAT
T98G	100	confirmed, in database	TTTTTTTTATWTTTAAATTTAATTTTWTW
			TWTTTAAAAAATTATATAT
TP365	77	unique sequence, no database	TTTTTTATTTTTTTTTTTTTATTTTTATATA
			AAATTTTATATTTTTAA
U87	100	confirmed, in database	ATTTAAAATTTTAAAAWTTTAATTTTATA
			TAAAAATATAATTWTTTAT

Table 17 Summary of *MALAT1* expression levels in RNA-centric pulldown eluates relative to *PGK1* and *GAPDH* housekeeper RNA levels determined by RT-qPCR (n=3). Results are listed with respective values for mean relative normalised *MALAT1* expression, the resulting variance value as well as the Student's t-test p-value obtained through the comparison of results from *MALAT1* specific and non-RNA binding probes in each cell line.

Tumour type	Cell line	*MALAT1* specific		Non-RNA binding		p-value
		Mean	Variance	Mean	Variance	
GBM	LN18	2.81	0.46	0.0048	0.0008	2.00E-06
	LN229	6.11	1.74	0.0073	0.0012	1.10E-05
	LN308	1.33	0.23	0.0015	0.0003	3.00E-06
	T98G	1.62	0.16	0.0099	0.0016	5.00E-06
	U251	3.25	0.37	0.0057	0.0015	1.84E-04
MB	CHLA-259	3.84	0.86	0.0058	0.0008	1.30E-05
	D283	0.70	0.10	0.0019	0.0009	1.61E-04
	Med8A	4.25	1.38	0.0071	0.0026	3.60E-05
	ONS76	1.58	0.15	0.0054	0.0005	2.75E-04
	UW-228-3	5.26	0.34	0.0056	0.0010	1.00E-06

Table 18 *MALAT1* expression levels in established GBM cell lines relative to *PGK1* and *GAPDH* housekeeper RNA levels determined by RT-qPCR (n=3). Results are listed with respective values for mean relative normalised *MALAT1* expression, and the resulting variance value in each cell line.

Cell line	Relative expression	Variance
LN18	0.42	0.08
LN229	0.99	0.35
LN308	0.43	0.05
U251	1.23	0.23
T98G	1.18	0.14
TP365	1.71	0.30
U87	0.87	0.22

Table 19 *MALAT1* expression levels in generated isogenic GBM cell lines relative to *PGK1* and *GAPDH* housekeeper RNA levels determined by RT-qPCR (n=3). Results are listed with respective values for mean relative normalised *MALAT1* expression, and the resulting variance value in each cell line.

Cell line	Control		KD		KD efficiency in %
	Relative expression	Variance	Relative expression	Variance	
U251	1.000	0.104	0.481	0.045	51.9
LN229	1.000	0.017	0.443	0.018	55.7
LN308	1.000	0.023	0.043	0.003	95.7
LN18	1.000	0.043	0.109	0.005	89.1

Table 20 Mutations in GBM cell lines; data from KMT laboratory, university hospital Düsseldorf.

Cell line	Gene	Mutation	Frequency in %
LN18	*NF1*	mutation	45.58
	TP53	mutation	99.91
LN229	*TERT*	*TERT* 228 mutation	66.67
	TP53	mutation	99.34
	MTAP	mutation	32.46
	PTPN1	mutation	21.12
LN308	*TERT*	*TERT* 228 mutation	38.89
	PTEN	splicesite mutation	100
	TP53	Homozygote deletion	
U251	*TERT*	*TERT* 228 mutation	81.61
	TP53	mutation	99.78
	NF1	mutation	99.84
T98G	*TERT*	*TERT* 250 mutation	73.13
	PTEN	mutation	99.89
	TP53	mutation	99.9
TP365	*TERT*	*TERT* 228 mutation	53.33
	TP53	mutation	21.91
	FGFR1	mutation	60.82
U87	*TERT*	*TERT* 250 mutation	85.71
	CDKN2A	stop-gain mutation	31.48
	PTEN	splicesite mutation	80.16
	TP53	mutation	15.19
	NF1	frameshift deletion	70.27
	NF1	mutation	33.22

Appendix C

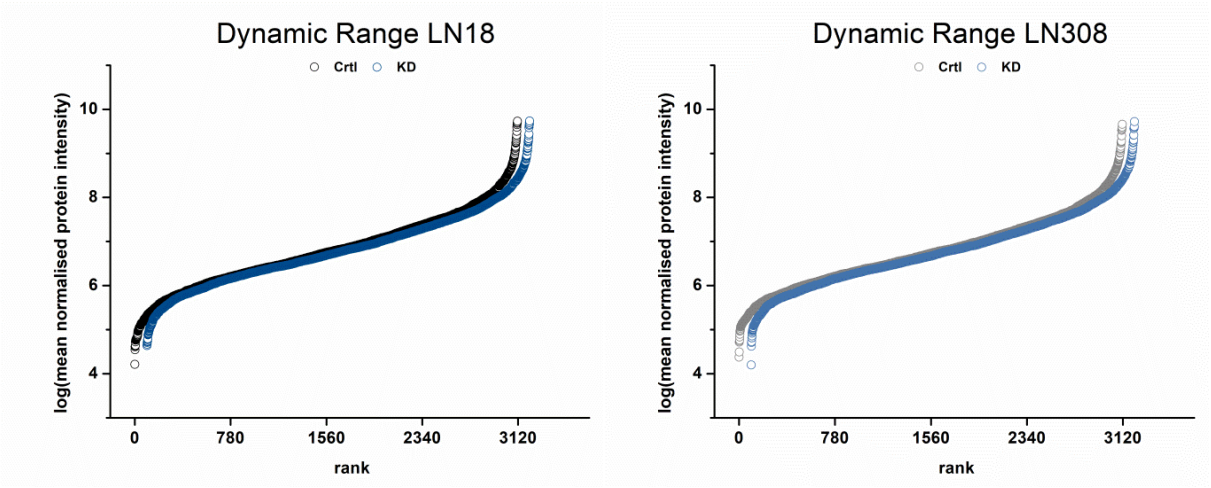

Figure 58 Dynamic range for all quantified proteins in isogenic LN18 and LN308 cell line pairs. Logarithmic mean normalised protein intensities were plotted against their abundance ranked from lowest to highest in the scatter plots. Abundance ranks for quantified proteins in KD samples start at 100 to increase visibility. Measurements for isogenic LN18 cell lines are depicted in the right graph and measurements for isogenic LN308 cell lines are depicted in the left graph with control cells in black and *MALAT1* KD cells in blue.

Table 21 List of differentially regulated proteins in LN18. Proteins are listed with their UniProt accession, associated gene name, peptide as well as unique peptide count in addition to p-value and FC measured.

Accession	Gene	Peptides	Unique peptides	p-value	FC
Q12805	*EFEMP1*	4	4	1.10E-05	-2.04
Q96QR8	*PURB*	2	2	7.83E-04	-1.64
P08962	*CD63*	2	2	1.22E-03	-1.57
Q684P5	*RAP1GAP2*	7	7	1.84E-03	-2.00
Q14192	*FHL2*	3	3	2.71E-03	-2.32
Q15836	*VAMP3*	2	2	3.21E-03	-1.57
Q96CV9	*OPTN*	2	2	4.29E-03	-1.69
Q5SRE5	*NUP188*	10	10	6.05E-03	-1.64
P39060	*COL18A1*	4	3	8.34E-03	-1.86
Q8IV38	*ANKMY2*	2	2	8.71E-03	-1.60
O75844	*ZMPSTE24*	10	9	9.27E-03	-1.84
Q8N653	*LZTR1*	2	2	9.82E-03	-1.65
Q9NUQ6	*SPATS2L*	2	2	1.19E-02	-1.52
Q9UPN9	*TRIM33*	3	3	1.24E-02	-1.56
P13645	*KRT10*	15	13	1.35E-02	-2.02
O43294	*TGFB1I1*	6	6	1.60E-02	-1.68
O76074	*PDE5A*	2	2	1.79E-02	-2.11
Q9NPQ8	*RIC8A*	6	6	1.96E-02	-1.72
Q8TD19	*NEK9*	2	2	2.53E-02	-2.16
Q0VDG4	*SCRN3*	2	2	2.93E-02	-1.70
Q9UPQ0	*LIMCH1*	3	2	3.09E-02	-1.73
P61587	*RND3*	2	2	3.38E-02	-2.43
Q13501	*SQSTM1*	8	8	3.42E-02	-1.55

Q6PJT7	*ZC3H14*	3	2	3.50E-02	-1.86
Q7L8L6	*FASTKD5*	2	2	4.45E-02	-1.72
Q9NQS7	*INCENP*	2	2	4.50E-02	-2.06
P23497	*SP100*	6	5	4.91E-02	-1.58
O95232	*LUC7L3*	2	2	4.98E-02	-1.57
Q96DB5	*RMDN1*	4	3	6.83E-05	1.87
P21506	*ZNF10*	5	5	1.51E-04	1.78
Q86X76	*NIT1*	4	3	1.57E-04	1.98
P29218	*IMPA1*	4	4	6.72E-04	1.59
Q96HP0	*DOCK6*	2	2	6.84E-04	2.55
Q6N075	*MFSD5*	2	2	7.57E-04	2.55
O94888	*UBXN7*	2	2	9.62E-04	2.76
Q8NFF5	*FLAD1*	2	2	1.15E-03	2.26
Q6P179	*ERAP2*	3	3	1.25E-03	2.43
P21589	*NT5E*	8	8	1.26E-03	1.96
Q8IV08	*PLD3*	4	4	1.27E-03	1.69
Q9ULX6	*AKAP8L*	2	2	1.56E-03	2.32
Q6PI48	*DARS2*	7	6	2.42E-03	1.51
Q13356	*PPIL2*	2	2	2.59E-03	1.94
Q9Y624	*F11R*	2	2	2.70E-03	1.82
Q99808	*SLC29A1*	2	2	2.71E-03	1.65
Q02388	*COL7A1*	10	9	2.97E-03	1.60
P12109	*COL6A1*	2	2	3.71E-03	1.64
P15291	*B4GALT1*	4	4	3.75E-03	1.51
Q6VY07	*PACS1*	2	2	4.06E-03	1.92
Q9H9T3	*ELP3*	2	2	4.72E-03	1.62
Q96GM5	*SMARCD1*	4	4	5.10E-03	1.57
O14492	*SH2B2*	9	9	5.35E-03	1.56
Q96S55	*WRNIP1*	5	5	5.62E-03	1.65
O75976	*CPD*	6	6	5.90E-03	1.66
Q8WU76	*SCFD2*	5	5	6.04E-03	1.68
P48651	*PTDSS1*	3	3	6.16E-03	1.59
Q5VT25	*CDC42BPA*	4	4	6.82E-03	1.56
Q9NV06	*DCAF13*	2	2	7.08E-03	1.71
Q9NVH0	*EXD2*	2	2	7.49E-03	1.60
O15305	*PMM2*	2	2	9.00E-03	2.28
Q9UM54-1	*MYO6*	2	2	9.13E-03	1.61
Q96II8	*LRCH3*	2	2	9.14E-03	2.19
Q8NBJ7	*SUMF2*	2	2	9.33E-03	1.53
P19086	*GNAZ*	5	5	1.01E-02	1.64
Q9NWT1	*PAK1IP1*	2	2	1.06E-02	1.74
Q9UQR1	*ZNF148*	3	2	1.07E-02	2.05
P55081	*MFAP1*	3	3	1.10E-02	2.05
Q8IZ07	*ANKRD13A*	3	3	1.14E-02	1.52
Q9BXR0	*QTRT1*	3	3	1.18E-02	1.55
Q5T1J5	*CHCHD2P9*	2	2	1.24E-02	4.73
Q15070	*OXA1L*	2	2	1.31E-02	1.72
P09493	*TPM1*	4	4	1.39E-02	1.94
P17480	*UBTF*	4	4	1.40E-02	1.51

Q9Y6I3	*EPN1*	2	2	1.49E-02	2.84
O95865	*DDAH2*	5	5	1.51E-02	1.58
P48634	*PRRC2A*	10	10	1.72E-02	1.57
Q8NE86	*MCU*	6	6	1.82E-02	1.51
Q9NP81	*SARS2*	3	3	2.16E-02	1.64
Q9Y6D6	*ARFGEF1*	3	3	2.16E-02	2.06
O15357	*INPPL1*	2	2	2.25E-02	1.60
Q9NXH9	*TRMT1*	3	3	2.30E-02	2.72
Q9BVQ7	*SPATA5L1*	2	2	2.31E-02	1.85
Q8IZ81	*ELMOD2*	2	2	2.36E-02	2.12
Q8NDX5	*PHC3*	3	3	2.44E-02	1.51
O14562	*UBFD1*	3	2	2.49E-02	1.64
P56524	*HDAC4*	2	2	2.57E-02	1.51
O60879	*DIAPH2*	5	4	2.71E-02	1.79
Q9BXK5	*BCL2L13*	4	4	2.82E-02	1.53
O76054	*SEC14L2*	4	3	2.99E-02	1.55
O94887	*FARP2*	3	2	3.03E-02	1.56
P42696	*RBM34*	2	2	3.13E-02	1.55
P38571	*LIPA*	2	2	3.15E-02	2.14
Q9Y3A6	*TMED5*	2	2	3.17E-02	1.56
Q99943	*AGPAT1*	3	3	3.20E-02	1.70
P61019	*RAB2A*	12	11	3.27E-02	1.55
Q15047	*SETDB1*	2	2	3.35E-02	1.65
Q5RKV6	*EXOSC6*	2	2	3.38E-02	1.64
Q4L180	*FILIP1L*	3	3	3.42E-02	1.63
O75886	*STAM2*	3	3	3.63E-02	2.30
P08648	*ITGA5*	2	2	3.69E-02	1.52
Q8IY95	*TMEM192*	2	2	3.93E-02	2.00
P62841	*RPS15*	6	6	3.99E-02	1.67
Q15363	*TMED2*	4	4	4.02E-02	2.14
Q8IY17	*PNPLA6*	3	3	4.17E-02	2.39
Q13635	*PTCH1*	3	3	4.21E-02	1.66
Q9H7D7	*WDR26*	6	5	4.22E-02	1.50
Q15113	*PCOLCE*	4	4	4.53E-02	1.62
Q8IYD1	*GSPT2*	4	4	4.59E-02	1.54
Q9BYD6	*MRPL1*	5	5	4.62E-02	1.58
P41212	*ETV6*	2	2	4.69E-02	4.81
Q9H4L7	*SMARCAD1*	3	2	4.89E-02	1.74
Q9UJY5	*GGA1*	3	3	4.97E-02	1.78

Table 22 List of differentially regulated proteins in LN308. Proteins are listed with their UniProt accession, associated gene name, peptide as well as unique peptide count in addition to p-value and FC measured.

Accession	Gene	Peptides	Unique peptides	p-value	FC
Q9Y316	*MEMO1*	3	3	7.85E-04	-1.64
P51808	*DYNLT3*	2	2	2.13E-03	-2.18
Q12805	*EFEMP1*	4	4	2.23E-03	-1.62
Q9BY42	*RTF2*	2	2	1.57E-02	-1.69
Q9NZN8	*CNOT2*	2	2	4.47E-02	-1.62
P21506	*ZNF10*	5	5	7.39E-04	1.56
Q9BZE9	*ASPSCR1*	2	2	3.71E-03	1.96
Q9NXR7-1	*BABAM2*	2	2	4.14E-02	1.76

Appendix D

Table 23 Inhibitor library employed in the HT drug screening experiment as provided by Lena Blümel, university hospital Düsseldorf.

	Inhibitor	Target/Mechanism
1	(-)-Epigallocatechin Gallate	Autophagy; DNA Methyltransferase; Telomerase;
2	(-)-p-Bromotetramisole (oxalate)	Phosphatase;
3	(±)-Equol	Estrogen Receptor/ERR;
4	(R,S)-Ivosidenib	Isocitrate Dehydrogenase (IDH);
5	(S)-10-Hydroxycamptothecin	Others;
6	(S)-MCPG	mGluR;
7	17-AAG	Autophagy; HSP;
8	2-Deoxy-D-glucose	Hexokinase;
9	2-Methoxyestradiol	Autophagy; HIF/HIF Prolyl-Hydroxylase; Microtubule/Tubulin;
10	3,3'-Diindolylmethane	Androgen Receptor;
11	3-Deazaneplanocin A (hydrochloride)	Epigenetic Reader Domain; Histone Methyltransferase;
12	4SC-202	HDAC;
13	5-Azacytidine	Autophagy; Nucleoside Antimetabolite/Analog;
14	5-Fluorouracil	Nucleoside Antimetabolite/Analog;
15	6-Mercaptopurine	Autophagy; Nucleoside Antimetabolite/Analog;
16	6-Thioguanine	Autophagy; DNA Methyltransferase;
17	Abarelix	GNRH Receptor;
18	ABC294640	SPHK;
19	Abiraterone	Cytochrome P450;
20	ABT-199	Bcl-2 Family;
21	ABT-737	Autophagy; Bcl-2 Family;
22	ABT-751	Autophagy; Microtubule/Tubulin;
23	Actinomycin D	Autophagy; DNA/RNA Synthesis;
24	ACY-1215	HDAC;
25	Adarotene	Apoptosis;
26	AEE788	EGFR;
27	Afatinib (dimaleate)	Autophagy; EGFR;
28	Afuresertib	Akt; PKA;
29	AGI-5198	Isocitrate Dehydrogenase (IDH);
30	AICAR	AMPK; Autophagy;
31	Alendronate (sodium hydrate)	Others;
32	Alisertib	Aurora Kinase; Autophagy;
33	Alprenolol (hydrochloride)	5-HT Receptor;
34	Altretamine	DNA Alkylator/Crosslinker;
35	Alvespimycin (hydrochloride)	HSP;
36	AMG 232	MDM-2/p53;

37	AMG 900	Aurora Kinase;
38	AMG 925	CDK; FLT3;
39	AMG-208	c-Met/HGFR;
40	AMG319	PI3K;
41	AMG-337	c-Met/HGFR;
42	Amifostine	Others;
43	Amiselimod (hydrochloride)	LPL Receptor;
44	Amisulpride	Dopamine Receptor;
45	Amonafide	Topoisomerase;
46	Amsacrine	Autophagy; Topoisomerase;
47	Amuvatinib	c-Kit; FLT3; PDGFR;
48	Amygdalin	Others;
49	Anacetrapib	CETP;
50	Anamorelin	GHSR;
51	Anastrozole	Aromatase;
52	Ancitabine (hydrochloride)	Autophagy;
53	Andrographolide	NF-κB;
54	Anethole	Others;
55	Apocynin	Autophagy;
56	APTO-253	PAK;
57	ARN-509	Androgen Receptor;
58	ARQ-092	Akt;
59	ARRY-520 (R enantiomer)	Kinesin;
60	AS703026	MEK;
61	ASC-J9	Androgen Receptor;
62	ASP3026	ALK;
63	AT13148	Akt;
64	AT13387	HSP;
65	AT7519 (Hydrochloride)	CDK;
66	AT9283	Aurora Kinase; Autophagy; JAK;
67	Atrasentan (hydrochloride)	Endothelin Receptor;
68	Auristatin PE	Microtubule/Tubulin;
69	Aurora A inhibitor I	Aurora Kinase;
70	AV-412 (free base)	EGFR;
71	AVL-292	Btk;
72	AVN-944	Others;
73	Axitinib	PDGFR; VEGFR;
74	AXL1717	IGF-1R;
75	AZ505 (ditrifluoroacetate)	Histone Methyltransferase;
76	AZ-5104	EGFR;
77	AZ6102	PARP;
78	AZD 6482	Autophagy; PI3K;
79	AZD1152	Aurora Kinase;

80	AZD1152-HQPA	Aurora Kinase;
81	AZD1208	Pim;
82	AZD-1480	JAK;
83	AZD2014	Autophagy; mTOR;
84	AZD-2461	PARP;
85	AZD3514	Androgen Receptor;
86	AZD3759	EGFR;
87	AZD3839 (free base)	Beta-secretase;
88	AZD3965	Monocarboxylate Transporter;
89	AZD4547	FGFR;
90	AZD5363	Akt; Autophagy; PKA; Ribosomal S6 Kinase (RSK);
91	AZD-5438	CDK;
92	AZD6738	ATM/ATR;
93	AZD-7762	Checkpoint Kinase (Chk);
94	AZD-8055	Autophagy; mTOR;
95	AZD8186	PI3K;
96	AZD8330	MEK;
97	AZD-9291	EGFR;
98	AZD-9291 (mesylate)	EGFR;
99	Bafetinib	Autophagy; Bcr-Abl;
100	Bakuchiol	p38 MAPK;
101	Bardoxolone (methyl)	Autophagy; Keap1-Nrf2;
102	Baricitinib (phosphate)	JAK;
103	BAY 80-6946	PI3K;
104	Bazedoxifene (acetate)	Estrogen Receptor/ERR;
105	Belinostat	Autophagy; HDAC;
106	Bendamustine (hydrochloride)	DNA Alkylator/Crosslinker;
107	Berberine (chloride hydrate)	Autophagy; Wnt; β-catenin;
108	Bergapten	Autophagy; Cytochrome P450;
109	Bestatin	Aminopeptidase;
110	Betahistine (dihydrochloride)	Histamine Receptor;
111	Betulinic acid	Apoptosis; Autophagy; Topoisomerase;
112	Bexarotene	Autophagy; RAR/RXR;
113	BEZ235	mTOR; PI3K;
114	BI 2536	Epigenetic Reader Domain; Polo-like Kinase (PLK);
115	BI-847325	Aurora Kinase; MEK;
116	BIBF 1120	FGFR; PDGFR; VEGFR;
117	BIBF 1120 (esylate)	FGFR; PDGFR; VEGFR;
118	BIBR 1532	Telomerase;
119	BIBX 1382	EGFR;
120	Bicalutamide	Androgen Receptor; Autophagy;
121	BIIB021	Autophagy; HSP;
122	Birinapant	IAP;

123	Bithionol	Parasite ;
124	BKT140	CXCR;
125	Bleomycin (sulfate)	Bacterial; DNA/RNA Synthesis;
126	BLU-554	FGFR;
127	BMN-673 (8R,9S)	PARP;
128	BMS 777607	c-Met/HGFR; TAM Receptor;
129	BMS-214662	Farnesyl Transferase;
130	BMS-599626 (Hydrochloride)	EGFR;
131	BMS-690514	EGFR; VEGFR;
132	BMS-708163	Notch; γ-secretase;
133	BMS-754807	IGF-1R; Insulin Receptor;
134	BMS-794833	c-Met/HGFR; VEGFR;
135	BMS-833923	Smo;
136	BMS-911543	JAK;
137	Bortezomib	Autophagy; Proteasome;
138	Bosutinib	Bcr-Abl; Src;
139	Briciclib	CDK;
140	Brigatinib	ALK;
141	Brivanib	Autophagy; VEGFR;
142	BSI-201	PARP;
143	Buserelin (Acetate)	GNRH Receptor;
144	Busulfan	DNA Alkylator/Crosslinker;
145	BYL-719	PI3K;
146	Cabazitaxel	Autophagy; Microtubule/Tubulin;
147	Cabozantinib (S-malate)	VEGFR;
148	CAL-101	Autophagy; PI3K;
149	Calcitonin (salmon)	Others;
150	Calcitriol	VD/VDR;
151	Canertinib	EGFR;
152	Canertinib (dihydrochloride)	EGFR;
153	Capecitabine	DNA/RNA Synthesis; Nucleoside Antimetabolite/Analog;
154	Capsaicin	Autophagy; TRP Channel;
155	Carboplatin	Autophagy; DNA Alkylator/Crosslinker;
156	Carfilzomib	Autophagy; Proteasome;
157	Carmofur	Nucleoside Antimetabolite/Analog;
158	Carmustine	DNA Alkylator/Crosslinker;
159	Catechin	Others;
160	CB-5083	p97;
161	CB-839	Autophagy;
162	CC-401 (hydrochloride)	JNK;
163	Cecropin B	Cytochrome P450;
164	Cediranib	VEGFR;

165	Cediranib (maleate)	Autophagy; VEGFR;
166	CEP-32496	Raf;
167	CEP-37440	ALK; FAK;
168	Cerdulatinib	JAK; Syk;
169	Cevipabulin	Microtubule/Tubulin;
170	CH5132799	PI3K;
171	CH5183284	FGFR;
172	CH5424802	ALK;
173	Chidamide	HDAC;
174	Chlorambucil	DNA Alkylator/Crosslinker;
175	Chlormethine (hydrochloride)	Others;
176	CI-1040	MEK;
177	CI-994	HDAC;
178	Cilengitide	Autophagy; Integrin;
179	Cinobufotalin	Others;
180	Cisplatin	Apoptosis;
181	Citarinostat	HDAC;
182	Cladribine	Adenosine Deaminase;
183	Clofarabine	Autophagy; Nucleoside Antimetabolite/Analog;
184	CO-1686	EGFR;
185	Cobimetinib	MEK;
186	Cortisone	Glucocorticoid Receptor;
187	CPI-613	Pyruvate Dehydrogenase;
188	Crenolanib	Autophagy; PDGFR;
189	Crizotinib	ALK; Autophagy; c-Met/HGFR;
190	CTS-1027	MMP;
191	CUDC-101	EGFR; HDAC;
192	CUDC-427	IAP;
193	CUDC-907	HDAC; PI3K;
194	Curcumin	Autophagy; Keap1-Nrf2;
195	Curcumol	Others;
196	CX-4945	Autophagy; Casein Kinase;
197	CX-5461	DNA/RNA Synthesis;
198	CYC-116	Aurora Kinase;
199	Cyclic somatostatin	Others;
200	Cyclophosphamide	DNA Alkylator/Crosslinker;
201	Cyclosporin A	Others;
202	CYT387	Autophagy; JAK;
203	Cytarabine	Autophagy; Nucleoside Antimetabolite/Analog;
204	D-3263 (hydrochloride)	TRP Channel;
205	Dabrafenib (Mesylate)	Raf;
206	Dacarbazine	Nucleoside Antimetabolite/Analog;
207	Dacomitinib	EGFR;

208	Dalcetrapib	CETP;
209	Danusertib	Aurora Kinase; Autophagy;
210	Dapagliflozin	SGLT;
211	Dasatinib	Bcr-Abl; Src;
212	Dasatinib (hydrochloride)	Autophagy; Bcr-Abl; Src;
213	Daunorubicin (Hydrochloride)	ADC Cytotoxin; Autophagy; Topoisomerase;
214	DCC-2036	Bcr-Abl; FLT3; Src;
215	DCC-2618	c-Kit; c-Met/HGFR;
216	Debio 0932	HSP;
217	Decitabine	DNA Methyltransferase;
218	Defactinib	FAK;
219	Deforolimus	mTOR;
220	Delamanid	Bacterial;
221	Delanzomib	Proteasome;
222	Dihydroartemisinin	JNK; NF-κB;
223	Dimethylenastron	Kinesin;
224	Dinaciclib	CDK;
225	DMXAA	Autophagy;
226	Docetaxel	Microtubule/Tubulin;
227	Dofequidar (fumarate)	P-glycoprotein;
228	Dovitinib	c-Kit;
229	Doxifluridine	Nucleoside Antimetabolite/Analog;
230	Doxorubicin (hydrochloride)	ADC Cytotoxin; Autophagy; Topoisomerase;
231	Dutasteride	5 alpha Reductase;
232	Duvelisib (R enantiomer)	PI3K;
233	E-3810	FGFR; VEGFR;
234	E-7050	c-Met/HGFR; VEGFR;
235	E7449	PARP;
236	E7820	Integrin;
237	Efaproxiral	Others;
238	Elesclomol	Apoptosis;
239	Ellipticine (hydrochloride)	Topoisomerase;
240	Embelin	IAP;
241	EMD-1214063	Autophagy; c-Met/HGFR;
242	Empagliflozin	SGLT;
243	Enasidenib	Isocitrate Dehydrogenase (IDH);
244	Endoxifen (E-isomer)	Estrogen Receptor/ERR;
245	ENMD-2076	Aurora Kinase; FLT3; VEGFR;
246	Ensartinib	ALK;
247	Entinostat	Autophagy; HDAC;
248	Entrectinib	ALK; Autophagy; ROS; Trk Receptor;
249	Enzastaurin	Autophagy; PKC;
250	Epirubicin (hydrochloride)	Topoisomerase;

251	Epothilone B	Microtubule/Tubulin;
252	EPZ-5676	Histone Methyltransferase;
253	EPZ-6438	Epigenetic Reader Domain; Histone Methyltransferase;
254	Eribulin (mesylate)	Microtubule/Tubulin;
255	Erlotinib	Autophagy; EGFR;
256	Estramustine (phosphate sodium)	Microtubule/Tubulin;
257	Etoposide	Autophagy; Topoisomerase;
258	Everolimus	mTOR;
259	Evodiamine	Others;
260	EW-7197	TGF-β Receptor;
261	Exatecan (Mesylate)	Topoisomerase;
262	Exemestane	Aromatase;
263	Exherin (trifluoroacetate)	Others;
264	Ezatiostat	Gutathione S-transferase;
265	Fasudil (Hydrochloride)	Autophagy; PKC; ROCK;
266	Fenretinide	Autophagy; RAR/RXR;
267	FG-4592	HIF/HIF Prolyl-Hydroxylase;
268	Finasteride	5 alpha Reductase;
269	FK866	Autophagy; Nampt;
270	Flavopiridol (Hydrochloride)	Autophagy; CDK;
271	Floxuridine	Nucleoside Antimetabolite/Analog;
272	Fludarabine (phosphate)	Nucleoside Antimetabolite/Analog;
273	Flumatinib	Bcr-Abl; c-Kit; PDGFR;
274	Flutamide	Androgen Receptor;
275	Foretinib	c-Met/HGFR; VEGFR;
276	Formestane	Aromatase;
277	Forodesine (hydrochloride)	Nucleoside Antimetabolite/Analog;
278	Fosbretabulin (disodium)	Microtubule/Tubulin;
279	Ganetespib	HSP;
280	GANT 61	Autophagy; Gli;
281	GDC-0032	PI3K;
282	GDC-0068	Akt;
283	GDC-0068 (dihydrochloride)	Akt;
284	GDC-0152	IAP;
285	GDC-0349	Autophagy; mTOR;
286	GDC-0623	MEK;
287	GDC-0941	Autophagy; PI3K;
288	GDC-0980	mTOR; PI3K;
289	GDC-0994	ERK;
290	Gefitinib	Autophagy; EGFR;
291	Gemcitabine	Autophagy; DNA/RNA Synthesis; Nucleoside Antimetabolite/Analog;

292	Genistein	Autophagy; EGFR;
293	Genz-644282	Topoisomerase;
294	Gilteritinib	FLT3; TAM Receptor;
295	Gimeracil	Others;
296	GLPG0634	JAK;
297	Gossypol (acetic acid)	Bcl-2 Family;
298	GS-9973	Syk;
299	GSK 525762A	Epigenetic Reader Domain;
300	GSK1059615	mTOR; PI3K;
301	GSK-1070916	Aurora Kinase;
302	GSK126	Epigenetic Reader Domain; Histone Methyltransferase;
303	GSK2110183 (hydrochloride)	Akt;
304	GSK2126458	mTOR; PI3K;
305	GSK2141795	Akt;
306	GSK2636771	PI3K;
307	GSK2879552	Histone Demethylase;
308	GSK343	Autophagy; Epigenetic Reader Domain; Histone Methyltransferase;
309	GSK461364	Polo-like Kinase (PLK);
310	GSK-690693	Akt; Autophagy;
311	GSK-923295	Kinesin;
312	Hesperidin	Autophagy;
313	Hexaminolevulinate (hydrochloride)	Others;
314	Homoharringtonine	STAT;
315	Honokiol	Akt; Autophagy; MEK;
316	Hydroxyfasudil	ROCK;
317	Hydroxyurea	Autophagy; DNA/RNA Synthesis;
318	Icaritin	Autophagy;
319	Icotinib (Hydrochloride)	EGFR;
320	Idarubicin (hydrochloride)	Autophagy; Topoisomerase;
321	Ifosfamide	DNA alkylator/crosslinker;
322	Imatinib (Mesylate)	Autophagy; Bcr-Abl; c-Kit; PDGFR;
323	Imisopasem manganese	Others;
324	INCB 024360	Indoleamine 2,3-Dioxygenase (IDO);
325	INCB28060	c-Met/HGFR;
326	Ingenol Mebutate	PKC;
327	INK-128	Autophagy; mTOR; PI3K;
328	INNO-206	ADC Cytotoxin; Topoisomerase;
329	INO-1001	PARP;
330	Inolitazone (dihydrochloride)	PPAR;
331	IPI-145	PI3K;
332	Irbinitinib	EGFR;

333	Irinotecan	Autophagy; Topoisomerase;
334	Isoliquiritigenin	Aldose Reductase; Autophagy;
335	Isotretinoin	RAR/RXR;
336	Ispinesib	Kinesin;
337	Itraconazole	Autophagy; Fungal;
338	Ivosidenib	Isocitrate Dehydrogenase (IDH);
339	Ixabepilone	Microtubule/Tubulin;
340	JNJ-38877605	c-Met/HGFR;
341	K-115	ROCK;
342	Kevetrin (hydrochloride)	MDM-2/p53;
343	KU-57788	CRISPR/Cas9; DNA-PK; Epigenetic Reader Domain;
344	KW-2449	FLT3;
345	KX2-391 (Mesylate)	Microtubule/Tubulin; Src;
346	Lapatinib	Autophagy; EGFR;
347	LB-100	Phosphatase;
348	LCL161	IAP;
349	LDE225	Smo;
350	LDK378	ALK; IGF-1R; Insulin Receptor;
351	LEE011	CDK;
352	LEE011 (hydrochloride)	CDK;
353	Lenvatinib	VEGFR;
354	Letrozole	Aromatase; Autophagy;
355	Lexibulin	Microtubule/Tubulin;
356	LGK974	Porcupine;
357	LGX818	Raf;
358	Licochalcone A	Autophagy;
359	Linifanib	Autophagy; PDGFR; VEGFR;
360	Linsitinib	IGF-1R; Insulin Receptor;
361	Lomustine	Autophagy; DNA Alkylator/Crosslinker;
362	Lonafarnib	Autophagy; Farnesyl Transferase;
363	Lonidamine	Hexokinase;
364	Losmapimod	Autophagy; p38 MAPK;
365	Lurbinectedin	Others;
366	Luteolin	Autophagy;
367	LY2090314	GSK-3;
368	LY2157299	TGF-β Receptor;
369	LY2228820	p38 MAPK;
370	LY2510924	CXCR;
371	LY-2584702 (free base)	Ribosomal S6 Kinase (RSK);
372	LY2603618	Autophagy; Checkpoint Kinase (Chk);
373	LY2606368 (dihydrochloride)	Checkpoint Kinase (Chk);
374	LY2784544	FGFR; FLT3; JAK;
375	LY2801653 (dihydrochloride)	c-Met/HGFR;

376	LY2835219	CDK;
377	LY2874455	FGFR;
378	LY2940680	Smo;
379	LY3009120	Autophagy; Raf;
380	LY3023414	DNA-PK; mTOR; PI3K;
381	LY3039478	Notch;
382	Malotilate	5-Lipoxygenase;
383	Marimastat	MMP;
384	Masitinib	c-Kit; PDGFR;
385	Masitinib (mesylate)	c-Kit; PDGFR;
386	Mc-Val-Cit-PABC-PNP	ADC Linker;
387	MEK162	Autophagy; MEK;
388	Melphalan	DNA Alkylator/Crosslinker;
389	Methotrexate	ADC Cytotoxin; Antifolate;
390	MI-773	MDM-2/p53;
391	Mibefradil (dihydrochloride)	Calcium Channel;
392	Miriplatin	DNA Alkylator/Crosslinker;
393	Mitomycin C	ADC Cytotoxin; Autophagy; DNA Alkylator/Crosslinker; DNA/RNA Synthesis;
394	Mitotane	Others;
395	Mitoxantrone (dihydrochloride)	Topoisomerase;
396	MK 2206 (dihydrochloride)	Akt; Autophagy;
397	MK-0752	γ-secretase;
398	MK-1775	Wee1;
399	MK-2461	c-Met/HGFR;
400	MK-4827 (Racemate)	PARP;
401	MK-4827 (tosylate)	PARP;
402	MK-5108	Aurora Kinase;
403	MLN 2480	Raf;
404	MLN1117	PI3K;
405	MLN2238	Autophagy; Proteasome;
406	MLN4924 (hydrochloride)	NEDD8-activating Enzyme;
407	MLN8054	Aurora Kinase;
408	MLN9708	Autophagy; Proteasome;
409	Mocetinostat	Autophagy; HDAC;
410	Motesanib (Diphosphate)	c-Kit; VEGFR;
411	Motolimod	Toll-like Receptor (TLR);
412	Mozavaptan	Vasopressin Receptor;
413	MSX-122	CXCR;
414	Mubritinib	EGFR;
415	Napabucasin	STAT;
416	Naringenin	Caspase; NF-κB; PPAR;
417	Navitoclax	Bcl-2 Family;

418	Nedaplatin	DNA/RNA Synthesis;
419	Nelarabine	Nucleoside Antimetabolite/Analog;
420	Nelotanserin	5-HT Receptor;
421	Neratinib	EGFR;
422	Nilotinib	Autophagy; Bcr-Abl;
423	NMS-1286937	Polo-like Kinase (PLK);
424	Nocodazole	Autophagy; Bcr-Abl; CRISPR/Cas9; Microtubule/Tubulin;
425	Noscapine	Autophagy; Sigma Receptor;
426	NVP-AUY922	Autophagy; HSP;
427	NVP-BKM120	PI3K;
428	NVP-BKM120 (Hydrochloride)	PI3K;
429	Obatoclax	Autophagy; Bcl-2 Family;
430	ODM-201	Androgen Receptor;
431	Olaparib	Autophagy; PARP;
432	Oleanolic Acid	Autophagy; STAT;
433	Oltipraz	HIF/HIF Prolyl-Hydroxylase;
434	Ombrabulin (hydrochloride)	Microtubule/Tubulin;
435	ONO-4059	Btk;
436	Oprozomib	Autophagy; Proteasome;
437	Orteronel	Cytochrome P450;
438	OSI-027	Autophagy; mTOR;
439	OSI-930	c-Fms; c-Kit; VEGFR;
440	Osilodrostat	Mineralocorticoid Receptor;
441	Ospemifene	Estrogen Receptor/ERR;
442	Ostarine	Androgen Receptor;
443	OTX-015	Epigenetic Reader Domain;
444	Oxaliplatin	Autophagy; DNA Alkylator/Crosslinker;
445	PAC-1	Autophagy; Caspase;
446	Paclitaxel	ADC Cytotoxin; Microtubule/Tubulin;
447	Pacritinib	FLT3; JAK;
448	Palbociclib	CDK;
449	Palifosfamide	DNA Alkylator/Crosslinker;
450	Palomid 529	mTOR;
451	Panobinostat	Autophagy; HDAC;
452	Parthenolide	Autophagy; DNA Methyltransferase; HDAC; NF-κB;
453	Pazopanib (Hydrochloride)	Autophagy; c-Fms; c-Kit; FGFR; PDGFR; VEGFR;
454	PCI-24781	HDAC;
455	PCI-32765	Btk;
456	PD0325901	Autophagy; MEK;
457	Pelitinib	EGFR;
458	Pemetrexed (disodium hemipenta hydrate)	Antifolate; Autophagy;

459	Pemetrexed (disodium hemipenta hydrate) (1:2:2.5)	Antifolate;
460	Pentostatin	Adenosine Deaminase;
461	Perifosine	Akt; Autophagy;
462	Pexidartinib	c-Fms; c-Kit;
463	PF-03814735	Aurora Kinase;
464	PF-04217903 (methanesulfonate)	c-Met/HGFR;
465	PF-04449913	Smo;
466	PF-04691502	mTOR; PI3K;
467	PF-06463922	ALK;
468	PFK-158	Others;
469	PH-797804	p38 MAPK;
470	PHA-793887	CDK;
471	PHA-848125	Autophagy; CDK;
472	Phenformin (hydrochloride)	AMPK;
473	Pipobroman	Others;
474	Pixantrone (dimaleate)	Topoisomerase;
475	PKC412	PKC;
476	Plinabulin	Microtubule/Tubulin;
477	PND-1186	FAK;
478	Ponatinib	Autophagy; Bcr-Abl; FGFR; PDGFR; Src; VEGFR;
479	Poziotinib	EGFR;
480	PQR620	mTOR;
481	Pracinostat	HDAC;
482	Pralatrexate	Antifolate;
483	Pranlukast (hemihydrate)	Leukotriene Receptor;
484	Prinaberel	Estrogen Receptor/ERR;
485	Procarbazine (Hydrochloride)	DNA Alkylator/Crosslinker;
486	Psoralen	Others;
487	Psoralidin	Notch;
488	PX-12	Others;
489	PX-478	Autophagy; HIF/HIF Prolyl-Hydroxylase;
490	Quercetin	Autophagy; PI3K; Sirtuin;
491	Quinacrine (dihydrochloride)	Autophagy; Phospholipase;
492	Quisinostat	HDAC;
493	Quizartinib	Autophagy; FLT3;
494	R406	Syk;
495	R428	TAM Receptor;
496	R788 (disodium hexahydrate)	Syk;
497	Raltitrexed	Nucleoside Antimetabolite/Analog; Thymidylate Synthase;
498	Rapamycin	mTOR;
499	Refametinib	MEK;

500	Regorafenib	Autophagy; VEGFR;
501	Resminostat (hydrochloride)	HDAC;
502	Resveratrol	Autophagy; IKK;
503	Retinoic acid	PPAR; RAR/RXR;
504	RG7112	MDM-2/p53;
505	RG7388	MDM-2/p53;
506	RGB-286638 (free base)	CDK;
507	RGFP966	HDAC;
508	Rigosertib (sodium)	Polo-like Kinase (PLK);
509	Ro 5126766	MEK; Raf;
510	RO4929097	Notch; γ-secretase;
511	RO4987655	MEK;
512	Romidepsin	HDAC;
513	Roscovitine	CDK;
514	Rotenone	Others;
515	Ruboxistaurin (hydrochloride)	PKC;
516	Rucaparib (phosphate)	PARP;
517	Ruxolitinib (phosphate)	Autophagy; JAK;
518	Ruxolitinib (S enantiomer)	Autophagy; JAK;
519	RVX-208	Epigenetic Reader Domain;
520	RX-3117	Nucleoside Antimetabolite/Analog;
521	Salinomycin	Autophagy; Bacterial; Wnt; β-catenin;
522	Salirasib	Autophagy; Ras;
523	SAR245409	mTOR; PI3K;
524	Saracatinib	Autophagy; Src;
525	Satraplatin	DNA Alkylator/Crosslinker;
526	Savolitinib	c-Met/HGFR;
527	SB1317	CDK; FLT3; JAK;
528	SB-743921	Kinesin;
529	SCIO-469	p38 MAPK;
530	Selumetinib	MEK;
531	Semagacestat	Amyloid-β; Notch; γ-secretase;
532	Seocalcitol	VD/VDR;
533	Serdemetan	MDM-2/p53;
534	SGI-1776	Autophagy; Pim;
535	SGX-523	c-Met/HGFR;
536	Silibinin	Autophagy;
537	SJG-136	DNA Alkylator/Crosslinker;
538	SN-38	Autophagy; Topoisomerase;
539	SNS-032	CDK;
540	SNS-314	Aurora Kinase;
541	Sorafenib (Tosylate)	Autophagy; c-Kit; FLT3; PDGFR; Raf; VEGFR;
542	Sotrastaurin	PKC;

543	SSR128129E	FGFR;
544	Staurosporine	PKA; PKC;
545	Stibogluconate (sodium)	Phosphatase;
546	Streptozocin	DNA Alkylator/Crosslinker; DNA/RNA Synthesis;
547	SU5416	VEGFR;
548	Sulfatinib	FGFR; VEGFR;
549	Sunitinib (Malate)	PDGFR; VEGFR;
550	TAK-285	EGFR;
551	TAK-593	PDGFR; VEGFR;
552	TAK-632	Aurora Kinase; Raf;
553	TAK-715	p38 MAPK;
554	TAK-733	MEK;
555	TAK-901	Aurora Kinase;
556	TAK-960	Polo-like Kinase (PLK);
557	Talabostat (mesylate)	Dipeptidyl Peptidase;
558	Tamibarotene	RAR/RXR;
559	Tamoxifen	Autophagy; Estrogen Receptor/ERR;
560	Tandutinib	FLT3;
561	Tariquidar	P-glycoprotein;
562	TAS-102	Nucleoside Antimetabolite/Analog; Thymidylate Synthase;
563	Tasquinimod	HDAC;
564	Tauroursodeoxycholate (Sodium)	ERK;
565	Telatinib	c-Kit; PDGFR; VEGFR;
566	Temozolomide	Autophagy; DNA Alkylator/Crosslinker;
567	Temsirolimus	mTOR;
568	Teniposide	Topoisomerase;
569	TG 100801	Src; VEGFR;
570	TG100-115	PI3K;
571	TG-101348	Epigenetic Reader Domain; JAK;
572	TGR-1202	PI3K;
573	TH-302	Others;
574	Thalidomide	Others;
575	Thioridazine (hydrochloride)	5-HT Receptor; Autophagy; Dopamine Receptor;
576	Thio-TEPA	DNA Alkylator/Crosslinker;
577	TIC10 isomer	Akt; ERK; TNF-alpha;
578	Tipifarnib	Farnesyl Transferase;
579	Tipifarnib (S enantiomer)	Farnesyl Transferase;
580	Tipiracil (hydrochloride)	Nucleoside Antimetabolite/Analog;
581	Tirapazamine	Topoisomerase;
582	Tivantinib	c-Met/HGFR;
583	Tivozanib	VEGFR;
584	Toceranib (phosphate)	PDGFR; VEGFR;

585	Tofacitinib (citrate)	JAK;
586	TOK-001	Cytochrome P450;
587	Topotecan (Hydrochloride)	Autophagy; Topoisomerase;
588	Toremifene (Citrate)	Estrogen Receptor/ERR;
589	Tozasertib	Aurora Kinase; Autophagy;
590	Trametinib	MEK;
591	Tramiprosate	Amyloid-β;
592	Treosulfan	DNA Alkylator/Crosslinker;
593	Triapine	DNA/RNA Synthesis;
594	Trichostatin A	HDAC;
595	Triciribine	Akt; DNA/RNA Synthesis; HIV; Nucleoside Antimetabolite/Analog;
596	Trifluorothymidine	Nucleoside Antimetabolite/Analog; Thymidylate Synthase;
597	Triptorelin	GNRH Receptor;
598	Troglitazone	Autophagy; PPAR;
599	TSU-68	PDGFR;
600	Tubastatin A (Hydrochloride)	Autophagy; HDAC;
601	Uramustine	DNA Alkylator/Crosslinker;
602	Ursolic acid	Autophagy;
603	VAL-083	DNA Alkylator/Crosslinker;
604	Valproic acid (sodium salt)	Autophagy; HDAC;
605	Valrubicin	PKC;
606	Valspodar	P-glycoprotein;
607	Vandetanib	Autophagy; VEGFR;
608	Vatalanib	VEGFR;
609	Vatalanib (dihydrochloride)	VEGFR;
610	VcMMAE	Drug-Linker Conjugates for ADC; Microtubule/Tubulin;
611	VE-822	ATM/ATR;
612	Veliparib (dihydrochloride)	Autophagy; PARP;
613	Vemurafenib	Autophagy; Raf;
614	Verteporfin	Autophagy; YAP;
615	Vinblastine (sulfate)	Autophagy; Microtubule/Tubulin;
616	Vincristine (sulfate)	Microtubule/Tubulin;
617	Vinflunine (Tartrate)	Microtubule/Tubulin;
618	Vismodegib	Autophagy; Hedgehog;
619	VLX1570	Deubiquitinase;
620	Volasertib	Polo-like Kinase (PLK);
621	Voreloxin (Hydrochloride)	Topoisomerase;
622	Vorinostat	Autophagy; HDAC;
623	VRT752271	ERK;
624	VS-5584	PI3K;
625	VT-464 (R enantiomer)	Cytochrome P450;

626	VX-661	CFTR;
627	WAY-362450	FXR;
628	WP1066	JAK; STAT;
629	Xanthohumol	COX; DGAT;
630	XL019	JAK;
631	XL-147	PI3K;
632	XL228	Aurora Kinase; Bcr-Abl; IGF-1R; Src;
633	YM-155	Autophagy; Survivin;
634	Zibotentan	Endothelin Receptor;
635	Zoledronic acid (monohydrate)	Autophagy; PKC;
636	Zosuquidar (trihydrochloride)	P-glycoprotein;
637	ZSTK474	Autophagy; PI3K;

Acknowledgements

I am extremely grateful to my supervisor Prof Dr Kai Stühler for all the constructive discussions as well as his patience and guidance throughout this journey.

I also could not have undertaken this journey without Prof Dr Lutz Schmitt my co-supervisor.

Many thanks to Dr Marc Remke and the members of his team at the Remke Lab for the fantastic collaboration as well as the biological discussions.

Special thanks to Dr Anja Stefanski and Dr Nan Qin for their important advice, all their suggestions throughout this time, and mostly for answering my never ending stream of questions. I learnt a lot from both of you.

I would like to extend my sincere thanks to my colleagues at the Molecular Proteomics Laboratory for all their help and the great working environment. My thanks to Eva Bruns for the initial training, to my office partners Leonie Grube, Nina Schmidt, and Omid Etemad-Parishanzadeh for the helpful discussions and the teamwork as well as to Christin Hafermann for all her help.

Lastly, I would like to thank my mother for her unconditional support and her belief in me as well as my sister and friends for reminding me of what life is about.

Affirmation in lieu of an oath

I hereby affirm that the thesis entitled:

“Investigating the role of MALAT1, a long non-coding RNA, in glioblastoma tumorigenesis”

is my own work, written independently and without assistance other than the resources cited.

I declare under oath that I have produced my thesis independently and without any undue assistance by third parties under consideration of the ‘Principles for the Safeguarding of Good Scientific Practice at Heinrich Heine University Düsseldorf'.

This thesis has not been submitted, in either identical or similar form, to any other examination authority or university and has not yet been published.

Macclesfield (UK), 25th August 2022 _____

place, date signature